

# Towards a Geometric Understanding of the 4-Dimensional Point Groups

Laith Rastanawi\*

Institut für Mathematik  
Freie Universität Berlin  
Arnimallee 2  
14195 Berlin, Germany

laith.rastanawi@fu-berlin.de

Günter Rote\*

Institut für Informatik  
Freie Universität Berlin  
Takustraße 9  
14195 Berlin, Germany

rote@inf.fu-berlin.de

October 14, 2024

## Abstract

We classify the finite groups of orthogonal transformations in 4-space, and we study these groups from the viewpoint of their geometric action, using polar orbit polytopes. For one type of groups (the toroidal groups), we develop a new classification based on their action on an invariant torus, while we rely on classic results for the remaining groups.

As a tool, we develop a convenient parameterization of the oriented great circles on the 3-sphere, which leads to (oriented) Hopf fibrations in a natural way.

## Contents

<b>1</b>	<b>Introduction and Results</b>	<b>4</b>
<b>2</b>	<b>Orbit Polytopes</b>	<b>5</b>
2.1	Geometric understanding through orbit polytopes: the pyritohedral group . . . .	5
2.1.1	The pyritohedral group for flatlanders . . . . .	6
2.1.2	Polar orbit polytopes and Voronoi diagrams . . . . .	7
2.2	Fundamental domains and orbifolds . . . . .	8
2.3	Left or right orientation of projected images: view from outside . . . . .	8
<b>3</b>	<b>Point groups</b>	<b>9</b>
3.1	The 4-dimensional orthogonal transformations . . . . .	9
3.1.1	Orientation-preserving transformations . . . . .	9
3.1.2	Absolutely orthogonal planes and circles . . . . .	9
3.1.3	Left and right rotations . . . . .	10
3.1.4	Orientation-reversing transformations . . . . .	10
3.1.5	Quaternion representation . . . . .	10
3.2	The classic approach to the classification . . . . .	11
3.3	Previous classifications . . . . .	11
3.3.1	Related work . . . . .	12
3.4	Conjugacy, geometrically equal groups . . . . .	12
3.5	Obtaining the achiral groups . . . . .	13
3.6	Point groups in 3-space and their quaternion representation . . . . .	13
3.7	Finite groups of quaternions . . . . .	14
3.8	Notations for the 4-dimensional point groups, diploid and haploid groups . . . .	14

---

\*Supported by the DFG Research Training Group GRK 2434 “Facets of Complexity”

Certain printers in combination with certain operating systems and printer drivers do not print some of our figures in the intended way. For example, the points on the back part of the sphere in Figure 8b on p. 31 should be visible behind the transparent front part, similar to Figure 8a. The difference is of minor importance except in Figure 7 on p. 28.

D35	<b>4 Hopf fibrations</b>	<b>15</b>
D36	4.1 Parameterizing the great circles in $S^3$	15
D37	4.1.1 Keeping a circle invariant	17
D38	4.1.2 Oriented great circles	18
D39	4.2 Hopf bundles	18
D40	4.2.1 Left and right screws	20
D41	4.2.2 Clifford-parallel circles	21
D42	<b>5 Classification of the point groups</b>	<b>21</b>
D43	5.1 The Clifford torus	22
D44	<b>6 The tubical groups</b>	<b>22</b>
D45	6.1 Orbit circles	23
D46	6.2 Tubes	24
D47	6.2.1 Mapping between adjacent cells	25
D48	6.3 The geometry of the tubes	25
D49	6.3.1 The spherical tubes	27
D50	6.3.2 The spherical tube boundaries	27
D51	6.3.3 The tangential slices	27
D52	6.3.4 The tangential tube boundaries	29
D53	6.4 Generic starting points	30
D54	6.5 Starting point close to a mirror	30
D55	6.6 Starting point on a mirror	31
D56	6.7 Starting point close to a rotation center	32
D57	6.8 Starting point on a rotation center	33
D58	6.8.1 Supergroups of cyclic type	35
D59	6.8.2 Supergroups of dihedral type, and flip symmetries	35
D60	6.9 Two examples of special starting points	35
D61	6.9.1 $\pm[I \times C_n]$ , 5-fold rotation center	35
D62	6.9.2 $\pm\frac{1}{2}[O \times C_{2n}]$ , 4-fold rotation center	37
D63	6.10 Consequences for starting points near rotation centers	40
D64	6.11 Mappings between different tubes	40
D65	6.12 Small values of $n$	40
D66	6.13 Online gallery of polar orbit polytopes	42
D67	6.14 $\pm[T \times C_n]$ versus $\pm\frac{1}{3}[T \times C_{3n}]$	42
D68	<b>7 The toroidal groups</b>	<b>43</b>
D69	7.1 The invariant Clifford torus	43
D70	7.2 Torus coordinates and the torus foliation	45
D71	7.3 Symmetries of the torus	47
D72	7.3.1 Torus translations	48
D73	7.3.2 The directional group: symmetries with a fixed point	49
D74	7.3.3 Choice of coordinate system	50
D75	7.3.4 The directional group and the translational subgroup	50
D76	7.4 Overview of the toroidal groups	51
D77	7.5 The torus translation groups, type $\square$	51
D78	7.5.1 Dependence on the starting point	54
D79	7.6 The torus flip groups, type $\boxdot$	54
D80	7.7 Groups that contain only one type of reflection	54
D81	7.7.1 The torus reflection groups, type $\boxplus$	55
D82	7.7.2 The torus swap groups	56
D83	7.8 The torus swaptorn groups, type $\boxtimes$	57
D84	7.9 Groups that contain two orthogonal reflections, type $\boxplus$ and $\boxtimes$	58
D85	7.10 The full torus groups, type $\boxtimes$	59
D86	7.11 Duplications	60
D87	7.11.1 List of Duplications	62
D88	7.11.2 A duplication example	62
D89	7.12 Comparison with the classification of Conway and Smith	65

D90	<b>8 The polyhedral groups</b>	<b>65</b>
D91	8.1 The Coxeter notation for groups . . . . .	67
D92	8.2 Strongly inscribed polytopes . . . . .	67
D93	8.3 Symmetries of the simplex . . . . .	67
D94	8.4 Symmetries of the hypercube (and its polar, the cross-polytope) . . . . .	67
D95	8.5 Symmetries of the 600-cell (and its polar, the 120-cell) . . . . .	68
D96	8.6 Symmetries of the 24-cell . . . . .	70
D97	8.6.1 A pair of enantiomorphic groups . . . . .	70
D98	<b>9 The axial groups</b>	<b>73</b>
D99	<b>10 Computer calculations</b>	<b>76</b>
D100	10.1 Representation of transformations and groups . . . . .	76
D101	10.2 Fingerprinting . . . . .	76
D102	10.3 Computer checks . . . . .	77
D103	10.4 Checking the achiral polyhedral and axial groups . . . . .	77
D104	10.5 Checking the toroidal groups . . . . .	78
D105	<b>11 Higher dimensions</b>	<b>78</b>
D106	<b>References</b>	<b>79</b>
D107	<b>A Generators for the polyhedral and axial groups</b>	<b>81</b>
D108	<b>B Orbit polytopes for tubical groups with special starting points</b>	<b>83</b>
D109	B.1 $\pm[I \times C_n]$ . . . . .	84
D110	B.1.1 $\pm[I \times C_n]$ , 3-fold rotation center . . . . .	84
D111	B.1.2 $\pm[I \times C_n]$ , 2-fold rotation center . . . . .	85
D112	B.2 $\pm[O \times C_n]$ . . . . .	86
D113	B.2.1 $\pm[O \times C_n]$ , 4-fold rotation center . . . . .	86
D114	B.2.2 $\pm[O \times C_n]$ , 3-fold rotation center . . . . .	87
D115	B.2.3 $\pm[O \times C_n]$ , 2-fold rotation center . . . . .	88
D116	B.3 $\pm\frac{1}{2}[O \times C_{2n}]$ . . . . .	89
D117	B.3.1 $\pm\frac{1}{2}[O \times C_{2n}]$ , 3-fold rotation center . . . . .	89
D118	B.3.2 $\pm\frac{1}{2}[O \times C_{2n}]$ , 2-fold rotation center . . . . .	90
D119	B.4 $\pm[T \times C_n]$ . . . . .	91
D120	B.4.1 $\pm[T \times C_n]$ , 3-fold rotation center . . . . .	91
D121	B.4.2 $\pm[T \times C_n]$ , 2-fold rotation center . . . . .	92
D122	B.5 $\pm\frac{1}{3}[T \times C_{3n}]$ . . . . .	93
D123	B.5.1 $\pm\frac{1}{3}[T \times C_{3n}]$ , 3-fold (type I) rotation center . . . . .	93
D124	B.5.2 $\pm\frac{1}{3}[T \times C_{3n}]$ , 3-fold (type II) rotation center . . . . .	94
D125	B.5.3 $\pm\frac{1}{3}[T \times C_{3n}]$ , 2-fold rotation center . . . . .	95
D126	<b>C The number of groups of given order</b>	<b>96</b>
D127	<b>D The crystallographic point groups</b>	<b>97</b>
D128	<b>E Geometric interpretation of oriented great circles</b>	<b>100</b>
D129	<b>F Subgroup relations between tubical groups</b>	<b>101</b>
D130	<b>G Conway and Smith's classification of the toroidal groups</b>	<b>101</b>
D131	G.1 Index-4 subgroups of $D_{4m}$ . . . . .	104
D132	<b>List of Tables</b>	
D133	1 Point groups in 3 dimensions . . . . .	14
D134	2 The 11 classes of left tubical groups . . . . .	23
D135	3 Relations among tubical groups . . . . .	36
D136	4 The group $D_8^{\mathbb{T}}$ , the directional parts of the torus symmetries . . . . .	49
D137	5 The 10 subgroups of $D_8^{\mathbb{T}}$ . . . . .	50

D138	6	Overview of the 25 classes of toroidal groups . . . . .	52
D139	7	Generators for torus reflection groups and torus swap groups . . . . .	57
D140	8	Generators for full torus reflection/swap groups and full torus groups . . . . .	59
D141	9	The duplications among toroidal groups . . . . .	63
D142	10	The 25 polyhedral groups . . . . .	66
D143	11	Analogy between symmetries of the four-dimensional and three-dimensional cube	68
D144	12	Analogies between symmetries of self-dual polytopes . . . . .	72
D145	13	The 14 pyramidal and prismatic axial groups . . . . .	74
D146	14	The 7 hybrid axial groups . . . . .	74
D147	15	Summary of the 21 axial groups . . . . .	75
D148	16	The 46 polyhedral and axial groups with generators . . . . .	82
D149	17	The 227 crystallographic point groups in four dimensions, part 1 . . . . .	98
D150	18	The 227 crystallographic point groups, part 2, and three pseudo-crystal groups .	99

## 1 Introduction and Results

A  $d$ -dimensional point group is a finite group of orthogonal transformations in  $\mathbb{R}^d$ , or in other words, a finite subgroup of  $O(d)$ . We propose the following classification for the 4-dimensional point groups.

**Theorem 1.1.** *The 4-dimensional point groups can be classified into*

- 25 polyhedral groups (Table 10),
- 21 axial groups (7 pyramidal groups, 7 prismatic groups, and 7 hybrid groups, Table 15),
- 22 one-parameter families of tubical groups (11 left tubical groups and 11 right tubical groups, Table 2), and
- 25 infinite families of toroidal groups (Table 6), among them
  - 2 three-parameter families,
  - 19 two-parameter families, and
  - 4 one-parameter families.

In contrast to earlier classifications of these groups (notably by Du Val in 1962 [15] and by Conway and Smith in 2003 [8], see Section 3.3), we emphasize a geometric viewpoint, trying to visualize and understand actions of these groups. Besides, we correct some omissions, duplications, and mistakes in these classifications.

**Overview of the groups.** The 25 *polyhedral* groups are related to the regular polytopes. The symmetries of the regular polytopes are well understood, because they are generated by reflections, and the classification of such groups as Coxeter groups is classic. We will deal with these groups only briefly, dwelling a little on just a few groups that come in enantiomorphic pairs (i.e., groups that are not equal to their own mirror.)

The 21 *axial* groups are those that keep one axis fixed. Thus, they essentially operate in the three dimensions perpendicular to this axis (possibly combined with a flip of the axis), and they are easy to handle, based on the well-known classification of the three-dimensional point groups.

The *tubical* groups are characterized as those that have (exactly) one Hopf bundle invariant. They come in left and right versions (which are mirrors of each other) depending on the Hopf bundle they keep invariant. They are so named because they arise with a decomposition of the 3-sphere into tube-like structures (discrete Hopf fibrations).

The *toroidal* groups are characterized as having an invariant torus. This class of groups is where our main contribution in terms of the completeness of the classification lies. We propose a new, geometric, classification of these groups. Essentially, it boils down to classifying the isometry groups of the two-dimensional square flat torus.

We emphasize that, regarding the completeness of the classification, in particular concerning the polyhedral and tubical groups, we rely on the classic approach (see Section 3.2). Only for the toroidal and axial groups, we supplant the classic approach by our geometric approach.

**Hopf fibrations.** We give a self-contained presentation of Hopf fibrations (Section 4). In many places in the literature, one particular Hopf map is introduced as “the Hopf map”, either in terms of four real coordinates or two complex coordinates, leading to “the Hopf fibration”. In some sense, this is justified, as all Hopf bundles are (mirror-)congruent. However, for our characterization, we require the full generality of Hopf bundles. As a tool for working with Hopf fibrations, we introduce a parameterization for great circles in  $S^3$ , which might be useful elsewhere.

**Orbit polytope.** Our main tool to understand tubical groups are polar orbit polytopes. (Section 2). In particular, we study the symmetries of a cell of the polar orbit polytope for different starting points.

## 2 Orbit Polytopes

### 2.1 Geometric understanding through orbit polytopes: the pyritohedral group

One can try to visualize a point group  $G \leq O(d)$  by looking at the orbit of some point  $0 \neq v \in \mathbb{R}^d$  and taking the convex hull. This is called the  $G$ -orbit *polytope* of  $v$ . For an in-depth study of orbit polytopes and their symmetries, refer to [17, 18].

The orbit polytope will usually depend on the choice of  $v$ , and it may have other symmetries in addition to those of  $G$ . For example, the  $C_n$ -orbit polytope in the plane is always a regular  $n$ -gon, and this orbit polytope has the larger dihedral group  $D_{2n}$  as its symmetry group.

We will illustrate the usefulness of orbit polytopes with a three-dimensional example. The pyritohedral group is perhaps the most interesting among the point groups in 3 dimensions. It is generated by a cyclic rotation of the coordinates  $(x_1, x_2, x_3) \mapsto (x_2, x_3, x_1)$  and by the coordinate reflection  $(x_1, x_2, x_3) \mapsto (-x_1, x_2, x_3)$ . It has order 24. Figure 1 shows a few examples of orbit polytopes for this group, and their polars. The elements of the pyritohedral group are simultaneously symmetries of the octahedron (where it is an index-2 subgroup of the full symmetry group) and the icosahedron (an index-5 subgroup), and of course of their polars, the cube and the dodecahedron. The group contains reflections, but it is not generated by its reflections.

The orbit of the points  $(1, 0, 0)$  and  $(1, 1, 1)$  generate the regular octahedron and the cube, respectively. These are each other’s polars, but they don’t give any specific information about the pyritohedral group.

Figure 1a shows the orbit polytope (in yellow) of a generic point  $(\frac{2}{3}, \frac{1}{2}, 1)$ , and its polar (in orange). The symmetries of these polytopes are exactly the pyritohedral group. That orbit polytope has 6 rectangular faces (lying in planes of the faces of a cube), 8 equilateral triangles (lying in the faces of an octahedron), and 12 trapezoids (going through the edges of some cube, but not of some regular octahedron). The polar has 24 quadrilateral faces, corresponding to the 24 group elements. For any pair of faces, there is a unique symmetry of the polytope that maps one face to the other.<sup>1</sup>

If we choose one coordinate of the starting point to be 0, the rectangles shrink to line segments, and the trapezoids become isosceles triangles. See Figure 1b. The orbit polytope is an icosahedron with 20 triangular faces: 8 equilateral triangles and 12 isosceles triangles. The polar polytope is a *pyritohedron*, that is, a dodecahedron with 12 equal but not necessarily regular pentagons. For this choice, the orbit contains only 12 points, but the polytope gains no additional symmetries beyond the pyritohedral symmetries. However, for  $(0, \frac{\sqrt{5}-1}{2}, 1)$ , we get the regular icosahedron and the regular dodecahedron. For the specific choice  $(0, \frac{1}{2}, 1)$ , the polar orbit polytope is one of the crystal forms of the mineral pyrite, which gave the polytope and group its name, see Figure 1b. This polytope is also an *alternahedron* on 4 symbols [13]. An alternahedron can be constructed as the orbit of a generic point  $(x_1, x_2, x_3, x_4) \in \mathbb{R}^4$  under all even permutations. Since the points lie in a hyperplane  $x_1 + x_2 + x_3 + x_4 = \text{const}$ , this is a three-dimensional polytope. For the starting point  $(0, 1, 2)$ , we obtain the alternahedron that results from the canonical choice  $(x_1, x_2, x_3, x_4) = (1, 2, 3, 4)$ , a scaled copy of Figure 1b.<sup>2</sup>

<sup>1</sup>In mineralogy, this shape is sometimes called a *diploid*, and *diploidal symmetry* is an alternative name for pyritohedral symmetry. In our context, the term diploid will show up in a different sense.

<sup>2</sup>The illustration of this polytope in [13, Fig. 1] may make the wrong impression of consisting of equilateral triangles only. However, its isosceles faces have base length 2 and two equal legs of length  $\sqrt{6} \approx 2.45$ .

The pyritohedral group differs from the symmetries of the cube (or the octahedron) by allowing only even permutations of the coordinates  $x_1, x_2, x_3$ . When two coordinates are equal, this distinction plays no role, and the resulting polyhedron will have all symmetries of the cube, see Figure 1f. (We mention that some special starting points of this form lead to Archimedean polytopes: The starting point  $(1, 1, \sqrt{2}+1)$  generates a rhombicuboctahedron with 8 regular triangles and 18 squares;  $(0, 1, 1)$  generates the cuboctahedron with 8 regular triangles and 6 squares; with  $(\frac{1}{\sqrt{2}+1}, 1, 1)$ , we get the truncated cube with 8 regular triangles and 8 regular octagons, similar to the yellow polytope in Figure 1f.)

For the purpose of visualizing the pyritohedral group, we will try to keep the three coordinates distinct. By choosing the point close to  $(1, 1, 1)$  or  $(0, 0, 1)$ , we can emphasize the cube-like or the octahedron-like appearance of the orbit polytope or its polar. For example, the polar orbit polytope for  $(0, \frac{1}{10}, 1)$  resembles a cube whose squares are subdivided into rectangles, like the orange polytope in Figure 1c. (Actually, the mineral pyrite has sometimes a cubic crystal form in which the faces carry parallel thin grooves, so-called *striations*.<sup>3</sup>) See also Figure 1d for  $(\frac{2}{10}, \frac{1}{10}, 1)$ . The orbit polytope in Figure 1c appears like an octahedron whose edges have been shaved off, but in an asymmetric way that provides a direction for the edges (see Figure 32a on p. 71 in Section 8.6).

On the other hand, the polar orbit polytope for  $(\frac{8}{10}, \frac{9}{10}, 1)$  resembles an octahedron, carrying a pinwheel-like structure on every face. See Figure 1e.

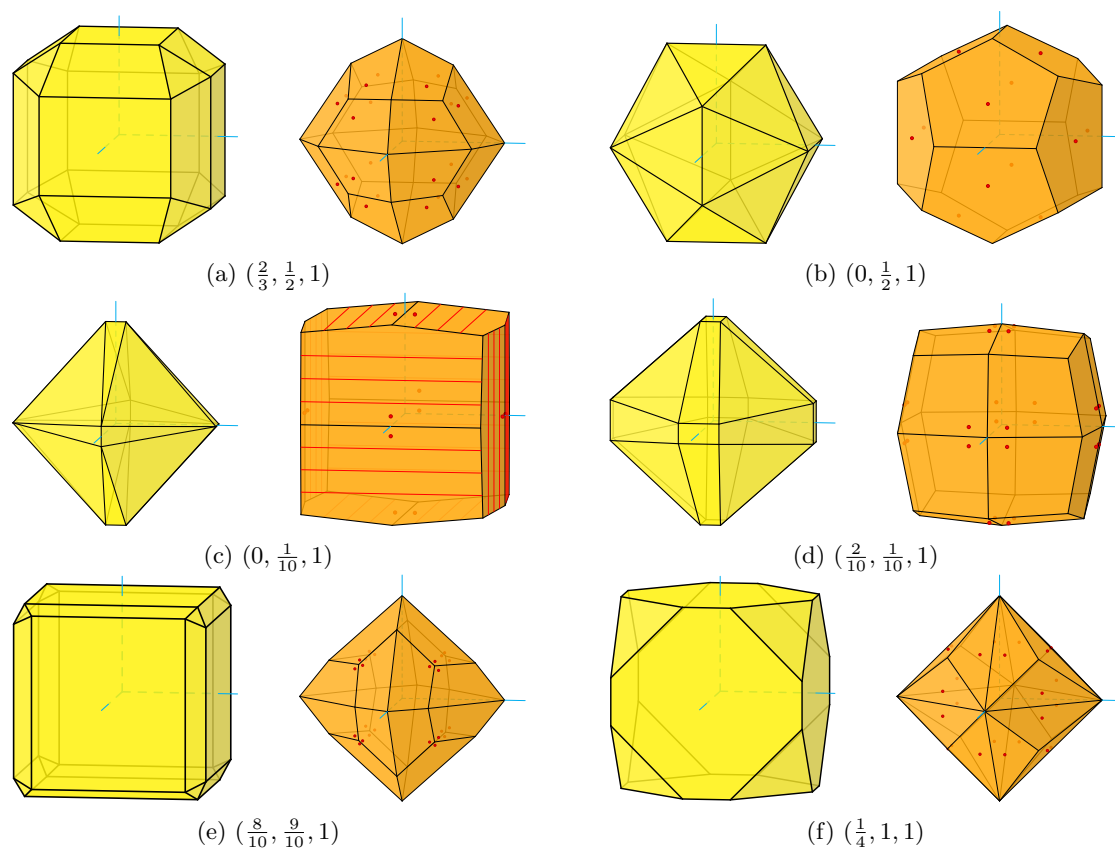


Figure 1: Orbit polytopes of the pyritohedral group (yellow, on the left) and their polar polytopes (orange, on the right) for various starting points. The pictures are rescaled to uniform size; the scale is not maintained between the pictures.

### 2.1.1 The pyritohedral group for flatlanders

We will be in the situation that we try to visualize 4-dimensional point groups through orbit polytopes or their polars. So let us go one dimension lower and imagine that we, as ordinary three-dimensional people, would like to explain the pyritohedral group to flatlanders. We will see that different options have different merits, and there may be no unique best way of visualizing a group.

<sup>3</sup>See <http://www.mineralogische-sammlungen.de/Pyrit-gestreift-engl.html>

Assuming that flatlanders accept the notions of a cube or an octahedron, we could tell them that we build a cube whose squares are striped in such a way that the patterns on adjacent squares never abut, similar to the orange polytope in Figure 1c. It is allowed to map any square to any other square (6 possibilities) in such a way that the stripes match (the dihedral group  $D_4$  with 4 possibilities, for a total of 24 transformations).

Alternatively, we could tell them that the edges of an octahedron are oriented such that each triangle forms a directed cycle (Figure 32a on p. 71). It is allowed to map any triangle to any other triangle (8 possibilities) in such a way that edge directions are preserved (the cyclic group  $C_3$  with 3 possibilities, for a total of 24 transformations).

Another option is the polar of  $(c, 1, 1)$ , where  $c \notin \{0, 1\}$ , see the orange polytope in Figure 1f. It has 24 isosceles triangles, one per group element. As  $c$  approaches 1 or 0, the polar orbit polytope converges to an octahedron or to a rhombic dodecahedron. As a shape, the triangle does not reveal much about the group, so we have to add the information that the base edge acts as a mirror, and the opposite vertex is a 3-fold *gyration point*, i.e., there are three rotated copies that fit together. (This is essentially what is expressed in the orbifold notation  $3*2$ .) We are not allowed to use the reflection that maps the triangle to itself, and we might indicate this by placing an arrow along the base edge.

In most cases, it was advantageous to describe the group in terms of the polar orbit polytope: We have many copies of one shape, and any shape can be mapped to any other. It is not necessarily the best option to insist that all points of the orbit are distinct. Sometimes it is preferable to allow also symmetries within each face. In this case, the information, which of these symmetries are in the group must be conveyed as side information, for example by decorations or patterns that should be left invariant, such as the stripes in Figure 1c.

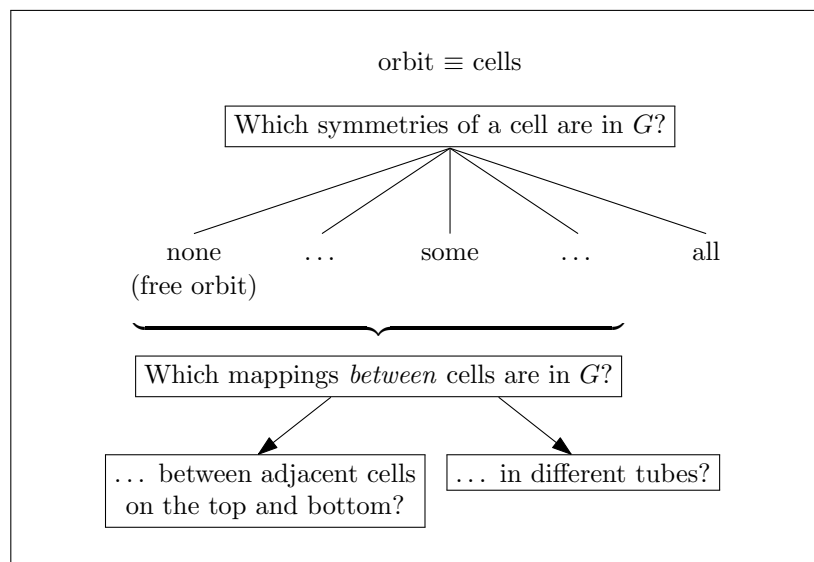


Figure 2: Geometric understanding of a group  $G$  through its polar orbit polytope

Figure 2 summarizes the relation between a polar orbit polytope and its group  $G$ . All cells are equal, and the cells correspond to the points of the orbit. We know that between any two cells, there is at least one transformation in  $G$  that carries one cell to the other. However, it is not directly apparent *which* transformations carry one cell to another cell, or to itself. If all symmetries of a cell belong to the group, the answer is clear; otherwise we have to discuss this question and describe the answer separately.

The bottom row of Figure 2 splits this question into two subproblems that are relevant only for tubical groups (Section 6), namely the relation between adjacent cells in a tube, and between cells of different tubes.

### 2.1.2 Polar orbit polytopes and Voronoi diagrams

There is a well-known connection between polar orbit polytopes and spherical Voronoi diagrams, or more generally, between polytopes whose facets are tangent to a sphere and spherical Voronoi diagrams: The central projection of the polytope to the sphere gives the spherical Voronoi

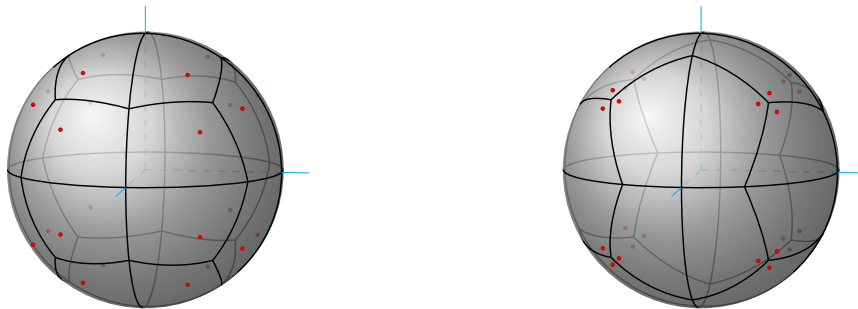


Figure 3: Spherical Voronoi diagrams of the orbits in Figure 1a and Figure 1e.

diagram of the tangency points (the orbit points). Figure 3 shows spherical Voronoi diagrams for two orbits of Figure 1.

Thus, when we look at polar orbit polytopes, we may think about partitioning the sphere according to the closest point from the orbit. The orbit polytope and the spherical Voronoi diagram have the same combinatorial structure, but the faces of the orbit polytope are true Euclidean polytopes, whereas the faces of the Voronoi diagram are spherical polytopes. The closer the orbit points are together, the smaller the distortion will be, and the more the orbit polytope will represent the true metric situation of the Voronoi diagram.

In our illustrations of 4-dimensional groups, we will prefer to show orbit polytopes, because these are easier to compute.

## 2.2 Fundamental domains and orbifolds

For comparison, we mention another way to characterize geometric groups, namely by showing a fundamental domain of the group, possibly extended by additional information that characterizes the type of rotations that fix an edge, such as in an orbifold. This is particularly appropriate for Coxeter groups, which are generated by reflections and for which the choice of fundamental domain is canonical.

Dunbar [16] studied orientation-preserving 4-dimensional point groups. He constructed fundamental domains for 10 out of the 14 orientation-preserving polyhedral groups (omitting  $\pm[I \times T]$  and  $\pm[I \times O]$  and their mirrors). For each of the 21 orientation-preserving polyhedral and axial groups, he showed the structure of the singular set (fixpoints of some group elements) of the corresponding orbifold, which is a 3-valent graph where each edge is labeled with the order of the rotational symmetry around the edge.<sup>4</sup>

The fundamental domain, possibly enriched by additional information, is a concise way for representing some groups, but it does not have the immediate visual appeal of polar orbit polytopes. For example, the fundamental domain of every Coxeter group is a simplex, and the distinctions between different groups lies only in the dihedral angles at the edges.

## 2.3 Left or right orientation of projected images: view from outside

We will illustrate many situations in 4-space by three-dimensional graphics that are derived through projection. Just as a plane in space has no preferred orientation, a 3-dimensional hyperplane in 4-space has no intrinsic orientation. It depends on the side from which we look at it. Hence, it is important to establish a convention about the orientation, in order to distinguish a situation from its mirror image.

Let us look at plane images of the familiar three-dimensional space “for orientation” in this matter. For a polytope or a sphere, we follow the convention that we want to look at it *from outside*, as for a map of some part of the Earth. Accordingly, when we interpret a plane picture with an  $x_1, x_2$ -coordinate system (with  $x_2$  counterclockwise from  $x_1$ ), the usual convention is to think of the third coordinate  $x_3$  as the “vertical upward” direction that is facing us, leading to a right-handed coordinate system  $x_1, x_2, x_3$ .

Similarly, when we deal with a 4-polytope and want to show a picture of one of its facets, which is a three-dimensional polytope  $F$ , we use a right-handed orthonormal  $x_1, x_2, x_3$ -coordinate sys-

<sup>4</sup>In the list of orientation-reversing polyhedral groups that are Coxeter groups [16, Figure 17], the 6th and 8th entries, which are the Coxeter-Dynkin diagrams for the orientation-reversing extensions of  $T \times_{C_3} T$  and  $J \times_J^* J^1$ , must be exchanged.



tem in the space of  $F$  that can be extended to a positively oriented coordinate system  $x_1, x_2, x_3, x_4$  of 4-space such that  $x_4$  points outward from the 4-polytope.

We use the same convention when drawing a cluster of adjacent facets, or when illustrating situations in the 3-sphere, either through central projection or through parallel projection. For example, a small region in the 3-sphere can be visualized as 3-space, with some distortion, and we will be careful to ensure that this corresponds to a view of the sphere “from outside”.

There are other contexts that favor the opposite convention. For example, stereographic projection is often done from the North Pole  $(x_1, x_2, x_3, x_4) = (0, 0, 0, 1)$  of  $S^3$ , and this yields a view “from inside” in the  $(x_1, x_2, x_3)$ -hyperplane. See for example [35, §7], or also [16, p. 123] for a different ordering of the coordinates with the same effect.

### 3 Point groups

The 2-dimensional point groups are the cyclic groups  $C_n$  and the dihedral groups  $D_{2n}$ , for  $n \geq 1$ . For  $n \geq 3$ , they can be visualized, respectively, as the  $n$  rotations of the regular  $n$ -gon, and the  $2n$  symmetries (rotations and reflections) of the regular  $n$ -gon. See Figure 4.

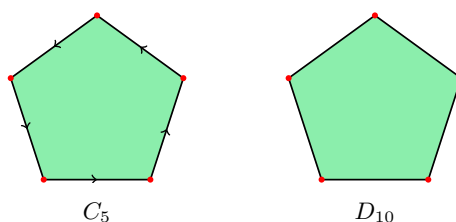


Figure 4: The group  $C_5$  consisting of the rotational symmetries of the regular pentagon, and the group  $D_{10}$  of all symmetries of the regular pentagon.

The 3-dimensional point groups are well-studied (see Section 3.6 below). In one sentence, they can be characterized as the symmetry groups of the five Platonic solids and of the regular  $n$ -side prisms, and their subgroups. This gives a frame for classifying these groups, but it does not give the full information. It remains to work out what the subgroups are, and moreover, there are duplications, for example: certain Platonic solids are polar to each other; the vertices of the cube are contained in the vertices of an icosahedron; and in turn, they contain the vertices of a tetrahedron; a cube is a special quadrilateral prism.

### 3.1 The 4-dimensional orthogonal transformations

#### 3.1.1 Orientation-preserving transformations

We call a 4-dimensional orientation-preserving transformation a *rotation*. In some appropriate basis with coordinates  $x_1, x_2, x_3, x_4$ , every rotation has the form

$$R_{\alpha_1, \alpha_2} = \begin{pmatrix} \cos \alpha_1 & -\sin \alpha_1 & 0 & 0 \\ \sin \alpha_1 & \cos \alpha_1 & 0 & 0 \\ 0 & 0 & \cos \alpha_2 & -\sin \alpha_2 \\ 0 & 0 & \sin \alpha_2 & \cos \alpha_2 \end{pmatrix}, \text{ or } R_{\alpha_1, \alpha_2} = \begin{pmatrix} R_{\alpha_1} & 0 \\ 0 & R_{\alpha_2} \end{pmatrix} = \text{diag}(R_{\alpha_1}, R_{\alpha_2}) \quad (1)$$

in block form, using the rotation matrices  $R_\alpha = \begin{pmatrix} \cos \alpha & -\sin \alpha \\ \sin \alpha & \cos \alpha \end{pmatrix}$  as building blocks [10, §12.1]. If  $\alpha_2 = 0$ , we have a *simple rotation*: a rotation in the  $x_1x_2$ -plane by the angle  $\alpha_1$ , leaving the complementary  $x_3x_4$ -plane fixed. Thus, the general rotation is the product of two simple rotations in two orthogonal planes, and we call it more specifically a *double rotation*. If  $\alpha_2 \neq \pm\alpha_1$  then the two planes are uniquely determined. Each plane is an *invariant plane*: as a set, it is fixed by the operation.

If  $\alpha_1 = \alpha_2 = \pi$ , the matrix is the negative identity matrix, and we have the *central inversion* or *antipodal map*, which we denote by  $-\text{id}$ . In  $\mathbb{R}^4$ , this is an orientation-preserving transformation.

#### 3.1.2 Absolutely orthogonal planes and circles

When we speak of orthogonal planes in 4-space, we always mean “absolutely” orthogonal, in the sense that every vector in one plane is orthogonal to every vector in the other plane.

We will mostly study the situation on the sphere. Here, an invariant plane becomes an *invariant great circle*, and there are *absolutely orthogonal great circles*.

### 3.1.3 Left and right rotations

The rotations with  $\alpha_2 = \pm\alpha_1$  play a special role: Every point is moved by the same angle  $|\alpha_1|$ , and there is no unique pair of invariant planes. The rotations with  $\alpha_2 = \alpha_1$  are *left rotations*, and the rotations with  $\alpha_2 = -\alpha_1$  are *right rotations*. It is easy to see that every rotation  $R_{\alpha_1, \alpha_2}$  is the product of a left and a right rotation (with angles  $(\alpha_1 \pm \alpha_2)/2$ ). This representation is unique, up to a multiplication of both factors with  $-\text{id}$ . Left rotations commute with right rotations. These facts are not straightforward, but they follow easily from the quaternion representation that is discussed below. The product of a left rotation by  $\beta_L$  and a right rotation by  $\beta_R$  is a rotation  $R_{\beta_L + \beta_R, \beta_L - \beta_R}$ .

### 3.1.4 Orientation-reversing transformations

An orientation-reversing transformation has the following form, in some appropriate basis with coordinates  $x_1, x_2, x_3, x_4$ :

$$\bar{R}_\alpha = \begin{pmatrix} \cos \alpha & -\sin \alpha & 0 & 0 \\ \sin \alpha & \cos \alpha & 0 & 0 \\ 0 & 0 & -1 & 0 \\ 0 & 0 & 0 & 1 \end{pmatrix} = \text{diag}(R_\alpha, -1, 1) \quad (2)$$

It operates in some three-dimensional subspace  $x_1, x_2, x_3$  and leaves one axis  $x_4$  fixed. The  $x_3$ -axis is inverted. For  $\alpha = 0$ , we have a mirror reflection in a hyperplane,  $\bar{R}_0 = \text{diag}(1, 1, -1, 1)$ . For  $\alpha = \pi$ , we have  $\bar{R}_\pi = \text{diag}(-1, -1, -1, 1)$ , which could be interpreted as a reflection in the  $x_4$ -axis. In general, we have a rotary-reflection, which has two unique invariant planes: In one plane, it acts as a rotation by  $\alpha$ ; in the other plane, it has two opposite fixpoints in  $S^3$ , and two other opposite points that are swapped. The square of an orientation-reversing transformation  $\bar{R}_\alpha$  is always a simple rotation.

### 3.1.5 Quaternion representation

The quaternions  $x_1 + x_2i + x_3j + x_4k$  are naturally identified with the vectors  $x = (x_1, x_2, x_3, x_4) \in \mathbb{R}^4$ . We identify the set of unit quaternions with  $S^3$ , the 3-sphere, and the set of pure unit quaternions  $v_1i + v_2j + v_3k$  with the points  $(v_1, v_2, v_3)$  on  $S^2$ , the 2-sphere.

Every 4-dimensional rotation can be represented by a pair  $[l, r]$  of unit quaternions  $l, r \in S^3$ . See [8, §4.1]. The pair  $[l, r]$  operates on the vectors  $x \in \mathbb{R}^4$ , treated as quaternions, by the rule

$$[l, r]: x \mapsto \bar{l}xr.$$

The representation of rotations by quaternion pairs is unique except that  $[l, r] = [-l, -r]$ . The rotations  $[l, 1]$  are the *left rotations*, and the rotations  $[1, r]$  are the *right rotations*: They correspond to quaternion multiplication from the left and from the right. A left or right rotation moves every point by the same angular distance  $\alpha$ . In fact, as we shall see (Proposition 4.14(ii)), a left or right rotation by an angle  $\alpha$  other than 0 or  $\pi$  defines a *Hopf bundle*, a decomposition of the 3-sphere  $S^3$  into great circles, each of which is rotated in itself by  $\alpha$ . As transformations on  $S^3$ , they operate as left screws and right screws, respectively. See Section 4.2.1.

We compose transformations by writing them from left to right, i.e.  $[l_1, r_1][l_2, r_2]$  denotes the effect of first applying  $[l_1, r_1]$  and then  $[l_2, r_2]$ .<sup>5</sup> Accordingly, composition can be carried out as componentwise quaternion multiplication:  $[l_1, r_1][l_2, r_2] = [l_1l_2, r_1r_2]$ .

Every orientation-reversing transformation can be represented as

$$*[l, r]: x \mapsto \bar{l}\bar{x}r.$$

See [8, §4.1]. The stand-alone symbol  $*$  is alternate notation for quaternion conjugation  $*[1, 1]: x \mapsto \bar{x}$ . Then  $*[a, b]$  can be interpreted as a composition of the operations  $*$  and  $[a, b]$ . Geometrically, the transformation  $*$  maps  $(x_1, x_2, x_3, x_4)$  to  $(x_1, -x_2, -x_3, -x_4)$ , and it is a reflection in the  $x_1$ -axis. The transformation  $-*$  maps  $(x_1, x_2, x_3, x_4)$  to  $(-x_1, x_2, x_3, x_4)$ , and it is a reflection in the hyperplane  $x_1 = 0$ .

<sup>5</sup>Du Val [15] used the opposite convention, and accordingly his notation  $[l, r]$  denotes the map  $x \mapsto lx\bar{r}$ .

The inverse transformations are given by these formulas:

$$\begin{aligned} [l, r]^{-1} &= [\bar{l}, \bar{r}] \\ (*[l, r])^{-1} &= *[\bar{r}, \bar{l}] = [\bar{l}, \bar{r}]* \end{aligned} \quad (3)$$

The last equation in (3) is also interesting: We may put the  $*$  operation on the other side of a transformation  $[l, r]$  after swapping the components  $l$  and  $r$ .

For  $l = r$ , it is easy to see that  $[l, l]$  maps the point 1 to itself, and thus operates only on the pure quaternion part. Thus, the pairs  $[l, l]$  act as 3-dimensional rotations. For  $l = \cos \alpha + \sin \alpha(ui + vj + wk)$ ,  $[l, l]$  performs a rotation by  $2\alpha$  around the axis with unit vector  $(u, v, w) \in \mathbb{R}^3$ . We will denote  $[l, l]$  by  $[l]: x \mapsto \bar{l}xl$ . When viewed as an operation on the unit sphere  $S^2$ ,  $[l]$  is a *clockwise* rotation by  $2\alpha$  around the point  $(u, v, w)$ .<sup>6</sup> Note that, when the quaternion  $l$  is used as a left rotation  $[l, 1]$  or a right rotation  $[1, l]$  in 4-space, every point is rotated only by  $\alpha$ , not by  $2\alpha$ .

### 3.2 The classic approach to the classification

For a finite subgroup  $G \leq \text{SO}(4)$ , we can consider the group

$$A = \{ (l, r) \in S^3 \times S^3 \mid [l, r] \in G \},$$

which is a two-fold cover of  $G$ , as each rotation  $[l, r] \in G$  is represented by two quaternion pairs  $(l, r)$  and  $(-l, -r)$  in  $A$ . The elements  $l$  and  $r$  of these pairs form the *left and the right group* of  $G$ :

$$L := \{ l \mid (l, r) \in A \}, \quad R := \{ r \mid (l, r) \in A \}$$

These are finite groups of quaternions.

**Proposition 3.1.** *There is a one-to-one correspondence between*

1. *The finite subgroups  $G$  of  $\text{SO}(4)$*
2. *The subgroups  $A$  of  $L \times R$  that contain the element  $(-1, -1)$ , where  $L$  and  $R$  are finite groups of unit quaternions.*

Since there are only five possibilities for finite groups of unit quaternions (including two infinite families, see Section 3.7), this makes it easy, in principle, to determine the finite subgroups of  $\text{SO}(4)$ .

One task of this program, the enumeration of the subgroups  $A$  of a direct product  $L \times R$  is guided by Goursat's Lemma, which was established by Goursat [20] in this very context: The groups

$$L_0 := \{ l \mid (l, 1) \in A \}, \quad R_0 := \{ r \mid (1, r) \in A \}$$

form normal subgroups of  $L$  and  $R$ , which we call the *left and right kernel* of  $G$ . The group  $A$ , and hence  $G$ , is determined by  $L, R, L_0, R_0$  and an isomorphism  $\Phi: L/L_0 \rightarrow R/R_0$  between the factor groups:

$$G = \{ [l, r] \in \text{SO}(4) \mid l \in L, r \in R, \Phi(lL_0) = rR_0 \}$$

The task reduces to the enumeration of all possibilities for the components  $L, R, L_0, R_0, \Phi$ , and to the less trivial task of determining which parameters lead to geometrically equal groups.

This approach underlies all classifications so far, and we call it the *classic* classification.

### 3.3 Previous classifications

- Goursat [20], in 1889, classified the finite groups of motions of *elliptic 3-space*. Elliptic 3-space can be interpreted as the 3-sphere  $S^3$  in which antipodal points are identified. Hence, these groups can be equivalently described as those groups in  $\text{O}(4)$  that contain the central inversion  $-\text{id}$  (the so-called diploid groups, see Section 3.8).

<sup>6</sup>Measuring the rotation angle clockwise is opposite to the usual convention of regarding the counterclockwise direction as the mathematically positive direction. This is a consequence of writing the operation  $[l]$  as  $x \mapsto \bar{l}xl$  (as opposed to the alternative  $x \mapsto lx\bar{l}$ , which was chosen, for example, by Du Val [15]) and regarding the quaternion axes  $i, j, k$  as a right-handed coordinate frame of 3-space, see [12, Exercise 6.4 on p. 67, answer on pp. 189–190].

- Threlfall and Seifert [35, 36], in a series of two papers in 1931 and 1933, extended this to the groups of Euclidean space, but they only concentrated on the chiral groups, i.e., the groups of  $SO(4)$ . Their goal was to study the quotient spaces of the 3-sphere under fixpoint-free group actions, because these lead to *space forms*, spaces of constant curvature without singularities.<sup>7</sup>
- Hurley [23], in 1951, independently of Threlfall and Seifert, built on Goursat’s classification and extended it to  $O(4)$ . However, he considered only the crystallographic groups, see Appendix D.
- Du Val [15], independently of Hurley, in a small monograph from 1964, took up Goursat’s classification and extended it to all groups. From a geometric viewpoint, he extensively discussed the symmetries of the 4-dimensional regular polytopes.
- Conway and Smith [8] in a monograph from 2003, took up the classification task again, correcting some omissions and duplications of the previous classifications. They gave geometric descriptions for the polyhedral and axial groups in terms of Coxeter’s notation.

### 3.3.1 Related work

- De Medeiros and Figueroa-O’Farrill [14], in 2012, classified the groups of order pairs  $(l, r) \in S^3 \times S^3$  of unit quaternions under componentwise multiplication (using Goursat’s Lemma again). These form the 4-dimensional spin group  $Spin(4)$ . Since this is a double cover of  $SO(4)$ , the results should confirm the classification of the chiral point groups. Indeed, Tables 16–18 in [14, Appendix B] give references to  $SO(4)$  and the classification of [8].<sup>8</sup>
- Marina Maerchik, in 1976 [29], investigated the groups that are generated by reflections and simple rotations (also in higher dimensions), as reported in Lange and Mikhaïlova [27], (The term “pseudoreflections” in the title of [29] refers to simple rotations.)
- We mention that the approach of understanding the 4-dimensional groups through their orbits was pioneered by Robinson [32], who, in 1931, studied the orbits of the polyhedral groups. He focused on the orbits themselves and their convex hulls (and not on the polar orbit polytopes as we do).

## 3.4 Conjugacy, geometrically equal groups

Conjugation with a rotation  $[a, b]$  transforms a group into a different group, which is geometrically the same, but expressed in a different coordinate system. Conjugation transforms an orientation-preserving transformation  $[l, r]$  as follows:

$$[a, b]^{-1}[l, r][a, b] = [a^{-1}la, b^{-1}rb]$$

Its effect is thus a conjugation of the left group by  $a$  and an independent conjugation of the right group by  $b$ . As a conclusion, we can represent the left group  $L$  and the right group  $R$  in any convenient coordinate system of our choice, and it is no loss of generality to choose a particular representative for each finite group of quaternions. (Section 3.7 specifies the representatives that we use.)

<sup>7</sup>The term “Diskontinuitätsbereich” in the title of [35, 36] is used like a well-established concept that does not require a definition. In the contemporary literature, it means what we today call a fundamental domain. Seifert and Threlfall were in particular interested in its topological properties, referring by “Diskontinuitätsbereich” to the quotient space under a group action, with a specification how the boundary faces of the fundamental domain are to be pairwise identified. Du Val [15, §30] also takes this interpretation and calls it a *group-set space*, where *group-set* is his term for orbit.

In modern usage, “region of discontinuity” has other meanings, closer to the literal meaning of the words, where discontinuity plays a role.

<sup>8</sup>However, besides noticing a few typographical errors, we found some discrepancies in these tables: (i) The 6th entry in Table 18 lists a group  $\pm[C_{2k+1} \times \bar{D}_{4m}]$ . We cannot match this with anything in the Conway–Smith classification, even allowing for one typo. (ii) The last entry in Table 4.2 of [8] is  $+\frac{1}{f}[C_{mf} \times C_{nf}]$ . This group does not appear in the tables of [14]. We don’t know whether these discrepancies arose in the translation from the classification in [14] to the notions of  $SO(4)$  or they indicate problems in the classification itself.

### 3.5 Obtaining the achiral groups

The classic approach by Goursat's Lemma leads only to the chiral groups. Since the chiral part of an achiral group is an index-2 subgroup, every achiral group  $G$  is obtained by extending a chiral group  $H$  with some orientation-reversing element

$$e = *[a, b].$$

We will now derive some conditions on  $e$ , and possibly by modifying the group  $G$  into a geometrically conjugate group, constrain  $e$  to a finite number of possibilities.

Let  $H$  be a chiral group with left group  $L$  and right group  $R$ . For each  $[l, r] \in H$ , we must have  $e^{-1}[l, r]e \in H$ , i.e.,  $H$  is normalized by  $e$ :

$$e^{-1}[l, r]e = *[\bar{b}, \bar{a}][l, r]*[a, b] = [\bar{a}ra, \bar{b}lb] \in H$$

This means that  $\bar{a}ra \in L$  and  $\bar{b}lb \in R$  for every  $[l, r] \in H$ , which implies  $\bar{a}Ra = L$  and  $\bar{b}Lb = R$ , i.e.,  $L$  and  $R$  are conjugate.

We conjugate  $G$  with  $[1, a]$ , transforming  $G$  to some geometrically equivalent group  $G'$  with left group  $L'$  and right group  $R'$ . Let us see what happens to an arbitrary element  $[l, r]$ :

$$[1, \bar{a}][l, r][1, a] = [l, \bar{a}ra] \quad (4)$$

The set of values  $\bar{a}ra$  forms the new right group  $R' = \bar{a}Ra = L$ , while the left group remains unchanged:  $L' = L$ . Thus, we have achieved  $L' = R'$ , i.e., the left and right groups are not just conjugate, but equal.

The extending element  $e = *[a, b]$  is transformed as follows:

$$e' := [1, \bar{a}]*[a, b][1, a] = *[1, ba] = *[1, c] \quad (5)$$

Thus we have simultaneously achieved  $e' = *[1, c]$ . Moreover,

$$e'e' = *[1, c]*[1, c] = [c, c] \in H,$$

and thus,  $c$  must be an element of  $L = R$ .

**Proposition 3.2.** *W.l.o.g., we can assume  $L = R$ , and the extending element is of the form  $e = *[1, c]$ , with  $c \in L$ .*

This reduces the extending element to a finite number of possibilities. Conway and Smith [8, p. 51] have sketched some additional considerations, which allow to further restrict the extending element, sometimes at the cost of giving up the condition  $L = R$ , see Figure 54 on p. 107.

Conjugation by  $[a, a]$  changes the transformations as follows:

$$\begin{aligned} [a, a]^{-1}[l, r][a, a] &= [a^{-1}la, a^{-1}ra] \\ [a, a]^{-1}*[l, r][a, a] &= *[a^{-1}la, a^{-1}ra] \end{aligned}$$

Its effect is thus a conjugation of the left and right group  $L = R$  by  $a$ . As for the chiral groups, we can therefore choose any convenient representation of the left and right group  $L$  in Proposition 3.2.

### 3.6 Point groups in 3-space and their quaternion representation

Table 1 lists the three-dimensional point groups that we will use. We will refer to them by the notation of Conway and Smith [8], given in the first column. As alternate notations, we give the orbifold notation, the Hermann-Mauguin notation or international symbol [21], and the Coxeter notation, which we will revisit in Section 8.

The table contains all 7 polyhedral groups (3 chiral and 4 achiral ones): groups consisting of symmetries of regular polytopes. The groups that are not polyhedral (subgroups of the symmetry groups of regular prisms, related to the frieze groups) include, besides  $+C_n$  and  $+D_{2n}$ , five additional classes of *achiral* groups, which are not listed here. In total, there are 14 types of three-dimensional point groups. Note that the subscript  $2n$  in  $D_{2n}$  is always even; we follow the convention of using the *order* of the group, not the number of sides of the polygon or prism of which it is the symmetry group.

The notations  $+I, \pm I$ , etc. for the polyhedral groups are easy to remember. The one that requires some attention is the full symmetry group of the tetrahedron, which is denoted by  $TO$ , as opposed to the pyritohedral group  $\pm T$ , which is obtained by extending  $+T$  by the central reflection, and which we have discussed extensively in Section 2.1.

the chiral groups					
CS	orbifold	I.T.	Coxeter name	order	orientation-preserving symmetries of ...
$+C_n$	<b>nn</b>	$n$	$[n]^+$	$n$	the $n$ -sided pyramid ( $n \geq 1$ )
$+D_{2n}$	<b>22n</b>	$n2$	$[2, n]^+$	$2n$	the $n$ -sided prism ( $n \geq 1$ )
$+T$	<b>332</b>	$23$	$[3, 3]^+$	$12$	the tetrahedron
$+O$	<b>432</b>	$432$	$[3, 4]^+$	$24$	the octahedron / the cube
$+I$	<b>532</b>	$532$	$[3, 5]^+$	$60$	the icosahedron / the dodecahedron
some achiral polyhedral groups					
CS	orbifold	I.T.	Coxeter name	order	description of the group
$TO$	<b>*332</b>	$\bar{4}3m$	$[3, 3]$	$24$	all symmetries of the tetrahedron
$\pm T$	<b>3*2</b>	$m\bar{3}$	$[3^+, 4]$ or $[^+3, 4]$	$24$	the pyritohedral group
$\pm O$	<b>*432</b>	$m\bar{3}m$	$[3, 4]$	$48$	all symmetries of the octahedron
$\pm I$	<b>*532</b>	$5\bar{3}m$	$[3, 5]$	$120$	all symmetries of the icosahedron

Table 1: Some point groups in 3 dimensions

### 3.7 Finite groups of quaternions

The finite groups of quaternions are [8, Theorem 12]:

$$\begin{aligned}
 2I &= \langle i_I, \omega \rangle & 2D_{2n} &= \langle e_n, j \rangle \\
 2O &= \langle i_O, \omega \rangle & 2C_n &= \langle e_n \rangle \\
 2T &= \langle i, \omega \rangle & 1C_n &= \langle e_{n/2} \rangle \quad (n \text{ odd})
 \end{aligned}$$

The generators are defined in terms of the following quaternions, which we will use throughout:

$$\begin{aligned}
 \omega &= \frac{1}{2}(-1 + i + j + k) & (\text{order } 3) \\
 i_O &= \frac{1}{\sqrt{2}}(j + k) & (\text{order } 4) \\
 i_I &= \frac{1}{2}(i + \frac{\sqrt{5}-1}{2}j + \frac{\sqrt{5}+1}{2}k) & (\text{order } 4) \\
 e_n &= \cos \frac{\pi}{n} + i \sin \frac{\pi}{n} & (\text{order } 2n)
 \end{aligned} \tag{6}$$

We follow Conway and Smith's notation for these groups. For each group  $+G < \text{SO}(3)$  (see the upper part of Table 1), there is quaternion group  $2G$  of twice the size, containing the quaternions  $\pm l$  for which  $[l]$  represents a rotation in  $+G$ . All these groups contain the quaternion  $-1$ . In addition, there are the odd cyclic groups  $1C_n$ , of order  $n$ . They cannot arise as left or right groups, because  $(-1, -1)$  is always contained in  $A$  and hence the left and right groups contain the quaternion  $-1$ .

### 3.8 Notations for the 4-dimensional point groups, diploid and haploid groups

We use the notation by Conway and Smith [8] for 4-dimensional point groups  $G$ , except for the toroidal groups, where we will replace it with our own notation. If  $L$  and  $R$  are 3-dimensional orientation-preserving point groups,  $\pm[L \times R]$  denotes full product group  $\{[l, r] \mid (l, r) \in 2L \times 2R\}$ , of order  $2|L| \cdot |R|$ . Note that the groups  $2L$  and  $2R$  that appear in the definition are quaternion groups, while the notation shows only the corresponding rotation groups  $L, R \in \text{SO}(3)$ .

A group that contains the negation  $-\text{id} = [1, -1]$  is called a *diploid* group. A diploid index- $f$  subgroup of  $\pm[L \times R]$  is denoted by  $\pm \frac{1}{f}[L \times R]$ . It is defined by two normal subgroups of  $2L$  and of  $2R$  of index  $f$ . Different possibilities for the normal subgroups and for the isomorphism  $\Phi$  are distinguished by various ornamentations of the notation, see Appendix G for some of these cases.

A *haploid* group, which does not contain the negation  $-\text{id}$ , is denoted by  $+\frac{1}{f}[L \times R]$ , and it is an index-2 subgroup of the corresponding diploid group  $\pm \frac{1}{f}[L \times R]$ . Achiral groups are index-2 extensions of chiral groups, and they are also denoted by various decorations.

Du Val [15] writes the groups as  $(\mathbf{L}/\mathbf{L}_0; \mathbf{R}/\mathbf{R}_0)$ , where the boldface letters distinguish quaternion groups from the corresponding 3-dimensional rotation groups. Again, various ornamentations denote different cases of normal subgroups and the isomorphism  $\Phi$ . Achiral extensions are denoted by a star. We will not work with this notation except for reference in our tables, and then we will omit the boldface font. In some cases, we had to adapt Du Val's names, see Tables 10 and 15.

## 4 Hopf fibrations

We give a self-contained presentation of Hopf fibrations and Hopf maps. Our treatment was inspired by Lyons [28], but we did not see it anywhere in this generality. As a tool, we introduce a parameterization of the great circles in  $S^3$ , which might be useful elsewhere. We also define *oriented* Hopf bundles: families of consistently oriented great circles.

We summarize the main statements:

- The great circles in  $S^3$  can be parameterized by pairs  $p, q$  of pure unit quaternions, or equivalently, by pairs of points  $p, q \in S^2$  (Section 4.1). The choice of parameters is unique except that  $K_p^q = K_{-p}^{-q}$ . The twofold ambiguity of the parameters can be used to specify an orientation of the circles (Section 4.1.2).
- The great circles  $K_p^q$  with fixed  $q$  form a partition of  $S^3$ , which we call the *left Hopf bundle*  $\mathcal{H}^q$ . It naturally comes with a *left Hopf map*  $h^q: S^3 \rightarrow S^2$ , which maps all points of  $K_p^q$  to the point  $p \in S^2$ .  
This map provides a bijection between the circles of the left Hopf bundle  $\mathcal{H}^q$  and the points on  $S^2$ .  
Similarly, the great circles  $K_p^q$  with fixed  $p$  form a *right Hopf bundle*  $\mathcal{H}_p$ , with a *right Hopf map*  $h_p$ , etc. In the following, we will mention only the left Hopf bundles, but all statements hold also with left and right reversed.
- Every great circle of  $S^3$  belongs to a unique left Hopf bundle. In other words, the left Hopf bundles form a partition of the set of great circles of  $S^3$ .
- For every left Hopf bundle  $\mathcal{H}^q$ , there is a one-parameter family of right rotations that maps every circle in  $\mathcal{H}^q$  to itself, rotating each circle by the same angle  $\alpha$ .  
Conversely, a right rotation by an angle  $\alpha \notin \{0, \pi\}$  rotates every point of  $S^3$  by the same angle  $\alpha$ , and the set of circles along which these rotations happen form a left Hopf bundle (Proposition 4.14).
- The following statements discuss the behavior of Hopf bundles under orthogonal transformations (Proposition 4.12):
  - Any left rotation leaves the left Hopf bundle  $\mathcal{H}^q$  fixed, as a partition. It permutes the great circles of the bundle.
  - Any rotation maps the left Hopf bundle  $\mathcal{H}^q$  to another left Hopf bundle. Any two left Hopf bundles are congruent (by some right rotation).
  - Left Hopf bundles and right Hopf bundles are mirrors of each other.
- The intersection of a left Hopf bundle and a right Hopf bundle consists of two absolutely orthogonal circles (Corollary 4.10).
- Any two great circles in the same Hopf bundle are Clifford-parallel (Proposition 4.15). This means that a point moving on one circle maintains a constant distance to the other circle.

### 4.1 Parameterizing the great circles in $S^3$

**Definition 4.1.** For any two pure unit quaternions  $p, q \in S^2$ , we define the following subset of unit quaternions:

$$K_p^q := \{ x \in S^3 \mid [x]p = q \} \quad (7)$$

This can be interpreted as the set of rotations on  $S^2$  that map  $p$  to  $q$ .

**Proposition 4.2.**  $K_p^q$  has an alternative representation

$$K_p^q = \{ x \in S^3 \mid [p, q]x = x \}, \quad (8)$$

and it forms a great circle in  $S^3$ . Moreover, every great circle in  $S^3$  can be represented in this way, and the choice of parameters  $p, q \in S^2$  is unique except that  $K_p^q = K_{-p}^{-q}$ .

This gives a convenient parameterization of the great circles in  $S^3$  (or equivalently, the planes in  $\mathbb{R}^4$ ) by pairs of points on  $S^2$ , which might be useful in other contexts. For example, they might be used to define a notion of distance between great circles (or planes in  $\mathbb{R}^4$ ). (Other distance measures are discussed in [26, 25] and [7]. The connection to these different distance notions remains to be explored.)

Before giving the proof, let us make a general remark about quaternions. Multiple meanings can be associated to a unit quaternion  $x$ : Besides treating it (i) as a point on  $S^3$ , we can regard it (ii) as a rotation  $[x]$  of  $S^2$ , or (iii) as a left rotation  $[x, 1]$  of  $S^3$ , or (iv) as a right rotation  $[1, x]$  of  $S^3$ . Rather than fixing an opinion on what a quaternion really *is* (cf. [1, p. 298]), we capitalize on this ambiguity and freely switch between the definitions (7) and (8).

*Proof of Proposition 4.2.* The two expressions (7) and (8) are equivalent by a simple rearrangement of terms:

$$[x]p = q \iff \bar{x}px = q \iff px = xq \iff x = \bar{p}xq \iff x = [p, q]x$$

The expression (8) shows that  $K_p^q$  is the set of fixpoints of the rotation  $[p, q]$ . Since  $p$  and  $q$  are unit quaternions, the rotation  $[p, q]$  is a simple rotation by  $180^\circ$  (a half-turn). Its set of fixpoints is a two-dimensional plane, or when restricted to unit quaternions, a great circle.

Conversely, if a great circle  $K$  is given and we want to determine  $p$  and  $q$ , we know that we are looking for a simple rotation by  $180^\circ$  whose set of fixpoints is  $K$ . This rotation is uniquely determined, and its quaternion representation  $[p, q]$  is unique up to flipping both signs simultaneously.  $\square$

The effect of orthogonal transformations on great circles is expressed easily in our parameterization:

**Proposition 4.3.** *Let  $p, q \in S^2$ . Then for any  $l, r \in S^3$ ,*

$$(i) \quad [l, r]K_p^q = K_{[l]p}^{[r]q}.$$

$$(ii) \quad (*[l, r])K_p^q = K_{[l]q}^{[r]p}, \text{ and in particular, } *K_p^q = K_q^p.$$

*Proof.* The following calculation proves part (i).

$$\begin{aligned} [l, r]K_p^q &= \{ \bar{l}xr \mid \bar{x}px = q \} \\ &= \{ y \mid r\bar{y}\bar{l}p\bar{l}y\bar{r} = q \} = \{ y \mid \bar{y}\bar{l}p\bar{l}y = \bar{r}qr \} = \{ y \mid [y][l]p = [r]q \} = K_{[l]p}^{[r]q}, \end{aligned}$$

where we have substituted  $x$  by  $y := \bar{l}xr$ . Part (ii) follows from part (i) and  $*K_p^q = K_q^p$ . This last statement expresses the fact that the inverse rotations  $[\bar{x}]$  of the rotations  $[x]$  that map  $p$  to  $q$  are the rotations mapping  $q$  to  $p$ . More formally,

$$*K_p^q = \{ \bar{x} \mid \bar{x}px = q \} = \{ y \mid yp\bar{y} = q \} = \{ y \mid p = \bar{y}qy \} = K_q^p,$$

with  $y := \bar{x}$ .  $\square$

The elements of  $K_p^p$  form a subgroup of the quaternions [16]: According to (7),  $K_p^p$  is the stabilizer of  $p$ . Its cosets can be characterized by Proposition 4.3(i):

**Corollary 4.4.** *The left cosets of  $K_p^p$  are the circles  $K_{p'}^p$ , and the right cosets of  $K_p^p$  are the circles  $K_p^{p'}$ , for arbitrary  $p' \in S^2$ .  $\square$*

We emphasize that the two parameters  $p$  and  $q$  in  $K_p^q$  “live on different spheres  $S^2$ ”: Any relation between them has no intrinsic geometric meaning, and will be changed by coordinate transformations according to Proposition 4.3. This is despite the fact that  $p = q$  has an algebraic significance, since the circle  $K_p^p$  goes through the special quaternion 1, which is one of the coordinate axes, and hence  $K_p^p$  forms a subgroup of quaternions.



#### 4.1.1 Keeping a circle invariant

The following proposition characterizes the transformations that map a given great circle to itself. Moreover, it describes the action of these transformations when restricted to that circle. For a pure unit quaternion  $p \in S^2$  and an angle  $\theta \in \mathbb{R}$  we use the notation

$$\exp p\theta := \cos \theta + p \sin \theta,$$

so that  $[\exp p\theta]$  is a clockwise rotation around  $p$  by  $2\theta$  on  $S^2$ .

**Proposition 4.5.** *Consider the circle  $K_p^q$ , for  $p, q \in S^2$ . The rotations  $[l, r]$  that leave  $K_p^q$  invariant fall into two categories, each of which is a two-parameter family.*

(a) *The orientation-preserving case:  $[l]p = p$  and  $[r]q = q$ .*

*Every transformation in this family can be written as  $[\exp p\varphi, \exp q\theta]$  for  $\varphi, \theta \in \mathbb{R}$ . This transformation acts on the circle  $K_p^q$  as rotation by  $|\theta - \varphi|$ .*

(b) *The orientation-reversing case:  $[l]p = -p$  and  $[r]q = -q$ .*

*After choosing two fixed quaternions  $p', q' \in S^2$  orthogonal to  $p$  and  $q$ , respectively, they can be written as the transformations  $[p' \exp p\varphi, q' \exp q\theta]$  for  $\varphi, \theta \in \mathbb{R}$ , and they act on  $K_p^q$  as reflections.*

Note that the transformations that we consider are always orientation-preserving when considered in 4-space; they can be orientation-reversing when considered as (2-dimensional) operations on the circle  $K_p^q$ .

*Proof.* Let  $[l, r] \in \text{SO}(4)$  be a rotation. Then we have the following equivalences.

$$[l, r]K_p^q = K_p^q \iff K_{[l]p}^{[r]q} = K_p^q \iff ([l]p = p \wedge [r]q = q) \vee ([l]p = -p \wedge [r]q = -q)$$

For the first case, the transformations  $[l]$  on  $S^2$  that leave the point  $p$  fixed are the rotations around  $p$ , and they are given by the quaternions  $l = \exp p\varphi$ , and similarly for  $r$ . For the second case, the transformations  $[l]$  on  $S^2$  that map  $p$  to  $-p$  can be written as a composition of  $[p']$ , which maps  $p$  to  $-p$ , and an arbitrary rotation around the axis through  $p$  and  $-p$ , which is expressed as  $[\exp p\varphi]$ . This establishes that  $[l, r]$  can be written in the claimed form.

We now investigate the action of these rotations on  $K_p^q$ .

(a) Let  $x \in K_p^q$ . Since  $xq = px$ , we have  $x \exp q\theta = (\exp p\varphi)x$ . In particular,

$$[\exp p\varphi, \exp q\theta]x = \exp(-p\varphi)x \exp q\theta = \exp(-p\varphi)(\exp p\theta)x = (\exp p(-\varphi + \theta))x.$$

Thus,  $[\exp p\varphi, \exp q\theta]$  acts on  $K_p^q$  like the left multiplication with  $\exp p(\theta - \varphi)$ , which (being a left rotation) moves every point by the angle  $|\theta - \varphi|$ .

(b) It is enough to show that  $[p', q']$  acts as a reflection on  $K_p^q$ . We will show that  $K_p^q \cap K_{p'}^{q'} \neq \emptyset$  and  $K_p^q \cap K_{p'}^{-q'} \neq \emptyset$ . Thus, there is a point  $x \in K_p^q$  with  $[p', q']x = x$  and another point  $y \in K_p^q$  with  $[p', q']y = -y$ , and this means that  $[p', q']$  fixes some, but not all, points on  $K_p^q$ , and thus its action cannot be a rotation.

Let  $[x_0]$  be a rotation that maps  $p$  to  $q$ . Then it maps  $p'$  to some point  $p''$  that is orthogonal to  $q$ . Let  $[y_0]$  be the rotation that fixes  $q$  and maps  $p''$  to  $q'$ . The rotation  $[x_0 y_0]$  maps  $p$  to  $q$  and  $p'$  to  $q'$ . Thus,  $x_0 y_0 \in K_p^q \cap K_{p'}^{q'}$ . Similarly, if  $[z_0]$  is the rotation that fixes  $q$  and maps  $p''$  to  $-q'$ , then  $x_0 z_0 \in K_p^q \cap K_{p'}^{-q'}$ .  $\square$

**Proposition 4.6.** *The great circles  $K_p^q$  and  $K_{-p}^{-q} = K_{-p}^q$  are absolutely orthogonal.*

*Proof.* The simple rotation  $[p, -q] = [-p, q]$  maps  $x \in K_p^q$  to  $-x \in K_{-p}^q$ . That is,  $[p, -q]$  preserves (not pointwise)  $K_p^q$ . Since  $K_{-p}^{-q}$  is the fixed circle of  $[p, -q]$  and the invariant circles of a simple rotation are absolutely orthogonal, we are done.  $\square$

### 4.1.2 Oriented great circles

By Proposition 4.5, the left rotation  $[\exp(-p\theta), 1]$  has the same effect on the circle  $K_p^q$  as the right rotation  $[1, \exp q\theta]$ . This allows us to specify an orientation for  $K_p^q$ . For some starting point  $x \in K_p^q$ , we write

$$K_p^q = \{ (\exp p\theta)x \mid \theta \in \mathbb{R} \} = \{ x \exp q\theta \mid \theta \in \mathbb{R} \}, \quad (9)$$

and both parameterizations traverse the circle in the same sense, for increasing  $\theta$ . We may thus introduce the notation  $\vec{K}_p^q$  to denote an *oriented great circle* on  $S^3$ . If we use  $\vec{K}_{-p}^{-q}$  in (9), the same circle will be traversed in the *opposite sense*. Thus, we obtain a notation for oriented great circles on  $S^3$ , and for this notation, the choice of parameters  $p, q \in S^2$  is unique. Only for an oriented circle, the phrase “rotation by  $\pi/4$ ” or “rotation by  $-\pi/3$ ” has a well-defined meaning, and we can give a more specific version of Proposition 4.5a: The operation  $[\exp p\varphi, \exp q\theta]$  rotates  $\vec{K}_p^q$  by  $\theta - \varphi$ .

In Appendix E, we give a direct geometric view of this orientation, based on the original interpretation of  $K_p^q$  as the set of rotations on  $S^2$  that map  $p$  to  $q$  (Definition 4.1).

Proposition 4.3 extends to oriented circles as follows:

**Proposition 4.7.**  $[l, r]\vec{K}_p^q = \vec{K}_{[l]_p}^{[r]_q}$  and  $*\vec{K}_p^q = \vec{K}_{-p}^{-q}$ .

*Proof.* For  $x \in K_p^q$ ,

$$[l, r](x \exp q\theta) = \bar{l}x(\exp q\theta)r = \bar{l}xr\bar{r}(\exp q\theta)r = (\bar{l}xr) \exp(\bar{r}qr\theta) = y \exp([r]q\theta)$$

with  $y = \bar{l}xr \in [l, r]K_p^q = K_{[l]_p}^{[r]_q}$ . Thus, the orientation that we get on  $[l, r]\vec{K}_p^q$  coincides with the orientation prescribed in (9) for  $\vec{K}_{[l]_p}^{[r]_q}$ . Similarly,

$$*(x \exp q\theta) = (\exp \bar{q}\theta)\bar{x} = \exp(-q\theta)y$$

with  $y = \bar{x} \in *K_p^q = K_q^p = K_{-q}^{-p}$ , and this is the correct orientation for  $\vec{K}_{-q}^{-p}$  in accordance with (9).  $\square$

## 4.2 Hopf bundles

Hopf bundles are families of circles  $K_p^q$  with fixed  $p$  or with fixed  $q$ :

**Definition 4.8.** Let  $q_0 \in S^2$  be a pure unit quaternion. The *left Hopf bundle*  $\mathcal{H}^{q_0}$  is

$$\mathcal{H}^{q_0} := \{ K_q^{q_0} \mid q \in S^2 \},$$

and the *right Hopf bundle*  $\mathcal{H}_{q_0}$  is

$$\mathcal{H}_{q_0} := \{ K_{q_0}^q \mid q \in S^2 \}.$$

The *oriented* left and right Hopf bundles are defined analogously:

$$\vec{\mathcal{H}}^{q_0} := \{ \vec{K}_q^{q_0} \mid q \in S^2 \}$$

$$\vec{\mathcal{H}}_{q_0} := \{ \vec{K}_{q_0}^q \mid q \in S^2 \}$$

The convention for left and right was adopted from Dunbar [16]: According to Corollary 4.4, the circles  $K_q^{q_0}$  of the left Hopf bundle  $\mathcal{H}^{q_0}$  are the *left* cosets of the circle  $K_{q_0}^{q_0}$ .

We can naturally assign a Hopf map to each bundle, such that the circles of a bundle become the fibers of the associated Hopf map:

**Definition 4.9.** Let  $q_0 \in S^2$  be a pure unit quaternion. The *left Hopf map* associated with  $q_0$  is

$$\begin{aligned} h^{q_0} : S^3 &\rightarrow S^2 \\ x &\mapsto [\bar{x}]q_0 = xq_0\bar{x}, \end{aligned}$$

and the *right Hopf map* associated with  $q_0$  is

$$\begin{aligned} h_{q_0} : S^3 &\rightarrow S^2 \\ x &\mapsto [x]q_0 = \bar{x}q_0x. \end{aligned}$$

**Corollary 4.10.** *The following statements are direct consequences of the definitions:*

- *The choice of the parameter  $q_0$  in the left Hopf bundle  $\mathcal{H}^{q_0}$  is unique except that  $\mathcal{H}^{q_0} = \mathcal{H}^{-q_0}$ . As oriented Hopf bundles,  $\vec{\mathcal{H}}^{q_0}$  and  $\vec{\mathcal{H}}^{-q_0}$  contain the same circles in opposite orientation.*

*The same statement holds for right Hopf bundles.*

- *No two different left Hopf bundles share a circle. That is,*

$$\mathcal{H}^{p_0} \cap \mathcal{H}^{p_1} = \emptyset \text{ if } p_0 \neq \pm p_1.$$

*A similar statement holds for right Hopf bundles.*

- *A left Hopf bundle intersects a right Hopf bundle in exactly two circles, which are absolutely orthogonal:*

$$\mathcal{H}_{q_0} \cap \mathcal{H}^{p_0} = \{K_{q_0}^{p_0}, K_{q_0}^{-p_0} = K_{-q_0}^{p_0}\}.$$

- *Every great circle  $K_{q_0}^{p_0}$  in  $S^3$  belongs to a unique left Hopf bundle  $\mathcal{H}^{p_0}$  and to a unique right Hopf bundle  $\mathcal{H}_{q_0}$ .*

From Proposition 4.7, we can directly work out the effect of a transformation on an (oriented) Hopf bundle:

**Proposition 4.11.** (a)  $[l, r]\vec{\mathcal{H}}^q = \vec{\mathcal{H}}^{[r]q}$  and  $[l, r]\vec{\mathcal{H}}_p = \vec{\mathcal{H}}_{[l]p}$ ; (b)  $*\vec{\mathcal{H}}^q = \vec{\mathcal{H}}_{-q}$  and  $*\vec{\mathcal{H}}_p = \vec{\mathcal{H}}^{-p}$ .

We get consequences about the operations that leave a Hopf bundle invariant and about mappings between Hopf bundles.

**Proposition 4.12.** *The following statements about the operations that leave a left Hopf bundle invariant hold, and similar statements hold for right Hopf bundles.*

- (i) *Any left rotation leaves an oriented left Hopf bundle  $\vec{\mathcal{H}}^q$  invariant. It permutes the great circles of the bundle.*
- (ii) *A right rotation  $[1, r]$  leaves the oriented left Hopf bundle  $\vec{\mathcal{H}}^q$  invariant iff  $[r]q = q$ .*
- (iii) *A right rotation  $[1, r]$  maps the oriented left Hopf bundle  $\vec{\mathcal{H}}^q$  to the opposite bundle  $\vec{\mathcal{H}}^{-q}$  iff  $[r]q = -q$ .*
- (iv) *Any two oriented left Hopf bundles are congruent, and can be mapped to each other by a right rotation.*
- (v) *Any oriented right Hopf bundle and any oriented left Hopf bundle are mirrors of each other.* □

We can summarize properties (i)–(iii) in the following statement, which characterizes the transformations that leave a given left Hopf bundle invariant, in analogy to Proposition 4.5.

**Proposition 4.13.**

- (i) *A rotation  $[l, r]$  preserves  $\mathcal{H}^{q_0}$  if and only if  $[r]q_0 = \pm q_0$ .*
- (ii) *More precisely, these rotations come in two families.*

- (a) *The rotations with  $[r]q_0 = q_0$  can be written as  $[l, \exp q_0 \theta]$  for  $\theta \in \mathbb{R}$ , and they map  $\vec{\mathcal{H}}^{q_0}$  to  $\vec{\mathcal{H}}^{q_0}$ , preserving the orientation of the circles.*
- (b) *The rotations with  $[r]q_0 = -q_0$  can be written as  $[l, q' \exp q_0 \theta]$  for  $\theta \in \mathbb{R}$ , where  $q' \in S^2$  is some fixed quaternion orthogonal to  $q_0$ . They map  $\vec{\mathcal{H}}^{q_0}$  to  $\vec{\mathcal{H}}^{-q_0}$ , reversing the orientation of the circles.*

Note that an orientation-reversing transformation sends a left Hopf bundle to a right one, and those two share exactly two circles. Thus, no orientation-reversing transformation can preserve a Hopf bundle.

### 4.2.1 Left and right screws

A generic rotation has two circles that it leaves invariant. The left and right rotations are special: they have infinitely many invariant circles, and as we will see, these circles form a Hopf bundle. In contrast to Proposition 4.13, we now discuss rotations that leave every *individual* circle of a Hopf bundle invariant:

#### Proposition 4.14.

- (i) For the oriented left Hopf bundle  $\vec{\mathcal{H}}^{q_0}$ , the one-parameter subgroup of right rotations  $[1, \exp q_0 \varphi]$  rotates every circle of  $\vec{\mathcal{H}}^{q_0}$  in itself by the same angle  $\varphi$ .
- (ii) Conversely, for a right rotation  $[1, r]$  with  $r \neq 1, -1$ , the set of circles that it leaves invariant forms a left Hopf bundle  $\mathcal{H}^{q_0}$ , and  $[1, r]$  rotates every circle of  $\vec{\mathcal{H}}^{q_0}$  in itself by the same angle  $\varphi$ .

*Proof.* Part (i) is a direct consequence of the definition (9) of oriented circles.

According to Proposition 4.5, the right rotation  $[1, r]$  leaves a circle  $K_p^q$  invariant iff  $[r]q = q$ . (Case (b) of Proposition 4.5, where  $[l]p = -p$ , does not apply since  $l = 1$ .) After writing  $r = \exp q_0 \varphi$  with  $\varphi \neq 0, \pi$ , the condition  $[r]q = q$  translates to  $q = \pm q_0$ , and the circles  $\{K_p^{\pm q_0} \mid p \in S^2\}$  form the Hopf bundle  $\mathcal{H}^{q_0}$ . The last part of the statement repeats (i).  $\square$

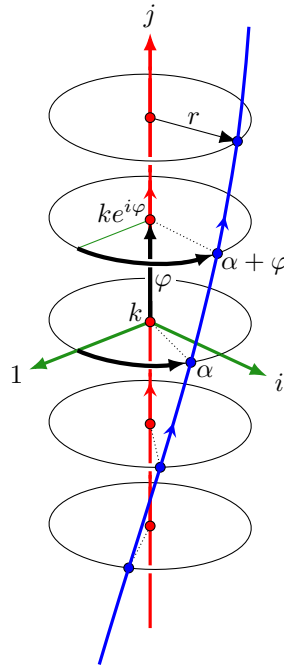


Figure 5: A right screw around the great circle  $K_{-i}^i$  (in red)

Geometrically, these rotations are *screw motions*. If we look at one circle  $K_p^{q_0}$  from the bundle, the adjacent circles form helices that wind around this circle, see Figure 5. The right multiplication by  $\exp q_0 \varphi$  effects a forward motion of  $\varphi$  *along* every circle, and a simultaneous clockwise rotation by the same angle  $\varphi$  *around* the circle, when seen in the direction of the forward movement, and is thus a *right screw*.<sup>9</sup> In contrast to the situation in Euclidean 3-space,

<sup>9</sup>While not everything that is associated to right rotations is “right”, it is a lucky coincidence that at least right rotations perform right screws, and left rotations perform left screws. This view depends on the convention that we have chosen in Section 2.3 for viewing parts of the 3-sphere as three-dimensional space.

Here is a check of this fact at an example: Figure 5 shows the situation around the point  $(x_1, x_2, x_3, x_4) = (0, 0, 0, 1) \equiv k \in K_{-i}^i$ . According to our conventions from Section 2.3, we draw this in 3-space by projecting to the tangent space  $x_4 = 1$ , i.e., omitting the  $x_4$ -coordinate, and drawing  $(x_1, x_2, x_3) \equiv (1, i, j)$  as a right-handed coordinate system. The great circle  $K_{-i}^i$  is invariant under the family of right rotations  $[1, \exp i\varphi]$ , which move the point  $k$  along the circle:

$$\vec{K}_{-i}^i = \{k \exp i\varphi\} = \{k(\cos \varphi + i \sin \varphi)\} = \{k \cos \varphi + j \sin \varphi\}$$

The tangent vector at  $\varphi = 0$  points in the direction  $j \equiv (0, 0, 1, 0)$ .

these screws have no distinguished axis. The blue circle seems to wind around the red circle, but this is an artifact of the projection of this picture. All circles are in fact equivalent, and the situation looks the same for every circle of the bundle.

#### 4.2.2 Clifford-parallel circles

We measure the *distance* between two points  $p, q \in S^3$  as the geodesic distance on the sphere, which equals the angular distance along the great circle through  $p$  and  $q$ :  $\text{dist}(p, q) := \arccos \langle p, q \rangle$ , where  $\langle p, q \rangle$  denotes the scalar product. The distance between two sets  $K, K' \subseteq S^3$  is  $\text{dist}(K, K') = \inf \{ \text{dist}(p, q) \mid p \in K, q \in K' \}$ .

Two great circles  $K$  and  $K'$  in  $S^3$  are called *Clifford-parallel* if  $\text{dist}(x, K')$  does not depend on  $x \in K$ . See for example [3, Section 18.8] for more information on Clifford parallelism.

**Proposition 4.15** ([3, Exercise 18.11.18]). *Great circles in the same Hopf bundle  $\mathcal{H}^q$  are Clifford-parallel, and  $\text{dist}(K_p^q, K_r^q) = \text{dist}(p, r)/2$ .*

*Proof.* By Proposition 4.5a, the right rotations  $[1, \exp q\theta]$  rotate  $x \in K_p^q$  along the circle  $K_p^q$  while keeping  $K_r^q$  invariant as a set. Thus,  $\text{dist}(x, K_r^q)$  is constant as  $x$  moves on  $K_p^q$ , showing that  $K_p^q$  and  $K_r^q$  are Clifford-parallel.

Since  $K_r^q$  is a left coset of  $K_q^q$ , we may assume that  $r = q$  by applying some left rotation to  $K_p^q$  and  $K_r^q$ . That is, it is enough to show that  $\text{dist}(K_p^q, K_q^q) = \text{dist}(p, q)/2$ . Since  $1 \in K_q^q$  and the circles  $K_p^q$  and  $K_q^q$  are Clifford parallel, it is enough to show that  $\text{dist}(K_p^q, 1) = \text{dist}(p, q)/2$ .

The points  $x = \cos \alpha + v \sin \alpha \in K_p^q$  represent the rotations  $[x]$  on  $S^2$  that map  $p$  to  $q$ , and  $\text{dist}(x, 1) = \arccos \cos \alpha = \alpha$ , assuming  $0 \leq \alpha \leq \pi$ . Thus, we are trying to minimize  $\alpha$ , which is half the rotation angle of  $[x]$ . The rotation that minimizes the rotation angle is the one that moves  $p$  to  $q$  along the great circle through  $p$  and  $q$ , and its rotation angle  $2\alpha$  is  $\text{dist}(p, q)$ .  $\square$

We mention that Clifford parallelism arises in two kinds: left and right, accordingly as the circles belong to a common left or right Hopf bundle. Each kind of Clifford parallelism is transitive, but Clifford parallelism in itself is not.

## 5 Classification of the point groups

We make a coarse classification of the groups by their invariant Hopf bundles. The following observation of Dunbar [16, p. 124] characterizes this in terms of the left and right groups.

**Proposition 5.1.** *A 4-dimensional point group leaves some left Hopf bundle invariant if and only if its right group is cyclic or dihedral. A similar statement holds for right Hopf bundles and the left group.*

*Proof.* By Proposition 4.13(i), a transformation  $[l, r] \in \text{SO}(4)$  preserves  $\mathcal{H}^{q_0}$  if and only if  $[r]$  keeps the line through  $q_0$  invariant. The set of such  $r$ 's form an infinite group that is isomorphic to  $\text{O}(2)$ . Its finite subgroups are either cyclic or dihedral.  $\square$

As we have seen, the left and right groups  $L$  and  $R$  are one of the five classes  $2I, 2O, 2T, 2D_{2n}$ , and  $2C_n$ . Besides the infinite families of cyclic groups  $2C_n$  and dihedral groups  $2D_{2n}$ , there are the three polyhedral groups  $2I, 2O, 2T$ . Accordingly, we get a rough classification into three classes of groups.

1. The left subgroup is cyclic or dihedral, and the right subgroup is polyhedral, or vice versa.

These groups leave some left or right Hopf bundle invariant, and they are the *tubical groups*, to be discussed in Section 6.

---

Let us look at a small circle of radius  $r$  around  $K_{-i}^i$ , centered at  $k$ : It lies in a plane parallel to the  $1, i$ -plane and can be written as

$$\frac{1}{\sqrt{1+r^2}}(k + r(\cos \alpha + i \sin \alpha)) = \frac{1}{\sqrt{1+r^2}}(k + r \exp i\alpha).$$

The right rotation  $[1, \exp i\varphi]$  maps this to

$$\frac{1}{\sqrt{1+r^2}}(k + r \exp i\alpha) \exp i\varphi = \frac{1}{\sqrt{1+r^2}}(k \exp i\varphi + r \exp i(\alpha + \varphi))$$

i.e., it increases  $\alpha$  together with  $\varphi$ . As can be seen in Figure 5, this is a right screw.

Du Val [15, § 14, p. 36], for example, considers right quaternion multiplications as left screws, without giving reasons for this choice, and he draws his illustrations accordingly. On the other hand, Coxeter [12, Chapter 6, p. 70] considers right quaternion multiplications as right screws.

2. Both the left and right subgroup are cyclic or dihedral.

These groups leave some both some left and some right Hopf bundle invariant. They form a large family, the *toroidal groups*, to be discussed in Section 7.

3. Both the left and right subgroup are polyhedral.

These groups leave no Hopf bundle invariant. There are finitely many groups of this class: the polyhedral groups and the axial groups.

For all classes except the tubical groups, there is the possibility that  $L = R$ , and hence we also consider the achiral extensions of these groups.

## 5.1 The Clifford torus

The toroidal groups are characterized as leaving both some left Hopf bundle  $\mathcal{H}_p$  and some right Hopf bundle  $\mathcal{H}^q$  invariant. By Corollary 4.10, these two bundles intersect in two orthogonal circles  $K_p^q \cup K_p^{-q}$ , and hence these two circles must also be invariant. We conclude that the set  $\mathbb{T}_p^q$  of points that are equidistant from these two circles is also invariant. We will see that this set is a *Clifford torus*. It has several alternative representations.

$$\begin{aligned} \mathbb{T}_p^q &= \{ x \in S^3 \mid \text{dist}(x, K_p^q) = \text{dist}(x, K_p^{-q}) \} \\ &= \{ x \in S^3 \mid \text{dist}(x, K_p^q) = \frac{\pi}{4} \} \\ &= \{ x \in S^3 \mid \text{dist}(x, K_p^{-q}) = \frac{\pi}{4} \} \\ &= \{ x \in S^3 \mid \text{dist}(x, K_p^q) = \text{dist}(x, K_{-p}^q) \} \end{aligned} \quad (10)$$

Proposition 4.3 tells us how an orthogonal transformation acts on the circle  $K_p^q$  that defines the torus  $\mathbb{T}_p^q$ . As an immediate corollary, we obtain:

**Proposition 5.2.** *Let  $p, q \in S^2$ . Then for any  $l, r \in S^3$ ,*

- (i)  $[l, r]\mathbb{T}_p^q = \mathbb{T}_{[l]p}^{[r]q}$ .
- (ii)  $(*[l, r])\mathbb{T}_p^q = \mathbb{T}_{[l]q}^{[r]p}$ , and as a special case,  $*\mathbb{T}_p^q = \mathbb{T}_q^p$ .

From  $\mathbb{T}_p^q$ , we can recover the two defining circles  $K_p^q \cup K_p^{-q}$  as those points whose distance from  $\mathbb{T}_p^q$  takes the extreme values  $\pi/4$ :

$$K_p^q \cup K_p^{-q} = \{ x \in S^3 \mid \text{dist}(x, \mathbb{T}_p^q) = \frac{\pi}{4} \}$$

Since the choice of parameters  $p, q$  for circles  $K_p^q$  is unique up to simultaneous sign changes, the choice of parameters  $p, q \in S^2$  for the torus  $\mathbb{T}_p^q$  is unique up to independent sign changes:  $\mathbb{T}_p^q = \mathbb{T}_{-p}^{-q} = \mathbb{T}_{-p}^q = \mathbb{T}_p^{-q}$ .

By Proposition 5.2, any two Clifford tori are related by an appropriate orientation-preserving transformation. There are no “left” or “right” Clifford tori. Thus, it is sufficient to study one special torus. In particular,  $\mathbb{T}_i^i$  is the “standard” Clifford torus:

$$\mathbb{T}_i^i = \{ \frac{1}{\sqrt{2}}(\cos \theta, \sin \theta, \cos \varphi, \sin \varphi) \mid 0 \leq \theta, \varphi < 2\pi \} = \{ x \in \mathbb{R}^4 \mid x_1^2 + y_1^2 = x_2^2 + y_2^2 = \frac{1}{2} \} \quad (11)$$

It is a square flat torus, and we name the coordinates  $(x_1, y_1, x_2, y_2)$  to emphasize that it is the Cartesian product of a circle of radius  $\sqrt{1/2}$  in the  $x_1, y_1$ -plane and a circle of radius  $\sqrt{1/2}$  in the  $x_2, y_2$ -plane. For this torus, the two circles of extreme distance are  $K_i^i$  and  $K_i^{-i}$ , the great circles in the  $x_1, y_1$ -plane and in the  $x_2, y_2$ -plane.

In Section 7.11.2, we will see another torus,  $\mathbb{T}_k^i$ , with a different, but equally natural equation (25).

## 6 The tubical groups

In this section we consider the point groups that preserve a left or a right Hopf bundle, but *not both*. By Proposition 5.1, these groups are characterized as the groups for which the left or the right group, but not both, is cyclic or dihedral. These groups will be called *tubical groups*. We

have chosen this name because, as we will see (see for instance Figure 6), for large enough order, the polar orbit polytope consists of intertwined congruent tube-like structures.<sup>10</sup>

Since any two left (resp. right) Hopf bundles are congruent, it is enough to consider the tubical groups that preserve a specific left (resp. right) Hopf bundle. We will call these the *left tubical groups* and the *right tubical groups*. Since left and right Hopf bundles are mirror-congruent, we can restrict our attention to the left tubical groups.

The classic classification leads to 11 classes of left tubical groups. Table 2 lists them with the notation from Conway and Smith [8, Table 4.1] in the first column, together with their generators. In Appendix F, we depict subgroup relations between these groups.

$G \leq \text{SO}(4)$	parameter $n$	generators	order	$G^h \leq \text{O}(3)$
cyclic type				
$\pm[I \times C_n]$	$n \geq 1$	$[i_I, 1], [\omega, 1]; [1, e_n]$	$120n$	$+I$
$\pm[O \times C_n]$	$n \geq 1$	$[i_O, 1], [\omega, 1]; [1, e_n]$	$48n$	$+O$
$\pm\frac{1}{2}[O \times C_{2n}]$	$n \geq 1$	$[i, 1], [\omega, 1]; [1, e_n]; [i_O, e_{2n}]$	$48n$	$+O$
$\pm[T \times C_n]$	$n \geq 1$	$[i, 1], [\omega, 1]; [1, e_n]$	$24n$	$+T$
$\pm\frac{1}{3}[T \times C_{3n}]$	$n \geq 1$	$[i, 1]; [1, e_n]; [\omega, e_{3n}]$	$24n$	$+T$
dihedral type				
$\pm[I \times D_{2n}]$	$n \geq 2$	$[i_I, 1], [\omega, 1]; [1, e_n], [1, j]$	$240n$	$\pm I$
$\pm[O \times D_{2n}]$	$n \geq 2$	$[i_O, 1], [\omega, 1]; [1, e_n], [1, j]$	$96n$	$\pm O$
$\pm\frac{1}{2}[O \times \overline{D}_{4n}]$	$n \geq 2$	$[i, 1], [\omega, 1]; [1, e_n], [1, j]; [i_O, e_{2n}]$	$96n$	$\pm O$
$\pm\frac{1}{2}[O \times D_{2n}]$	$n \geq 2$	$[i, 1], [\omega, 1]; [1, e_n]; [i_O, j]$	$48n$	$TO$
$\pm\frac{1}{6}[O \times D_{6n}]$	$n \geq 1$	$[i, 1]; [1, e_n]; [i_O, j], [\omega, e_{3n}]$	$48n$	$TO$
$\pm[T \times D_{2n}]$	$n \geq 2$	$[i, 1], [\omega, 1]; [1, e_n], [1, j]$	$48n$	$\pm T$

Table 2: Left tubical groups [8, Table 4.1]. See (6) on p. 14 for definitions of the quaternions  $i_I, i_O, \omega, e_n$ .

According to the right group, there are 5 tubical group classes of *cyclic type* and 6 tubical group classes of *dihedral type*. The left Hopf bundle that they leave invariant is  $\mathcal{H}^i$ . This follows from Proposition 4.13(ii) and our choice for the generators of  $2C_n$  and  $2D_{2n}$ . The cyclic-type groups are those tubical groups that moreover preserve the consistent orientation of the circles in  $\mathcal{H}^i$ . That is, they preserve  $\vec{\mathcal{H}}^i$ . Each of these classes is parameterized by a positive integer  $n$ , which is the largest integer  $n$  such that  $[1, e_n]$  is in the group.

In some cases the parameter  $n$  starts from 2 in order to exclude the groups  $D_2$ , which is geometrically the same as  $C_2$ . We also exclude  $\pm\frac{1}{2}[O \times \overline{D}_4]$  because the notation  $\overline{D}_{4n}$  indicates that the normal subgroup  $D_{2n}$  of  $D_{4n}$  is used, and not  $C_{2n}$ . For  $n = 1$ , this distinction disappears, and hence  $\pm\frac{1}{2}[O \times \overline{D}_4]$  is geometrically the same as  $\pm\frac{1}{2}[O \times D_4]$  (see also Appendix G.1). In this case and in all other cases where  $C_2$  and  $D_2$  are exchanged, the respective groups are conjugate under  $[1, \frac{1}{\sqrt{2}}(i + j)]$ , which exchanges  $[1, i]$  with  $[1, j]$ .

**Convention.** For ease of use, we drop the word “left” from “left tubical group” and call it simply “tubical group” in this section. We will denote  $\mathcal{H}^i$  by  $\mathcal{H}$  and call it *the* Hopf bundle. We will also denote  $h^i(x) = xi\bar{x}$  by  $h(x)$  and call it *the* Hopf map.

## 6.1 Orbit circles

An element of a tubical group has one of the following two forms, and Proposition 4.5 describes its action on the circles of  $\mathcal{H}$ :

- $[l, e_m^s]$ , which maps  $\vec{K}_p$  to  $\vec{K}_{[l]p}$ , and
- $[l, je_m^s]$ , which maps  $K_p$  to  $K_{-[l]p}$  with a reversal of orientation. More precisely, this rotation maps  $\vec{K}_p = \vec{K}_p^i$  to  $\vec{K}_{[l]p}^{-i}$ , which is the reverse of  $\vec{K}_{-[l]p}^i = \vec{K}_{-[l]p}$ . These elements occur only in the groups of dihedral type.

Thus, the rotations permute the Hopf circles of  $\mathcal{H}$ . Via the one-to-one correspondence of the Hopf map, they induce mappings on the Hopf sphere  $S^2$ :

<sup>10</sup>There is a notion of *tubular groups*, which is something completely different, see for example [5].

**Proposition 6.1.** *A tubical group  $G$  induces a 3-dimensional point group  $G^h$  via the Hopf map  $h$ . This group  $G^h$  is isomorphic to  $G/\langle[1, e_n]\rangle$ , where  $n$  is the largest integer such that  $[1, e_n] \in G$ .*

*Proof.* The above considerations show that  $[l, e_m^s]$  induces the orientation-preserving transformation  $[l]$  on  $S^2$ , and  $[l, je_m^s]$  induces the orientation-reversing transformation  $-[l]$  on  $S^2$ . We are done since the image of  $G$  in the homomorphism

$$\begin{aligned} G &\rightarrow \mathrm{O}(3) \\ [l, e_m^s] &\mapsto [l] \\ [l, je_m^s] &\mapsto -[l] \end{aligned}$$

is  $G^h$ , and the kernel is  $\langle[1, e_n]\rangle$ .  $\square$

The column “ $G^h \leq \mathrm{O}(3)$ ” in Table 2 lists the induced group for each tubical group  $G$ . Tubical groups of cyclic type induce chiral groups  $G^h$ , and tubical groups of dihedral type induce achiral groups  $G^h$ .

As a consequence, the orbit of some starting point  $v \in S^3$  can be determined as follows:

1. The starting point lies on the circle  $K_{h(v)}$ . The subgroup  $\langle[1, e_n]\rangle$  generates a regular  $2n$ -gon in this circle.
2. For each  $t \in G^h$ , there is a coset of elements that map  $K_{h(v)}$  to the circle  $K_{t(h(v))}$ , and these elements generate a regular  $2n$ -gon in this circle.

**Proposition 6.2.** *Let  $G$  be a tubical group. The orbit of a point  $v \in S^3$  is the union of regular  $2n$ -gons on the circles  $K_{t(h(v))}$  for  $t \in G^h$ .*  $\square$

We call these circles the *orbit circles* of  $G$ .

If the  $G^h$ -orbit of  $h(v)$  is not free, several of these  $2n$ -gons will share the same circle, and they may overlap. The  $2n$ -gons may coincide, or they may form polygons with more vertices. It turns out that they can intersperse to form a regular  $2fn$ -gon or, in the case of dihedral-type groups, the union of two regular  $2fn$ -gons, for some  $1 \leq f \leq 5$ .

The  $G^h$ -orbit of  $h(v)$  is always free when the starting point does not lie on a rotation center or a mirror of  $G^h$ . The following corollary follows directly from the previous proposition.

**Corollary 6.3.** *Let  $G$  be a tubical group and let  $v \in S^3$  be a point. If the  $G^h$ -orbit of  $h(v)$  is free, then the  $G$ -orbit of  $v$  is also free.*  $\square$

For tubical groups of cyclic type, the orbit has the following nice property.

**Proposition 6.4.** *Let  $G$  be a cyclic-type tubical group. The  $G$ -orbit of a point  $v \in S^3$ , up to congruence, depends only on the circle of  $\mathcal{H}$  on which  $v$  lies.*

*Proof.* Rotation of  $v$  along  $K_{h(v)}$  can be performed by a right rotation of the form  $[1, \exp \theta i]$ . Since the right group of  $G$  is cyclic, elements of  $G$  have the form  $[l, e_m^s]$ . These elements commute with right rotations of the form  $[1, \exp \theta i]$ . In particular,

$$\mathrm{orbit}([1, \exp \theta i]v, G) = [1, \exp \theta i]\mathrm{orbit}(v, G). \quad \square$$

## 6.2 Tubes

If  $n$  is large, the orbit fills the orbit circles densely. Figure 6a shows the cells (i.e. facets) of the polar orbit polytope that correspond to orbit points on three orbit circles. Here orbit points form a regular 80-gon on each orbit circle. We clearly see twisted and intertwined tubes, which are characteristic for these groups, and which we have used to assign their names. Figures 6c and 6e show a single cell. It has two large flat faces, where successive cells are stacked on top of each other with a slight twist. On the boundary of the tubes in Figure 6a we can distinguish two different sets of “parallel” curves. One set of curves comes from the boundaries between successive *slices* (cells) of the tubes, and the other set of curves is a trace of the slices of the adjacent tubes. At first sight, it is hard to know which of the two line patterns is which. In Figure 6b, we have cut the tubes open to show where the boundaries between the slices are, revealing also the three orbit circles.

If we let  $n$  grow to infinity, the tubes become smooth, see Figure 6d. We explore the limiting shape of these tubes in Section 6.3. We will see that the tubes are either 3-sided, 4-sided, or



5-sided, and their shape as well as their structure, how they share common boundaries and how they meet around edges, can be understood in terms of the spherical Voronoi diagram on the Hopf sphere  $S^2$ . Figure 6f shows this Voronoi diagram for our example.

We will show some more examples of cells below (Figures 12 and 13) and in Appendix B. In general, the cell of a polar orbit polytope of a tubical group for large enough  $n$  will always exhibit the following characteristic features.

- It is a thin slice with a roughly polygonal shape.
- The top and bottom faces are parallel.
- Moreover, the top and bottom faces are congruent and slightly twisted with a right screw. (There are, however exceptions for tubical groups of dihedral type: With some choices of starting points, there is an alternative way of stacking the slices: every other slice is upside down, as in Figure 9.)
- The top and bottom faces approach the shape of a triangle, quadrilateral or pentagon with curved sides.
- The sides are decorated with slanted patterns, which come from the boundaries of the adjacent tubes.
- The tube twists around the orbit circle by one full  $360^\circ$  turn as it closes up on itself.

If  $n$  is small, these properties break down: The circles are not filled densely enough to ensure that the cells are thin slices. Sometimes they are regular or Archimedean polytopes, and the orbit polytopes coincide with those of polyhedral groups, and the “tubes” may even be disconnected, see for example Figures 36 or 44 in Appendix B. See Section 6.12 for more examples.

Figure 6 shows a case where the  $2n$ -gons lie on different circles. Then the orbit is free: for any two cells, there is a unique transformation in the group that moves one cell to the other. If the starting point is generic enough, the cells have no symmetries. (See Proposition 6.10 below for a precise statement.) Then the given group is the symmetry group of its orbit polytope: There is a unique transformation mapping one cell to the other even among *all* orthogonal transformations, not just the group elements.

### 6.2.1 Mapping between adjacent cells

**Definition 6.5.** The *cell axis* of a cell of the polar orbit polytope is the orthogonal projection of the orbit circle into the 3-dimensional hyperplane of the cell.

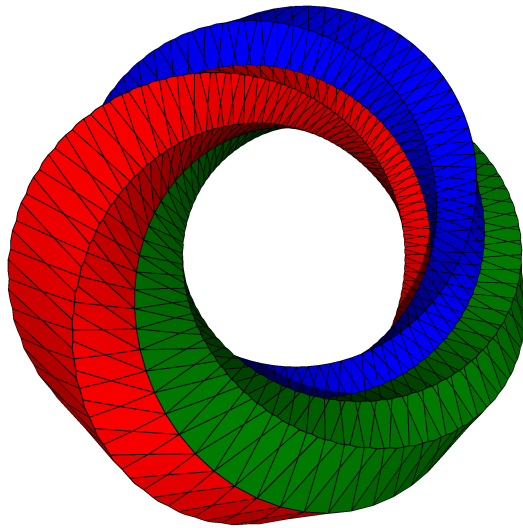
The cell axis thus gives the direction in which consecutive cells are stacked upon each other along the orbit circle. It is a line going through the orbit point. Figure 6c shows a cell together with its axis. The cell axis is not necessarily a symmetry axis. The cell axis intersects the boundary of the cell in two *poles*.

This is where consecutive cells are attached to each other (unless  $n$  is too small and the tubes are disconnected.) More precisely: For the orbit polytope of a generic starting point, the next cell is attached as follows. We translate the cell  $C$  from the bottom pole to the top pole. Call the new cell  $C'$ . We rotate  $C'$  slightly until its bottom face matches the top face of  $C$ , and we attach it there (with a bend into the fourth dimension, as for every polytope).

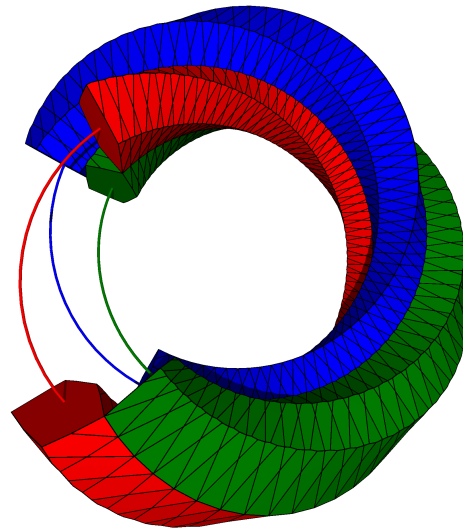
## 6.3 The geometry of the tubes

We investigate the structure of the tubes in the limiting case as  $n \rightarrow \infty$ , where they become smooth objects. As  $n$  gets larger, the orbit circle is filled more and more densely, and the slices get thinner. In the limit, every slice becomes a flat plane convex region, which we call a *tangential slice*. The tangential slices around an orbit circle sweep out the *tangential tube* as  $v$  moves around the circle. The limit of the polar orbit polytope consists of tangential tubes, and this is what is shown in Figure 6d. The central projections of these tubes and slices to the sphere are the *spherical tubes* and the *spherical slices* of these tubes. The spherical tubes are the Voronoi diagram on  $S^3$  of the orbit circles.

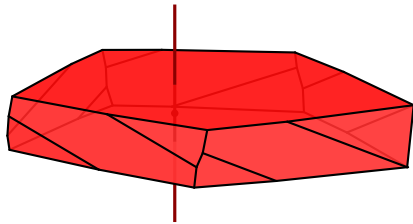
This gives us a way to generalize these notations to any finite set of circles from a common Hopf bundle. For that we first need the definition of the spherical Voronoi diagram. Let  $\mathcal{X}$  be a



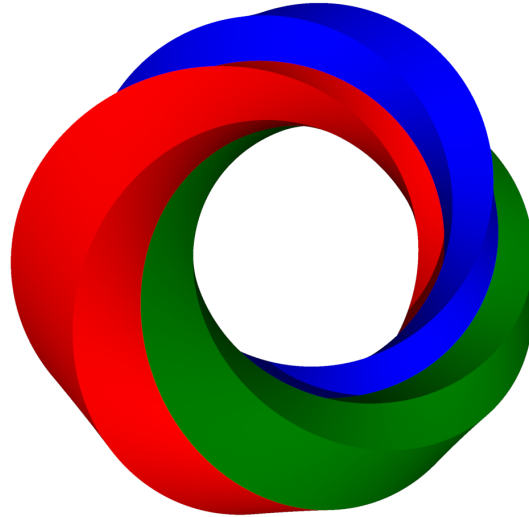
(a) Three tubes



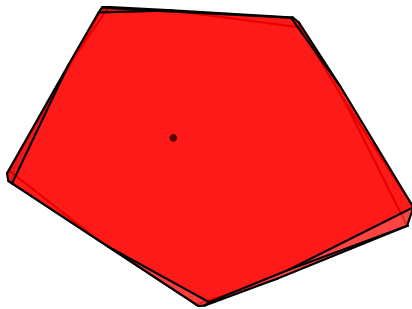
(b) Three partial tubes



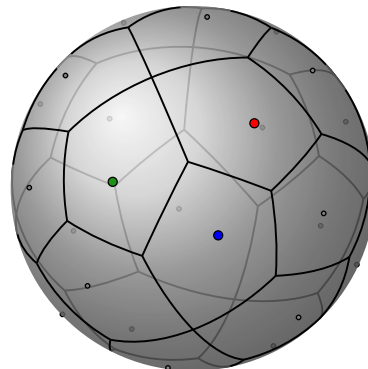
(c) A single cell



(d) Three smooth tubes



(e) Top view of a cell in orthogonal projection



(f) Voronoi diagram on the Hopf sphere

Figure 6: (a) Three tubes (out of twenty-four) of the polar  $\pm[O \times C_n]$ -orbit polytope for a generic starting point  $v$  and  $n = 40$ . Each tube consists of 80 cells (slices). The tubes are shown in a central projection. (b) Some of the cells are removed to make the slices visible. We also show the corresponding orbit circles. (c) A single cell (with its cell axis) from those tubes, in a perspective view from the side, and (e) a top view in orthogonal projection. (f) The spherical Voronoi diagram of the  $+O$ -orbit of  $h(v)$ . The colored points correspond to the tubes of the same color. (d) The tubes as  $n$  goes to infinity.

finite collection of nonempty subsets of  $S^d$ , and let  $X \in \mathcal{X}$  be one of these subsets. The *spherical Voronoi cell* of  $X$  with respect to  $\mathcal{X}$  is

$$\text{Vor}_{\mathcal{X}}(X) := \{x \in S^d \mid \text{dist}(x, X) \leq \text{dist}(x, Y) \text{ for all } Y \in \mathcal{X}\}.$$

The spherical Voronoi cells of the subsets in  $\mathcal{X}$  give a decomposition of  $S^d$ , denoted by  $\text{Vor}_{\mathcal{X}}$  and called the *spherical Voronoi diagram*. If the subsets in  $\mathcal{X}$  are singletons, we get the usual spherical Voronoi diagram.

Let  $\mathcal{C}$  be a finite set of at least two circles from a common Hopf bundle, and let  $K \in \mathcal{C}$  be one of them. We can assume that the common Hopf bundle is  $\mathcal{H}$ . The Voronoi cell of  $K$  with respect to  $\mathcal{C}$  is called a *spherical tube*. The intersection of  $\text{Vor}_{\mathcal{C}}(K)$  with the hyperplane perpendicular to  $K$  at a point  $v \in K$  gives two (2-dimensional) patches. One contains  $v$  and one contains  $-v$ . These are *spherical slices*. The *tangential slices* and *tangential tubes* are defined as above in the special case of orbit circles.

We will show that the spherical tubes are bounded by patches of Clifford tori (Theorem 6.7), and the tangential slices are polygons of circular arcs (Theorem 6.8).

### 6.3.1 The spherical tubes

Given that the circles belong to a common Hopf bundle and the Hopf map transforms distances appropriately (Proposition 4.15), it is no surprise that the Voronoi diagram of the set of *circles* on  $S^3$  is closely related to the Voronoi diagram of the corresponding *points* on  $S^2$  (see Figure 6f.)

**Proposition 6.6.** *Let  $\mathcal{C} \subset \mathcal{H}$  be a finite set of circles from  $\mathcal{H}$ , and let  $K \in \mathcal{C}$  be one of them. The spherical tube  $\text{Vor}_{\mathcal{C}}(K)$  is the union of circles from  $\mathcal{H}$  that are the preimages under  $h$  of the points in  $\text{Vor}_{h(\mathcal{C})}(h(K))$ , where  $h(\mathcal{C}) := \{h(C) \mid C \in \mathcal{C}\}$ .*

*Proof.* First we will show that for any point  $x' \in \text{Vor}_{\mathcal{C}}(K)$ , the great circle  $K'$  from  $\mathcal{H}$  on which  $x'$  lies is also in  $\text{Vor}_{\mathcal{C}}(K)$ . Since all the circles in  $\mathcal{H}$  are Clifford-parallel (Proposition 4.15),  $\text{dist}(K', C) = \text{dist}(x', C)$  for all  $C \in \mathcal{C}$ . Thus, we get the following equivalence.

$$\text{dist}(x', K) \leq \text{dist}(x', C) \iff \text{dist}(K', K) \leq \text{dist}(K', C),$$

for all  $C \in \mathcal{C}$ . That is,  $K' \subset \text{Vor}_{\mathcal{C}}(K)$ . By Proposition 4.15 we know that

$$\text{dist}(K', K) \leq \text{dist}(K', C) \iff \text{dist}(h(K'), h(K)) \leq \text{dist}(h(K'), h(C)),$$

for all  $C \in \mathcal{C}$ . That is,  $K' \in \text{Vor}_{\mathcal{C}}(K)$  if and only if  $h(K') \in \text{Vor}_{h(\mathcal{C})}(h(K))$ . □

### 6.3.2 The spherical tube boundaries

**Theorem 6.7.** *Let  $\mathcal{C} \subset \mathcal{H}$  be a finite set of circles from  $\mathcal{H}$ . The boundaries of the corresponding spherical tubes consist of patches of Clifford tori. The edges of these tubes are great circles from  $\mathcal{H}$ .*

*Proof.* As in Proposition 6.6, the boundary between two tubes is the preimage, under the Hopf map  $h$ , of the boundary between the two corresponding Voronoi regions in  $\text{Vor}_{h(\mathcal{C})}$ . Such a boundary edge on the Hopf sphere  $S^2$  is contained in a great circle. A great circle can be described as the points that are equidistant from two antipodal points  $\pm p$  on  $S^2$ , and under the inverse Hopf map, these become the points on  $S^3$  that are equidistant from two absolutely orthogonal circles  $K_p$  and  $K_{-p}$ , and this is, by definition, a Clifford torus.

The tube edges, where three or more tubes meet, are the preimages of the Voronoi vertices of  $\text{Vor}_{h(\mathcal{C})}$ . Thus, they are circles from  $\mathcal{H}$ . □

### 6.3.3 The tangential slices

**Theorem 6.8.** *Let  $\mathcal{C} \subset \mathcal{H}$  be a finite set of circles from  $\mathcal{H}$ . The corresponding tangential slices are (flat) convex regions bounded by circular arcs.*

*Proof.* Let  $K \in \mathcal{C}$  be one of the circles. We want to consider the tangential slice of  $K$  at a point  $v \in K$ . Without loss of generality, we may assume that  $v = i$ , because the left rotation  $[-vi, 1]$  preserves  $\mathcal{H}$  (see Proposition 4.12(i)) and maps  $v$  to  $i$ . Then  $K$  is actually  $K_i$ , the great circle through the points 1 and  $i$ .

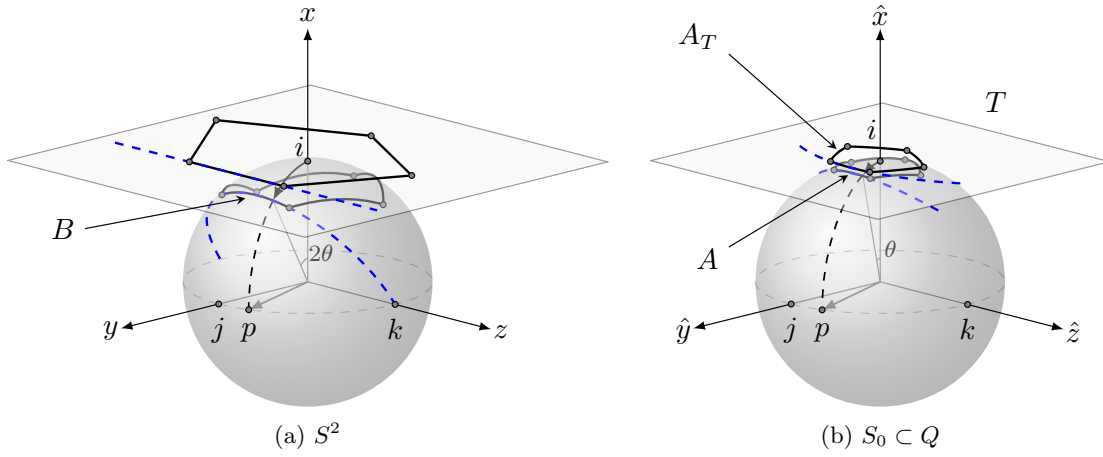


Figure 7: The procedure to get the tangential slice  $A_T$ . (a) The spherical pentagon  $B$  is the Voronoi cell of the point  $i = h(K_i)$  with respect to  $h(\mathcal{C})$ . The pentagon in the plane passing through  $i$  is the central projection of  $B$  onto that plane. (b) The spherical pentagon  $A$  is the spherical slice at  $i$ , which we get from a radial contraction of  $B$ . The circular-arc pentagon  $A_T$  in the tangent plane  $T$  passing through  $i$  is the corresponding tangential slice, which we get from a central projection of  $A$  to  $T$ . This example is constructed from the orbit circles of Figure 6.

The tangent direction of  $K$  at  $v$  is the quaternion 1. The hyperplane  $Q$  perpendicular to  $K$  at  $v$  is spanned by  $i, j$  and  $k$ , which we represent in a 3-dimensional coordinate system  $\hat{x}, \hat{y}, \hat{z}$ , see Figure 7b.  $Q$  intersects  $S^3$  in a great 2-sphere  $S_0$ . The spherical tube  $\text{Vor}_{\mathcal{C}}(K)$  cuts out two opposite patches from  $S_0$ : the spherical slices. Denote by  $A$  the slice that contains  $v$ . The slice  $A$  intersects each circle of  $\text{Vor}_{\mathcal{C}}(K)$ . Thus, by Proposition 6.6,  $h(A)$  equals  $\text{Vor}_{h(\mathcal{C})}(h(v))$ , which we will denote by  $B$ .

Using spherical coordinates, a point in  $S_0$  has the form  $i \cos \theta + p \sin \theta$ , where the direction vector  $p$  is a unit vector in the  $\hat{y}, \hat{z}$ -plane that plays the role of the longitude, and  $\theta \in \mathbb{R}$  is the angular distance on  $S_0$  between that point and  $i$ . See Figure 7. Since  $p$  and  $i$  are pure unit quaternions, they anticommute, and in particular,  $pip = -ipp = i$ . We will now apply the Hopf map  $h$  to a point in  $S_0$ :

$$\begin{aligned} h(i \cos \theta + p \sin \theta) &= (i \cos \theta + p \sin \theta) i (-i \cos \theta - p \sin \theta) \\ &= i \cos^2 \theta - pip \sin^2 \theta + p \cos \theta \sin \theta + p \cos \theta \sin \theta \\ &= i(\cos^2 \theta - \sin^2 \theta) + 2p \cos \theta \sin \theta \\ &= i \cos 2\theta + p \sin 2\theta. \end{aligned}$$

That is,  $h$  maps a point whose angular distance from  $i$  is  $\theta$  to the point in the same direction but with angular distance  $2\theta$ . Thus, if we identify  $S_0$  with  $S^2$  using the natural identification (on  $S^2$ , we denote the  $i, j$  and  $k$  directions by  $x, y$  and  $z$ , respectively), we see that  $A$  is obtained from  $B$  by a *radial contraction*. That is, we look from  $i$  in all directions and multiply the angular distance between  $i$  and each point in  $B$  by  $1/2$ .

The intersection of  $Q$  with the (3-dimensional) tangent space of  $S^3$  at  $v$  is the 2-dimensional tangent plane  $T$  of  $S_0$  at  $v$ . For our choice  $v = i$ ,  $T$  is the plane in  $Q$  defined by  $\hat{x} = 1$ . The tangential slice lies in this plane.

So to get the tangential slice  $A_T$  at  $v$ , we radially contract  $B$  to get  $A$ , and then centrally project  $A$  to  $T$ . We will describe this procedure algebraically. The radial contraction towards  $i$  is the map

$$i \cos \theta + p \sin \theta \mapsto i \cos \frac{\theta}{2} + p \sin \frac{\theta}{2}.$$

This map is not uniquely determined at the South Pole ( $\theta = \pi$ ), and we will tacitly exclude this point from further consideration. Writing  $p$  as  $j \cos \varphi + k \sin \varphi$ , the map can be described as follows:

$$\begin{pmatrix} x \\ y \\ z \end{pmatrix} = \begin{pmatrix} \cos \theta \\ \cos \varphi \sin \theta \\ \sin \varphi \sin \theta \end{pmatrix} \mapsto \begin{pmatrix} \hat{x} \\ \hat{y} \\ \hat{z} \end{pmatrix} = \begin{pmatrix} \cos \frac{\theta}{2} \\ \cos \varphi \sin \frac{\theta}{2} \\ \sin \varphi \sin \frac{\theta}{2} \end{pmatrix}$$

Using the identities  $\cos \frac{\theta}{2} = \frac{\sqrt{1+\cos \theta}}{\sqrt{2}}$  and  $\sin \theta = 2 \sin \frac{\theta}{2} \cos \frac{\theta}{2}$ , the map is written as follows.

$$(x, y, z) \mapsto (\hat{x}, \hat{y}, \hat{z}) = \frac{1}{\sqrt{2}} \left( \sqrt{1+x}, \frac{y}{\sqrt{1+x}}, \frac{z}{\sqrt{1+x}} \right)$$

Combining this with the central projection from the origin onto  $T$  gives the following map  $f$ .

$$f: (x, y, z) \mapsto (\hat{x}, \hat{y}, \hat{z}) = \left( 1, \frac{y}{1+x}, \frac{z}{1+x} \right) = \left( 1, \frac{y/x}{1+1/x}, \frac{z/x}{1+1/x} \right)$$

If we apply  $f$  to a boundary edge of  $B$ , it will turn out the resulting curve is part of a circle. The boundary edges of  $B$  are arcs of great circles on  $S^2$ . We obtain such an arc by centrally projecting to  $S^2$  a straight segment in the tangent plane of  $S^2$  at  $h(v) = i$ . Without loss of generality suppose that one of these segments lies on the line  $(x, y, z) = (1, c_0, t)$ ,  $t \in \mathbb{R}$ , for some constant  $c_0 \neq 0$ , see the blue line in Figure 7a. The central projection of this line to  $S^2$  lies on the great circle

$$\left\{ \frac{\pm 1}{\sqrt{c_0^2 + t^2 + 1}} (1, c_0, t) \mid t \in \mathbb{R} \right\}.$$

See the blue curve in Figure 7a. The map  $f$  transforms this great circle into the set

$$\left\{ \left( 1, \frac{c_0}{1 \pm \sqrt{c_0^2 + t^2 + 1}}, \frac{t}{1 \pm \sqrt{c_0^2 + t^2 + 1}} \right) \mid t \in \mathbb{R} \right\}. \quad (12)$$

See the blue curve in the tangent plane in Figure 7b. Straightforward manipulations show that this set is a circle:

$$\begin{aligned} \hat{y} = \frac{c_0}{1 \pm \sqrt{c_0^2 + t^2 + 1}} &\iff \pm \hat{y} \sqrt{c_0^2 + t^2 + 1} = c_0 - \hat{y} \\ &\iff \hat{y}^2 c_0^2 + \hat{y}^2 t^2 + \hat{y}^2 = \hat{y}^2 - 2c_0 \hat{y} + \hat{y}_0^2 \iff \hat{y}^2 c_0^2 + \hat{y}^2 t^2 + 2c_0 \hat{y} = c_0^2 \end{aligned}$$

Dividing both sides by  $c_0^2$  and then substituting the relation  $\frac{\hat{z}}{\hat{y}} = \frac{t}{c_0}$ , which follows from (12), gives

$$\hat{y}^2 + \hat{z}^2 + \frac{2}{c_0} \hat{y} = 1 \iff \left( \hat{y} + \frac{1}{c_0} \right)^2 + \hat{z}^2 = \frac{c_0^2 + 1}{c_0^2}, \quad (13)$$

which is the equation of a circle. □

The circle defined in (13) belongs to the pencil of circles through the points  $(\hat{x}, \hat{y}, \hat{z}) = (1, 0, \pm 1)$ , because these points fulfill the equations (13). The center  $(\hat{x}, \hat{y}, \hat{z}) = (1, -\frac{1}{c_0}, 0)$  lies on the axis  $(\hat{x}, \hat{y}, \hat{z}) = \lambda(c_0, -1, 0)$  perpendicular to the plane  $c_0 x = y$  containing the great circle and the line that started the construction.

If the set of great circles  $\mathcal{C}$  in the previous theorem are the orbit circles of a tubical group  $G$ , then the spherical Voronoi cell  $B$  on  $S^2$  can have 3, 4 or 5 sides, because the cells form a tiling of the sphere with equal cells. Thus, the spherical slice is also 3, 4 or 5 sided. In particular, we get the following corollary.

**Corollary 6.9.** *The tangential slice of an orbit of a tubical group is a convex plane region whose boundary consists of 3, 4, or 5 circular arcs.*

### 6.3.4 The tangential tube boundaries

The boundary surfaces of the tangential tubes (shown in Figure 6d) carry some interesting structures, but we don't know what these surfaces are.

The points on such a surface are equidistant from two circles  $K$  and  $K'$ , and we denote the surface by  $B(K, K')$ . We know from Theorem 6.7 that its central projection to the sphere is a Clifford torus  $\mathbb{T}$ , whose image  $h(\mathbb{T})$  is the bisector between  $h(K)$  and  $h(K')$  on  $S^2$ . According to the relation between Voronoi diagrams and polar orbit polytopes (as briefly discussed in Section 2.1.2), a circle  $K \in \mathcal{H}$  that belongs to  $\mathbb{T}$  is expanded by some factor, depending on the distance to  $K$  and  $K'$ , to become a circle on  $B(K, K')$ . Thus, the surface  $B(K, K')$  is fibered by circles (of different radii) around the origin.

Another fibration by circles, this time of equal radii, can be obtained by taking the circular arc that forms the boundary of the tangential slice towards  $K'$ , and sweeping it along the circle  $K$ .

In Figure 7b, the circle  $K$  proceeds from the point  $i$  into the fourth dimension, and the circular boundary arc must simultaneously wind around  $K$  as it moves along  $K$ . A third fibration, by circles of the same radius, is obtained in an analogous way from  $K'$ . Each of these fibrations leads to a straightforward parametric description of  $B(K, K')$ .

Alternatively, an implicit description  $B(K, K')$  by two equations can be obtained as the intersection of two “tangential hypercylinders” in which the two tangential tubes of  $K$  and  $K'$  lie. (If the circle  $K$  is described by the system  $x_1^2 + x_2^2 = 1$ ,  $x_3 = x_4 = 0$  in an appropriate coordinate system, its tangential hypercylinder is obtained by omitting the equations  $x_3 = x_4 = 0$ .)

## 6.4 Generic starting points

We return to the analysis of the polar orbit polytope, and start with the easy generic case.

**Proposition 6.10.** *Let  $G$  be a tubical group whose right group is  $C_n$  or  $D_n$  for  $n \geq 6$ . Let  $v \in S^3$  be a point. If the  $G^h$ -orbit of  $h(v)$  has no symmetries other than  $G^h$ , then the same holds for the  $G$ -orbit of  $v$ : the symmetry group of this orbit is  $G$ .*

*Proof.* Since no  $C_n$  or  $D_n$  for  $n \geq 6$  is contained in a polyhedral group, the only groups containing  $G$  are tubical. In particular, the symmetry group  $H$  of the  $G$ -orbit of  $v$  is tubical. Since the symmetry group of the  $G^h$ -orbit of  $h(v)$  is  $G^h$  by assumption, the point  $h(v)$  does not lie on any rotation center or a mirror of a supergroup of  $G^h$ . In particular, the  $H^h$ -orbit of  $h(v)$  is free. Thus, by Corollary 6.3, the  $H$ -orbit of  $v$  is free. So  $G$  and  $H$  have the same order. Since  $G \leq H$ , we get  $G = H$ .  $\square$

According to our goal of obtaining a geometric understanding through the orbit polytope, as described in Figure 2 in Section 2, we are done, in principle. Since the cell has no nontrivial symmetries, *all* symmetries of a cell are in  $G$ . We are in the branch of Figure 2 that requires no further action. Every cell can be mapped to every other cell in a unique way.

In particular, for two consecutive cells on a tube it is obvious what the transformation between them is: a small translation along the orbit circle combined with a slight twist around the orbit circle, or in other words, a right screw, effected by the right rotation  $[1, e_n]$ .

Between cells on different tubes, the transformation is not so obvious. For example, in Figure 6c, we see a vertical zigzag of three short edges between the front corner of the upper (roughly pentagonal) face and the corresponding corner of the lower face. These edges are part of a longer sequence of edges, where 3 tubes meet, and which closes in a circular way. How are the cells arranged around this “axis”, and how does the group map between them? To investigate this question, it is helpful to move the starting point closer to the axis to look what happens there. In particular, this will help us to distinguish different classes of groups  $G$  with the same group  $G^h$ . We will see an example in Section 6.14. Eventually, we will also consider starting points *on* the axis.

## 6.5 Starting point close to a mirror

Let  $G$  be a dihedral-type tubical group, and  $p \in S^2$  be a point close to the mirror of a reflection of  $G^h$ . Moreover, assume that  $p$  does not lie on any rotation center of  $G^h$ . The point  $p$  has a *neighboring partner*  $p'$ , which is obtained from  $p$  by reflecting it across that mirror. We call the corresponding circles  $K_p$  and  $K_{p'}$  *neighboring circles*. The red point and the blue point in Figure 8a form a neighboring pair for the group  $\pm T$ .

We will now discuss the  $G$ -orbit under different choices for the starting point  $v$  on  $K_p$ .

**Case 1.** Choose  $v \in K_p$  such that for each orbit point, the closest point on the neighboring circle is also in the orbit. See Figure 8c. Thus, in the polar  $G$ -orbit polytope, each cell has a “big” face that directly faces the closest point on the neighboring circle.

**Case 2.** If we move  $v$  in one direction, the orbit points on the neighboring circle move in the opposite direction. We choose  $v$  such that the orbit points on neighboring circles are in “alternating positions”. That is, the distance between orbit points on neighboring circles is maximized. See Figure 8d. Thus, in every cell of the polar  $G$ -orbit polytope, the side that is close to the neighboring circle is divided into two faces, on each a cell of the neighboring tube is stacked.

**Case 3.** Figure 8e shows an intermediate situation.

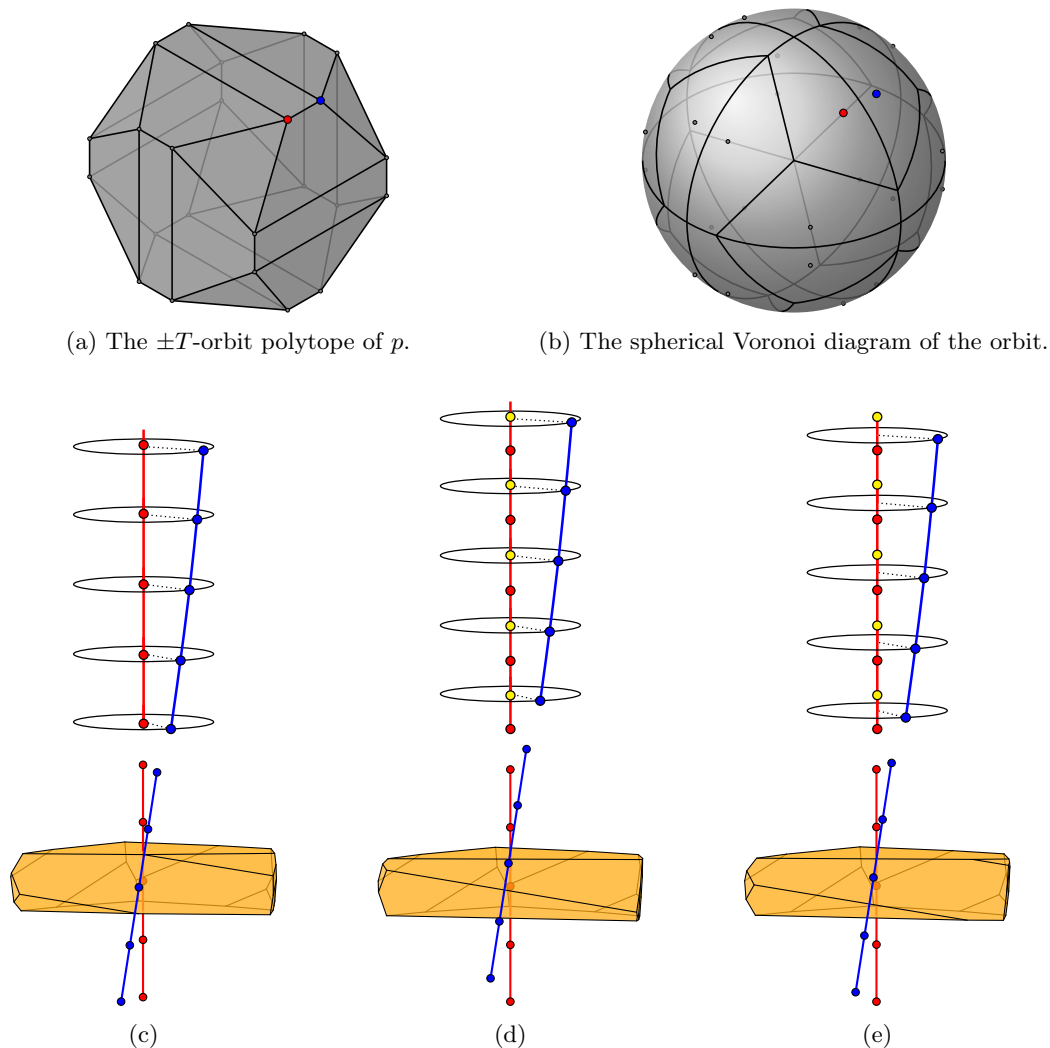


Figure 8: Orbits of the group  $G = \pm[T \times D_{20}]$  for a starting point  $v$  whose image  $p := h(v)$  lies near a mirror of  $G^h = \pm T$ . The top row shows the three-dimensional  $\pm T$ -orbit polytope of  $p$  and the corresponding spherical Voronoi diagram. The red and the blue points form a neighboring pair. The next row shows different possible configurations for orbit points on the corresponding neighboring circles. Red points and blue points are orbit points on the two neighboring circles. Yellow points are midpoints of orbit points on the red circle. They are not orbit points. The third row shows a cell of the corresponding polar orbit polytope.

## 6.6 Starting point on a mirror

It is also interesting to see what happens if we move  $p$  to lie on that mirror of  $G^h$ . We still assume that  $p$  does not lie on any rotation center of  $G^h$ . In this case, the neighboring pairs on  $S^2$  coincide, and thus the corresponding neighboring circles also coincide. We describe next what happens in each of the previous cases.

**Case 1.** The orbit points coincide in pairs, and thus they form a regular  $2n$ -gon on  $K_p$ . Each orbit point can be mapped to any other orbit point by two different elements of  $G$ , one of which rotates  $K_p$  and one of which reverses the orientation of  $K_p$ . Thus, in the polar orbit polytope, each cell has a half-turn symmetry that flips the direction of the cell axis, and exchanges the top and bottom faces. We call it a *flip symmetry*. (For small  $n$ , top and bottom faces might not be defined.)

It is interesting to notice that for this choice of the starting point, the  $G$ -orbit of  $v$  coincides with the orbit of  $v$  under the cyclic-type index-2 subgroup  $G_C$  of  $G$ . Since the  $G_C$ -orbit is the same up to congruence for any starting point on  $K_p$  (Proposition 6.4), the  $G_C$ -orbit of *any* starting point on  $K_p$  has the extra symmetries coming from a dihedral-type group that is geometrically equal to  $G$ . (This geometrically equal group

D1153  
 D1154  
 D1155

has the generators of  $G$  with  $j$  replaced by a different unit quaternion  $q'$  orthogonal to  $i$ , which is the quaternion  $q'$  from Proposition 4.5(b). We put this in a proposition since we will need it later.

D1156  
 D1157  
 D1158  
 D1159

**Proposition 6.11.** *Let  $G_C$  be a cyclic-type tubical group, and let  $G_D$  be a dihedral-type tubical group containing  $G_C$  as an index-2 subgroup. If  $p$  lies on a mirror of  $G_D^h$ , then the  $G_C$ -orbit of any point on  $K_p$  has the symmetries from (a geometrically equal copy of)  $G_D$ .*

D1160  
 D1161  
 D1162  
 D1163  
 D1164

**Case 2.** Orbit points on  $K_p$  form a regular  $4n$ -gon. Each orbit point can be mapped to any other orbit point by a unique element of  $G$ . However, this orbit has extra symmetries, which come from the supergroup of  $G$  that we obtain by extending  $G$  by the new symmetry  $[1, e_{2n}]$ . This orbit of the supergroup follows the behavior described in Case 1. Accordingly, each cell of the polar  $G$ -orbit polytope has a flip symmetry.

D1165  
 D1166  
 D1167

In almost all choices for  $G$ , the supergroup has the same class as  $G$  but with twice the parameter  $n$ . The only exceptional case is  $G = \pm \frac{1}{2}[O \times \overline{D}_{4n}]$ . In this case, the supergroup is  $\pm[O \times D_{4n}]$ .

D1168  
 D1169  
 D1170  
 D1171

**Case 3.** Orbit points on  $K_p$  form two regular  $2n$ -gons whose union is a  $4n$ -gon with equal angles, and side lengths alternating between two values. The orbit points come in close pairs. Accordingly, the cells of the polar orbit polytope come in a sequence of alternating “up-and-down pancakes” stacked upon each other. See the two cells in Figure 9.

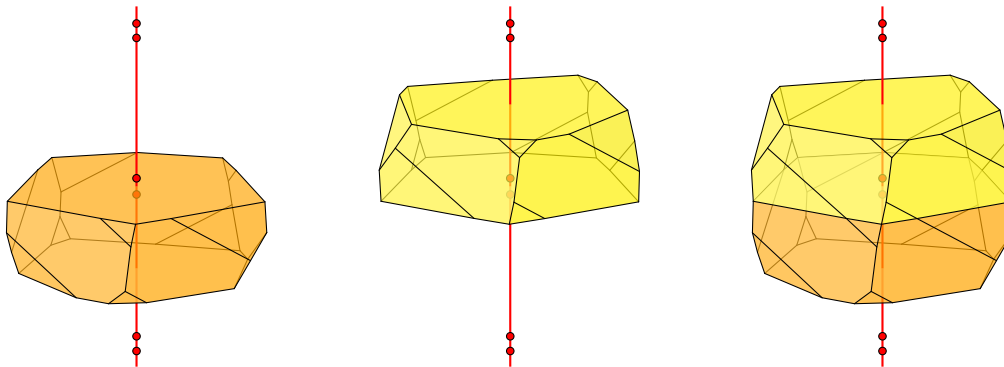


Figure 9: Two cells stacked upon each other with a  $180^\circ$  rotation. The two left figures show each cell individually.

D1172

## 6.7 Starting point close to a rotation center

D1173  
 D1174

Let  $G$  be a cyclic-type tubical group, and let  $p$  be an  $f$ -fold rotation center<sup>11</sup> of  $G^h$ . Let  $[g] \in G^h$  be the clockwise rotation of  $G^h$  around  $p$  by  $\frac{2\pi}{f}$ . That is,  $g = \cos \frac{\pi}{f} + p \sin \frac{\pi}{f}$ .

Choose a point  $p_1 \in S^2$  close to  $p$ . Since  $p_1$  avoids rotation centers of  $G^h$ , its images under  $[g]$  are all distinct:

$$p_1, p_2 := [g]p_1, \dots, p_f := [g]^{f-1}p_1$$

D1175  
 D1176

Figure 10a and Figure 11a show these points around a 4-fold rotation center and a 5-fold rotation center, respectively.

D1177  
 D1178  
 D1179

We want to describe the  $G$ -orbit for a starting point on  $K_{p_1}$ . By Proposition 6.4, any point on  $K_{p_1}$  will give the same  $G$ -orbit, up to congruence. Thus, let  $v \in K_{p_1}$  be any point on  $K_{p_1}$  and consider its  $G$ -orbit.

D1180  
 D1181

We will now discuss the  $G$ -orbit of  $v$  under different assumptions on the subgroup  $H$  of elements of  $G$  that preserve  $K_p$ .

D1182  
 D1183

**Case 1.**  $H$  contains a simple rotation fixing  $K_p$  of order  $f$ : Orbit points around  $K_p$  can be grouped into regular  $f$ -gons (if  $f \geq 3$ ) or pairs (if  $f = 2$ ). See Figure 10c and Figure 11c.

<sup>11</sup>We call  $p$  an  $f$ -fold rotation center of some 3-dimensional point group if  $f$  is the largest order of a rotation around  $p$  in that group. Hence, a 4-fold rotation center of a group is *not* a 2-fold rotation center of that group.



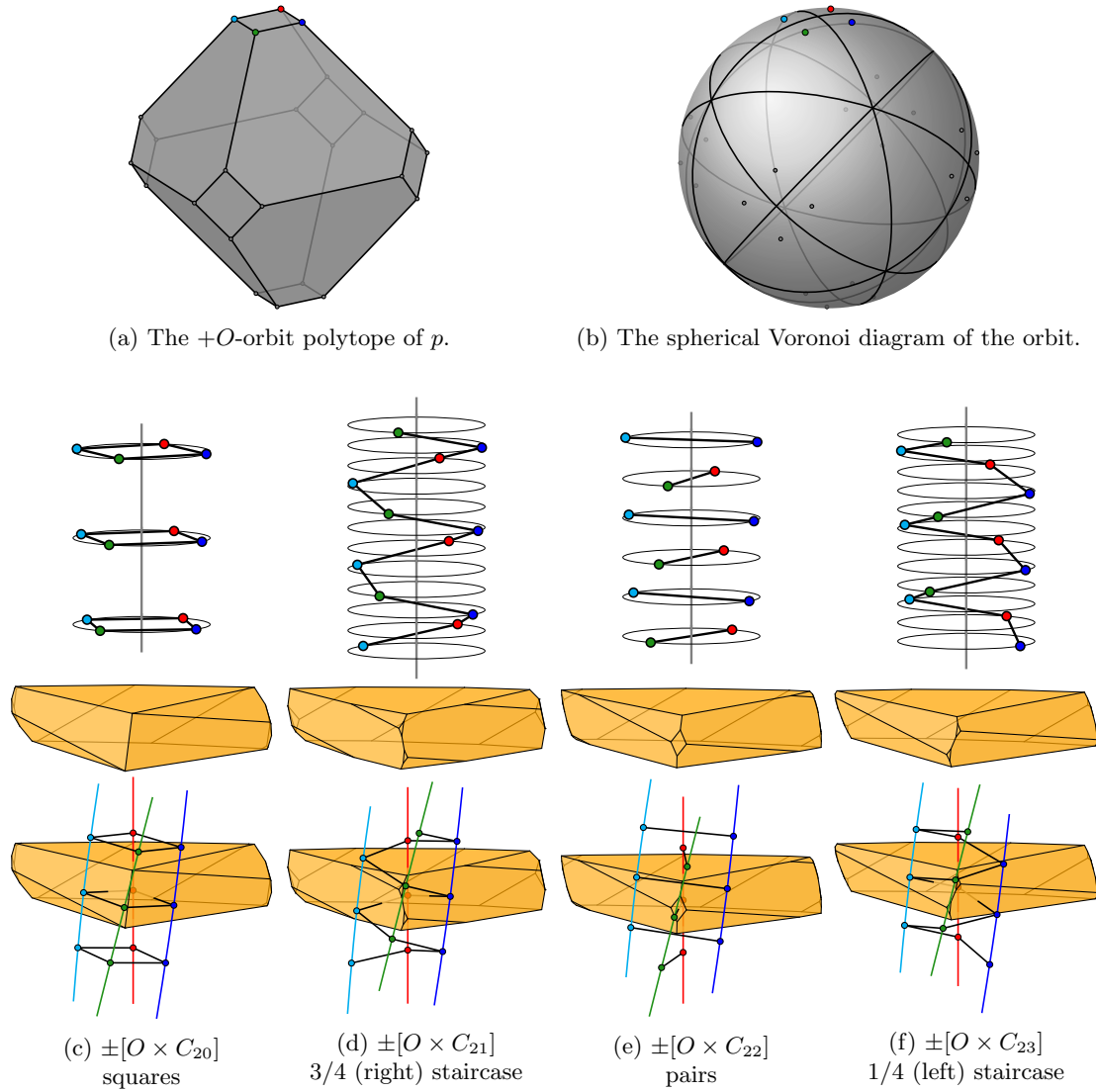


Figure 10: Orbits of the groups  $G = \pm[O \times C_n]$  for a starting point  $v$  whose image  $p := h(v)$  lies near a 4-fold rotation center of  $G^h = +O$ . The top row shows the three-dimensional  $+O$ -orbit polytope of  $p$  and the corresponding spherical Voronoi diagram. The four images of  $p$  under the 4-fold rotation are colored. The next row shows all possible configurations for orbit points on the corresponding colored circles. The vertical line in each figure is the great circle of  $\mathcal{H}$  that correspond to the rotation center. The third row shows a cell of the corresponding polar orbit polytope, and the bottom row combines the previous two rows.

- D1184 **Case 2.**  $H$  contains no simple rotation fixing  $K_p$ : Orbit points around  $K_p$  form different types  
 D1185 of staircases. See Figures 10d and 10f, and Figures 11d–11g.  
 D1186 **Case 3.**  $H$  contains a simple rotation fixing  $K_p$  of order not equal to  $f$ : This case can only occur  
 D1187 when  $f = 4$  and the order of that simple rotation is 2. Orbit points around  $K_p$  can be  
 D1188 grouped into pairs. See Figure 10e.

## D1189 6.8 Starting point on a rotation center

D1190 It is also interesting to see what happens if we move  $p_1$  to  $p$ . In this case, the points  $p_1, \dots, p_f$   
 D1191 coincide with  $p$ , and thus the corresponding circles  $K_{p_1}, \dots, K_{p_f}$  coincide with  $K_p$ . We describe  
 D1192 next what happens in each of the previous cases.

- D1193 **Case 1.** The orbit points coincide in groups of size  $f$ , and thus they form a regular  $2n$ -gon on  
 D1194  $K_p$ . Each orbit point can be mapped to itself by  $f$  different elements of  $G$ . Thus, in  
 D1195 the polar orbit polytope, each cell has an  $f$ -fold rotational symmetry whose axis is the  
 D1196 cell axis.

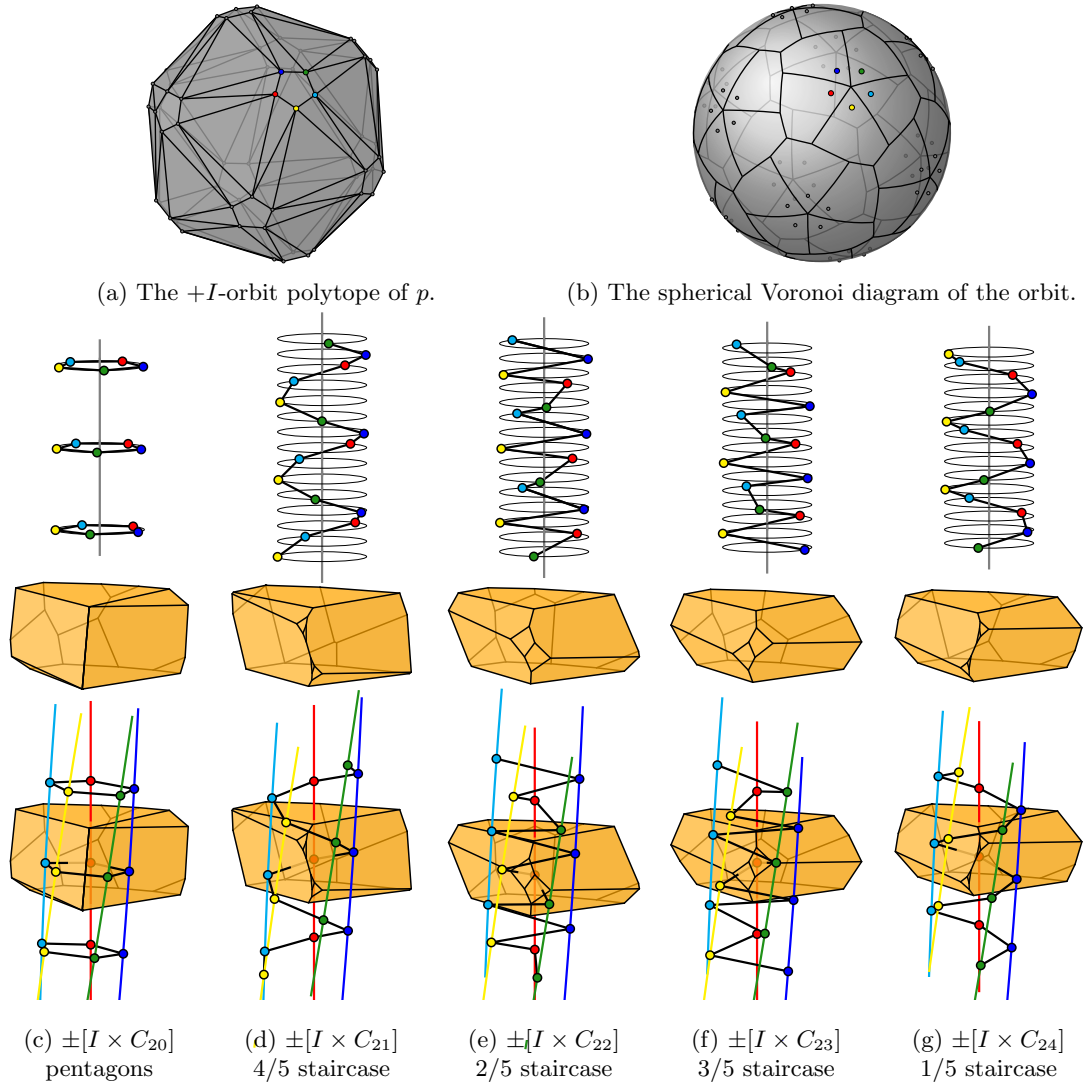


Figure 11: Orbits of the groups  $G = \pm[I \times C_n]$  for a starting point  $v$  whose image  $p := h(v)$  lies near a 5-fold rotation center of  $G^h = +I$ . The top row shows the three-dimensional  $+I$ -orbit polytope of  $p$  and the corresponding spherical Voronoi diagram. The five images of  $p$  under the 5-fold rotation are colored. The next row shows all possible configurations for orbit points on the corresponding colored circles. The vertical line in each figure is the great circle of  $\mathcal{H}$  that correspond to the rotation center. The third row shows a cell of the corresponding polar orbit polytope, and the bottom row combines the previous two rows.

D1197

D1198

D1199

D1200

D1201

D1202

**Case 2.** Orbit points on  $K_p$  form a regular  $2fn$ -gon. Each orbit point can be mapped to itself by a unique element of  $G$ . However, the orbit has extra symmetries, which come from the supergroup of  $G$  that we obtain by extending  $G$  by the new symmetry  $[1, e_{fn}]$ . Thus, in total, each orbit point can be mapped to itself by  $f$  symmetries. Accordingly, in the polar orbit polytope, each cell has an  $f$ -fold rotational symmetry whose axis is the cell axis.

D1203

D1204

D1205

D1206

D1207

D1208

**Case 3.** Orbit points on  $K_p$  form a regular  $4n$ -gon. Each orbit point can be mapped to itself by 2 different elements of  $G$ . However, the orbit has extra symmetries, which come from the supergroup of  $G$  that we obtain by extending  $G$  by the new symmetry  $[1, e_{2n}]$ . Thus, each orbit point can be mapped to itself by *extra* 2 symmetries. Accordingly, in the polar orbit polytope, each cell has a 4-fold rotational symmetry whose axis is the cell axis.

D1209

See Section 6.9 for particular examples and Appendix B for a coverage of all groups.

### 6.8.1 Supergroups of cyclic type

The cyclic-type supergroups described in Case 2 and Case 3 are listed in Table 3 for each group class and each type of rotation center. For large enough  $n$ , this supergroup is the largest cyclic-type symmetry group of the orbit. In most cases, this is the same class of group with a larger parameter  $n$ . The only exception are the groups  $G = \pm[T \times C_n]$  when  $p$  is a 2-fold rotation center of  $G^h = +T$ . As can be seen in Table 3, the symmetry groups of cyclic type of the orbit are then of the form  $\pm[O \times C_{n'}]$  or  $\pm\frac{1}{2}[O \times C_{n'}]$ .

The reason for this exceptional behavior can already be seen at the level of the groups  $G^h$  in three dimensions: On  $S^2$ , the group  $+T$  is an index-2 subgroup of  $+O$ . The 2-fold rotation centers  $p$  of  $+T$  coincide with the 4-fold rotation centers of  $+O$ , and the orbit has size 6 in both cases.

The group  $G_1 := \pm[T \times C_n]$  is an index-2 subgroup of  $G_2 := \pm[O \times C_n]$ . One can show that when  $n \equiv 0 \pmod{4}$ , the orbits of both groups have a simple rotation fixing  $K_p$  of order 2 (for  $G_1$ ) and of order 4 (for  $G_2$ ). In particular, both orbits follow Case 1 above and they form a regular  $2n$ -gon on each orbit circle. Since they also have the same orbit circles, these two orbits coincide. The other cases ( $n \equiv 2 \pmod{4}$ , and  $n$  odd) are similar.

Accordingly, all cells of the groups  $\pm[T \times C_n]$  when  $p$  is a 2-fold rotation center (Section B.4.2), appear also as cells of the groups  $\pm\frac{1}{2}[O \times C_{n'}]$  when  $p$  is a 4-fold rotation center (Figure 13), and those when  $n$  is a multiple of 4 also appear for the groups  $\pm[O \times C_{n'}]$  (Section B.2.1).

It is perhaps instructive to look at a particular example and compare the groups  $\pm[T \times C_{24}]$  (Figure 44) and  $\pm\frac{1}{2}[O \times C_{24}]$  (Figure 13 for  $n = 12$ ), which have equal, 4-sided cells. The allowed rotations between consecutive cells, apart from the necessary adjustment of  $\pi/24$ , are  $0^\circ$  and  $180^\circ$  in the first case and  $\pm 90^\circ$  in the second case. The common supergroup that has all four rotations is  $\pm[O \times C_{24}]$  (Figure 38).

### 6.8.2 Supergroups of dihedral type, and flip symmetries

For each cyclic-type tubical group and for each rotation center  $p$  of its induced group on  $S^2$ , there is a dihedral-type tubical group whose induced group on  $S^2$  has a mirror through  $p$ , and the cyclic-type group is an index-2 subgroup of the dihedral-type group. Thus, by Proposition 6.11, the orbit of the cyclic-type group for a starting point on  $K_p$  has extra symmetries coming from (a geometrically equal copy of) that dihedral-type tubical group. In particular, each cell of the polar orbit polytope will have a flip symmetry. See the figures in Section 6.9 and Appendix B. The dihedral-type supergroups are listed in Table 3.

## 6.9 Two examples of special starting points

In this section we will discuss two cases of non-generic starting points. In particular, we want to consider orbits of cyclic-type tubical groups where the image of the starting point under  $h$  is a rotation center of the induced group. In Table 3 and Appendix B, we summarize the results for the remaining groups and rotation centers.

### 6.9.1 $\pm[I \times C_n]$ , 5-fold rotation center

Let  $G = \pm[I \times C_n]$ . We want to consider the  $G$ -orbit of a point whose image under  $h$  is a 5-fold rotation center  $p$  of  $+I$ . By Proposition 6.4, any starting point on  $K_p$  will give the same orbit, up to congruence. Notice also that the other orbit circles correspond to the other 5-fold rotation centers of  $+I$ . Thus, choosing  $p$  to be an arbitrary 5-fold rotation center will yield the same orbit, up to congruence.

So let  $p$  be the 5-fold rotation center  $p = \frac{1}{\sqrt{\varphi^2+1}}(0, 1, \varphi)$ , where  $\varphi = \frac{1+\sqrt{5}}{2}$ . Then  $g = -\omega i_I = \cos \frac{\pi}{5} + p \sin \frac{\pi}{5} \in 2I$  defines the  $72^\circ$  clockwise rotation  $[g] \in +I$  around  $p$ . By Proposition 4.5, we know the elements of  $G$  that preserve  $K_p$ . These elements form a subgroup  $H = \langle [g, 1], [1, e_n] \rangle$  of order  $10n$ . Proposition 4.5 also tells us the  $H$  acts on  $K_p$  as a 2-dimensional cyclic group.

The rotation  $[g, 1]$  rotates  $\vec{K}_p$  by  $-\frac{\pi}{5}$ , while  $[1, e_n]$  rotates it by  $\frac{\pi}{n}$ . Thus, the  $G$ -orbit of a point on  $K_p$  forms a regular  $\text{lcm}(2n, 10)$ -gon on  $K_p$ . We will discuss the orbit of a point  $v \in K_p$  depending on the value of  $n$ . Figure 12 shows cells of the polar orbit polytopes for different values of  $n$ .

- If  $n$  is a multiple of 5, then the orbit points form a regular  $2n$ -gon on each orbit circle. So, every orbit point can be mapped to itself by 5 different elements of  $G$ . This is reflected

center type	#tubes	$n$	orbit size	cyclic-type supergroup	dihedral-type supergroup	figure
$\pm [I \times C_n]$						
5-fold	12	0 mod 5 else	$24n$ $120n$	$-$ $\pm [I \times C_{5n}]$	$\pm [I \times D_{2n}]$ $\pm [I \times D_{10n}]$	12
3-fold	20	0 mod 3 else	$40n$ $120n$	$-$ $\pm [I \times C_{3n}]$	$\pm [I \times D_{2n}]$ $\pm [I \times D_{6n}]$	36
2-fold	30	0 mod 2 else	$60n$ $120n$	$-$ $\pm [I \times C_{2n}]$	$\pm [I \times D_{2n}]$ $\pm [I \times D_{4n}]$	37
$\pm [O \times C_n]$						
4-fold	6	0 mod 4 2 mod 4 else	$12n$ $24n$ $48n$	$-$ $\pm [O \times C_{2n}]$ $\pm [O \times C_{4n}]$	$\pm [O \times D_{2n}]$ $\pm [O \times D_{4n}]$ $\pm [O \times D_{8n}]$	38
3-fold	8	0 mod 3 else	$16n$ $48n$	$-$ $\pm [O \times C_{3n}]$	$\pm [O \times D_{2n}]$ $\pm [O \times D_{6n}]$	39
2-fold	12	0 mod 2 else	$24n$ $48n$	$-$ $\pm [O \times C_{2n}]$	$\pm [O \times D_{2n}]$ $\pm [O \times D_{4n}]$	40
$\pm \frac{1}{2}[O \times C_{2n}]$						
4-fold	6	2 mod 4 0 mod 4 else	$12n$ $24n$ $48n$	$-$ $\pm [O \times C_{2n}]$ $\pm [O \times C_{4n}]$	$\pm \frac{1}{2}[O \times \overline{D}_{4n}]$ $\pm [O \times D_{4n}]$ $\pm [O \times D_{8n}]$	13
3-fold	8	0 mod 3 else	$16n$ $48n$	$-$ $\pm \frac{1}{2}[O \times C_{6n}]$	$\pm \frac{1}{2}[O \times \overline{D}_{4n}]$ $\pm \frac{1}{2}[O \times \overline{D}_{12n}]$	41
2-fold	12	0 mod 2 else	$24n$ $48n$	$-$ $\pm \frac{1}{2}[O \times C_{4n}]$	$\pm \frac{1}{2}[O \times \overline{D}_{4n}]$ $\pm \frac{1}{2}[O \times \overline{D}_{8n}]$	42
$\pm [T \times C_n]$						
3-fold	4	0 mod 3 else	$8n$ $24n$	$-$ $\pm [T \times C_{3n}]$	$\pm \frac{1}{2}[O \times D_{2n}]$ $\pm \frac{1}{2}[O \times D_{6n}]$	43
2-fold	6	0 mod 4 2 mod 4 else	$12n$ $12n$ $24n$	$\pm [O \times C_n]$ $\pm \frac{1}{2}[O \times C_{2n}]$ $\pm \frac{1}{2}[O \times C_{4n}]$	$\pm [O \times D_{2n}]$ $\pm \frac{1}{2}[O \times \overline{D}_{4n}]$ $\pm \frac{1}{2}[O \times \overline{D}_{8n}]$	44
$\pm \frac{1}{3}[T \times C_{3n}]$						
3-fold I	4	1 mod 3 else	$8n$ $24n$	$-$ $\pm [T \times C_{3n}]$	$\pm \frac{1}{6}[O \times D_{6n}]$ $\pm \frac{1}{2}[O \times D_{6n}]$	46
3-fold II	4	2 mod 3 else	$8n$ $24n$	$-$ $\pm [T \times C_{3n}]$	$\pm \frac{1}{6}[O \times D_{6n}]$ $\pm \frac{1}{2}[O \times D_{6n}]$	45
2-fold	6	0 mod 2 else	$12n$ $24n$	$-$ $\pm \frac{1}{3}[T \times C_{6n}]$	$\pm \frac{1}{6}[O \times D_{6n}]$ $\pm \frac{1}{6}[O \times D_{12n}]$	47

Table 3: The columns “cyclic-type supergroup” and “dihedral-type supergroup” indicate the largest symmetry group of the orbit that is tubical of that type. In Section 6.9, we extensively discuss two cases from the table. For the other cases, we summarize the results in Appendix B. The last column refers to the figure that shows cells of the corresponding polar orbit polytope with different values for  $n$ . The two types of 3-fold rotation centers for  $\pm \frac{1}{3}[T \times C_{3n}]$  (3-fold I and 3-fold II) are defined in Section 6.14.

on the cells of the polar orbit polytope where each cell has a 5-fold rotational symmetry whose axis is the cell axis.

This case corresponds to Case 1 in Section 6.8, where  $H$  contains a simple rotation of order 5 fixing  $K_p$ .

The element  $[1, e_n]$  of  $G$  maps an orbit point to an adjacent one on the same circle. Correspondingly, on each tube, the cells of the polar orbit polytope are stacked upon each other with a right screw by  $\frac{\pi}{n}$ .

• If  $n$  is not a multiple of 5, then the orbit points form a regular  $10n$ -gon on each orbit circle. That is, the orbit is free. So, every orbit point can be mapped to itself by a unique element of  $G$ . However, this orbit has extra symmetries. In particular, the rotation  $[1, e_{5n}]$  maps each orbit point to an adjacent one on the same circle. Adjoining  $[1, e_{5n}]$  to  $G$  gives the supergroup  $\pm[I \times C_{5n}]$ , whose orbit of  $n$  follows the first case. Accordingly, each cell of the polar orbit polytope has a 5-fold symmetry whose axis is the cell axis.

This case corresponds to Case 2 in Section 6.8, where  $H$  does not contain any simple rotation fixing  $K_p$ .

The symmetry  $[1, e_{5n}]$  (which is not in  $G$ ) maps an orbit point to an adjacent one on the same circle. Correspondingly, on each tube, the cells of the polar orbit polytope are stacked upon each other with a right screw by  $\frac{\pi}{5n}$ .

In accordance with Section 6.8.2, every cell has a flip symmetry, which is not included in  $G$ . It comes from (a group geometrically equal to) the group  $\pm[I \times D_{2n}]$ , which contains  $G$  as an index-2 subgroup.

The top and bottom faces in each cell are congruent. They resemble the shape of a pentagon. This corresponds to the fact that the spherical Voronoi cell of the  $+I$ -orbit of  $p$  on the 2-sphere is a spherical regular pentagon, as shown in the top right picture of Figure 12. (Refer to the discussion in Section 6.3.)

Since the  $+I$ -orbit of  $p$  has size 12, the  $G$ -orbit of  $v$  lies on 12 orbit circles. Accordingly, the cells of the polar orbit polytope can be decomposed into 12 tubes, each with  $\text{lcm}(2n, 10)$  cells. In the PDF-file of this article, the interested reader can click on the pictures in Figure 12 for an interactive visualization of these tubes. We refer to Section 6.13 for more details.

In accordance with the program set out in Figure 2 in Section 2 to understand the group by its action on the orbit polytope, we will now work out how each cell is mapped to the adjacent cell in the same tube. This requires a small number-theoretic calculation. The mapping between adjacent cells is obtained in cooperation between the right group and the left group. In particular, to get a rotation by  $\frac{2\pi}{\text{lcm}(2n, 10)}$  along the orbit circle  $\vec{K}_p$ , we have to combine a left rotation by  $-a \cdot \frac{\pi}{5}$  with a right rotation by  $b \cdot \frac{\pi}{n}$ , resulting in the angle

$$\frac{b\pi}{n} - \frac{a\pi}{5} = \frac{2\pi}{\text{lcm}(2n, 10)}. \quad (14)$$

For example, for  $n = 12$  we can solve this by  $a = 2, b = 5$ . The right screw angle between consecutive slices (or orbit points) is then  $\frac{b\pi}{n} + \frac{a\pi}{5}$ . Using (14), this can be rewritten as

$$\frac{a\pi}{5} + \frac{b\pi}{n} = \frac{2a\pi}{5} + \frac{2\pi}{\text{lcm}(2n, 10)} = \left( \frac{a}{5} + \frac{1}{\text{lcm}(2n, 10)} \right) \cdot 2\pi, \quad (15)$$

which is  $(\frac{2}{5} + \frac{\pi}{120}) \cdot 2\pi$  in our example. This angle is always of the form  $(\frac{a}{5} + \frac{1}{\text{lcm}(2n, 10)}) \cdot 2\pi$  for some integer  $a$ , in accordance with the requirement to match the pentagonal shape. The value  $a$  can never be 0. The rotation angles for different values of  $n$  are listed in Figure 12.

When  $n$  is not a multiple of 5, there is one element of the group that maps a cell to the upper adjacent one. Thus,  $a$  has a unique value. When  $n$  is a multiple of 5, each cell has a 5-fold symmetry included in the group. Thus, all values of  $a$  are permissible.

### 6.9.2 $\pm\frac{1}{2}[O \times C_{2n}]$ , 4-fold rotation center

Let  $G = \pm\frac{1}{2}[O \times C_{2n}]$ . We want to consider the  $G$ -orbit of a point whose image under  $h$  is a 4-fold rotation center  $p$  of  $+O$ . The discussion will closely parallel that of the group from the previous section, but in connection with the 4-fold rotation, we will also meet Case 3. Any of the 4-fold rotation centers  $p$  gives the same orbit. So let  $p$  be the 4-fold rotation center

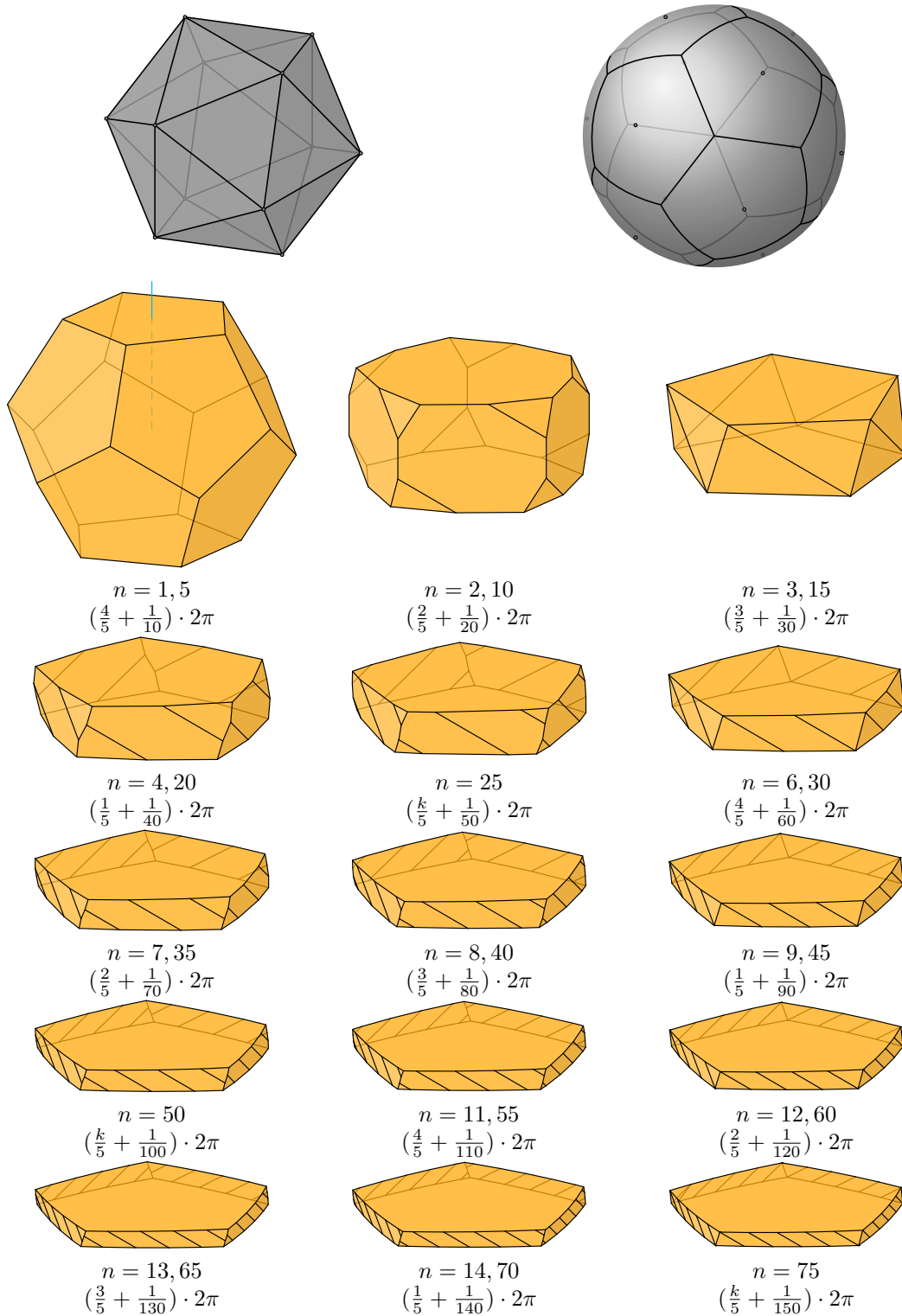


Figure 12: The  $+I$ -orbit polytope of the 5-fold rotation center  $p = (1/\sqrt{\varphi^2 + 1})(0, 1, \varphi)$  of  $+I$ , where  $\varphi = (1 + \sqrt{5})/2$  (top left), and the spherical Voronoi diagram of that orbit (top right). The remaining pictures show cells of polar  $\pm[I \times C_n]$ -orbit polytopes for a starting point on  $K_p$  for different values of  $n$ . In addition we indicate the counterclockwise angle (as seen from the top) by which the group rotates as it proceeds from a cell to the consecutive cell above. When the same orbit arises for several values of  $n$ , then the indicated angle is the unique valid angle only for the smallest value  $n_0$  that is specified. For a larger value  $n = 5n_0$ , this can be combined with arbitrary multiples of a 5-fold rotation. The polar orbit polytope can be decomposed into 12 tubes, each with  $\text{lcm}(2n, 10)$  cells. The blue vertical line indicates the cell axis, the direction towards the next cell along  $K_p$ . For an appropriate choice of starting point on  $K_p$ , the group  $\pm[I \times D_{2n}]$  produces the same orbit.

$p = (0, 1, 0)$ . Then  $g = -\omega i_O = \cos \frac{\pi}{4} + p \sin \frac{\pi}{4} \in 2O$  defines the  $90^\circ$  clockwise rotation  $[g] \in +O$  around  $p$ . By Proposition 4.5, we determine the elements of  $G$  that preserve  $K_p$  as the subgroup  $H = \langle [g, e_{2n}], [1, e_n] \rangle$  of order  $8n$ , which acts on  $K_p$  as a 2-dimensional cyclic group. The rotation  $[g, e_{2n}]$  rotates  $\vec{K}_p$  by  $-\frac{\pi}{4} + \frac{\pi}{2n} = -\frac{(n-2)\pi}{4n}$ . Its order is

$$\frac{2\pi}{\gcd(\frac{(n-2)\pi}{4n}, 2\pi)} = \frac{2\pi}{\frac{\pi}{4n} \gcd(n-2, 8n)} = \frac{8n}{\gcd(n-2, 8n-8(n-2))} = \frac{8n}{\gcd(n-2, 16)}.$$

The other operation,  $[1, e_n]$  rotates it by  $\frac{\pi}{n}$ . Thus, the  $G$ -orbit of a point on  $K_p$  forms a regular polygon with  $\text{lcm}(2n, \frac{8n}{\gcd(n-2, 16)})$  sides on  $K_p$ . The denominator  $\gcd(n-2, 16)$  can take the values 1, 2, 4, 8, 16, but in the overall expression, the values 4, 8, 16 make no distinction, and thus we can simplify the expression for the number of sides to  $\frac{8n}{\gcd(n-2, 4)}$ .

The structure of the orbit of a point  $v \in K_p$  depends on  $n$ . Cells of the polar orbit polytopes for different values of  $n$  are shown in Figure 13.

- If  $n-2$  is a multiple of 4, then  $\gcd(n-2, 4) = 4$  and  $\frac{8n}{\gcd(n-2, 4)} = 2n$ . The orbit points form a regular  $2n$ -gon on each orbit circle, and every point can be mapped to itself by 4 different elements of  $G$ . This is reflected on the polar orbit polytope where each cell has a 4-fold symmetry whose axis is the cell axis.

This corresponds to Case 1 in Section 6.8, where  $H$  contains a simple rotation of order 4 fixing  $K_p$ .

The element  $[1, e_n]$  of  $G$  maps an orbit point to an adjacent one on the same circle. Correspondingly, on each tube, the cells of the polar orbit polytope are stacked upon each other with a right screw by  $\frac{\pi}{2n}$ .

- If  $n-2 \equiv 2 \pmod{4}$ , then  $\gcd(n-2, 4) = 2$  and  $\frac{8n}{\gcd(n-2, 4)} = 4n$ . The orbit points form a regular  $4n$ -gon on each orbit circle, and every point can be mapped to itself by 2 different elements of  $G$ . However, this orbit has extra symmetries. In particular, the rotation  $[1, e_{2n}]$  maps each orbit point to an adjacent one on the same circle. Adjoining  $[1, e_{2n}]$  to  $G$  gives the supergroup  $\pm[O \times C_{2n}]$ , which contains  $G$  as an index-2 subgroup. Thus, each orbit point can be mapped to itself by 2 extra symmetries that are not in  $G$ . Accordingly, as in the first case, every cell of the polar orbit polytope has a 4-fold symmetry whose axis is the cell axis.

This corresponds to Case 3 in Section 6.8, where  $H$  contains a simple rotation of order 2 fixing  $K_p$ .

The symmetry  $[1, e_{2n}]$  (which is not in  $G$ ) maps an orbit point to adjacent one on the same circle. Correspondingly, on each tube, the cells of the polar orbit polytope are stacked upon each other with a right screw by  $\frac{\pi}{2n}$ .

- If  $n-2$  is odd, then  $\gcd(n-2, 4) = 1$  and  $\frac{8n}{\gcd(n-2, 4)} = 8n$ . The orbit is free. The orbit forms a regular  $8n$ -gon on each orbit circle. Every point can be mapped to any other point by a unique element of  $G$ . Again, the orbit has extra symmetries. In particular, the rotation  $[1, e_{4n}]$  maps each orbit point to an adjacent one on the same circle. Adjoining  $[1, e_{4n}]$  to  $G$  gives the supergroup  $\pm[O \times C_{4n}]$ , which contains  $G$  as an index-4 subgroup. Thus, each orbit point can be mapped to itself by 4 symmetries. Accordingly, as in the other cases, every cell of the polar orbit polytope has a 4-fold symmetry whose axis is the cell axis.

This corresponds to Case 2 in Section 6.8, where  $H$  does not contain a simple rotation fixing  $K_p$ .

The symmetry  $[1, e_{4n}]$  (which is not in  $G$ ) maps an orbit point to the next one on the same circle. Correspondingly, on each tube, the cells of the polar orbit polytope are stacked upon each other with a right screw by  $\frac{\pi}{4n}$ .

In accordance with Section 6.8.2, every cell has a flip symmetry, which is not included in  $G$ . It comes from (a group geometrically equal to) the group  $\pm\frac{1}{2}[O \times \overline{D}_{4n}]$ , which contains  $G$  as an index-2 subgroup.

The top and bottom faces in each cell are congruent. They resemble the shape of a rounded square, in agreement with the quadrilateral Voronoi cell on the 2-sphere, as shown in the top right figure in Figure 13.

Since the  $+O$ -orbit of  $p$  has size 6, the  $G$ -orbit of  $v$  lies on 6 orbit circles. Accordingly, the cells of the polar orbit polytope can be decomposed into 6 tubes, each with  $\frac{8n}{\gcd(n-2,4)}$  cells.

Similar to the previous section, one can work out the right screw angle (in  $G$ ) between consecutive slices. To summarize: When  $n - 2$  is odd, there is a unique angle of the form:  $(\frac{k_0}{4} + \frac{1}{8n}) \cdot 2\pi$  (with specific  $k_0 = 1, 2$ , or  $3$ ). When  $n - 2 \equiv 2 \pmod{4}$ , there are two angles:  $(\frac{2k+1}{4} + \frac{1}{4n}) \cdot 2\pi$  (with arbitrary  $k$ ). When  $n - 2$  is a multiple of 4, there are four angles:  $(\frac{k}{4} + \frac{1}{2n}) \cdot 2\pi$  (with arbitrary  $k$ ).

## 6.10 Consequences for starting points near rotation centers

In Sections 6.7 and 6.8 we have discussed the different cases that can arise for an orbit *near* a rotation axis and *on* a rotation axis. Indeed, we can confirm this relation by comparing Figure 11 and Figure 12. By the analysis that lead to Figure 11, an orbit of  $\pm[I \times C_n]$  near a 5-fold rotation axis forms a  $4/5$ ,  $2/5$ ,  $3/5$ , or  $1/5$  staircase if  $n \equiv 1, 2, 3, 4 \pmod{5}$ , respectively, and it forms pentagons if  $n$  is a multiple of 5. We can check in Figure 12 that these values are precisely the specified rotations (up to the twist by  $\frac{\pi}{5n}$ ), except when  $n$  is a multiple of 5, and in that case all five rotations are allowed. Similarly, Figure 10 corresponds with Figure 38.

Conversely, we can consult the appropriate entries in Appendix B for orbits *on* a rotation axis to conclude what type of pentagons, quadrilaterals, triangles, pairs, or staircases to expect for an orbit *near* this rotation axis.

## 6.11 Mappings between different tubes

Continuing the discussion of the tubes for the groups  $G = \pm\frac{1}{2}[O \times C_{2n}]$ , from Section 6.9.2, we will now continue with the program set out in Figure 2 in Section 2, by asking, for this example, how cells in different tubes are mapped to each other. The cells in Figure 13 have a roughly four-sided shape. At *corners* of these quadrilaterals, three tubes meet.

To understand what is happening there, we imagine putting a starting point  $v'$  near a corner. Then  $h(v')$  is near a three-fold rotation center of  $+O$ . Near such a rotation center, the orbit forms either a set of triangles, or a left or right staircase. As just discussed, we can check this by consulting the pictures for the orbit *on* a three-fold rotation axis: Figure 41.

We see that those cells of Figure 13 that have a straight line segment  $A$  between the top and the bottom face at the corners ( $n = 6, 3, 18, 12$ ) correspond to cases where the orbit of  $v'$  consists of triangles. Indeed, one can imagine three cells arranges around a common edge  $A$ . (The cells don't lie perpendicular to the axis  $A$ , but they are twisted.)

For the remaining cases ( $n = 1, 4, 10, 14, 8, 5, 22$ ) the edge is broken into three parts between the top and the bottom face, and this is where the cells are arranged in a staircase-like fashion.

## 6.12 Small values of $n$

For small values of  $n$ , some of the cyclic-type tubical groups recover well-known decompositions of regular/uniform polytopes into tubes (or more commonly knows as rings). These appear in various places in the literature. We list some of the references. Next to each group, we state the rotation center of the induced group that is the image of the starting point.

- $\pm[I \times C_1]$  and 5-fold rotation center (Figure 12): We get the decomposition of the 120-cell into 12 tubes, each with 10 regular dodecahedra.<sup>12</sup> Figure 30 shows a picture of three dodecahedra from one tube, see also [15, Figure 21], [9, p. 75] and Coxeter [12, p. 53].
- $\pm[O \times C_1]$  and 4-fold rotation center (Figure 38): We get the decomposition of the bi-truncated 24-cell (the 48-cell) into 6 tubes, each with 8 truncated cubes, stacked upon the octagonal faces.
- $\pm[O \times C_1]$  and 3-fold rotation center (Figure 39): We get the decomposition of the bi-truncated 24-cell (the 48-cell) into 8 tubes, each with 6 truncated cubes, stacked upon the triangular faces. [9, p. 75-76].
- $\pm[T \times C_1]$  and 3-fold rotation center (Figure 43): We get the decomposition of the 24-cell into 4 tubes, each with 6 octahedra [9, p. 74], [2].

<sup>12</sup>A remarkable paper model of a Schlegel diagram with two rings was produced by Robert Webb, <https://youtu.be/2nTLI89vdzg>. An interesting burr puzzle was made in [33] using pieces of these rings.



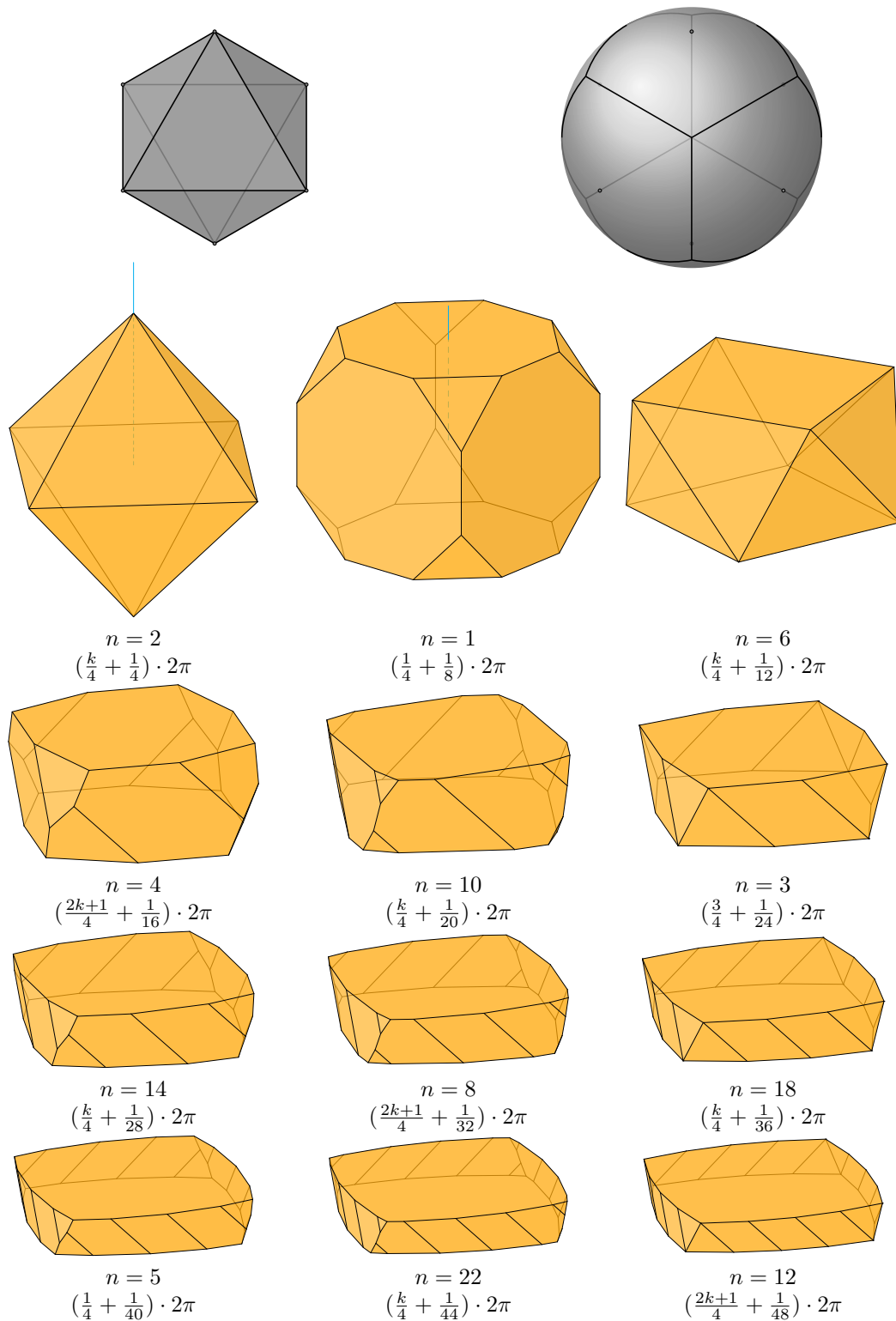


Figure 13: The  $+O$ -orbit polytope of the 4-fold rotation center  $p = (0, 1, 0)$  of  $+O$  (top left), and the spherical Voronoi diagram of that orbit (top right). The remaining pictures show cells of polar  $\pm \frac{1}{2}[O \times C_{2n}]$ -orbit polytopes for a starting point on  $K_p$  for different values of  $n$ . In addition we indicate the counterclockwise angle (as seen from the top) by which the group rotates as it proceeds from a cell to the consecutive cell above. The polar orbit polytope can be decomposed into 6 tubes, each with  $\frac{8n}{\gcd(n-2, 4)}$  cells. The blue vertical line indicates the cell axis, the direction towards the next cell along  $K_p$ . For an appropriate choice of starting point on  $K_p$ , the group  $\pm \frac{1}{2}[O \times \bar{D}_{4n}]$  produces the same orbit. When  $n = 2$ , the cells that should form a tube touch each other only in a vertex.

- $\pm[T \times C_1]$  and 2-fold rotation center (Figure 44): We get the decomposition of the 24-cell into 6 tubes, each with 4 octahedra, touching each other via vertices.
- $\pm\frac{1}{3}[T \times C_3]$  and 3-fold (type I) rotation center (Figure 45): This is a degenerate case. We get the decomposition of the hypercube into 4 “tubes”, but each “tube” is just a pair of opposite cube faces.

We remark that the orbit of  $G = \pm[L \times C_1]$ , is the same, up to congruence, for any starting point. This follows since the  $G$ -orbit of a point  $v \in \mathbb{R}^4$  can be obtained from the  $G$ -orbit of the quaternion 1 by applying the rotation  $[1, v]$ :

$$\text{orbit}(v, G) = \{\bar{l}v \mid l \in L\} = [1, v]\{\bar{l} \mid l \in L\} = [1, v]\text{orbit}(1, G).$$

### 6.13 Online gallery of polar orbit polytopes

The interested reader can explore polar orbit polytopes for the cyclic-type tubical groups with all special choices of starting points in an online gallery that provides interactive three-dimensional views.<sup>13</sup>

The polytopes are shown in a central projection to the three-dimensional tangent space at the starting point  $v$  of the orbit. The projection center lies outside the polytope, close to the cell  $F_0$  opposite to  $v$ . In the projection,  $F_0$  becomes the outer cell that (almost) encloses all remaining projected cells. The orientation of the outer cell is reversed with respect to the other cells. We are mostly interested not in  $F_0$  but in the cells near  $v$ , which are distorted the least in the projection, and as a consequence, we go with the majority and ensure that *these* cells are oriented according to our convention (Section 2.3). For large values on  $n$ , we have refrained from constructing true Schlegel diagrams, because this would have resulted in tiny inner cells. As a result, cells near the boundary of the projection wrap around and overlap.

The goal of the gallery is to show the decomposition of the polytopes into tubes, and how these tubes are structured and interact with each other. It is possible to remove cells one by one to see more structure. The order of the cells is based on the distances of their orbit points to the starting point  $v$ .

### 6.14 $\pm[T \times C_n]$ versus $\pm\frac{1}{3}[T \times C_{3n}]$

Looking at the tubical groups in Table 2, we see that there are groups  $G$  with the same induced symmetry group  $G^h$  on  $S^2$ . Thus, for the same starting point, these groups have the same orbit circles. However, they differ in the way how the points on different circles are arranged relative to each other.

In this section we will consider the case where the induced group is  $+T$ . For the same  $n$ , we will compare the actions of  $\pm[T \times C_n]$  and  $\pm\frac{1}{3}[T \times C_{3n}]$  on and around the circles of  $\mathcal{H}$  that correspond to rotation centers of  $+T$ . We will see that these two groups have different sets of fixed circles of  $\mathcal{H}$ , which correspond to 3-fold rotation centers of  $+T$ . On such a fixed circle, the size of the orbit is reduced by a factor of 3 (from  $24n$  to  $8n$ , see Table 3). In Figures 15 and 16, we visualize the effect of that difference on the orbit points and the cells of the polar orbit polytope around these circles. We will see that triangles and both types of staircases appear in  $\pm[T \times C_n]$  and  $\pm\frac{1}{3}[T \times C_{3n}]$ , depending on  $n$ . In this sense, there is no sharp geometric distinction between the two families.

**2-fold rotation center.** Let  $p \in S^2$  be a 2-fold rotation center of  $+T$  and let  $[g] \in +T$  be the  $180^\circ$  rotation around  $p$ . If  $n$  is even, then  $[g, e_2]$  is in both groups, and it is a simple rotation that fixes  $K_p$ . If  $n$  is odd, then  $K_p$  is not fixed. Thus, for the same  $n$ ,  $\pm[T \times C_n]$  and  $\pm\frac{1}{3}[T \times C_{3n}]$  have the same set of fixed circles that correspond to 2-fold rotation centers of  $+T$ .

**3-fold rotation center.** The eight 3-fold rotation centers of  $+T$  belong to two conjugacy classes, depending on which  $+T$ -orbit they are in. The rotation centers of *type I*, are the ones in the orbit of  $p_0 = (-1, -1, -1)$ , and the rotation centers of *type II*, are the ones in the orbit of  $-p_0 = (1, 1, 1)$ . We will see that the group  $\pm[T \times C_n]$  does not distinguish between the circles

<sup>13</sup><https://www.inf.fu-berlin.de/inst/ag-ti/software/DiscreteHopfFibration/>. In the PDF-file of this article, the pictures of the cells in the figures in Section 6.9 and Appendix B are linked to the corresponding entries in the gallery.

$K_{p_0}$  and  $K_{-p_0}$ . In particular, the orbit of a starting point on  $p_0$  is congruent to the one of a starting point on  $-p_0$ . However, this is not the case for  $\pm \frac{1}{3}[T \times C_{3n}]$ .

The quaternion  $-\omega \in 2T$  defines the  $120^\circ$  clockwise rotation  $[-\omega]$  around  $p_0$ . That is  $-\omega = \cos \frac{\pi}{3} + p_0 \sin \frac{\pi}{3}$ . The quaternion  $-\omega^2 \in 2T$  defines the  $120^\circ$  clockwise rotation  $[-\omega^2]$  around  $-p_0$ . That is  $-\omega^2 = \cos \frac{\pi}{3} - p_0 \sin \frac{\pi}{3}$ .

By Proposition 4.5, the set of rotations that preserve  $K_{p_0}$  is the same as the set of rotations that preserve  $K_{-p_0}$ . Let's look at these rotations inside each of the two groups.

- The elements of  $\pm[T \times C_n]$  that preserve  $K_{p_0}$  (and  $K_{-p_0}$ ) form the subgroup

$$\langle [-\omega, 1], [1, e_n] \rangle = \langle [-\omega^2, 1], [1, e_n] \rangle$$

of order  $6n$ . The rotation  $[-\omega, 1]$  rotates  $K_{p_0}$  by  $\frac{\pi}{3}$  in one direction, while  $[1, e_n]$  rotates it by  $\frac{\pi}{n}$  in the other direction. Thus, the  $\pm[T \times C_n]$ -orbit of a starting point on  $K_{p_0}$  forms a regular  $\text{lcm}(2n, 3)$ -gon on  $K_{p_0}$ . Similarly, the  $\pm[T \times C_n]$ -orbit of a starting point on  $K_{-p_0}$  forms a regular  $\text{lcm}(2n, 3)$ -gon on  $K_{-p_0}$ . In particular, if  $n$  is a multiple of 3,  $\pm[T \times C_n]$  has a simple rotation  $([-\omega, e_3])$  fixing  $K_p$  and a simple rotation  $([-\omega^2, e_3])$  fixing  $K_{-p_0}$ . If  $n$  is not a multiple of 3,  $\pm[T \times C_n]$  has no simple rotation fixing  $K_{p_0}$  or  $K_{-p_0}$ , and the orbit points on the three circles form a left or right staircase.

- The elements of  $\frac{1}{3}[T \times C_{3n}]$  that preserve  $K_{p_0}$  (and  $K_{-p_0}$ ) form the subgroup

$$\langle [-\omega, e_{3n}], [1, e_n] \rangle = \langle [-\omega^2, e_{3n}^2], [1, e_n] \rangle$$

of order  $6n$ . We will now consider the action of this subgroup on the circles  $K_{p_0}$  and  $K_{-p_0}$ . On  $K_{p_0}$ , the rotation  $[-\omega, e_{3n}]$  rotates  $K_{p_0}$  by  $\frac{\pi}{3} - \frac{\pi}{3n} = \frac{(n-1)\pi}{3n}$ . Its order is

$$\frac{2\pi}{\gcd(\frac{(n-1)\pi}{3n}, 2\pi)} = \frac{2\pi}{\gcd(\frac{\pi}{3n}(n-1), 6n\frac{\pi}{3n})} = \frac{2\pi}{\frac{\pi}{3n} \gcd(n-1, 6n)} = \frac{6n}{\gcd(n-1, 6)}.$$

Thus, the  $\pm \frac{1}{3}[T \times C_{3n}]$ -orbit of a starting point on  $K_{p_0}$  forms a regular polygon with  $\text{lcm}(2n, \frac{6n}{\gcd(n-1, 6)}) = \frac{6n}{\gcd(n-1, 3)}$  sides. In particular, if  $n-1$  is a multiple of 3,  $\pm \frac{1}{3}[T \times C_{3n}]$  has a simple rotation fixing  $K_{p_0}$ . Otherwise,  $G$  has no simple rotation fixing  $K_{p_0}$ . On  $K_{-p_0}$ , the rotation  $[-\omega^2, e_{3n}^2]$  rotates  $K_{-p_0}$  by  $\frac{\pi}{3} - \frac{2\pi}{3n} = \frac{(n-2)\pi}{3n}$ . Its order is

$$\frac{2\pi}{\gcd(\frac{(n-2)\pi}{3n}, 2\pi)} = \frac{2\pi}{\gcd(\frac{\pi}{3n}(n-2), 6n\frac{\pi}{3n})} = \frac{2\pi}{\frac{\pi}{3n} \gcd(n-2, 6n)} = \frac{6n}{\gcd(n-2, 12)}.$$

Thus, the  $\pm \frac{1}{3}[T \times C_{3n}]$ -orbit of a starting point on  $K_{-p_0}$  forms a regular polygon with  $\text{lcm}(2n, \frac{6n}{\gcd(n-2, 12)}) = \frac{6n}{\gcd(n-2, 3)}$  sides. In particular, if  $n-2$  is a multiple of 3,  $\pm \frac{1}{3}[T \times C_{3n}]$  has a simple rotation fixing  $K_{-p_0}$ . Otherwise,  $G$  has no simple rotation fixing  $K_{-p_0}$ .

To summarize,  $\pm[T \times C_n]$  fixes  $K_{p_0}$  and  $K_{-p_0}$  if and only if  $n \equiv 0 \pmod{3}$ . While,  $\pm \frac{1}{3}[T \times C_{3n}]$  fixes  $K_{p_0}$  if and only if  $n \equiv 1 \pmod{3}$ , and it fixes  $K_{-p_0}$  if and only if  $n \equiv 2 \pmod{3}$ .

Here, we have discussed the situation in terms of orbits near the axis. As discussed in Section 6.10, the results can be checked against Figures 43, 46, and 45.

## 7 The toroidal groups

### 7.1 The invariant Clifford torus

We will now study the large class of groups of type  $[D \times D]$  or  $[C \times C]$  or  $[C \times D]$ , where both the left and the right group are cyclic or dihedral. At the beginning of Section 5.1, we have seen that these groups have an invariant Clifford torus  $\mathbb{T}_p^q$ . All tori  $\mathbb{T}_p^q$  are the same up to orthogonal transformations. We can thus, without loss of generality, restrict our attention to the standard torus  $\mathbb{T}_i^i$ . Indeed this is the torus that is left invariant by the left and right multiplication with the groups  $\pm[D_{2m} \times D_{2n}]$  and their subgroups, as follows from Proposition 4.13. When we speak of *the torus* in this section, we mean the torus  $\mathbb{T}_i^i$  and we denote it by  $\mathbb{T}$ .

Since we also have cases where the left and right subgroup are equal, we also have to deal with their achiral extensions. According to Proposition 3.2, the extending element can be taken as  $e = *[1, c]$ , which is a composition of  $*$ :  $(x_1, y_1, x_2, y_2) \mapsto (x_1, -y_1, -x_2, -y_2)$ , which leaves



Figure 14: The  $+T$ -orbit polytope of a starting point near a 3-fold rotation center of  $+T$  (left), and the spherical Voronoi diagram of this orbit (right). The picture looks the same for a Type I or a Type II center.

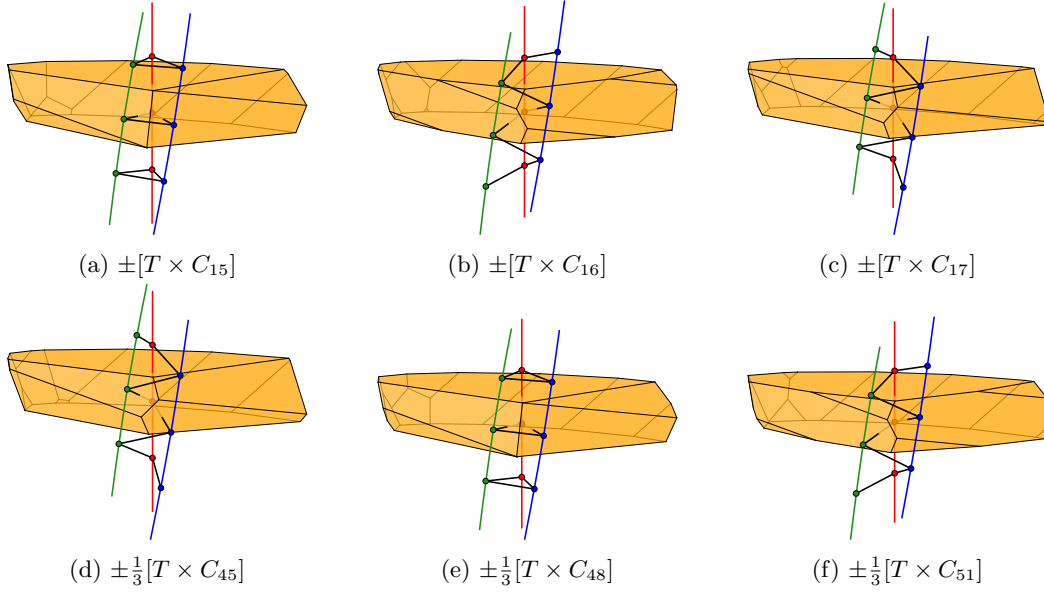


Figure 15: Cells of polar orbit polytopes of the corresponding groups, where the image of the starting point lies near a 3-fold rotation center of type I. The colors are in correspondence with Figure 14.

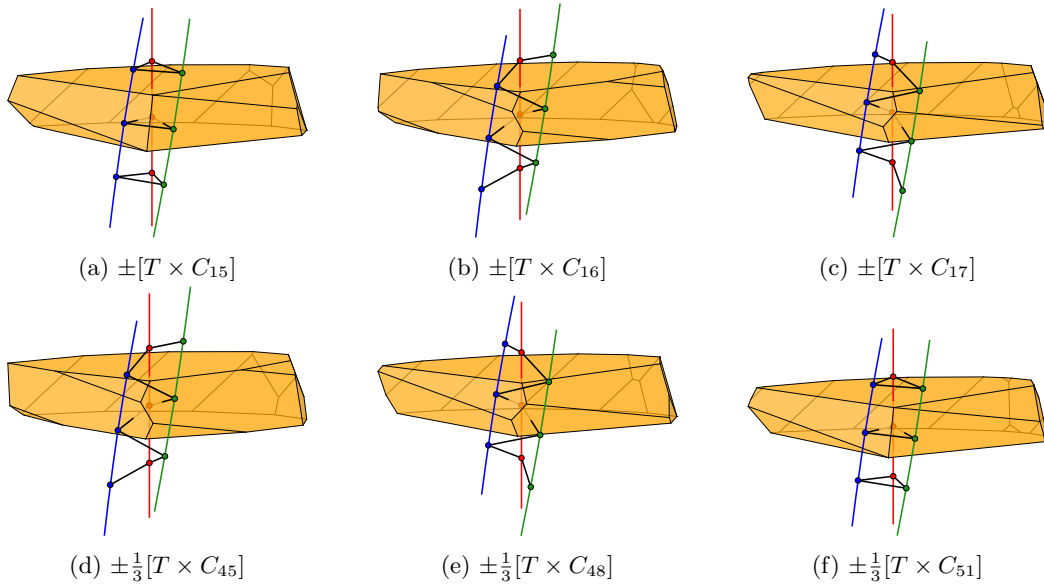


Figure 16: Cells of polar orbit polytopes of the corresponding groups, where the image of the starting point lies near a 3-fold rotation center of type II. The colors are in correspondence with Figure 14.

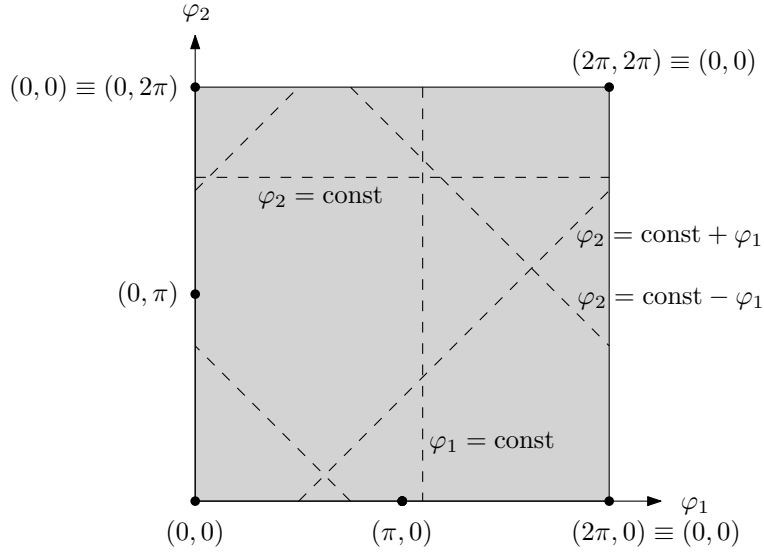


Figure 17: Torus coordinates for the Clifford torus

the torus fixed, with  $[1, c]$ , for an element  $c$  of the right group, which also leaves the torus fixed. This means that the achiral extensions can also be found among the groups that leave the torus fixed.

We call these groups, namely the subgroups  $\pm[D_{2m} \times D_{2n}]$  and their achiral extensions, the *toroidal groups*.

We will study and classify these groups by focusing on their action on  $\mathbb{T}$ . In particular, it will be of secondary interest whether the groups are chiral or achiral, or which Hopf bundles they preserve. These properties were important to derive the existence of the invariant torus, but we will not use them for the classification.

Since  $\mathbb{T}$  is a two-dimensional flat surface, the symmetry groups acting on  $\mathbb{T}$  bear much resemblance to the discrete symmetry groups of the plane, i.e., the wallpaper groups. These groups are well-studied and intuitive. All wallpaper groups except those that contain 3-fold rotations will make their appearance (12 out of the 17 wallpaper groups). The reason for excluding 3-fold rotations is that a Clifford torus has two distinguished directions, which are perpendicular to each other, and these directions must be preserved. We don't assume familiarity with the classification of the wallpaper groups. We will develop the classification as we go and adapt it to our needs.

## 7.2 Torus coordinates and the torus foliation

The Clifford torus belongs to a foliation of  $S^3$  by a family of tori, which, in terms of Cartesian coordinates  $(x_1, y_1, x_2, y_2)$ , have the equations

$$x_1^2 + y_1^2 = r_1^2, \quad x_2^2 + y_2^2 = r_2^2 \quad (16)$$

for fixed radii  $r_1, r_2$  with  $0 < r_1, r_2 < 1$  and  $r_1^2 + r_2^2 = 1$ . The standard Clifford torus has the parameters  $r_1 = r_2 = \sqrt{1/2}$ . As limiting cases,  $r_1 = 1$  gives the great circle in the  $x_1, y_1$ -plane, and  $r_1 = 0$  gives the great circle in the  $x_2, y_2$ -plane. Every torus in this family is the Cartesian product of two circles, and thus is a flat torus, with a locally Euclidean metric, forming a  $2\pi r_1 \times 2\pi r_2$  rectangle with opposite sides identified.

The best way to see the mapping to the rectangle is to use double polar coordinates:

$$\begin{pmatrix} x_1 \\ y_1 \\ x_2 \\ y_2 \end{pmatrix} = \begin{pmatrix} r_1 \cos \varphi_1 \\ r_1 \sin \varphi_1 \\ r_2 \cos \varphi_2 \\ r_2 \sin \varphi_2 \end{pmatrix} \quad (17)$$

Then  $\varphi_1$  and  $\varphi_2$  (appropriately scaled) can be used as rectangular two-dimensional coordinates, see Figure 17.

The lines with  $\varphi_1 = \text{const}$  and  $\varphi_2 = \text{const}$  are what we would normally call meridian circles and parallel circles of the torus, except that there is no natural way to distinguish the two classes.

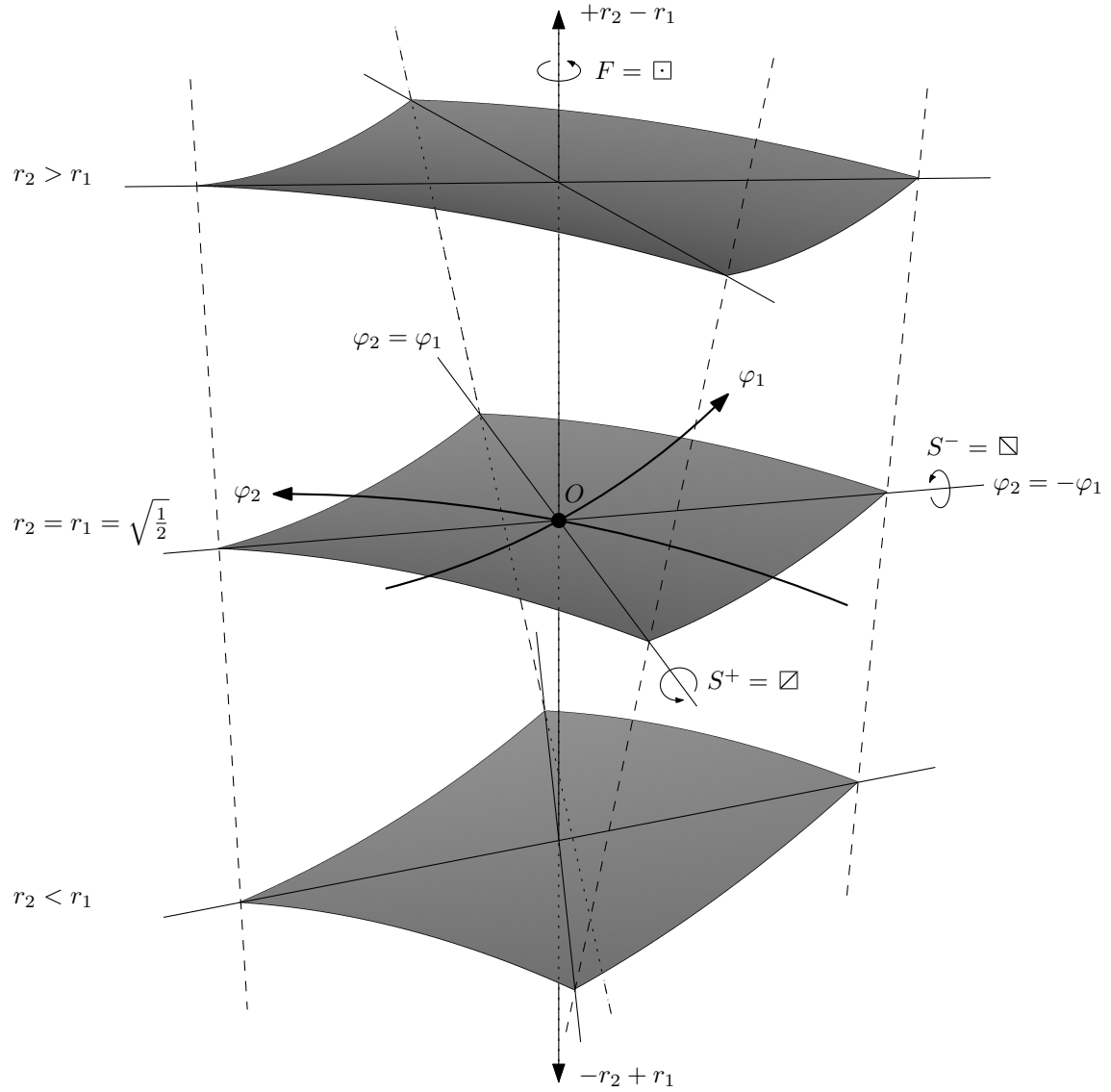


Figure 18: Patches of flat tori in the 3-sphere. This illustration is a central projection from the 3-sphere to the 3-dimensional tangent hyperplane at the point  $O = (\sqrt{1/2}, 0, \sqrt{1/2}, 0)$ , which is the marked point in the center. Great circles, i.e. geodesics on the 3-sphere, appear as straight lines. The axes of the *flip* half-turns  $F$  and the *swap* half-turns  $S^+$  and  $S^-$  are indicated.

The tangent in direction  $\varphi_1$  points in the direction  $(0, 1, 0, 0)$  and the tangent vector in direction  $\varphi_2$  points in the direction  $(0, 0, 0, 1)$ . The “perpendicular direction”, which is the vertical axis  $+r_2 - r_1$  in the figure, is the direction  $(-\sqrt{1/2}, 0, \sqrt{1/2}, 0)$ .

These circles have radius  $\sqrt{1/2}$ . The  $45^\circ$  lines with  $\varphi_2 = \text{const} + \varphi_1$  and  $\varphi_2 = \text{const} - \varphi_1$  are great circles. They are the circles from the Hopf bundles  $\mathcal{H}_i$  and  $\mathcal{H}^i$ .

Figure 18 gives a picture of corresponding patches around the origin  $\varphi_1 = \varphi_2 = 0$  for three tori. The middle one is the Clifford torus with  $r_1 = r_2 = \sqrt{1/2} \approx 0.7$ , the top one has  $r_1 = 0.55 < r_2 \approx 0.835$ , and the bottom one has the reversed values  $r_1$  and  $r_2$ .

Each torus is intrinsically flat, i.e., isometric to the Euclidean plane in every small patch, but, as the figure suggests, it is embedded as a “curved” surface inside  $S^3$ . The only “lines” in the torus that are geodesics of  $S^3$  are those that are parallel to the diagonal lines  $\varphi_2 = \pm\varphi_1$ . The dotted “vertical” lines connect points with the same  $\varphi_1, \varphi_2$ -coordinates on different tori. They are great circles, and they intersect every torus of the family orthogonally.

In Section 7.11.2, we will see the easy equation  $x_1x_3 = x_2x_4$  (24) for the same torus in a different coordinate system.

### 7.3 Symmetries of the torus

Since the torus is locally like the Euclidean plane, and the plane is the universal covering space of the torus, we can investigate the isometric symmetries of the torus by studying the isometries of the plane. However, not every isometry of the plane can be used as a symmetry of the torus; it must be “compatible” with the torus structure. The following theorem makes this precise:

**Theorem 7.1.** *There is a one-to-one correspondence between*

- groups  $G$  of isometries of the torus  $[0, 2\pi) \times [0, 2\pi)$ ,
- groups  $\hat{G}$  of isometries  $x \mapsto Ax + t$  of the  $(\varphi_1, \varphi_2)$ -plane with the following properties:
  - (i) The directional part  $A$  of every isometry in  $\hat{G}$  keeps the integer grid  $\mathbb{Z}^2$  invariant.
  - (ii) The group contains the two translations  $\varphi_1 \mapsto \varphi_1 + 2\pi$  and  $\varphi_2 \mapsto \varphi_2 + 2\pi$ .

The proof uses the following lemma, which shows how to lift torus isometries to plane isometries:

**Lemma 7.2.** *Let  $\Lambda$  denote the scaled integer grid  $\{(k_1 2\pi, k_2 2\pi) \mid k_1, k_2 \in \mathbb{Z}\}$ , and let  $p: \mathbb{R}^2 \rightarrow \mathbb{R}^2|_\Lambda$  be the quotient map from the plane to the torus  $[0, 2\pi) \times [0, 2\pi)$ :*

$$p(\varphi_1, \varphi_2) = (\varphi_1 \bmod 2\pi, \varphi_2 \bmod 2\pi)$$

*For every isometry  $T$  of the torus  $[0, 2\pi) \times [0, 2\pi)$ , there is an isometry  $\hat{T}$  of the plane with the following properties.*

- (a)  $T(p(x)) = p(\hat{T}(x))$  for all  $x \in \mathbb{R}^2$ .
- (b)  $\hat{T}$  maps the grid  $\Lambda$  to a translate of  $\Lambda$ .

*The isometry  $\hat{T}$  is unique up to translation by a grid vector  $t \in \Lambda$ .*

*Proof.* Pick some point  $y_0$  of the torus and let  $T(y_0) = y'_0$ . Find points  $x_0, x'_0 \in \mathbb{R}^2$  with  $y_0 = p(x_0)$  and  $y'_0 = p(x'_0)$ . Since  $p$  is locally injective, the mapping  $T$  can be lifted to a mapping  $\hat{T}(x) = p^{-1}(T(p(x)))$  in some neighborhood  $N(x_0)$  of  $x_0 \in \mathbb{R}^2$ :

$$\begin{array}{ccc} \mathbb{R}^2: & x_0 & \xrightarrow{\hat{T}} x'_0 \\ & \downarrow p & \downarrow p \\ \mathbb{T}: & y_0 & \xrightarrow{T} y'_0 \end{array} \quad (18)$$

In other words,  $\hat{T}(x_0) = x'_0$ , and for all  $x \in N(x_0)$ :

$$p(\hat{T}(x)) = T(p(x)) \quad (19)$$

Moreover, since both  $p$  and  $T$  are locally isometries,  $\hat{T}$  is an isometry in  $N(x_0)$ . This isometry can be extended to a unique isometry  $\hat{T}$  of the plane.

To extend the validity of (19) from  $N(x_0)$  to the whole plane, we look at a path  $x_0 + \lambda t$  from  $x_0$  to an arbitrary point  $x_0 + t$  of the plane, where  $(0 \leq \lambda \leq 1)$ . On the torus, it corresponds to a path  $p(x_0 + \lambda t)$ , which is mapped to an image path  $T(p(x_0 + \lambda t))$ , which in turn can be lifted

to a path on  $\mathbb{R}^2$ . Since  $p$  is locally invertible and an isometry, (19) must hold along the whole path, and therefore for an arbitrary point  $x_0 + t$  of the plane. This is claim (a).

To show claim (b), consider any  $t \in \Lambda$ . By (19),

$$p(\hat{T}(t)) = T(p(t)) = T(p(0))$$

that is, all values  $\hat{T}(t)$  for  $t \in \Lambda$  project to the same point  $T(p(0))$  on the torus. It follows that the image of  $\Lambda$  under  $\hat{T}$  is contained in a translate of  $\Lambda$ . But then it must be *equal* to this translate of  $\Lambda$ .

Once  $x_0$  and  $x'_0$  have been chosen, the construction gives a unique transformation  $\hat{T}$ . The result can be varied by adding an arbitrary translation  $t \in \Lambda$  to  $x_0$  (before applying  $\hat{T}$ ) or  $t' \in \Lambda$  to  $x'_0$  (after applying  $\hat{T}$ ). By property (b), it makes no difference whether we are allowed to translate by an element of  $\Lambda$  before applying  $\hat{T}$  or after (or both). This proves the uniqueness claim of the lemma.  $\square$

As a consequence, we can write a torus isometry like a plane isometry in the form  $x \mapsto Ax + t$  with an orthogonal matrix  $A$  and a translation vector  $t$ , bearing in mind that  $t$  is unique only up to grid translations.

*Proof of Theorem 7.1.* Given a group  $G$ , we can construct the lifted group  $\hat{G}$  as the set of lifted isometries  $\hat{T}$  of the transformations  $T \in G$  according to the lemma. The group property of  $\hat{G}$  can be easily shown by extending the diagram (18):

$$\begin{array}{ccccc} \mathbb{R}^2: & x_0 & \xrightarrow{\hat{T}} & x'_0 & \xrightarrow{\hat{T}'} & x''_0 \\ & \downarrow p & & \downarrow p & & \downarrow p \\ \mathbb{T}: & y_0 & \xrightarrow{T} & y'_0 & \xrightarrow{T'} & y''_0 \end{array}$$

$\hat{T}\hat{T}'$  (top arc) and  $TT'$  (bottom arc)

The translations  $\varphi_1 \mapsto \varphi_1 + 2\pi$  and  $\varphi_2 \mapsto \varphi_2 + 2\pi$  arise as lifts of the identity  $\text{id} \in G$ . It is clear that a matrix  $A$  keeps the scaled integer grid  $\Lambda := \{(k_1 2\pi, k_2 2\pi) \mid k_1, k_2 \in \mathbb{Z}\}$  invariant (Property (b)) if and only if it keeps the standard integer grid  $\mathbb{Z}^2$  invariant (Property (i)).

Conversely, given a transformation  $\hat{T}$  in the group  $\hat{G}$ , we can define  $T$  as follows: For a point  $y_0$  of the torus, pick a point  $x_0$  with  $p(x_0) = y_0$ , and define  $T(y_0)$  through the relation (18):  $T(y_0) := p(\hat{T}(x_0))$ . The choice of  $x_0$  is ambiguous. It is determined only up to a translation by  $t \in \Lambda$ , but we see that this has no effect on  $T(y_0)$ :

$$p(\hat{T}(x_0 + t)) = p(\hat{T}(x_0) + t') = p(\hat{T}(x_0))$$

By property (i), or property (b),  $t' \in \Lambda$ , and therefore the ambiguity evaporates through the projection  $p$ .  $\square$

### 7.3.1 Torus translations

The simplest operations are the ones that appear as translations on the torus, modulo  $2\pi$ . We denote them by

$$R_{\alpha_1, \alpha_2}: (\varphi_1, \varphi_2) \mapsto (\varphi_1 + \alpha_1, \varphi_2 + \alpha_2)$$

in accordance with (1). In this notation, a left rotation  $[\exp \alpha i, 1]$  turns out to be a negative translation along the  $45^\circ$  direction:  $T_{-\alpha, -\alpha}$ . A right rotation  $[1, \exp \alpha i]$  is a translation in the  $-45^\circ$  direction:  $R_{\alpha, -\alpha}$ . Arbitrary torus translations can be composed from left and right rotations, and the general translation is written in quaternion notation as

$$R_{\alpha_1, \alpha_2} = [\exp(\frac{-\alpha_1 - \alpha_2}{2} i), \exp(\frac{\alpha_1 - \alpha_2}{2} i)].$$

The torus translations  $R_{\alpha, 0}$  and  $R_{0, \alpha}$  along the  $\varphi_1$  and  $\varphi_2$ -axis are simple rotations, leaving the  $x_2, y_2$ -plane or the  $x_1, y_1$ -plane fixed, respectively.

One should bear in mind that all “translations”, as they appear on the torus, are actually rotations of  $S^3$ . (Only the left and right rotations among them may be called *translations of  $S^3$*  with some justification, because they correspond to the translations in elliptic 3-space.)



symbol	name	$[l, r]$	$(\varphi_1, \varphi_2) \rightarrow$	order	side	det	conj.	mirror
$\square$	identity	$[1, 1]$	$(\varphi_1, \varphi_2)$	1	+	+	—	$\square$
$\square$	horizontal reflection	$*[i, i]$	$(-\varphi_1, \varphi_2)$	2	+	—	$\square$	—
$\square$	vertical reflection	$*[k, k]$	$(\varphi_1, -\varphi_2)$	2	+	—	$\square$	—
$\square$	torus flip $F = \square \cdot \square$	$[j, j]$	$(-\varphi_1, -\varphi_2)$	2	+	+	—	$\square$
$\square$	torus swap $S^+$	$[i, k]$	$(\varphi_2, \varphi_1)$	2	—	+	—	$\square$
$\square$	alternate torus swap $S^-$	$[-k, i]$	$(-\varphi_2, -\varphi_1)$	2	—	+	—	$\square$
$\square$	left swaptorn $\square \cdot \square$	$*[-j, 1]$	$(\varphi_2, -\varphi_1)$	4	—	—	$\square$	—
$\square$	right swaptorn $\square^{-1}$	$*[1, j]$	$(-\varphi_2, \varphi_1)$	4	—	—	$\square$	—

Table 4: The directional parts of the torus symmetries, the elements of the group  $D_8^T$ . Some come in conjugate pairs, as indicated in the column “conj.”, meaning that they are geometrically equivalent. The conjugacy is established by any of the operations  $\square$  or  $\square$  in these cases. The torus flip  $\square$  commutes with all other operations. The last column shows the mirror transformation for each transformation of determinant +1 (the orientation-preserving transformations).

### 7.3.2 The directional group: symmetries with a fixed point

We pick the point  $O = (\sqrt{1/2}, 0, \sqrt{1/2}, 0)$  with torus coordinates  $\varphi_1 = \varphi_2 = 0$  as a reference point or origin on  $\mathbb{T}$ . Every isometry of  $\mathbb{T}$  can be decomposed in a unique way into a symmetry that leaves  $O$  fixed (the *directional part*), plus a torus translation (the *translational part*).

Let us therefore study the symmetries that leave  $O$  fixed. In the plane, these would be all rotations and reflections. However, according to Theorem 7.1 we can only use symmetries that leave the standard square grid  $\mathbb{Z}^2$  invariant, apart from a translation. This allows rotations by multiples of  $90^\circ$ , as well as reflections in the coordinate axes and in the  $45^\circ$ -lines.

In the plane, these seven operations together with the identity form the dihedral group  $D_8$ , the symmetries of the square. We denote the group by  $D_8^T$ , to indicate that we think of the transformations of  $S^3$  that leave the torus  $\mathbb{T}$  invariant. Table 4 summarizes these operations and their properties. For each operation, we have chosen a symbol indicating the axis direction in case of a reflection, or otherwise some suggestive sign, and a name. We also give the quaternion representation, the effect in terms of the  $\varphi_1, \varphi_2$ -coordinates, and the order of the group element.

Some transformations may *swap* the two sides of  $\mathbb{T}$ , exchanging the tori with parameters  $r_1, r_2$  and  $r_2, r_1$ . This is indicated by a “—” in the column “side”, and the names of these operations include the term “swap”. The nonswapping operations leave every torus of the foliation (16) invariant, not just the “central” Clifford torus.

The column “det” indicates whether the operation is orientation-preserving (+) or orientation-reversing (—). One must keep in mind that the operation on the torus  $\mathbb{T}$  induces a transformation of the whole  $S^3$ , and what appears as a reflection in the planar  $\varphi_1, \varphi_2$ -picture of  $\mathbb{T}$  may or may not be an orientation-reversing transformation of  $S^3$ . Thus, it may at first sight come as a surprise that the *torus swap*  $\square$  is orientation-preserving. The reason is that it goes together with a swap of the sides. As shown in Figure 18, it is actually a half-turn around the axis  $S^+$ . (The product of the signs in the “side” and “det” columns tells whether the operation is orientation-preserving when considered purely in the plane.)

Figure 18 makes it clear why there is no “pure swap”, no “inversion” at the central torus that would keep the torus pointwise fixed and swap the two sides of the torus: such a mapping would flip the dashed perpendicular lines and thus map the long side of the rectangular patch on the top to the short side of the rectangular patch at the bottom. We see that a swap is only possible if it goes hand in hand with an exchange of the  $\varphi_1$  and  $\varphi_2$  axes. In particular, such an exchange comes with the rotations by  $\pm 90^\circ$ , the right and left *swaptorn* operations, which are accordingly orientation-reversing.

The column “conj.” indicates operations that are conjugate to each other, i.e., geometrically equivalent. Thus, for example, the operation  $\square$  may, in a different coordinate system, appear as the operation  $\square$ . By contrast,  $\square$  and  $\square$  are distinguished: the axis of  $\square$  belongs to the invariant left Hopf bundle  $\mathcal{H}^i$ , and the axis of  $\square$  belongs to the invariant right Hopf bundle  $\mathcal{H}_i$ . The operations  $\square$  and  $\square$  are mirrors of each other, i.e., conjugate under an orientation-reversing transformation. This is indicated in the last column.

When viewed in isolation, the half-turns  $S^+ = \square$ ,  $S^- = \square$ , and  $F = \square$  are conjugate to each other. However, they are distinct when considering only transformations that leave the torus invariant.

group	name	chirality	swapping	conjugate	mirror
$\square = \{\square\}$	translation	chiral	no	—	$\square$
$\square\square = \{\square, \square\square\}$	reflection	achiral	no	$\square\square$ , by $\square$	—
$\square\square = \{\square, \square\square\}$	reflection	achiral	no	$\square\square$ , by $\square$	—
$\square\cdot = \{\square, \square\cdot\}$	flip	chiral	no	—	$\square\cdot$
$\square\square\square = \{\square, \square\square, \square\square\square\}$	full reflection	achiral	no	—	—
$\square\square = \{\square, \square\square\}$	swap	chiral	yes	—	$\square\square$
$\square\square = \{\square, \square\square\}$	swap	chiral	yes	—	$\square\square$
$\square\square\square = \{\square, \square\square, \square\square\square\}$	full swap	chiral	yes	—	$\square\square\square$
$\square\square\square = \{\square, \square\square, \square\square\square\} \cong C_4$	swaptorn	achiral	yes	—	—
$\square\square\square = \{\square, \square\square, \square\square\square, \square\square\square, \square\square, \square\square, \square\square, \square\square\}$	full torus	achiral	yes	—	—

Table 5: The 10 subgroups of  $D_8^\mathbb{T}$ . A group is achiral if it contains an orientation-reversing transformation. A group is swapping if it contains a transformation that swaps the two sides of the torus. The fifth column shows to which other groups the group is conjugate by an orientation-preserving transformation. The last column shows the mirror group of each chiral group, i.e., the conjugate group by an orientation-reversing transformation. (Each achiral group in this list is its own mirror image.)

### 7.3.3 Choice of coordinate system

The conjugacies discussed above introduces ambiguities in the representation of torus translations, which depend on the choice of the coordinate system for a given invariant torus.  $R_{\alpha_1, \alpha_2}$  may, in a different coordinate system, appear as  $R_{-\alpha_1, -\alpha_2}$  (conjugacy by  $\square$ ), or as  $R_{\alpha_2, \alpha_1}$  (conjugacy by  $\square$ ), or as  $R_{-\alpha_2, -\alpha_1}$  (conjugacy by  $\square$ ). (The operation  $R_{\alpha_1, -\alpha_2}$  or  $R_{-\alpha_1, \alpha_2}$  is its mirror operation.) The choice of origin in the  $\varphi_1, \varphi_2$ -plane, on the other hand, has no influence on the torus translations. It only affects the other operations.

### 7.3.4 The directional group and the translational subgroup

We have mentioned that every symmetry of the torus can be decomposed in a unique way (after fixing an origin) into a directional part and a translational part.

For a group  $G$ , the torus translations contained in it form a normal subgroup, the *translational subgroup*, which we denote by  $G_\square$ . The directional parts of the group operations form the *directional group* of  $G$ . It is a subgroup of  $D_8^\mathbb{T}$ , and we will use it as a coarse classification of the toroidal groups. (The directional group is isomorphic to the factor group  $G/G_\square$ .)

The ten subgroups of  $D_8^\mathbb{T}$  are listed in Table 5, together with a characteristic symbol and a name. Figure 19 shows their pictorial representation.

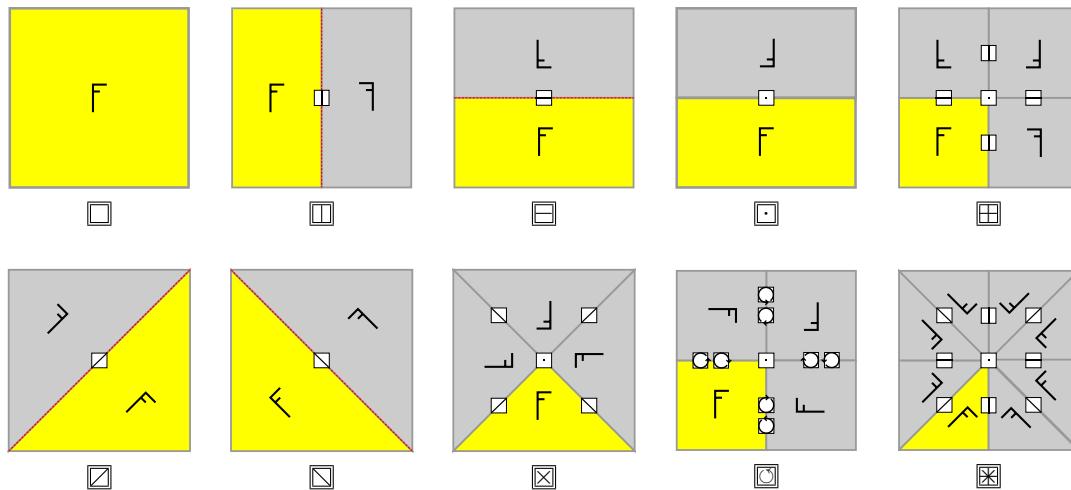


Figure 19: The 10 subgroups of  $D_8^\mathbb{T}$ . See Table 5.

The following lemma is useful in order to restrict the translational subgroup for a given directional group.

**Lemma 7.3.** *For a group  $G$  of torus symmetries, the translational subgroup  $G_{\square}$  is closed under every symmetry in the directional group of  $G$ .*

*Proof.* Assume that  $t \in G_{\square}$ , and we have an operation in  $G/G_{\square}$  that is represented by an orthogonal  $2 \times 2$  matrix  $A$ . This means that  $G$  contains some transformation  $x \mapsto Ax + b$ . If we conjugate the translation  $x \mapsto x + t$  with this transformation, we get  $x \mapsto A(A^{-1}(x - b) + t) + b = x + At$ , i.e., a translation by  $At$ .  $\square$

## 7.4 Overview of the toroidal groups

After fixing the directional group, we have to look at the translational subgroup, and the interaction between the two. The result is summarized as follows.

**Proposition 7.4.** *The 4-dimensional point groups that have an invariant torus can be classified into 25 infinite families of toroidal groups, among them*

- 2 three-parameter families
- 19 two-parameter families
- 4 one-parameter families

as shown in Table 6.

The last column of Table 6 shows the names of these groups in the classification of Conway and Smith.<sup>14</sup> We make a comparison in Section 7.12.

There is one difficulty that we have not addressed: We look at the groups that leave one particular Clifford torus invariant. However, there are some groups, in particular small groups, that have several invariant Clifford tori. This leads to ambiguities. For example, a torus translation by  $180^\circ$  on one torus may appear as a swaptorn  $\square$  on a different torus. We investigate these cases in detail in Section 7.11.

The natural constraint on the parameters  $m$  and  $n$  is  $m, n \geq 1$  in all cases of Table 6, in the sense that all these choices (in a few cases under the additional constraint that  $m \equiv n \pmod{2}$ ) lead to valid groups. (But note that some extra evenness constraints are already built into the notation, for example, when we write  $\square_{2m, 2n}^{\text{pm}}$  instead of  $\square_{m, n}^{\text{pm}}$ .) For the swaptorn groups  $\square_{a, b}$ , the natural choices are  $a, b \geq 0$  except for  $(a, b) = (0, 0)$ . The stricter conditions on  $m$  and  $n$  in Table 6 are imposed in order to exclude duplications.

We will now go through the categories one by one. This closely parallels the classification of the wallpaper groups. When appropriate, we use the established notations for wallpaper groups to distinguish the torus groups. We have to choose suitable parameters for the different dimensions of each wallpaper group, and in some cases, we have to refine the classification of wallpaper groups because different axis directions are distinguished.

## 7.5 The torus translation groups, type $\square$

These are the groups that contain only torus translations. The pure translation groups are the simplest class, but they are also the richest type of groups, requiring three parameters for their description. The translations  $(\alpha_1, \alpha_2)$  with  $R_{\alpha_1, \alpha_2} \in G$  form an additive group modulo  $(2\pi, 2\pi)$ , and hence a lattice modulo  $(2\pi, 2\pi)$ . In accordance with Theorem 7.1 we can also view it as a lattice in the plane that contains all points whose coordinates are multiples of  $2\pi$ , see Figure 20.

We parameterize these lattices with three parameters  $m, n, s$ : The lattice subdivides the principal diagonal from  $(0, 0)$  to  $(2\pi, 2\pi)$  into some number  $m \geq 1$  of segments. Then we choose  $t_1 = (\frac{2\pi}{m}, \frac{2\pi}{m})$  as the first generator of the lattice. The second parameter  $n \geq 1$  is the number of lattice lines parallel to the principal diagonal that run between  $(0, 0)$  and  $(2\pi, 0)$ , including the last one through  $(2\pi, 0)$ . In the figure, we have  $m = 2$  and  $n = 5$ . On each such line, the points are equidistant with distance  $\frac{2\pi}{m} \cdot \sqrt{2}$ . The first parallel lattice line thus contains a unique point  $t_2 = (\frac{\pi}{n}, -\frac{\pi}{n}) + (x, x)$  with  $0 \leq x < \frac{2\pi}{m}$ , and we choose  $x$  as the third parameter. The range from which  $t_2$  can be chosen is indicated by a double arrow in the figure.

<sup>14</sup>To get a closer correspondence with our parameterization for the groups of type  $\square$  and  $\square$  in the first two rows, we swap the role of the left and right factors in the generators given in Conway and Smith. Effectively, we consider the mirror groups. Accordingly, we have adapted the Conway–Smith convention of writing  $\frac{1}{f}[C_m \times C_n^{(s)}]$ , by decorating the *left* factor with the parameter  $s$ . More details are given in Appendix G.

group	order	parameters	names in Conway–Smith [8, Tables 4.1–4.3]		
torus translation groups (chiral, wallpaper group <b>p1</b> )					
$\square_{m,n}^{(s)}$	$mn$	$m, n \geq 1, -\frac{m}{2} \leq s \leq \frac{n-m}{2}$	$m \equiv 0 \pmod{2}$ : $\pm \frac{1}{f}[C_{mf/2}^{(s')} \times C_n]$ $m \equiv 1 \pmod{2}$ : $\pm \frac{1}{f}[C_{mf}^{(s')} \times C_n]$		
torus flip groups (chiral, wallpaper group <b>p2</b> )					
$\square_{m,n}^{(s)}$	$2mn$	$m, n \geq 1, -\frac{m}{2} \leq s \leq \frac{n-m}{2}$ $(m, n) \neq (1, 1), (2, 1)$	$m \equiv 0 \pmod{2}$ : $\pm \frac{1}{2f}[D_{mf}^{(f-s')} \times D_{2n}]$ $m \equiv 1 \pmod{2}$ : $\pm \frac{1}{2f}[D_{2mf}^{(2f-s')} \times D_{2n}]$		
torus swap groups (chiral)			$n$ even	$n$ odd	
$\square_{2m,2n}^{\mathbf{pm}}$	$4mn$	$m, n \geq 2$	$\pm[D_{2m} \times C_n]$	$\pm\frac{1}{2}[D_{2m} \times C_{2n}]$	
$\square_{2m,2n}^{\mathbf{pg}}$	$4mn$	$m \geq 2, n \geq 1$	$\pm\frac{1}{2}[D_{2m} \times C_{2n}]$	$\pm[D_{2m} \times C_n]$	
$\square_{m,n}^{\mathbf{cm}}$	$2mn$	$m \geq 3, n \geq 2, m - n$ even	$\pm\frac{1}{2}[\overline{D}_{2m} \times C_n]$	$\pm\frac{1}{2}[D_{2m} \times C_{2n}]$	
$\square_{2m,2n}^{\mathbf{pm}}$	$4mn$	$m, n \geq 2$	mirrors of the groups $\square_{2n,2m}^{\mathbf{pm}}$		
$\square_{2m,2n}^{\mathbf{pg}}$	$4mn$	$m \geq 1, n \geq 2$	mirrors of the groups $\square_{2n,2m}^{\mathbf{pg}}$		
$\square_{m,n}^{\mathbf{cm}}$	$2mn$	$m \geq 2, n \geq 3, m - n$ even	mirrors of the groups $\square_{n,m}^{\mathbf{cm}}$		
full torus swap groups (chiral)			$m$	$n$ even	$n$ odd
$\square_{2m,2n}^{\mathbf{p2mm}}$	$8mn$	$m, n \geq 2$	$m$ even	$\pm[D_{2m} \times D_{2n}]$	$\pm\frac{1}{2}[D_{2m} \times \overline{D}_{4n}]$
			$m$ odd	$\pm\frac{1}{2}[\overline{D}_{4m} \times D_{2n}]$	$\pm\frac{1}{4}[D_{4m} \times \overline{D}_{4n}]$
$\square_{2m,2n}^{\mathbf{p2mg}}$	$8mn$	$m, n \geq 2$	$m$ even	$\pm\frac{1}{2}[D_{2m} \times \overline{D}_{4n}]$	$\pm[D_{2m} \times D_{2n}]$
			$m$ odd	$\pm\frac{1}{4}[D_{4m} \times \overline{D}_{4n}]$	$\pm\frac{1}{2}[\overline{D}_{4m} \times D_{2n}]$
$\square_{2m,2n}^{\mathbf{p2gm}}$	$8mn$	$m, n \geq 2$	$m$ even	$\pm\frac{1}{2}[\overline{D}_{4m} \times D_{2n}]$	$\pm\frac{1}{4}[D_{4m} \times \overline{D}_{4n}]$
			$m$ odd	$\pm[D_{2m} \times D_{2n}]$	$\pm\frac{1}{2}[D_{2m} \times \overline{D}_{4n}]$
$\square_{2m,2n}^{\mathbf{p2gg}}$	$8mn$	$m, n \geq 2$	$m$ even	$\pm\frac{1}{4}[D_{4m} \times \overline{D}_{4n}]$	$\pm\frac{1}{2}[\overline{D}_{4m} \times D_{2n}]$
			$m$ odd	$\pm\frac{1}{2}[D_{2m} \times \overline{D}_{4n}]$	$\pm[D_{2m} \times D_{2n}]$
$\square_{m,n}^{\mathbf{c2mm}}$	$4mn$	$m, n \geq 3, m - n$ even	$m \equiv n$	$\pm\frac{1}{2}[\overline{D}_{2m} \times \overline{D}_{2n}]$	$\pm\frac{1}{4}[D_{4m} \times \overline{D}_{4n}]$
torus reflection groups (achiral)					
$\square_{m,n}^{\mathbf{pm}}$	$2mn$	$m, n \geq 1$	$\left\{ \begin{array}{l} + \text{ or } \pm \frac{1}{f}[C_{n'f} \times C_{n'f}^{(s)}] \cdot 2^{(0)} \text{ or} \\ + \frac{1}{f}[C_{n'f} \times C_{n'f}^{(s)}] \cdot 2^{(2)} \\ + \text{ or } \pm \frac{1}{f}[C_{n'f} \times C_{n'f}^{(s)}] \cdot 2^{(1)} \text{ or} \\ + \frac{1}{f}[C_{n'f} \times C_{n'f}^{(s)}] \cdot 2^{(0)} \end{array} \right.$ $\pm \frac{1}{f}[C_{n'f} \times C_{n'f}^{(s)}] \cdot 2^{(0)} \text{ or } + \frac{1}{f}[C_{n'f} \times C_{n'f}^{(s)}] \cdot 2^{(0)}$		
$\square_{m,n}^{\mathbf{pg}}$	$2mn$	$m, n \geq 1$			
$\square_{m,n}^{\mathbf{cm}}$	$4mn$	$m, n \geq 1$			
full torus reflection groups (achiral)					
$\square_{m,n}^{\mathbf{p2mm}}$	$4mn$	$m \geq n \geq 1, (m, n) \neq (1, 1)$	$\left\{ \begin{array}{l} \pm \frac{1}{2f}[D_{2n'f} \times D_{2n'f}^{(s)}] \cdot 2^{(\alpha,\beta)} \text{ or} \\ + \frac{1}{2f}[D_{2n'f} \times D_{2n'f}^{(s)}] \cdot 2^{(\alpha,\beta)} \end{array} \right.$ $\pm \text{ or } + \frac{1}{2f}[D_{2n'f} \times D_{2n'f}^{(s)}] \cdot 2^{(0,0)}$		
$\square_{m,n}^{\mathbf{p2mg}}$	$4mn$	$m, n \geq 1, (m, n) \neq (1, 1)$			
$\square_{m,n}^{\mathbf{p2gg}}$	$4mn$	$m \geq n \geq 1, (m, n) \neq (1, 1)$			
$\square_{m,n}^{\mathbf{c2mm}}$	$8mn$	$m \geq n \geq 1, (m, n) \neq (1, 1)$			
torus swapturn groups (achiral, wallpaper group <b>p4</b> )					
$\square_{a,b}$	$4(a^2+b^2)$	$a \geq b \geq 0$ $a \geq 2, (a, b) \neq (2, 0)$	$a \equiv b \pmod{2}$ : $\pm \frac{1}{2f}[D_{2nf} \times D_{2nf}^{(s)}] \cdot \overline{2}$ $a \not\equiv b \pmod{2}$ : $\pm \frac{1}{2f}[D_{2nf} \times D_{2nf}^{(s)}] \cdot \overline{2}$		
full torus groups (achiral)			$n$ even	$n$ odd	
$\square_n^{\mathbf{p4mmU}}$	$8n^2$	$n \geq 3$	$\pm\frac{1}{2}[\overline{D}_{2n} \times \overline{D}_{2n}] \cdot 2$	$\pm\frac{1}{4}[D_{4n} \times \overline{D}_{4n}] \cdot 2_1$	
$\square_n^{\mathbf{p4gmU}}$	$8n^2$	$n \geq 3$	$\pm\frac{1}{2}[\overline{D}_{2n} \times \overline{D}_{2n}] \cdot \overline{2}$	$\pm\frac{1}{4}[D_{4n} \times \overline{D}_{4n}] \cdot 2_3$	
$\square_n^{\mathbf{p4mmS}}$	$16n^2$	$n \geq 2$	$\pm[D_{2n} \times D_{2n}] \cdot 2$	$\pm\frac{1}{4}[D_{4n} \times \overline{D}_{4n}] \cdot 2$	
$\square_n^{\mathbf{p4gmS}}$	$16n^2$	$n \geq 2$	$\pm\frac{1}{4}[D_{4n} \times \overline{D}_{4n}] \cdot 2$	$\pm[D_{2n} \times D_{2n}] \cdot 2$	

Table 6: Overview of the toroidal groups. In the Conway–Smith names, we write  $n'$  and  $s'$  when these parameters don't directly correspond to our parameters  $n, s$ .

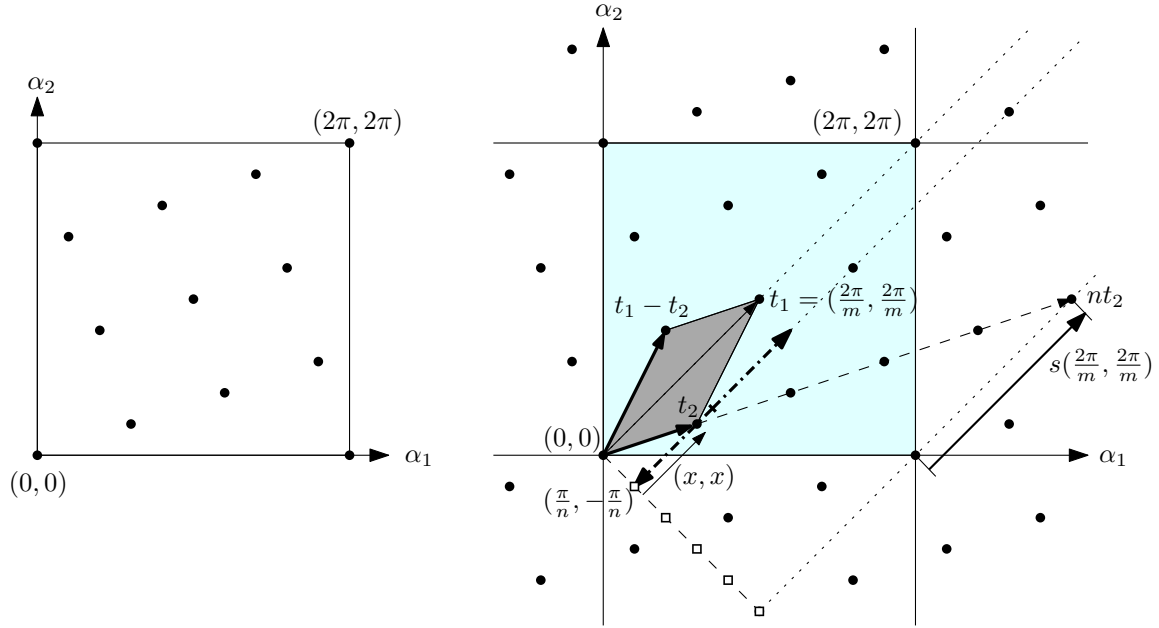


Figure 20: A lattice of torus translations. In the right part, we see that it is given by the parameters  $m = 2$ ,  $n = 5$ , and  $s = 1$ . The vectors  $t_1 = (\pi, \pi)$  and  $t_2 = (\frac{\pi}{5}, -\frac{\pi}{5}) + (\frac{2\pi}{5}, \frac{2\pi}{5}) = (\frac{3\pi}{5}, \frac{\pi}{5})$  generate the group  $\square_{2,5}^{(1)}$ . This lattice happens to be a square lattice, but this plays no role.

We still have to take into account the ambiguity from the choice of the coordinate system (Section 7.3.3). The choice of origin is no problem, since a translation does not depend on the origin. Also, the “flip” ambiguity from  $\square$  is no problem at all: Rotating the coordinate system by  $180^\circ$  maps the lattice to itself. The “swap” ambiguity from  $\square$ , however, is more serious, as it exchanges the coordinate axes:  $\alpha_1 \leftrightarrow \alpha_2$ . (From  $\square$ , we get no extra ambiguity, since  $\square = \square \cdot \square$ .)

To eliminate this ambiguity, we look at the vectors  $t_1 - t_2$  and  $t_2$ . They form also a lattice basis, and they span a parallelogram whose diagonal  $t_1$  lies on the  $\alpha_1 = \alpha_2$  axis. The alternate choice of the basis will reflect the parallelogram at this diagonal. Thus, the choices  $x$  and  $\frac{2\pi}{m} - x$  will lead to the same group. We can achieve a unique representative by stipulating that  $t_2$  is not longer than  $t_1 - t_2$ . This means that we restrict  $t_2$  to the lower half of the range, including the midpoint, which is marked in the figure:  $0 \leq x \leq \frac{\pi}{m}$ .<sup>15</sup>

Finally, we look at the point  $nt_2$ , which lies on the  $45^\circ$  line through  $(2\pi, 0)$ . We have to ensure that it is one of the existing lattice points on this line because additional points would contradict the choice of  $m$ . Thus

$$nt_2 = (\pi, -\pi) + (nx, nx) = (2\pi, 0) + s(\frac{2\pi}{m}, \frac{2\pi}{m})$$

for some integer  $s$ , or in other words

$$x = \frac{\pi}{n} + s \cdot \frac{2\pi}{mn}$$

Combining this with the constraint  $0 \leq x \leq \frac{\pi}{m}$ , we get

$$-\frac{m}{2} \leq s \leq -\frac{m}{2} + \frac{n}{2} \quad (20)$$

This range contains  $\lceil \frac{n}{2} \rceil$  integers if  $m$  is odd and  $\lceil \frac{n+1}{2} \rceil$  integers if  $m$  is even. In particular, there is always at least one possible value  $s$ .

<sup>15</sup>This easy way of dealing with the duplications caused by  $\square$  is the reason for preferring the oblique axes of Figure 20 for measuring the parameters  $m$  and  $n$  over the more natural  $\alpha_1, \alpha_2$ -axes. This oblique system is also aligned with the specification of the group by its left and right group (of left translations and right translations) that underlies the classic classification, see Appendix G. Curiously, these duplications caused by  $\square$  were overlooked by Conway and Smith [8], although they had escaped none of the previous classifications [20, p. 62, groupe I], [35, p. 20, item §1, formula (2)], [15, p. 55, first paragraph].

**Proposition 7.5.** *The point groups that contain only torus translations can be classified as follows:*

*For any integers  $m, n \geq 1$  and any integer  $s$  in the range (20), there is one such group, the torus translation group  $\square_{m,n}^{(s)}$ , of order  $mn$ . It is generated by  $R_{\frac{2\pi}{m}, \frac{2\pi}{m}}$  and  $R_{\frac{2\pi}{n} + \frac{2s\pi}{mn}, \frac{2s\pi}{mn}}$ .*

In terms of quaternions, these generators are  $[\exp(-\frac{2\pi}{m}i), 1]$  and  $[\exp(-\frac{(m+2s)\pi}{mn}i), \exp \frac{\pi i}{n}]$ . We emphasize that the two parameters  $m$  and  $n$  play different roles in this parameterization, and there is no straightforward way to read off the parameters of the mirror group from the original parameters  $m, n, s$ . (See for example the entries 11/01 and 11/02 in Table 17.)

We have observed above that  $x$  and  $x' = \frac{2\pi}{m} - x$  lead to the same group, and the same is true for  $x' = \frac{2\pi}{m} + x$ . In terms of  $s$  this means that the parameters  $s' = -m - s$  and  $s' = s + n$  lead to the same group as  $s$ . In Section 7.11, when we discuss duplications, it will be convenient to allow values  $s$  outside the range (20). In particular, it is good to remember that  $s = 0$  corresponds to a generating point on the  $\alpha_1$ -axis.

### 7.5.1 Dependence on the starting point

**Proposition 7.6.** *Any two full-dimensional orbits of a toroidal translation group are linearly equivalent.*

*Proof.* Let  $G$  be a toroidal translation group. We will show that any full-dimensional  $G$ -orbit can be obtained from the  $G$ -orbit of the point  $(\frac{1}{\sqrt{2}}, 0, \frac{1}{\sqrt{2}}, 0)$  by applying an invertible linear transformation.

Let  $v \in \mathbb{R}^4$  be a point whose  $G$ -orbit is full-dimensional. This is equivalent to requiring that the projections of  $v$  to the  $x_1, y_1$ -plane and to the  $x_2, y_2$ -plane are not zero. We can map  $v$  to a point  $v'$  of the form  $(r_1, 0, r_2, 0)$ , with  $r_1 \neq 0$  and  $r_2 \neq 0$ , by applying a rotation of the form

$$R_{\alpha_1, \alpha_2} = \begin{pmatrix} R_{\alpha_1} & 0 \\ 0 & R_{\alpha_2} \end{pmatrix}. \quad (21)$$

The new point  $v'$  can be mapped to the point  $(\frac{1}{\sqrt{2}}, 0, \frac{1}{\sqrt{2}}, 0)$  by applying a matrix of the form

$$\text{diag}(\lambda_1, \lambda_1, \lambda_2, \lambda_2) = \begin{pmatrix} \lambda_1 & 0 & 0 & 0 \\ 0 & \lambda_1 & 0 & 0 \\ 0 & 0 & \lambda_2 & 0 \\ 0 & 0 & 0 & \lambda_2 \end{pmatrix}. \quad (22)$$

Since torus translations commute with the linear transformations (21) and (22), we are done.  $\square$

Frieder and Ladisch [17, Proposition 6.3 and Corollary 8.4] proved that the same conclusion holds for any abelian group: All full-dimensional orbits are linearly equivalent to each other in this case.

## 7.6 The torus flip groups, type $\square$

These groups are generated by torus translations together with a single torus flip. Adding the flip operation is completely harmless. Conjugation with a flip changes  $R_{\alpha_1, \alpha_2}$  to  $R_{-\alpha_1, -\alpha_2}$ , and therefore does not change the translation lattice at all. The order of the group doubles.

If we choose the origin at the center of a 2-fold rotation induced by a torus flip, then  $\square_{m,n}^{(s)}$  is generated by

$$[\exp(-\frac{2\pi i}{m}), 1], [\exp(-\frac{(m+2s)\pi i}{mn}), \exp \frac{\pi i}{n}], [j, j].$$

## 7.7 Groups that contain only one type of reflection

These are the torus reflection groups  $\square$  and  $\square$ , as well as the torus swap groups  $\square$  and  $\square$ . The groups of type  $\square$  and  $\square$  are geometrically the same, because  $\square$  (or  $\square$ ) exchanges vertical mirrors with horizontal mirrors. Thus, Table 6 contains no entries for  $\square$ . The groups  $\square$  and  $\square$  are mirrors, and their treatment is similar.

If the directional part of a transformation is a reflection (in the plane), the transformation itself can be either a reflection or a glide reflection. In both cases there is an invariant line. We will classify the groups by placing a letter F on the invariant line and looking at its orbit.

We need a small lemma that is familiar from the classification of the wallpaper groups:

**Lemma 7.7.** *If a two-dimensional lattice has an axis of symmetry, then the lattice is either*

- (1) *a rectangular lattice that is aligned with the axis, or*
- (2) *a rhombic lattice, which contains in addition the midpoints of the rectangles.*

*In case (1), the symmetry axis goes through a lattice line or half-way between two lattice lines. In case (2), the symmetry axis goes through a lattice line.*

For an example, see the upper half of Figure 22, where the mirror lines are drawn as solid lines.

*Proof.* Assume without loss of generality that the symmetry axis is the  $y$ -axis. (We may have to translate the lattice so that it no longer contains the origin.) With every lattice point  $(x, y)$ , the lattice contains also the mirror point  $(-x, y)$ , and thus  $(2x, 0)$  is a horizontal lattice vector. It follows that there must be a lattice point  $(x_0, y_0)$  with smallest positive  $x$ -coordinate, since otherwise there would be arbitrarily short lattice vectors.

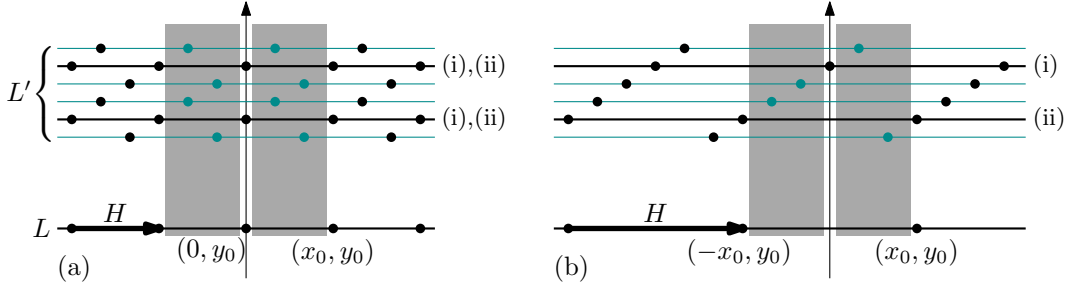


Figure 21: Different possibilities for the lattice line  $L'$ . The gray area is forbidden.

Consider the horizontal lattice line  $L$  through  $(x_0, y_0)$ . There are two cases, see Figure 21. (a)  $(0, y_0)$  is also a lattice point, and  $(H, 0) = (x_0, 0)$  is a lattice basis vector. (b)  $(0, y_0)$  is not a lattice point, and  $(H, 0) = (2x_0, 0)$  is a lattice basis vector. Now look at the next-higher horizontal lattice line  $L'$  above  $L$ , and choose a lattice point  $(x', y')$  on  $L'$ .  $L'$  contains the points  $(x' + kH, y')$  for  $k \in \mathbb{Z}$ , and therefore a point  $(x, y')$  in the interval  $-H/2 \leq x \leq H/2$ . The value of  $x$  cannot be in the range  $-x_0 < x < 0$  or  $0 < x < x_0$  because this would contradict the choice of  $(x_0, y_0)$ . Thus, either (i)  $x = 0$  or (ii) both points  $(\pm x_0, y')$  are in the lattice. In case (a), both possibilities (i) and (ii) hold simultaneously, and this leads to a rectangular lattice with the axis through lattice points. If (b) and (ii) holds, we have a rectangular lattice with the axis between lattice lines. If (b) and (i) holds, we have a rhombic lattice.  $\square$

### 7.7.1 The torus reflection groups, type $\square$

We distinguish two major cases.

- M) The group contains a mirror reflection.
- G) The group contains only glide reflections.

In both cases, every orientation-reversing transformation has a vertical invariant line. (Actually, since the translation  $\varphi_1 \mapsto \varphi_1 + 2\pi$  is always an element of the group, by Theorem 7.1, the invariant lines come in pairs  $\varphi_1 = \beta$  and  $\varphi_1 = \beta + \pi$ .)

As announced, we observe the orbit of the letter F. We put the bottom endpoint of the F on an invariant line  $\ell$ . First we look at the orbit under those transformations that leave  $\ell$  invariant, see the left side of Figure 22. In case G, the images with and without reflection alternate along  $\ell$ . In case M, they are mirror images of each other.

In case M, we have a mirror symmetry, and by Lemma 7.3, the translational subgroup must be closed under the mirror symmetry. Lemma 7.7 gives the two possibilities of a rectangular or a rhombic translational subgroup. Combining these translations with the mirror operations leads to the two cases in the top row of Figure 22.

In case G, we cannot apply Lemma 7.7 right away. Let  $H$  be the vertical distance between consecutive points on the axis. If we combine each glide reflection with a vertical translation by  $-H$ , we get mirror reflections, as in case M. To this modified group, we can apply Lemma 7.7, and we conclude that the translational group must either form a rectangular or a rhombic pattern. Adding back the translation by  $H$  to the orientation-reversing transformations leads to the results

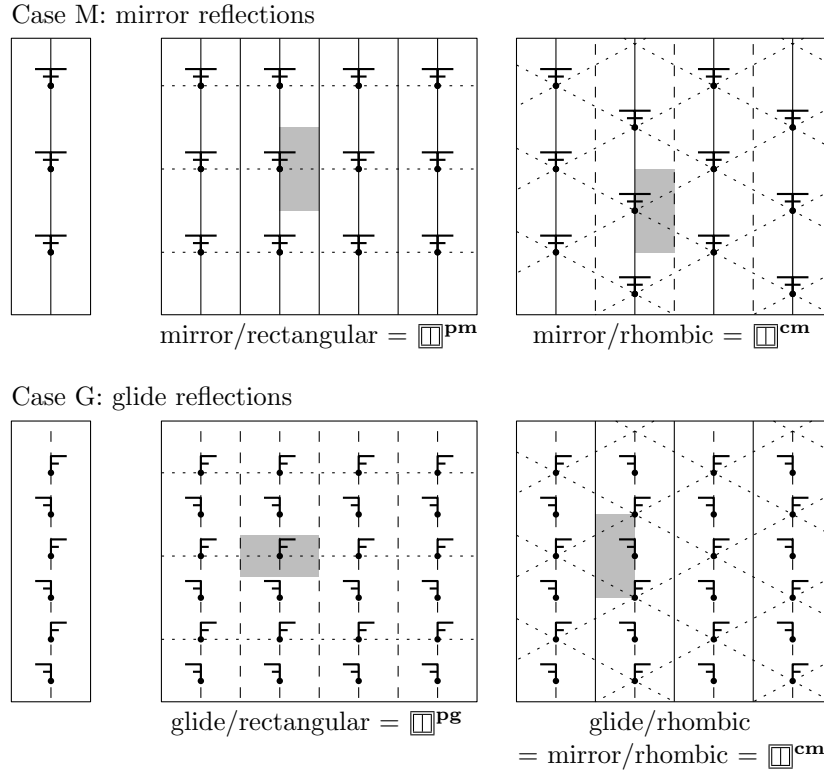


Figure 22: Torus reflection groups, type  $[mm]$ . Combinations of a vertical mirror/glide reflection axis with either a rectangular or a rhombic grid. Invariant lines are shown as solid lines if they act as mirrors, otherwise dashed. The dotted lines indicate the lattice of translations, and the shaded area is a fundamental domain.

in the lower row of Figure 22. In the rhombic case in the lower right picture we see that, when we try to combine glide reflections with a rhombic translational subgroup, we generate mirror symmetries, and thus, this case really belongs to case M. The picture looks different from the corresponding picture in the upper row because there are two alternating types of invariant lines: mirror lines, and lines with a glide reflection. Depending on where we put the F, we get different pictures.

We are thus left with three cases, which we denote by superscripts that are chosen in accordance with the International Notation for these wallpaper groups:

- mirror/rectangular:  $[mm]^{pm}$ ,
- mirror/rhombic:  $[mm]^{cm}$ , and
- glide/rectangular:  $[mg]^{pg}$ .

The groups are parameterized by two parameters  $m \geq 1$  and  $n \geq 1$ , the dimensions of the rectangular grid of translations in the  $\varphi_1$  and  $\varphi_2$  directions, see the left part of Figure 23.

Since the invariant lines give a distinguished direction, we need not worry about duplications when exchanging  $m$  and  $n$ . The order of each group  $G$  is twice the order of the translational subgroup  $G_{\square}$ .

### 7.7.2 The torus swap groups

For the groups of type  $[m]$ , we have to turn the picture by  $45^\circ$ . We have the same three cases,  $[m]^{pm}$ ,  $[m]^{cm}$ , and  $[m]^{pg}$ , but we must adapt the definition of  $m$  and  $n$ , see the right part of Figure 23. We divide the principal diagonal from  $(0,0)$  to  $(2\pi, 2\pi)$  into  $m$  parts and the secondary diagonal from  $(0,0)$  to  $(2\pi, -2\pi)$  into  $n$  parts. We cannot choose  $m$  and  $n$  freely because the midpoint  $(2\pi, 0)$  of the square spanned by these two diagonal directions, which represents the identity mapping, is always part of the lattice. Therefore, for the rectangular lattice cases  $[m]^{pm}$  and  $[m]^{pg}$ ,  $m$  and  $n$  must be even, and the number of lattice points on the torus is  $mn/2$ . (We loose a factor of 2 compared to  $[m]$ , because the tilted square in the figure covers the torus twice.) For the rhombic lattice case  $[m]^{cm}$ ,  $m$  and  $n$  must have the same parity, and the number of lattice points on the torus is  $mn$ .



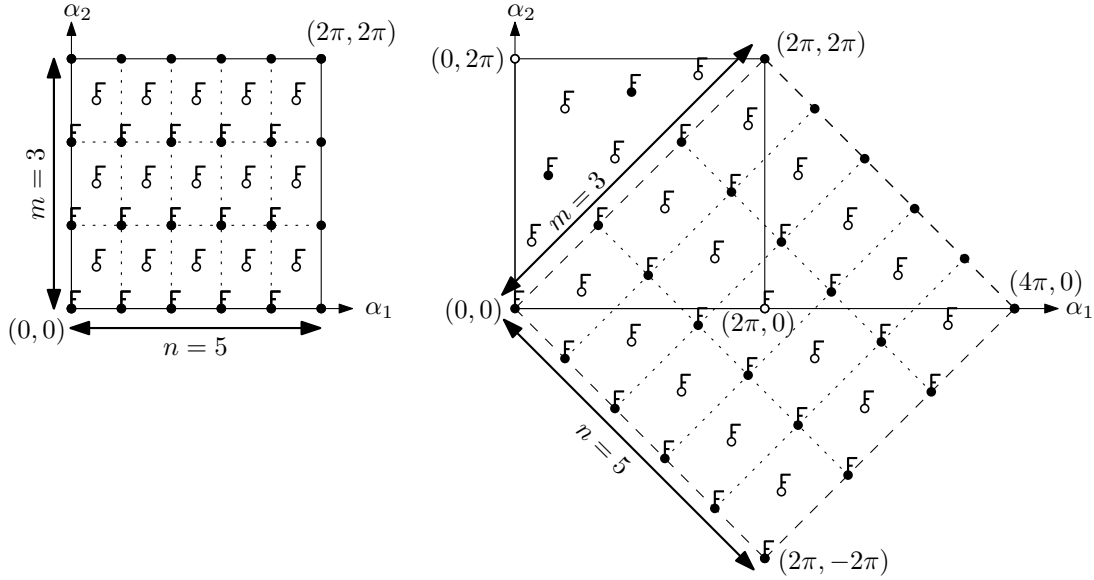


Figure 23: Left: Parameters for the translational subgroup of the groups with vertical invariant lines, type  $\square$ . We divide the vertical axis into  $m$  equal parts and the horizontal axis into  $n$  equal parts. In the rectangular case, the grid consists only of the  $mn$  black points. In the rhombic case, the white points are also present, for  $2mn$  translations in total.

Right: For the groups of type  $\square$ , the axes are tilted clockwise by  $45^\circ$  and longer by the factor  $\sqrt{2}$ .

We mention that the parameter  $m$  in this case coincides with the parameter  $m$  for the translations-only case  $\square$  of Figure 20. The parameter  $n$  coincides in the rhombic case; in the rectangular case, it is twice as big.

As mentioned, the groups of type  $\square$  are mirrors of the groups of type  $\square$ , and we need not discuss them separately.

**Generators for  $\square$ ,  $\square$  and  $\square$ .** Whenever a mirror line exists (**cm** and **pm**), we choose the origin of the coordinate system on such a line; otherwise (**pg**), we place it on an axis of glide reflection. With these conventions, the groups can be generated by the generators listed in Table 7.

group	generators
$\square_{m,n}^{\text{pm}}$	$[e^{\frac{\pi i}{m}}, e^{\frac{\pi i}{n}}], [e^{\frac{\pi i}{n}}, e^{-\frac{\pi i}{n}}], *[i, i]$
$\square_{m,n}^{\text{pg}}$	$[e^{\frac{\pi i}{m}}, e^{\frac{\pi i}{n}}], [e^{\frac{\pi i}{n}}, e^{-\frac{\pi i}{n}}], *[i, i][e^{\frac{\pi i}{2m}}, e^{\frac{\pi i}{2n}}]$
$\square_{m,n}^{\text{cm}}$	$[e^{\frac{\pi i}{m}}, e^{\frac{\pi i}{n}}], [e^{\frac{\pi i}{n}}, e^{-\frac{\pi i}{n}}], [e^{\frac{\pi i}{2m} + \frac{\pi i}{2n}}, e^{\frac{\pi i}{2m} - \frac{\pi i}{2n}}], *[i, i]$
$\square_{2m,2n}^{\text{pm}}$	$[e^{\frac{\pi i}{m}}, 1], [1, e^{\frac{\pi i}{n}}], [-k, i]$
$\square_{2m,2n}^{\text{pg}}$	$[e^{\frac{\pi i}{m}}, 1], [1, e^{\frac{\pi i}{n}}], [1, e^{\frac{\pi i}{2n}}] [-k, i]$
$\square_{m,n}^{\text{cm}}$	$[e^{\frac{i2\pi}{m}}, 1], [1, e^{\frac{i2\pi}{n}}], [e^{\frac{\pi i}{n}}, e^{\frac{\pi i}{m}}], [-k, i]$
$\square_{2m,2n}^{\text{pm}}$	$[e^{\frac{\pi i}{m}}, 1], [1, e^{\frac{\pi i}{n}}], [i, k]$
$\square_{2m,2n}^{\text{pg}}$	$[e^{\frac{\pi i}{m}}, 1], [1, e^{\frac{\pi i}{n}}], [e^{\frac{\pi i}{2m}}, 1][i, k]$
$\square_{m,n}^{\text{cm}}$	$[e^{\frac{i2\pi}{m}}, 1], [1, e^{\frac{i2\pi}{n}}], [e^{\frac{\pi i}{n}}, e^{\frac{\pi i}{m}}], [i, k]$

Table 7: Generators for torus reflection groups and torus swap groups

## 7.8 The torus swaptorn groups, type $\square$

By Lemma 7.3, the lattice of translations must be a square grid. The left part of Figure 24 shows how we parameterize a square grid on the torus. We take the sides  $a \geq 0$  and  $b \geq 0$  of the grid rectangle spanned by the two points  $(0, 0)$  and  $(2\pi, 0)$ , measured in grid units. Since  $(0, b)$  leads to the same grid rectangle as  $(b, 0)$ , we require  $a \geq 1$ .

Conjugation by  $\square$  reflects the grid at the principal diagonal. Since the grid is symmetric under  $90^\circ$  rotations, this has the same effect as reflection at a vertical axis, and it is easy to see

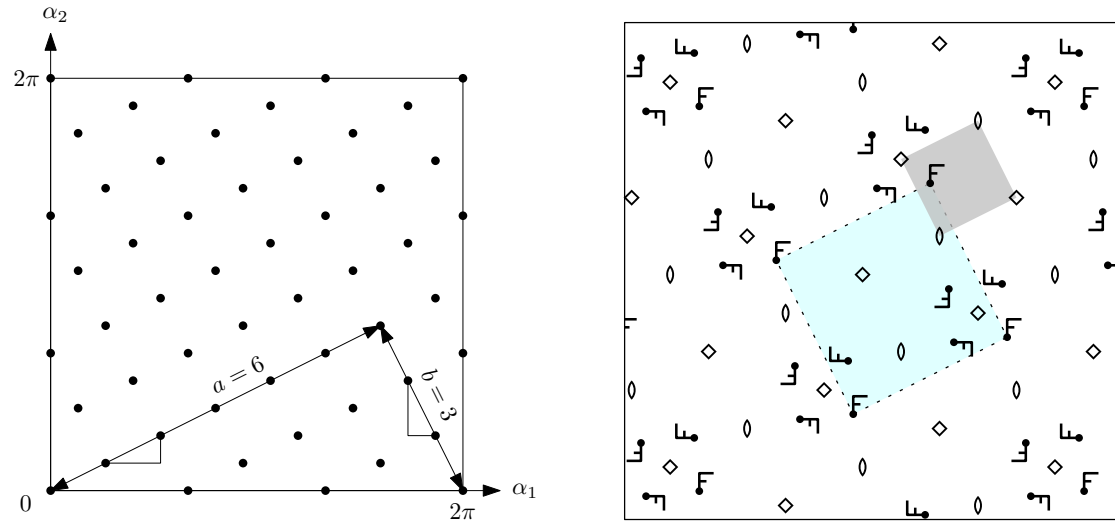


Figure 24: Left: Parameterizing a square grid. Right: The wallpaper group  $\mathbf{p4}$  corresponding to the groups  $\square$ . The centers of 4-fold rotations are marked by diamonds, the centers of 2-fold rotations are marked by “digons” in the form of a lense. The dotted light-blue square indicates the square lattice of the subgroup of translations, arbitrarily anchored at an upright F.

that such a reflection swaps the parameters  $a$  and  $b$ . Thus,  $(a, b)$  and  $(b, a)$  describe the same group, and we can assume  $a \geq b$  without loss of generality.

The number of grid points, i.e., the size of the translational subgroup, is  $a^2 + b^2$ , and the order is  $4(a^2 + b^2)$ . The right part of Figure 24 shows the various centers of 2-fold and 4-fold rotations, and a typical orbit. This corresponds to the wallpaper group  $\mathbf{p4}$ .

The grid is generated by the two orthogonal vectors  $(\alpha_1, \alpha_2) = 2\pi(\frac{a}{a^2+b^2}, \frac{b}{a^2+b^2})$  and  $(\alpha_1, \alpha_2) = 2\pi(\frac{b}{a^2+b^2}, -\frac{a}{a^2+b^2})$ , with  $c = \sqrt{a^2 + b^2}$ . If we choose the origin at the center of a 4-fold rotation induced by a swapturn, then  $\square_{a,b}$  can be generated by

$$[\exp(\frac{(-a-b)\pi i}{a^2+b^2}), \exp(\frac{(a-b)\pi i}{a^2+b^2})], [\exp(\frac{(a-b)\pi}{a^2+b^2}), \exp(\frac{(a+b)\pi i}{a^2+b^2})], *[-j, 1].$$

## 7.9 Groups that contain two orthogonal reflections, type $\boxplus$ and $\boxtimes$

As in the case of  $\square$ , we distinguish, for each axis separately, whether there are mirror reflections or only glide reflections. We know that the glide reflection case is inconsistent with the rhombic lattice (cf. Section 7.7.1). Hence, we have the following cases, see Figure 25.

- The grid of translations is a rhombic grid. In this case, both axes directions must be mirrors: **c2mm**.
- The grid of translations is a rectangular grid. In this case each axis direction can be a mirror direction or a glide reflection
  - **p2mm**. Two mirror directions
  - **p2mg**. One mirror direction and one glide direction
  - **p2gg**. Two glide directions

In **p2mg**, the two families of invariant lines are distinguishable: one family of parallel lines consists of mirror lines, whereas the perpendicular family has only glide reflections. Thus, there are two different types, where the two directions change roles.

However, for  $\boxplus$ , we need not distinguish two versions of  $\boxplus\mathbf{p2mg}$ , because conjugation with  $\square$  maps one to the other. For  $\boxtimes$ , on the other hand, the two versions are distinct. They are mirror images. We distinguish  $\boxtimes\mathbf{p2mg}$ , where the mirror lines are parallel to the principal diagonal  $\varphi_2 = +\varphi_1$ , and  $\boxtimes\mathbf{p2gm}$ , where the mirror lines are parallel to the secondary diagonal direction  $\varphi_2 = -\varphi_1$ .<sup>16</sup> The parameters  $m$  and  $n$  have the same meaning as in the corresponding groups  $\square$  and  $\square$ .

<sup>16</sup>This is in accordance with previous editions of the International Tables of X-Ray Crystallography, which explicitly provided variations of the symbols for different “settings” [21, Table 6.1.1, p. 542 in the 1952/1969 edition]: short symbol **pmg**, full symbol **p2mg**, or **p2gm** for other setting.

group	generators
$\boxplus \mathbf{p2mm}_{m,n}$	$[e^{\frac{\pi i}{m}}, e^{\frac{\pi i}{m}}], [e^{\frac{\pi i}{n}}, e^{-\frac{\pi i}{n}}], *[i, i], *[k, k]$
$\boxplus \mathbf{p2mg}_{m,n}$	$[e^{\frac{\pi i}{m}}, e^{\frac{\pi i}{m}}], [e^{\frac{\pi i}{n}}, e^{-\frac{\pi i}{n}}], *[i, i][e^{\frac{\pi i}{2n}}, e^{-\frac{\pi i}{2n}}], *[k, k][e^{\frac{\pi i}{2n}}, e^{-\frac{\pi i}{2n}}]$
$\boxplus \mathbf{p2gg}_{m,n}$	$[e^{\frac{\pi i}{m}}, e^{\frac{\pi i}{m}}], [e^{\frac{\pi i}{n}}, e^{-\frac{\pi i}{n}}], *[i, i][e^{\frac{\pi i}{2m} + \frac{\pi i}{2n}}, e^{\frac{\pi i}{2m} - \frac{\pi i}{2n}}], *[k, k][e^{\frac{\pi i}{2m} + \frac{\pi i}{2n}}, e^{\frac{\pi i}{2m} - \frac{\pi i}{2n}}]$
$\boxplus \mathbf{c2mm}_{m,n}$	$[e^{\frac{\pi i}{m}}, e^{\frac{\pi i}{m}}], [e^{\frac{\pi i}{n}}, e^{-\frac{\pi i}{n}}], [e^{\frac{\pi i}{2m} + \frac{\pi i}{2n}}, e^{\frac{\pi i}{2m} - \frac{\pi i}{2n}}], *[i, i], *[k, k]$
$\boxtimes \mathbf{p2mm}_{2m,2n}$	$[e^{\frac{\pi i}{m}}, 1], [1, e^{\frac{\pi i}{n}}], [i, k], [-k, i]$
$\boxtimes \mathbf{p2mg}_{2m,2n}$	$[e^{\frac{\pi i}{m}}, 1], [1, e^{\frac{\pi i}{n}}], [1, e^{\frac{\pi i}{2n}}][i, k], [1, e^{\frac{\pi i}{2n}}][-k, i]$
$\boxtimes \mathbf{p2gm}_{2m,2n}$	$[e^{\frac{\pi i}{m}}, 1], [1, e^{\frac{\pi i}{n}}], [e^{\frac{\pi i}{2m}}, 1][i, k], [e^{\frac{\pi i}{2m}}, 1][-k, i]$
$\boxtimes \mathbf{p2gg}_{2m,2n}$	$[e^{\frac{\pi i}{m}}, 1], [1, e^{\frac{\pi i}{n}}], [e^{\frac{\pi i}{2m}}, e^{\frac{\pi i}{2n}}][i, k], [e^{\frac{\pi i}{2m}}, e^{\frac{\pi i}{2n}}][-k, i]$
$\boxtimes \mathbf{c2mm}_{m,n}$	$[e^{\frac{i2\pi}{m}}, 1], [1, e^{\frac{i2\pi}{n}}], [e^{\frac{\pi i}{m}}, e^{\frac{\pi i}{n}}], [i, k], [-k, i]$
$\boxtimes \mathbf{p4mm}_n^U$	$[e^{\frac{\pi i}{n}}, e^{\frac{\pi i}{n}}], [e^{\frac{\pi i}{n}}, e^{-\frac{\pi i}{n}}], [i, k], *[i, i]$
$\boxtimes \mathbf{p4gm}_n^U$	$[e^{\frac{\pi i}{n}}, e^{\frac{\pi i}{n}}], [e^{\frac{\pi i}{n}}, e^{-\frac{\pi i}{n}}], [i, k][e^{\frac{\pi i}{n}}, 1], *[i, i][e^{\frac{\pi i}{n}}, 1]$
$\boxtimes \mathbf{p4mm}_n^S$	$[e^{\frac{\pi i}{n}}, 1], [1, e^{\frac{\pi i}{n}}], [i, k], *[i, i]$
$\boxtimes \mathbf{p4gm}_n^S$	$[e^{\frac{\pi i}{n}}, 1], [1, e^{\frac{\pi i}{n}}], [i, k][e^{\frac{\pi i}{2n}}, e^{\frac{\pi i}{2n}}], *[i, i][e^{\frac{\pi i}{2n}}, e^{\frac{\pi i}{2n}}]$

Table 8: Generators for full torus reflection groups, full torus swap groups, and full torus groups

These groups contain torus flips, as the product of two perpendicular reflections. We choose the origin on the center of a 2-fold rotation induced by a torus flip. For the groups **c2mm**, we place origin at the intersection of two mirror lines. Then the groups can be generated by the generators given in Table 8.

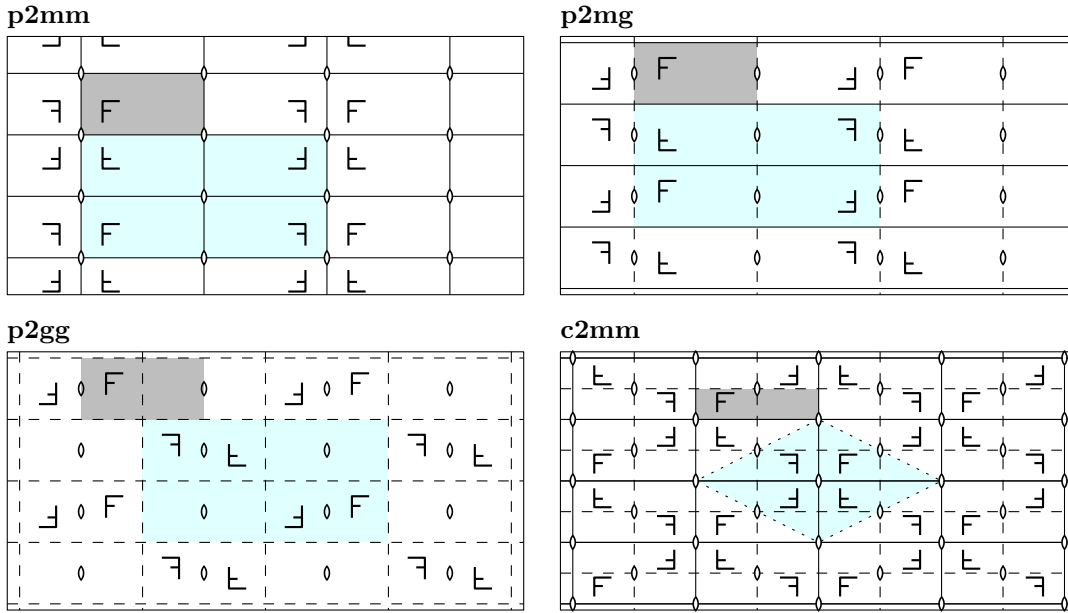
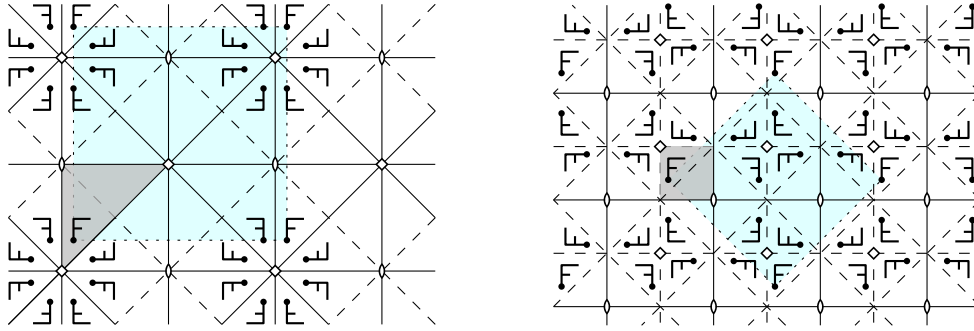


Figure 25: The four types of groups with two orthogonal families of invariant lines. The light-blue region indicates the lattice of translations. For better visibility, the letter F is moved away from the mirror lines. Axes of mirror reflection are shown as solid lines, and axes of glide reflection are dashed. As in Figure 24, lenses mark centers of 2-fold rotations.

## 7.10 The full torus groups, type $\boxtimes$

Finally, we have the groups where all directional transformations are combined. The conditions of  $\boxplus$  and  $\boxtimes$  force the lattice to be a rectangular lattice both in the  $\varphi_1, \varphi_2$  axis direction and in the  $\pm 45^\circ$  direction, possibly with added midpoints (rhombic case). This means that the lattice is a *square* lattice. It appears as a *rectangular* lattice in one pair of perpendicular directions and as a *rhombic* lattice in the other directions.

Thus, there are only two cases for the translation lattice: The square  $n \times n$  lattice with  $n^2$  translations (the upright grid “U”, Figure 26a), and its rhombic extension with  $2n^2$  translations (the slanted grid “S”, Figure 26b).



(a) mirror reflections, upright grid ( $\text{p4mmU}$ ) (b) glide reflections, slanted grid ( $\text{p4gmS}$ )

Figure 26: Two of the four types of groups  $\boxtimes$ . Small squares denote centers of 4-fold rotations. For each figure, there exists a rotated version by  $45^\circ$ , where  $\boxtimes\text{p4mmU}$  becomes  $\boxtimes\text{p4mms}$ , and  $\boxtimes\text{p4gmS}$  becomes  $\boxtimes\text{p4gmU}$ .

Let us first consider the slanted case, see Figure 26b. The lattice appears as a rhombic lattice for the  $\boxplus$  directions. From the point of view of the subgroups of type  $\boxplus$ , we know that this means that the “glide reflection” case is excluded (cf. the discussion in Section 7.7.1). There must be mirror reflections in the horizontal and vertical axes.

For the  $\boxtimes$  directions, the lattice appears as a rectangular lattice. According to Section 7.9 we can have the cases mirror/mirror, mirror/glide, glide/glide. But since  $90^\circ$  rotations are included, the mixed mirror/glide case is impossible. Two cases remain, which we call  $\boxtimes\text{p4mms}$  and  $\boxtimes\text{p4gmS}$ . The latter is shown in Figure 26b. When the lattice appears as a square lattice for the  $\boxplus$  directions, the two pairs of directions  $\boxplus$  and  $\boxtimes$  change roles, and we have two more groups,  $\boxtimes\text{p4mmU}$  and  $\boxtimes\text{p4gmU}$ . The first one is shown in Figure 26a. The groups  $\boxtimes\text{p4mm}$  have mirrors in all four directions, whereas the groups  $\boxtimes\text{p4gm}$  have mirrors in two directions only.

To list the generators for the full torus groups, we choose the origin of the coordinate system on the center of a 4-fold rotation induced by a swaptorn, see Table 8.

This concludes the discussion of the toroidal groups. The reader who wishes to practice the understanding of these classes might try to count, as an exercise, all groups of order 100, see Appendix C.

## 7.11 Duplications

As we have seen, every subgroup of a group  $\pm[D_{2m} \times D_{2n}]$  has an invariant torus. So far, we have analyzed the groups that leave a *fixed* torus invariant. We have already mentioned that some subgroups have more than one invariant Clifford torus, and this leads to duplications. Unfortunately, when it comes to weeding out duplications, all classifications (including the classic classification) become messy.<sup>17</sup>

We analyze the situation as follows. Every orientation-preserving transformation is of the form  $R_{\alpha_1, \alpha_2}$ , with  $-\pi \leq \alpha_1, \alpha_2 \leq \pi$ . If  $\alpha_1 \neq \pm\alpha_2$ , there is a unique pair of absolutely orthogonal invariant planes, and hence, there is a unique invariant Clifford torus *on which the transformation appears as a torus translation*. We call this torus the *primary* invariant torus.

Our strategy is to analyze the situation backwards. We look at all orientation-preserving transformations that are not torus translations, we write them in the form  $R_{\alpha_1, \alpha_2}$  and determine the translation vector  $(\alpha_1, \alpha_2)$  by which they would appear on their primary invariant torus. The result is summarized in the following proposition. The torus translations that lead to ambiguity are shown in Figure 27:

**Proposition 7.8.** *The orientation-preserving transformations that have more than one invariant torus are the following:*

(a) *Simple half-turns of the form  $\text{diag}(-1, -1, 1, 1)$ .*

*On their primary torus, they appear as torus translation by  $(\pi, 0)$  or  $(0, \pi)$ . There is an infinite family of alternate tori for which they are interpreted as torus flips or torus swaps.*

<sup>17</sup>The difficulty caused by these ambiguous transformations, in particular in connection with achiral groups, was already acknowledged by Hurley [23, p. 656–7].

(b) Double rotations  $R_{\alpha, \pi \pm \alpha}$ .

On an alternate torus, they appear as reflections or glide reflections associated to torus swaps  $\square$  or  $\square$ .

(c) Left and right rotations  $R_{\alpha, \pm \alpha}$ , including  $\text{id}$  and  $-\text{id}$ . (For  $\alpha = \pm \pi/2$ , these fall also under case (b).)

A left rotation  $R_{\alpha, \alpha}$  with  $\alpha \neq \pm \pi/2$  appears as a torus translation by  $(\alpha, \alpha)$  or by  $(-\alpha, -\alpha)$  on every invariant torus.

Similarly, a right rotation  $R_{\alpha, -\alpha}$  with  $\alpha \neq \pm \pi/2$  appears as a torus translation by  $(\alpha, -\alpha)$  or by  $(-\alpha, \alpha)$  on every invariant torus.

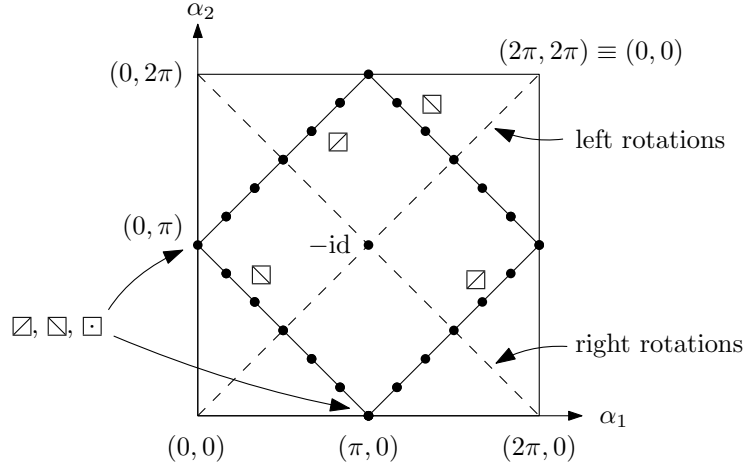


Figure 27: The torus translations on the tilted square are ambiguous: they can appear as rotations of different types, as indicated. Left and right rotations (on the diagonal) also have no unique invariant torus, but they appear as left and right rotations on any invariant torus.

*Proof.* The orientation-preserving transformations that are not torus translations are  $\square$  (torus flips) and  $\square$  and  $\square$  (reflections and glide reflections associated to torus swaps).

Every torus flip is a half-turn, and these are covered in case (a).

Let us look at reflections and glide reflections associated to the torus swaps  $\square$ . The torus swap  $\square$  at the principal diagonal is the transformation  $[i, k]$ . Both  $i$  and  $k$  are pure quaternions, in accordance with the fact that  $\square$  is a half-turn. The general torus swap of type  $\square$  is obtained by combining  $[i, k]$  with an arbitrary torus translation  $[\exp \beta_l i, \exp \beta_r i]$ :

$$[i \exp \beta_l i, k \exp \beta_r i] = [\exp(\frac{\pi}{2} i) \exp \beta_l i, k(\cos \beta_r + i \sin \beta_r)] = [\exp((\frac{\pi}{2} + \beta_l) i), k \cos \beta_r + j \sin \beta_r]$$

The right component  $k \cos \beta_r + j \sin \beta_r$  is still a unit quaternion (rotation angle  $\pi/2$ ), and hence the right rotation  $[1, \exp \beta_r i]$  has no effect on the type of the transformation. This is in accordance with the fact that, on the  $\varphi_1, \varphi_2$ -torus, a right rotation is a translation perpendicular to the reflection axis of  $\square$ , whose effect is just to move the reflection axis. The left rotation, however, changes the rotation angle from  $\pi/2$  to  $\pi/2 + \beta_l$ . The result is a rotation of type  $R_{\pi + \beta_l, \beta_l}$ . As a torus translation  $R_{\alpha_1, \alpha_2}$ , it lies on the line  $\alpha_1 = \alpha_2 + \pi$  (and  $\alpha_1 = \alpha_2 - \pi$ , considering that angles are taken modulo  $2\pi$ ), see Figure 27.

The operations of type  $\square$  are the mirrors of  $\square$ , and hence they appear on the reflected lines  $\alpha_1 = -(\alpha_2 \pm \pi)$ .

Left and right rotations have infinitely many invariant tori, but cause no confusion for our classification, because a left rotation will appear as the same left rotation on *any* invariant torus (possibly with an inverted angle), except when it falls under case (b).  $\square$

We note the curious fact that the operations that don't have a unique invariant torus coincide with the operations whose squares are left or right rotations.

**Corollary 7.9.** *A group may have more than one invariant torus only if the translational subgroup contains only elements on the diagonals and on the tilted square in Figure 27.*

This excludes from the search for duplications those groups for which the translational subgroup is sufficiently rich, i.e., when both parameters  $m$  and  $n$  are large. Still it leaves a large number of cases where one of the parameters is small. We present the list of duplications below.

### 7.11.1 List of Duplications

As mentioned, we have imposed the stricter conditions on  $m$  and  $n$  (and  $a$  and  $b$ ) in Table 6 in order to exclude all duplications. As a rule, among equal groups, we have chosen the group with the larger subgroup of torus translations (with the chosen invariant torus) to stay in the table.

Table 9 lists every group  $G_1$  that is excluded from Table 6, together with a group  $G_2$  to which it is conjugate, and a conjugation that converts the second group to the first one. The conjugations depend on the specific parameterizations that we have chosen and that were given with each class of groups discussed above, in particular in Tables 7 and 8.

In this section, we use the notation  $G_1 \doteq G_2$  for groups that are geometrically the same, i.e., conjugate under an orientation-preserving transformation, and we reserve the sign “=” for groups that are equal in our chosen coordinate system.

In some classes, the choice of the two parameters  $m$  and  $n$  is symmetric (e.g.,  $\boxtimes_{m,n}^{p2mm} \doteq \boxtimes_{n,m}^{p2mm}$ ). In those cases, we have achieved uniqueness by requiring  $m \geq n$  in Table 6. Such symmetries between the parameters, and other general relations are listed first for each type of group in Table 9. This is followed by a list of groups with small parameters that are explicitly excluded in Table 6.

We have made some simplifications to keep the table compact. As mentioned previously, we sometimes refer to groups  $\boxtimes_{m,n}^{(s)}$  or  $\boxtimes_{m,n}^{(s)}$  where the parameter  $s$  lies outside the “legal” range (20), in order to avoid case distinctions. The parameter  $s$  can be brought into that range by using the equalities  $\boxtimes_{m,n}^{(s)} = \boxtimes_{m,n}^{(s \pm m)} \doteq \boxtimes_{m,n}^{(-n-s)}$ , and similarly for  $\boxtimes$ . If the permissible range of parameters  $s$  contains only one integer, we omit the parameter and denote the group simply by  $\boxtimes_{m,n}$  or  $\boxtimes_{m,n}$ . In such a case, any choice of  $s$  will lead to the same group.

We have a few cases with more than two equal groups:

$$\begin{aligned} \boxtimes_{1,1}^{cm} &\doteq \boxtimes_{1,1}^{cm} \doteq \boxtimes_{1,1}^{(0)} \doteq \boxtimes_{1,2}^{(0)} = \langle \text{diag}(1, 1, -1, -1) \rangle \text{ (order 2)} \\ \boxtimes_{2,2}^{pm} &\doteq \boxtimes_{2,2}^{pm} \doteq \boxtimes_{2,1}^{(-1)} \doteq \boxtimes_{2,2}^{(0)} = \langle \text{diag}(1, 1, -1, -1), \text{diag}(-1, -1, 1, 1) \rangle \cong D_4 \text{ (order 4)} \\ \boxtimes_{2,2}^{p2gg} &\doteq \boxtimes_{4,2}^{pm} \doteq \boxtimes_{2,4}^{pm} \doteq \boxtimes_{4,2}^{(-2)} = \langle \text{diag}(R_{\pi/2}, R_{\pi/2}), \text{diag}(R_{\pi/2}, R_{-\pi/2}) \rangle \text{ (order 8)} \\ \boxtimes_{2,2}^{p2gm} &\doteq \boxtimes_{2,2}^{cm} \doteq \boxtimes_{2,4}^{pm} \doteq \boxtimes_{2,2}^{(-1)} = \langle -\text{id}, \text{diag}(1, -1, 1, -1), \text{diag}(R_{\pi/2}, R_{-\pi/2}) \rangle \text{ (order 8)} \\ \boxtimes_{2,2}^{p2mg} &\doteq \boxtimes_{2,2}^{cm} \doteq \boxtimes_{4,2}^{pm} \doteq \boxtimes_{4,1}^{(-2)} = \langle -\text{id}, \text{diag}(1, -1, 1, -1), \text{diag}(R_{\pi/2}, R_{\pi/2}) \rangle \text{ (order 8)} \\ \boxtimes_1^{p4gmU} &\doteq \boxtimes_{2,1}^{p2gg} \doteq \boxtimes_{1,2}^{p2gg} \doteq \langle \text{diag}(-1, -1, 1, 1), \text{diag}(1, 1, -1, 1), \text{diag}(1, 1, 1, -1) \rangle \text{ (order 8)} \\ \boxtimes_{2,2}^{c2mm} &\doteq \boxtimes_{4,2}^{p2mm} \doteq \boxtimes_{2,4}^{p2mm} \doteq \boxtimes_{4,2}^{(-2)} \text{ (order 16)} \end{aligned}$$

To reduce case distinctions, some of these groups  $G_1$  point to groups  $G_2$  that are themselves excluded in Table 6, and which must be looked up again in Table 9.

The conjugations in Table 9 were found by computer search for particular values of  $m$ . In many cases, the conjugate group or the conjugacy mapping depends on the parity of some parameter. We tried to simplify the entries of the table by manually adjusting them. All conjugations were checked by computer for  $m \leq 100$ .

When the groups are translated to the Conway-Smith classification using Table 6, the duplications have easy algebraic justifications: For example,  $C_2$  and  $D_2$  are obviously the same group. Also,  $\bar{D}_4$  can be replaced by  $D_4$ , see Appendix G.1 for more information.

### 7.11.2 A duplication example

By way of example, we treat one duplication in detail:

$$\boxtimes_{1,n}^{c2mm} \doteq \boxtimes_{1,2n}^{(\frac{n-1}{2})}, \text{ for odd } n. \quad (23)$$

Figure 28 shows the action of these groups on the torus for  $n = 5$ . We can confirm that, in accordance with Corollary 7.9, the 10 torus translations of  $\boxtimes_{1,10}^{(2)}$  lie only on a diagonal and on the line  $\alpha_1 + \alpha_2 = \pm\pi$ . The latter 5 translations become reflections and glide reflections in  $\boxtimes_{1,5}^{c2mm}$ . More precisely, in accordance with Figure 27, they are the reflections at the  $\boxtimes$  diagonal

$G_1$	$G_2$	$[\hat{l}, \hat{r}]$	$G_1$	$G_2$	$[\hat{l}, \hat{r}]$
chiral groups					
$\square_{m,n}^{(s)}$ $\square_{m,n}^{(s)}$	$\square_{m,n}^{(s+n)}$ $\square_{m,n}^{(-m-s)}$	$[1, 1]$ (equal) $[i, k] = \square$	$\square_{m,n}^{(s)}$ $\square_{m,n}^{(s)}$ $\square_{1,1}$ $\square_{2,1}$	$\square_{m,n}^{(s+n)}$ $\square_{m,n}^{(-m-s)}$ $\square_{1,2}$ $\square_{2,2}^{(0)}$	$[1, 1]$ (equal) $[i, k] = \square$ $[i + j, 1 + k]$ $[i + j, i + j]$
$\square_{4m-2,2}^{\text{pm}}$ $\square_{4m,2}^{\text{pm}}$ $\square_{2,4m-2}^{\text{pm}}$ $\square_{2,4m}^{\text{pm}}$	$\square_{4m-2,1}^{\text{pm}}$ $\square_{4m,1}^{\text{pm}}$ $\square_{2,4m-2}^{(2m-2)}$ $\square_{4,2m}^{(-2)}$	$[j + k, i + j]$ $[1, i + j]$ $[i + k, 1]$ $[i + k, 1]$	$\square_{2,4m-2}^{\text{pm}}$ $\square_{2,4m}^{\text{pm}}$ $\square_{2m,2}^{\text{pm}}$	$\square_{2,2m-1}^{(-1)}$ $\square_{2,2m}^{(-1)}$ $\square_{2m,2}^{(0)}$	$[i + j, j + k]$ $[i + j, 1]$ $[1, i + k]$
$\square_{2,4m-2}^{\text{pg}}$ $\square_{2,4m}^{\text{pg}}$	$\square_{4,2m-1}^{(-2)}$ $\square_{2,4m}^{(2m-1)}$	$[i + k, 1]$ $[i + k, 1]$	$\square_{2m,2}^{\text{pg}}$	$\square_{2m,2}^{(1)}$	$[1, i + k]$
$\square_{2m+1,1}^{\text{cm}}$ $\square_{1,4m-3}^{\text{cm}}$ $\square_{1,4m-1}^{\text{cm}}$ $\square_{2,4m-2}^{\text{cm}}$ $\square_{2,4m}^{\text{cm}}$	$\square_{2m+1,1}^{\text{cm}}$ $\square_{1,8m-6}^{(2m-2)}$ $\square_{1,8m-2}^{(2m-1)}$ $\square_{4,4m-2}^{\text{pm}}$ $\square_{4,4m}^{\text{pg}}$	$[j + k, 1 - k]$ $[i + k, 1]$ $[1 - j, 1]$ $[i + j, 1]$ $[i + k, 1]$	$\square_{1,2m+1}^{\text{cm}}$ $\square_{4m-3,1}^{\text{cm}}$ $\square_{4m-1,1}^{\text{cm}}$ $\square_{4m-2,2}^{\text{cm}}$ $\square_{4m,2}^{\text{cm}}$	$\square_{1,2m+1}^{(m)}$ $\square_{4m-3,2}^{\text{cm}}$ $\square_{4m-1,2}^{\text{cm}}$ $\square_{4m-2,4}^{\text{pm}}$ $\square_{4m,4}^{\text{pg}}$	$[i + j, j + k]$ $[1, 1 - j]$ $[1, i + k]$ $[1, i + j]$ $[1, i + k]$
$\square_{2m,2}^{\text{p2mm}}$	$\square_{2m,2}^{(0)}$	$[1, i + k]$	$\square_{2,4m-2}^{\text{p2mm}}$ $\square_{2,4m}^{\text{p2mm}}$	$\square_{2,4m-2}^{(2m-2)}$ $\square_{4,2m}^{(-2)}$	$[i + k, 1]$ $[i + k, 1]$
$\square_{2m,2}^{\text{p2gm}}$  $\square_{2,4m-2}^{\text{p2gm}}$ $\square_{2,4m}^{\text{p2gm}}$	$\square_{2m,2}^{(1)}$  $\square_{2,4m-2}^{\text{cm}}$ $\square_{4,4m}^{\text{pm}}$	$[1, i + k]$  $[i + j, j + k]$ $[i + j, 1]$	$\square_{2,4m-2}^{\text{p2mg}}$ $\square_{2,4m}^{\text{p2mg}}$ $\square_{4m-2,2}^{\text{p2mg}}$ $\square_{4m,2}^{\text{p2mg}}$	$\square_{4,2m-1}^{(-2)}$ $\square_{2,4m}^{(2m-1)}$ $\square_{4m-2,2}^{\text{cm}}$ $\square_{4m,4}^{\text{pm}}$	$[i + k, 1]$ $[i + k, 1]$ $[j + k, i + j]$ $[1, i + j]$
$\square_{4m-2,2}^{\text{p2gg}}$ $\square_{2,4m-2}^{\text{p2gg}}$	$\square_{4m-2,4}^{\text{pm}}$ $\square_{4,4m-2}^{\text{pm}}$	$[j + k, i + j]$ $[i + j, j + k]$	$\square_{4m,2}^{\text{p2gg}}$ $\square_{2,4m}^{\text{p2gg}}$	$\square_{4m,2}^{\text{cm}}$ $\square_{2,4m}^{\text{cm}}$	$[1, i + j]$ $[i + j, 1]$
$\square_{4m-3,1}^{\text{c2mm}}$ $\square_{4m-1,1}^{\text{c2mm}}$ $\square_{1,4m-3}^{\text{c2mm}}$ $\square_{1,4m-1}^{\text{c2mm}}$	$\square_{4m-3,2}^{\text{c2mm}}$ $\square_{4m-1,2}^{\text{c2mm}}$ $\square_{1,8m-6}^{(2m-2)}$ $\square_{1,8m-2}^{(2m-1)}$	$[1, 1 - j]$ $[1, 1 + j]$ $[1 + j, 1]$ $[1 - j, 1]$	$\square_{4m-2,2}^{\text{c2mm}}$ $\square_{4m,2}^{\text{c2mm}}$ $\square_{2,4m-2}^{\text{c2mm}}$ $\square_{2,4m}^{\text{c2mm}}$	$\square_{4m-2,4}^{\text{p2mm}}$ $\square_{4m,4}^{\text{p2gm}}$ $\square_{4,4m-2}^{\text{p2mm}}$ $\square_{4,4m}^{\text{p2mg}}$	$[j + k, i + j]$ $[1, i + k]$ $[i + j, j + k]$ $[i + k, 1]$
achiral groups					
$\square_{m,n}^{\text{p2mm}}$ $\square_{m,n}^{\text{p2gg}}$ $\square_{m,n}^{\text{c2mm}}$ $\square_{1,1}^{\text{p2mm}}$ $\square_{1,1}^{\text{p2mg}}$ $\square_{1,1}^{\text{p2gg}}$ $\square_{1,1}^{\text{c2mm}}$	$\square_{n,m}^{\text{p2mm}}$ $\square_{n,m}^{\text{p2gg}}$ $\square_{n,m}^{\text{c2mm}}$ $\square_{1,2}^{\text{pm}}$ $\square_{2,1}^{\text{pm}}$ $\square_{1,2}^{\text{pg}}$ $\square_{2,2}^{\text{pm}}$	$[i, k] = \square$ $[i, k] = \square$ $[i, k] = \square$ $[1 + k, 1 - k]$ $[1 + k, i - j]$ $[1 + k, 1 - k]$ $[1 + k, 1 - k]$	$\square_{a,b}$ $\square_{1,0}$ $\square_{1,1}$ $\square_{2,0}$	$\square_{b,a}$ $\square_{2,1}^{\text{pg}}$ $\square_{2,2}^{\text{pg}}$ $\square_{2,2}^{\text{p2gg}}$	$[i, k] = \square$ $[1 + k, 1 - i + j + k]$ $[1 + k, 1 + i - j + k]$ $[1 + k, 1 + k]$
$\square_1^{\text{p4mmU}}$ $\square_2^{\text{p4mmU}}$ $\square_1^{\text{p4mmS}}$	$\square_{1,2}^{\text{p2mg}}$ $\square_{2,2}^{\text{c2mm}}$ $\square_{2,2}^{\text{p2mg}}$	$[1 + k, 1 - i - j - k]$ $[1 + k, 1 + k]$ $[1 + k, 1 + i + j - k]$	$\square_1^{\text{p4gmU}}$ $\square_2^{\text{p4gmU}}$ $\square_1^{\text{p4gmS}}$	$\square_{2,1}^{\text{p2gg}}$ $\square_{2,2}^{\text{c2mm}}$ $\square_{2,2}^{\text{cm}}$	$[1 + k, 1 + i - j + k]$ $[1 + j, 1 + j]$ $[1 + k, 1 + k]$

Table 9: Duplications. The range of the parameter  $m$  is  $m \geq 1$  in all cases. The group  $G_1$  is obtained from  $G_2$  by conjugation with  $h := [\frac{\hat{l}}{\|\hat{l}\|}, \frac{\hat{r}}{\|\hat{r}\|}]$ . That is,  $G_1 = h^{-1}G_2h$ .

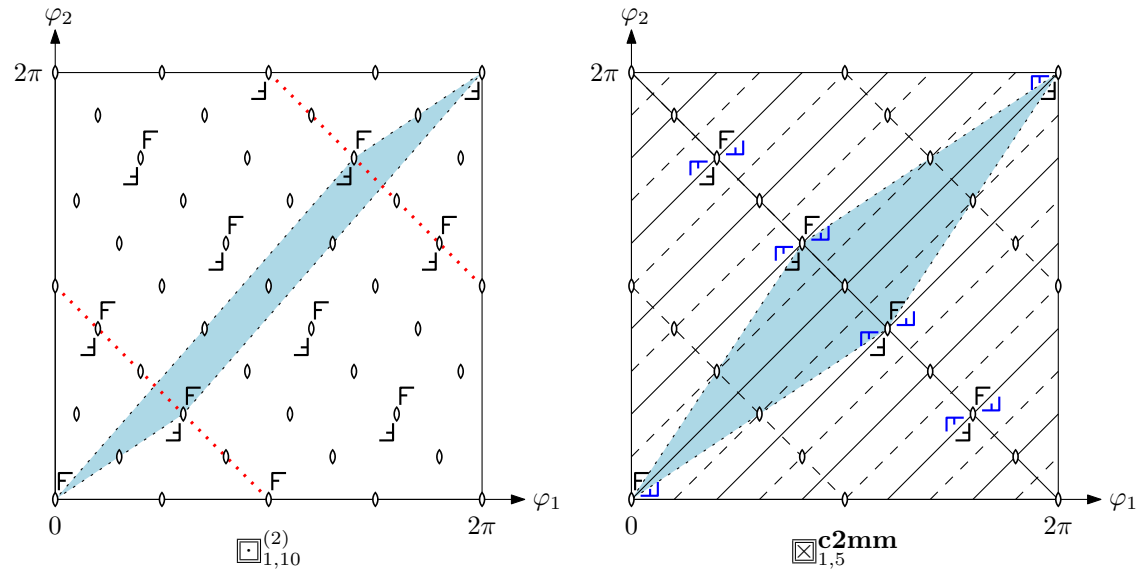


Figure 28: Duplication example,  $\boxed{1,10}^{(2)} \doteq \boxed{1,5} \text{c2mm}$

(4 glide reflections and one reflection). The picture shows actually more glide reflections and reflection axes than the order of the group would allow. The reason is that every glide reflection in this group can also be interpreted as a reflection, at a different axis.

We now prove the conjugacy formally. Since these groups have the same order  $4n$ , it is enough to show that  $G_2 = \boxed{1,2n}^{(\frac{n-1}{2})}$  is contained in  $G_1 = \boxed{1,n} \text{c2mm}$ . We do this by checking that the generators of  $G_2$ , under conjugation by the element  $h$  from Table 9, are elements of  $G_1$ . Here are the generators we gave for these groups:

$$G_1 = \boxed{1,n} \text{c2mm} = \langle [1, 1], [1, e^{\frac{i2\pi}{n}}], [-1, e^{\frac{\pi i}{n}}], [i, k], [-k, i] \rangle \quad (\text{see Table 8})$$

$$G_2 = \boxed{1,2n}^{(\frac{n-1}{2})} = \langle [e^{-2\pi i}, 1], [-i, e^{\frac{\pi i}{2n}}], [j, j] \rangle = \langle [-i, e^{\frac{\pi i}{2n}}], [j, j] \rangle \quad (\text{see Section 7.6})$$

We have to choose different conjugations depending on the value of  $n$  modulo 4.

- For  $\boxed{1,4m-1} \text{c2mm} \doteq \boxed{1,8m-2}^{(2m-1)}$ , we do conjugation by  $h_1 = [1 - j, 1]$ :

$$\begin{aligned} \left[\frac{1+j}{2}, 1\right] [-i, e^{\frac{\pi i}{8m-2}}] [1 - j, 1] &= [k, e^{\frac{\pi i}{8m-2}}] = [k, e^{\frac{i(14m-3)\pi}{8m-2}}] = [k, -i] [1, e^{\frac{i2\pi}{4m-1}}]^m \in G_1 \\ \left[\frac{1+j}{2}, 1\right] [j, j] [1 - j, 1] &= [j, j] = [i, k] [-k, i] \in G_1 \end{aligned}$$

- For  $\boxed{1,4m-3} \text{c2mm} \doteq \boxed{1,8m-6}^{(2m-2)}$ , we do conjugation by  $h_2 = [1 + j, 1]$ :

$$\begin{aligned} \left[\frac{1-j}{2}, 1\right] [-i, e^{\frac{\pi i}{8m-6}}] [1 + j, 1] &= [-k, e^{\frac{\pi i}{8m-6}}] = [j, j] [1, e^{\frac{i2\pi}{4m-3}}]^{m-1} [i, k] \in G_1 \\ \left[\frac{1-j}{2}, 1\right] [j, j] [1 + j, 1] &= [j, j] = [i, k] [-k, i] \in G_1 \end{aligned}$$

We can also study this transformation geometrically: What happens to the torus under this coordinate transformation? On which other torus do the glide reflections of  $\boxed{1,n} \text{c2mm}$  appear as torus translations? Indeed, there is another simple equation for a Clifford torus that is commonly used. We can transform our equation for the torus  $\mathbb{T}$  as follows:

$$\begin{aligned} x_1^2 + x_2^2 &= x_3^2 + x_4^2 \\ x_2^2 - x_4^2 &= x_3^2 - x_1^2 \\ (x_2 - x_4)(x_2 + x_4) &= (x_3 + x_1)(x_3 - x_1) \end{aligned} \tag{24}$$

$$\tilde{x}_2 \tilde{x}_4 = \tilde{x}_1 \tilde{x}_3, \tag{25}$$

with transformed coordinates  $(\tilde{x}_1, \tilde{x}_2, \tilde{x}_3, \tilde{x}_4)$ . This is, for example, how the torus is introduced in Coxeter [12, Eq. (4.41)], who has a separate section on “the spherical torus” [12, §4.4, p. 35–37].

Now, the coordinate change from (24) to (25) is precisely what the transformation  $h_1 = [1 - j, 1]$  in our example achieves:  $[1 - j, 1]$  maps the quaternion units  $(1, i, j, k) \equiv (x_1, x_2, x_3, x_4)$



to  $(1 + j, i - k, -1 + j, i + k) \equiv (x_1 + x_3, x_2 - x_4, -x_1 + x_3, x_2 + x_4) = (\tilde{x}_1, \tilde{x}_2, \tilde{x}_3, \tilde{x}_4)$ . Many conjugations in Table 9 are of this form.

The reason why we have chosen the example (23) for manual confirmation is that it corresponds to one of two duplications in the Conway-Smith classification that are not literally mentioned there:

$$\begin{aligned} +\tfrac{1}{4}[D_4 \times \bar{D}_{4n}] &\doteq +\tfrac{1}{4}[D_4 \times D_{4n}^{(1)}] \text{ for odd } n. \\ \pm\tfrac{1}{4}[D_4 \times \bar{D}_{4n}] &\doteq \pm\tfrac{1}{4}[D_4 \times D_{4n}^{(1)}] \end{aligned}$$

The second equality appears in Table 9 as  $\boxtimes_{2,2m}^{\mathbf{p}2\mathbf{mm}}$  for odd  $m$  and  $\boxtimes_{2,2m}^{\mathbf{p}2\mathbf{gm}}$  for even  $m$ . The reason behind these duplications is discussed in Section G.1.

## 7.12 Comparison with the classification of Conway and Smith

Looking at the right column of Table 6, we see that our classification and the classification of Conway and Smith [8] have some similarity in the rough categorization. For example the “mixed” groups of type  $[C \times D]$  are the torus swap groups (type  $\boxtimes$ ). In the finer details, however, the two classifications are often quite at odds with each other. Groups that come from one geometric family correspond to different classes in the CS classification from the algebraic viewpoint, depending on parity conditions. On the other hand, some groups that belong together algebraically appear in different categories of our classification.

While we acquired some understanding of the classic classification of the toroidal groups according to Conway and Smith [8], in particular, of the simplest case of the torus translation groups (type  $\boxtimes$ , corresponding to  $[C \times C]$ , see Appendix G), most entries in the right column of Table 6 were filled with the help of a computer, by generating the groups from the specified generators and comparing them by the fingerprints described in Section 10.2, and recognizing patterns.

One reason for the difficulty is the distinction between haploid and diploid groups, a term borrowed from biology by Conway and Smith [8]. A group is *diploid* if it contains the central reflection  $-\text{id}$ ; otherwise, it is *haploid*.<sup>18</sup> In the classic classification, the diploid groups arise easily, but the haploid groups must be specially constructed as index-2 subgroups of diploid groups. Thus, the presence or absence of  $-\text{id}$  appears at the very beginning of the classic classification by quaternions. In the notation of [8], diploid and haploid groups are distinguished by the prefix  $\pm$  and  $+$ .

For our geometric construction of the toroidal groups, this distinction is ephemeral. The central reflection  $-\text{id}$  is the torus translation  $R_{\pi,\pi}$  in the center of the parameter square. It depends on some parity conditions of the translation parameters whether this element belongs to  $G_{\boxtimes}$ . (For example, one can easily work out from Figure 23 that the groups  $\boxtimes^{\mathbf{pm}}$  and  $\boxtimes^{\mathbf{pg}}$  are diploid if  $m$  and  $n$  are even. The groups  $\boxtimes^{\mathbf{cm}}$  are diploid if  $m$  and  $n$  have the same parity.)

In elliptic geometry, where opposite points of  $S^3$  are identified, the distinction between haploid and the corresponding diploid groups disappears, or in other words, only diploid groups play a role in elliptic space.

## 8 The polyhedral groups

We will now explain the polyhedral groups, which are related to the regular 4-dimensional polytopes. The regular 4-dimensional polytopes have a rich and beautiful structure. They and their symmetry groups have been amply discussed in the literature, see for example [10, Chapters VIII and XIII], [15, §26, §27], and therefore we will be brief, except that we study in some more detail the groups that come in enantiomorphic pairs. Table 10 gives an overview, and Table 16 in Appendix A lists these groups with generators and cross references to other classifications.

We mention that pictures of the cube, the 120-cell, the 24-cell, and the bitruncated 24-cell (also known as the 48-cell, defined in Section 8.6.1) arise among the illustrations for the tubical groups, see Section 6.12.

<sup>18</sup>Threlfall and Seifert [35, § 5] used the terms *zweistufig* and *einstufig* for these groups.

CS name	Du Val # and name	Coxeter name	order	method
symmetries of the 120-cell $Q_{120} = \{5, 3, 3\}$ / the 600-cell $P_{600} = \{3, 3, 5\}$				
$\pm[I \times I] \cdot 2$	50. $(I/I; I/I)^*$	$[3, 3, 5]$	14400	chiral part inscribed polar & swap inscribed polar & swap inscribed polar inscribed polar
$\pm[I \times I]$	30. $(I/I; I/I)$	$[3, 3, 5]^+$	7200	
$\pm[I \times O]$	29. $(I/I; O/O)$	$[[3, 3, 5]_{\frac{1}{5}L}^+]$	2880	
$\pm[O \times I]$	29. $(O/O; I/I)$	$[[3, 3, 5]_{\frac{1}{5}R}^+]$	2880	
$\pm[I \times T]$	24. $(I/I; T/T)$	$[3, 3, 5]_{\frac{1}{5}L}^+$	1440	
$\pm[T \times I]$	24. $(T/T; I/I)$	$[3, 3, 5]_{\frac{1}{5}R}^+$	1440	
symmetries of the 24-cell $P_T = \{3, 4, 3\}$ and its polar 24-cell $P_{T_1}$				
$\pm[O \times O] \cdot 2$	48. $(O/O; O/O)^*$	$[[3, 4, 3]]$	2304	chiral part nonswapping swap with mirror chiral & nonswapping
$\pm[O \times O]$	25. $(O/O; O/O)$	$[[3, 4, 3]]^+$	1152	
$\pm\frac{1}{2}[O \times O] \cdot 2$	45. $(O/T; O/T)^*$	$[3, 4, 3]$	1152	
$\pm\frac{1}{2}[O \times O] \cdot \bar{2}$	46. $(O/T; O/T)^*_-$	$[[3, 4, 3]^+]$	1152	
$\pm\frac{1}{2}[O \times O]$	28. $(O/T; O/T)$	$[3, 4, 3]^+$	576	
$\pm[T \times T] \cdot 2$	43. $(T/T; T/T)^*$	$[3, 4, 3^+]$	576	edge orientation
$\pm[O \times T]$	23. $(O/O; T/T)$	$[[^+3, 4, 3^+]]_L$	576	diagonal marking
$\pm[T \times O]$	23. $(T/T; O/O)$	$[[^+3, 4, 3^+]]_R$	576	diagonal marking
$\pm[T \times T]$	20. $(T/T; T/T)$	$[^+3, 4, 3^+]$	288	2 dual edge orientations
symmetries of the hypercube $\{4, 3, 3\}$ / the cross-polytope $\{3, 3, 4\}$				
$\pm\frac{1}{6}[O \times O] \cdot 2$	47. $(O/V; O/V)^*$	$[3, 3, 4]$	384	chiral part even permutations 2-coloring 2-coloring & chiral
$\pm\frac{1}{6}[O \times O]$	27. $(O/V; O/V)$	$[3, 3, 4]^+$	192	
$\pm\frac{1}{3}[T \times T] \cdot 2$	41. $(T/V; T/V)^*$	$[^+3, 3, 4]$	192	
$\pm\frac{1}{3}[T \times \bar{T}] \cdot 2$	42. $(T/V; T/V)^*_-$	$[3, 3, 4^+]$	192	
$\pm\frac{1}{3}[T \times T]$	22. $(T/V; T/V)$	$[^+3, 3, 4^+]$	96	
symmetries of the simplex $\{3, 3, 3\}$ and its polar				
$\pm\frac{1}{60}[I \times \bar{I}] \cdot 2$	51. $(I^\dagger/C_2; I/C_2)^{\dagger*}$	$[[3, 3, 3]]$	240	chiral part nonswapping swap with mirror chiral & nonswapping
$\pm\frac{1}{60}[I \times \bar{I}]$	32. $(I^\dagger/C_2; I/C_2)^\dagger$	$[[3, 3, 3]]^+$	120	
$+\frac{1}{60}[I \times \bar{I}] \cdot 2_1$	51'. $(I^\dagger/C_1; I/C_1)^{\dagger*}$	$[3, 3, 3]$	120	
$+\frac{1}{60}[I \times \bar{I}] \cdot 2_3$	51'. $(I^\dagger/C_1; I/C_1)^{\dagger*}_-$	$[[3, 3, 3]^+]$	120	
$+\frac{1}{60}[I \times \bar{I}]$	32'. $(I^\dagger/C_1; I/C_1)^\dagger$	$[3, 3, 3]^+$	60	

Table 10: The polyhedral groups.

The second column give a cross-reference to the classification of Du Val [15]. We remark that, in Du Val's enumeration of the achiral groups [15, p. 61], the descriptions of the orientation-reversing elements of the groups #41  $(T/V; T/V)^*$  and #42  $(T/V; T/V)^*_-$  are swapped by mistake. We follow Goursat and Hurley and go with the convention that the group with the more natural choice of elements should be associated to the name without a distinguishing subscript. Du Val himself, in the detailed discussion of these groups [15, p. 73], follows the same (correct) interpretation.

## 8.1 The Coxeter notation for groups

For the geometric description of the groups, we will use the notations of Coxeter, with adaptations by Conway and Smith [8, §4.4].

In the basic Coxeter group notation, a sequence of  $n - 1$  numbers  $[p, q, \dots, r, s]$  stands for the symmetry group of a certain  $n$ -dimensional regular polytope (if it exists), which is denoted by  $\{p, q, \dots, r, s\}$ . (See the headings of Table 10 for the 4-dimensional regular polytopes.) This group is generated by  $n$  reflections  $R_1, \dots, R_n$ . Each reflection is its own mirror:  $(R_i)^2 = 1$ , and any two adjacent reflections generate a rotation whose order is specified in the sequence:  $(R_1 R_2)^p = (R_2 R_3)^q = \dots = (R_{n-1} R_n)^s = 1$ . Nonadjacent mirrors are perpendicular:  $R_i R_j = R_j R_i$  for  $|i - j| \geq 2$ .

$G^+$  denotes the chiral part of the group  $G$ , which contains products of an even number of reflections. When just one of the numbers  $p, q, \dots, r, s$  is even, say that between  $R_k$  and  $R_{k+1}$ , there are three further subgroups. The two subgroups  $[^+p, q, \dots, r, s]$  and  $[p, q, \dots, r, s^+]$  consist of words that use respectively  $R_1, \dots, R_k$  and  $R_{k+1}, \dots, R_n$  an even number of times. Their intersection is the index-4 subgroup  $[^+p, q, \dots, r, s^+]$ . Coxeter's original notation for  $[^+p, q, \dots]$  is  $[p^+, q, \dots]$ .

A second pair of brackets, like in  $[[3, 3, 3]]$ , indicates a swap between a polytope and its polar, following [11]. Some further extensions of the notation will be needed for the axial groups in Section 9, see Table 15. In some cases, we have extended the Coxeter notations in an ad-hoc manner, allowing us to avoid other ad-hoc extensions of [8].

## 8.2 Strongly inscribed polytopes

We say that a polytope  $P$  is *strongly inscribed* in a polytope  $Q$  if every vertex of  $P$  is a vertex of  $Q$ , and every facet of  $Q$  contains a facet of  $P$ . Figure 29 shows two three-dimensional examples. This relation between  $P$  and  $Q$  is reversed under polarity: With respect to an origin that lies inside  $P$ , the polar polytope  $Q^\Delta$  will be strongly inscribed in  $P^\Delta$ .

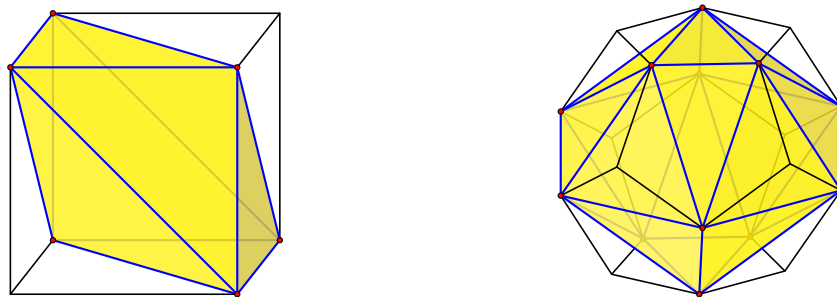


Figure 29: A cube with a strongly inscribed (non-regular) octahedron (left). A dodecahedron with a strongly inscribed (non-regular) icosahedron (right).

In four dimensions, we will show two instances of this phenomenon where a rotated copy of the polar polytope  $P^\Delta$  of a polytope  $P$  can be strongly inscribed into  $P$ . Among the *regular* polytopes in three dimensions, there are just some degenerate cases, where every facet of  $Q$  contains only an *edge* of  $P$ : In a cube  $Q$ , a regular tetrahedron  $P$  can be inscribed, with the six edges of  $P$  on the six square sides of  $Q$ . In a dodecahedron  $Q$ , a cube  $P$  can be inscribed, with its twelve edges on the twelve pentagons of  $Q$ . The tetrahedron inscribed in a dodecahedron does not fall in this category, since its edges go through the interior of the dodecahedron.

## 8.3 Symmetries of the simplex

The full symmetry group of the 4-simplex is  $[3, 3, 3]$ . The group  $[[3, 3, 3]]$  additionally swaps (by negation) the simplex with its polar. The chiral versions are  $[3, 3, 3]^+$  and  $[[3, 3, 3]]^+$ . The group  $[[3, 3, 3]]^+$  allows the flip to the polar only in connection with a reversal of orientation.

## 8.4 Symmetries of the hypercube (and its polar, the cross-polytope)

The full symmetry group of the hypercube is  $[3, 3, 4]$ . It is isomorphic to the semidirect product of coordinate permutations with sign flips  $\{(\pm 1, \pm 1, \pm 1, \pm 1)\} \rtimes S_4$ . This group has four subgroups.

The cube has a natural 2-coloring of the vertices that gives alternating colors to adjacent vertices. One can check that the vertices of each color form a cross-polytope. This cross-polytope is strongly inscribed in the cube: Each facet of the hypercube contains exactly one (tetrahedral) facet of that cross-polytope. The subgroup  $[3, 3, 4^+]$  contains those elements that preserve the 2-coloring. Equivalently, these are the elements that have an even number of sign changes.

The subgroup  $[^+3, 3, 4]$  contains those elements that have an even permutation of coordinates. It is isomorphic to  $\{(\pm 1, \pm 1, \pm 1, \pm 1)\} \rtimes A_4$ . The subgroup  $[^+3, 3, 4^+]$  is their intersection. The subgroup  $[3, 3, 4]^+$  contains the orientation-preserving transformations. These are the transformations where the parity of the sign changes matches the parity of the permutation.

It is interesting to note that the 3-dimensional group  $[3, 4]$  closely mirrors the picture for  $[3, 3, 4]$ , see Table 11. Both in three and four dimensions, the “half-cube” is itself a regular polytope: in 3 dimensions, it is the regular tetrahedron, while in 4 dimensions, it is the cross-polytope. The subgroup  $[3, 4^+] = TO$  preserves the 2-coloring of the vertices, i.e. it contains all symmetries of the tetrahedron. Its subgroup  $[^+3, 4^+] = +T$  contains the orientation-preserving symmetries of the tetrahedron. The group  $[^+3, 4] = \pm T$  contains the orientation-preserving symmetries of the tetrahedron together with its central reflection. It is also characterized as those symmetries that subject the three space axes to an even permutation. The group  $[3, 4]^+$  contains all orientation-preserving transformations in  $[3, 4]$ . For the groups  $+T$  and  $TO$  we have used alternate Coxeter names, which are equivalent to the standard ones, in order to highlight the analogy with 4 dimensions, cf. [6, p. 390].

4 dimensions	order	3 dimensions	order	description
$[3, 3, 4]$	384	$[3, 4] = \pm O$	48	the full symmetry group
$[3, 3, 4]^+$	192	$[3, 4]^+ = +O$	24	chiral part (preserves orientation)
$[^+3, 3, 4]$	192	$[^+3, 4] = \pm T$	24	even permutation of coordinates
$[3, 3, 4^+]$	192	$[3, 4^+] = [3, 3] = TO$	24	preserves the 2-coloring
$[^+3, 3, 4^+]$	96	$[^+3, 4^+] = [3, 3]^+ = +T$	12	all three constraints above

Table 11: Analogy between symmetries of the four-dimensional and three-dimensional cube

## 8.5 Symmetries of the 600-cell (and its polar, the 120-cell)

The 120 quaternions  $2I$  form the vertices of a 600-cell  $P_{600} = \{3, 3, 5\}$ . These quaternions are the centers of the 120 dodecahedra of the polar 120-cell  $Q_{120} = \{5, 3, 3\}$ , which has 600 vertices. The full symmetry group of  $P_{600}$  (or  $Q_{120}$ ) is  $[3, 3, 5]$ . Its chiral version is  $[3, 3, 5]^+$ .

The group has four interesting subgroups, which come in enantiomorphic versions. Under the left rotations by elements of  $2I$ , or in other words, under the group  $\pm[I \times C_1]$ , the 600 vertices of  $Q_{120}$  decompose into five orbits, as shown by the five labels  $A, B, C, D, E$  for the cell  $F_0$  in Figure 30a, cf. [15, Figure 22, p. 84]. We can regard this as a 5-coloring of the vertices. (The points of each color are labeled  $X, X', X'', X'''$  according to the horizontal levels in this picture, but this grouping has otherwise no significance.) One can indeed check that the mapping from a pentagonal face to the opposite face with a left screw by  $\pi/5$ , as effected by the elements of  $\pm[I \times C_1]$ , preserves the coloring.

The vertices of one color form a regular tetrahedron inscribed in a regular dodecahedron, and there are thus five ways inscribe such a “left” tetrahedron in a regular dodecahedron. There is an analogous “right” 5-coloring by the orbits under  $\pm[C_1 \times I]$ , and correspondingly, there are five ways of inscribing a “right” tetrahedron in a regular dodecahedron. One such tetrahedron is shown in Figure 30b.<sup>19</sup> The left and right tetrahedra are mirrors of each other, and they can be distinguished by looking at the paths of length 3 on the dodecahedron between vertices of a tetrahedron: These paths are either S-shaped zigzag paths (for left tetrahedra) or they have the shape of an inverted S (for right tetrahedra).

Every color class consists of the points  $2I \cdot p_0$  for some starting point  $p_0$ , and hence it forms a rotated copy  $P'_{600}$  of the 600-cell  $P_{600}$ . This polytope is strongly inscribed in  $Q_{120}$ : For each dodecahedron of  $Q_{120}$ , there is a unique left rotation in  $\pm[I \times C_1]$  mapping  $F_0$  to this dodecahedron, and in this way we get 120 images of the starting tetrahedron. Figure 30a shows these tetrahedra in three adjacent dodecahedra. (As a sanity check, one can perform

<sup>19</sup>The unions of these five or ten tetrahedra inside a dodecahedron form nice nonconvex star-like polyhedral compounds, see [15, Figures 14 and 15a–b]. See also <https://blogs.ams.org/visualinsight/2015/05/15/dodecahedron-with-5-tetrahedra/> from the AMS blog “Visual Insight”.

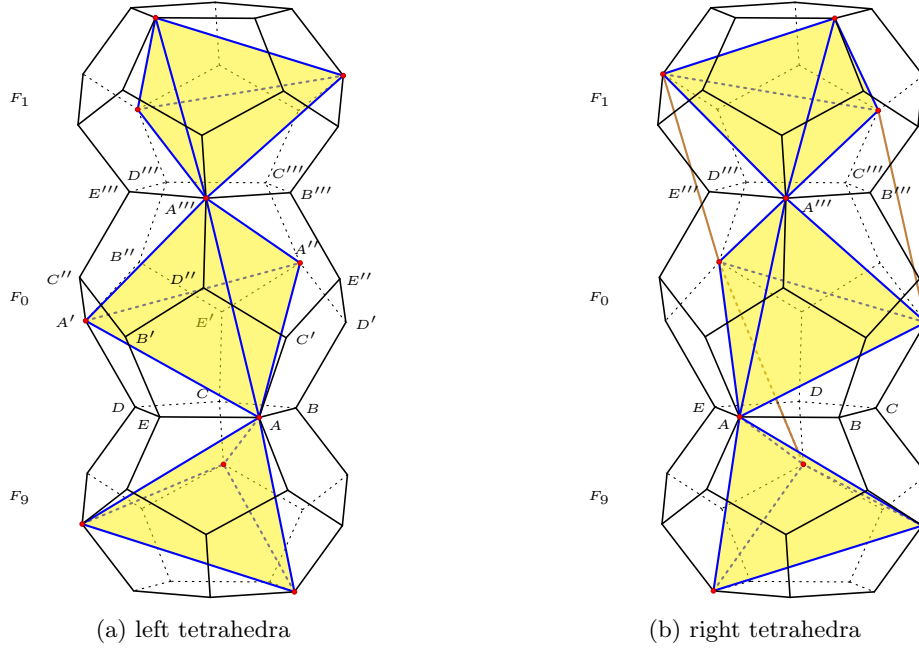


Figure 30: A sequence of inscribed tetrahedra in three successive dodecahedra of the 120-cell  $Q_{120}$ . The red vertices form a 600-cell  $P'_{600}$ . This is an orthogonal projection to the tangent space in the center of the middle cell, and this is why the top and bottom cells are foreshortened.

a small calculation: A vertex is shared by four tetrahedra—one tetrahedron in each of the four dodecahedra meeting in the vertex—and this gives a consistent vertex count, since every tetrahedron has four vertices and  $120 \cdot 4/4 = 120$ .)

The red points in Figure 30b form part of an analogous 600-cell  $P'^R_{600}$  spanned by right inscribed tetrahedra. Some additional edges of this  $P'^R_{600}$ , which don't lie in the three dodecahedra that are shown, are drawn in brown.

The group  $\pm[I \times T]$  consists of those symmetries of that simultaneously preserve the 120-cell  $Q_{120}$  and its strongly inscribed “left” 600-cell  $P'_{600}$ . To see this, consider the dodecahedral cell  $F_0$  that is centered at the quaternion 1. As mentioned, each left multiplication by an element  $2I$  maps  $F_0$ , together with its inscribed tetrahedron  $AA'A''A'''$  to a unique dodecahedral cell of  $Q_{120}$  with the corresponding tetrahedron. To understand the full group, we have to consider those group elements that keep  $F_0$  fixed.  $\pm[I \times T]$  consists of the elements  $[l, r]$  with  $(l, r) \in 2I \times 2T$ . The transformation  $[l, r]$  keeps  $F_0$  fixed iff it maps 1 to 1, and this is the case iff  $l = r$ . These elements are the elements  $[r, r] = [r]$  with  $r \in 2T$ , in other words, they form the tetrahedral group  $\pm T$ . And indeed, the symmetries of  $F_0$  that keep the tetrahedron  $AA'A''A'''$  invariant form a tetrahedral group.

We chose  $[3, 3, 5]_{\frac{1}{5}L}^+$  as an ad-hoc extension of Coxeter's notation for the group  $\pm[I \times T]$ , to indicate a  $1/5$  fraction of the group  $[3, 3, 5]^+$ .

Now, there is also the original 600-cell  $P_{600}$ , the polar of the  $Q_{120}$ , having one vertex in the center of each dodecahedron. This gives rise to a larger group  $[3, 3, 5]_{\frac{1}{5}L}^+ = \pm[I \times O]$  where the two 600-cells  $P_{600}$  and  $P'_{600}$  (properly scaled) are swapped. This group is not a subgroup of any other 4-dimensional point group.

When the starting point  $s$  is chosen in the center of the dodecahedral cell of  $Q_{120}$ , the polar orbit polytope of this group has 240 cells. Figure 31 shows such a cell  $C$ . The points of the orbit closest to  $s$  are four vertices of the dodecahedron (say, those of color  $A$ , the red points in Figure 30a). They form a tetrahedral cell of  $P'_{600}$ , and they are responsible for the rough tetrahedral shape of  $C$ . The centers of the twelve neighboring dodecahedra in  $Q_{120}$  give rise to the twelve small triangular faces, which are the remainders of the twelve pentagons of the original dodecahedral cell, when the polar is not present. In addition, there are four neighboring cells that are adjacent through hexagonal faces, opposite the large 12-gons. They are centered at vertices of  $P'_{600}$ . Two of these are shown as red points in Figure 30a, the point adjacent to  $C$  in the lower cell  $F_9$ , and the point adjacent to  $D'''$  in the upper cell  $F_1$ . The cell has chiral tetrahedral symmetry  $+T$ . In particular, it is not mirror-symmetric. In [16, Figure 9], this cell

is shown together with a fundamental domain inside it. Incidentally, this cell (and the orbit polytope) coincides with that of the tubical group  $\pm[I \times C_4]$  when the starting point is chosen on a two-fold rotation center (Figure 37).

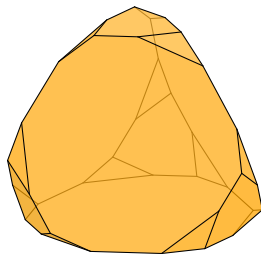


Figure 31: A cell  $C$  of the polar orbit polytope of the group  $\pm[I \times O]$

If we use the “right” 5-coloring we get the corresponding groups  $[3, 3, 5]_{\frac{1}{5}R}^+ = \pm[T \times I]$  and  $[[3, 3, 5]_{\frac{1}{5}R}^+] = \pm[O \times I]$ . See Figure 30b. These four groups come in two enantiomorphic pairs. The two corresponding groups are mirrors of each other. (They are therefore *metachiral groups* in the terminology of Conway and Smith [8, §4.6].)

## 8.6 Symmetries of the 24-cell

The set of 24 quaternions of  $2T$  form the vertices of a regular 24-cell  $P_T$ . The complete symmetry group of  $P_T$  is  $[3, 4, 3]$ , and its chiral version is  $[3, 4, 3]^+$ .

The points of  $P_T$  can be 3-colored: There are 8 vertices of  $P_T$  whose coordinates are the permutations of  $(\pm 1, 0, 0, 0)$ . They form a cross-polytope. The 16 remaining vertices are of the form  $(\pm 1/2, \pm 1/2, \pm 1/2, \pm 1/2)$ . They are the vertices of a 4-cube, and they can be naturally divided into two color groups of 8, as mentioned in Section 8.4. In total, we have three groups of 8 vertices, which we interpret as a *3-coloring* of the vertices by the colors  $a, b, c$ , see Figure 32a. Every triangular face contains vertices from all three colors. Thus, every symmetry of  $P_T$  induces a permutation of the colors.

We can look at those symmetries for which the permutations of the colors is even. In other words, besides the identity, we allow only cyclic shifts. These form the subgroup  $[3, 4, 3^+]$ . Another way to express this is to establish an *orientation of the edges* according to some cyclic ordering of the colors  $a \rightarrow b \rightarrow c \rightarrow a$  (a *coherent orientation* [10, §8.3]). The subgroup  $[3, 4, 3^+]$  consists of those elements that preserve this edge orientation. (This is analogous to the pyritohedral group  $\pm T$  in three dimensions, which can also be described as preserving the orientation of the edges of the octahedron shown in Figure 32a.)

The 24-cell is a self-dual polytope. In fact, the vertices of the polar polytope  $P_{T_1}$  (properly scaled) are the quaternions in the coset of  $2T$  in  $2O$ . If we add to  $[3, 4, 3]$  the symmetries that swap  $P_T$  and  $P_{T_1}$ , we get the group  $[[3, 4, 3]]$ , the symmetry group of the joint configuration  $P_O = P_T \cup P_{T_1}$ . Its chiral version is  $[[3, 4, 3]]^+$ . The subgroup  $[[3, 4, 3]]^+$  contains the symmetries that exchange  $P_T$  and  $P_{T_1}$  only in combination with a reversal of orientation. This group is interesting, because it is achiral, but it contains no reflections.

The polar polytope also has a three-coloring of its vertices. (One can give the partition explicitly in terms of the coordinates, as for  $P_T$ : The vertices of  $P_{T_1}$  are the centers of the facets of  $P_T$ , properly scaled, and their coordinates  $(x_1, x_2, x_3, x_4)$  are all permutations of the coordinates  $(\pm 1, \pm 1, 0, 0)/\sqrt{2}$ . The three color classes are characterized by the condition  $|x_1| = |x_2|$ ,  $|x_1| = |x_3|$ , and  $|x_1| = |x_4|$ , respectively.) We can interpret this 3-coloring as a 3-coloring of the *cells* of  $P_T$ , which we denote by  $A, B, C$ . The group  $[^+3, 4, 3]$  contains those symmetries of  $P_T$  for which the permutation of the colors of the *cells* is even. This group is of course geometrically the same as  $[3, 4, 3^+]$ , but we can also have both conditions:  $[^+3, 4, 3^+]$ .

### 8.6.1 A pair of enantiomorphic groups

Finally, we have two more groups, which are mirrors of each other. To understand these groups, let us look at the polar orbit polytope of  $P_O = P_T \cup P_{T_1}$ : The octahedral cells of the 24-cell shrink to truncated cubes with 6 regular octagons and 8 triangles as faces, see Figure 32b. This polytope is sometimes called the bitruncated 24-cell, or truncated-cubical tetraconta-octachoron.

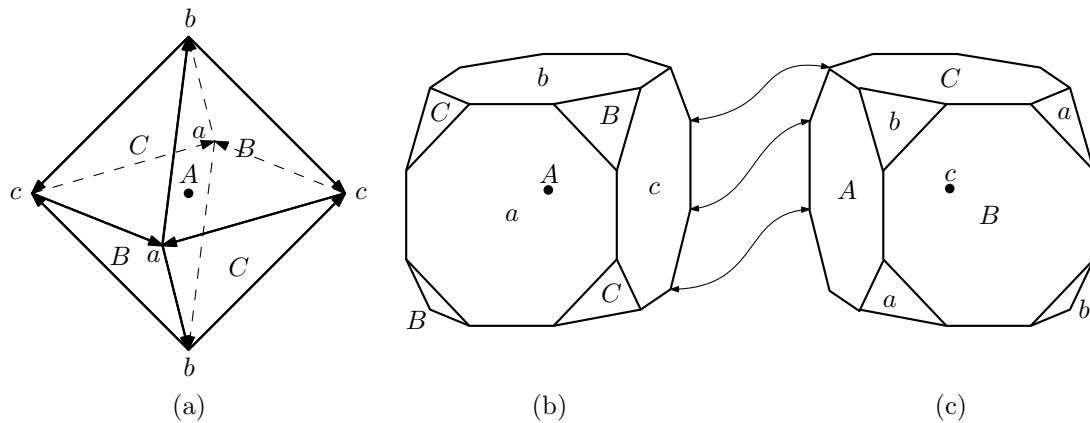


Figure 32: (a) An octahedral cell of the 24-cell with a consistent edge orientation. (b) The 48-cell consists of 48 truncated cubes.

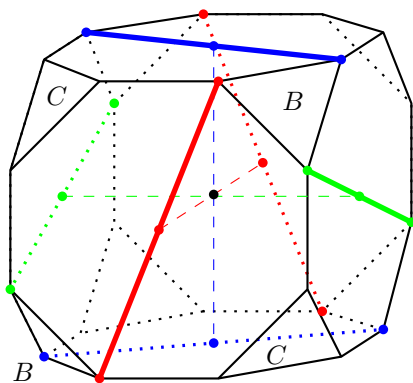


Figure 33: Decoration of the truncated cube by diagonals.

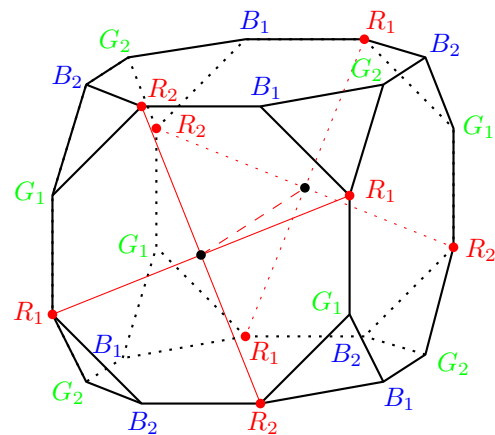


Figure 34: The 6 orbits of the vertices under  $\pm[O \times C_1]$  (left multiplication with  $2O$ )

We will simply refer to it as the *48-cell*. The small triangles are remainders from the triangular faces of the original octahedral cells of the 24-cell, which are centered at the points  $P_T$ .

Figure 32b shows a cell of color *A*. The triangles lead to adjacent cells, colored *B* or *C*, and we have labeled the triangles accordingly. The octagons lead to cells centered at points of  $P_T$ , and we have labeled them with the corresponding color *a*, *b*, or *c*.

Figure 32c shows an adjacent “dual” cell of the 48-cell, centered at a point of color *c*. Note that these two cells are not attached in a straight way, but by a screw of  $45^\circ$ . We can enforce the screw to be a left screw by decorating each of the six octagonal faces with a diagonal, as shown in Figure 33. The group  $\pm[O \times C_1]$  will map one selected cell to each cell by a unique left multiplication with an element of  $2O$  and hence will carry the diagonal pattern to every truncated cube of the 48-cell. The diagonals on adjacent cells match: A left rotation that maps a cell to the adjacent cell performs a left screw by  $45^\circ$ , and one can check in Figure 33 that the screw that maps an octagon to the opposite octagon while maintaining the diagonal is a left screw.

The group  $\pm[O \times T]$  is the group that preserves the set of diagonals (ignoring the colors). This can be confirmed as in the case  $\pm[I \times T]$  in Section 8.5: The group that fixes a cell should be the tetrahedral group  $+T$ , and indeed, the diagonal pattern of Figure 33 has tetrahedral symmetry: The diagonals connect only the *B*-triangles, and the *B*-triangles form a tetrahedral pattern. We have chosen the ad-hoc extension of Coxeter’s notation  $[+3, 4, 3^+]_L$  for the group  $\pm[O \times T]$  to indicate that it extends the operations  $[+3, 4, 3^+]$  by a swap between  $P_T$  and the polar polytope  $P_{T_1}$ , and this swap is effected by *left* rotations.

Of course, there is a mirror pattern of Figure 33, which leads to the mirror group  $\pm[T \times O] = [[+3, 4, 3^+]]_R$ , and these two groups are enantiomorphic.

D2215  
D2216  
D2217  
D2218  
D2219  
D2220  
D2221  
D2222  
D2223  
D2224  
D2225  
D2226  
D2227  
D2228  
D2229  
D2230  
D2231  
D2232  
D2233  
D2234  
D2235  
D2236  
D2237



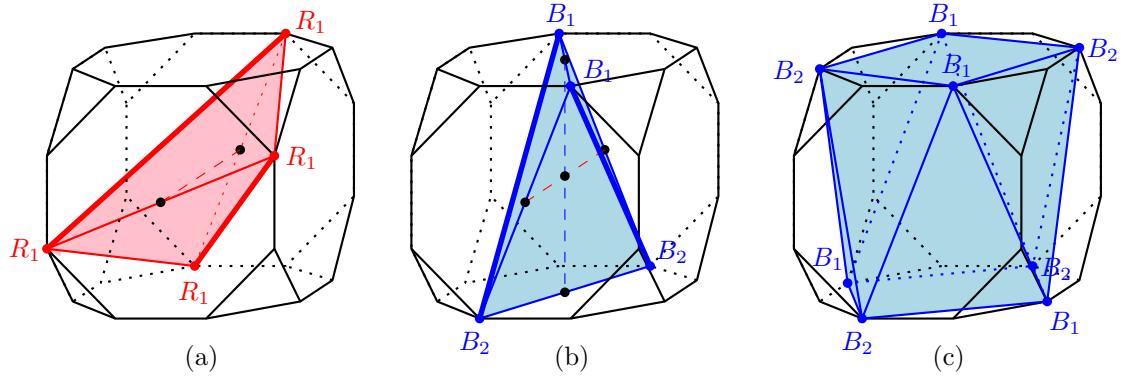


Figure 35: Facets inscribed in the truncated cube

**Analogies with three dimensions.** As pointed out by Du Val [15, p. 71], there is a strong analogy between the symmetries of the different self-dual polytopes in three and in four dimensions, as shown in Table 12. The simplex is a self-dual regular polytope, both in 4 dimensions (Section 8.3) and in 3 dimensions. In 3 dimensions, moreover, the simplex and its polar form the cube, and thus we have used alternate Coxeter notations to highlight the analogy (opposite ones from Table 11, where the analogy with the cube is emphasized). Only five of the symmetries of the 24-cell and its polar are used.

From the viewpoint of the cross-polytope, one could also match the group  $\pm[T \times T] \cdot 2 = [3, 4, 3^+] = [+3, 4, 3]$  of order 576 with the pyritohedral group  $\pm T = [+3, 4]$  of order 24, because they are both based on consistent edge orientations.

4-simplex	order	24-cell	order	3-simplex	order	description
$[3, 3, 3]$	240	$[3, 4, 3]$	2304	$[3, 3] = [3, 4] = \pm O$	48	all symmetries
$[3, 3, 3]^+$	120	$[3, 4, 3]^+$	1152	$[3, 3]^+ = [3, 4]^+ = +O$	24	chiral part
$[3, 3, 3]$	120	$[3, 4, 3]$	1152	$[3, 3] = TO$	24	nonswapping
$[3, 3, 3]^+$	120	$[3, 4, 3]^+$	1152	$[3, 3]^+ = [+3, 4] = \pm T$	24	swap with mirror
$[3, 3, 3]^+$	60	$[3, 4, 3]^+$	576	$[3, 3]^+ = +T$	12	chiral & nonswapping

Table 12: Analogies between symmetries of self-dual polytopes

**A strongly inscribed polar polytope.** The convex hull of the points  $P_O = P_T \cup P_{T_1}$  is a polytope with 288 equal tetrahedral facets, which we call the *288-cell*. It is polar to the 48-cell. We perform the same procedure as in Section 8.5 and split the vertices of the 48-cell into orbits under the action of  $\pm[O \times C_1]$ . We will see that this leads to another instance of a polytope with a strongly inscribed copy of its polar. However, we won't get any new groups.

The 48-cell has 288 vertices, and they are partitioned into 6 orbits of size 48, as shown in Figure 34, cf. Du Val [15, Figure 24, p. 85]: There is a natural partition of the colors into three pairs  $R_1, R_2$ ;  $G_1, G_2$ ; and  $B_1, B_2$ , according to the opposite octagons to which the colors belong. (The partition of each pair into  $R_1$  and  $R_2$ , etc., is arbitrary.) Indeed, one can check that the transition from an octagon to the opposite octagon with a left screw of  $45^\circ$  preserves the six colors (indicated for the red colors by two corresponding crosses.) Likewise, the transition from a triangle to the opposite triangle with a left screw of  $60^\circ$  preserves the colors.

Now, as in Section 8.5, the points of one color form a right coset of  $2O$ , and hence they form a rotated and scaled copy  $P'_O$  of the 288-cell  $P_O$ . This polytope is strongly inscribed in the 48-cell: Each truncated cube of the 48-cell contains one tetrahedron of  $P'_O$ . Figure 35a shows one such tetrahedron, spanned by the vertices of color  $R_1$ .

The geometry of this tetrahedron becomes clearer after rotating it by  $45^\circ$  around the midpoints of the front and back octagons, as in Figure 35b. We see that the tetrahedron has four equal edges, whose length is the diagonal of the octagons, and two opposite edges of larger length, equal to the diagonal of a circumscribed square. The 2-faces are therefore congruent isosceles triangles. Such a tetrahedron is called a *tetragonal disphenoid*.<sup>20</sup>

<sup>20</sup>The side length of the “untruncated” cube is  $\sqrt{8} - 2 \approx 0.8$ , which equals the edge length of a circumscribed 8-gon around a unit circle. Hence the two long edges of the tetrahedra, highlighted in bold, have length  $\sqrt{2}(\sqrt{8} - 2) =$



The symmetry group of the 48-cell together with its strongly inscribed 288-cell  $P'_O$  is the tubical group  $\pm[O \times D_4]$ , because the symmetry group of the disphenoid inside the truncated cube is only the vierergruppe  $D_4$ , consisting of half-turns through edge midpoints.

We can try to start with the rotated tetrahedra of Figure 35b, spanned by two opposite diagonals used for the decoration in Figure 34, hoping to recover the group  $\pm[O \times T]$ . However, this tetrahedron contains vertices of *two* colors  $B_1$  and  $B_2$ , and its orbit will thus contain the union of the orbits  $B_1$  and  $B_2$ . Inside each truncated cube, the convex hull forms a quadratic antiprism, as shown Figure 35c. (The convex hull contains 48 such antiprisms plus 192 tetrahedral cells, for a total of 240 facets.)

## 9 The axial groups

These are the finite subgroups of the direct product  $O(3) \times O(1)$ . The subgroup  $O(1)$  operates on the 4-th coordinate  $x_4$ , and we denote its elements by  $O(1) = \{+x_4, -x_4\}$ . Here  $+x_4$  is the identity, and  $-x_4$  denotes the reflection of the 4-th coordinate.

Let  $G$  be such an axial group. Let  $G_3 \in O(3)$  be the “projection” of  $G$  on  $O(3)$ . That is,

$$G_3 := \{g \in O(3) \mid (g, +x_4) \in G \text{ or } (g, -x_4) \in G\}.$$

If  $G_3$  itself is a 3-dimensional axial group, i.e.  $G \leq O(2) \times O(1)$ , then we may call  $G$  a *doubly axial group*. In this case, we prefer to regard  $G$  as a toroidal group in  $O(2) \times O(1) \times O(1) \leq O(2) \times O(2)$  and classify it as such. (These groups are the subgroups of  $\boxplus_{m,2}^{p2mm}$ .) Hence from now on, we assume that  $G_3$  is not an axial 3-dimensional group, i.e., we assume that  $G_3 \leq O(3)$  is one of the seven *polyhedral* 3-dimensional groups (see Section 3.6). These are well-understood, and thus the axial groups are quite easy to classify. There are 21 axial groups (excluding the doubly axial groups), and their full list is given below in Table 15, with references to other classifications from the literature. Together with the polyhedral groups in Table 10, these groups exhaust all entries in [8, Tables 4.2 and 4.3] except the toroidal groups. Table 16 in Appendix A lists them with generators and cross-references to other classifications.

Note that the product  $O(3) \times O(1)$  used here is different from the product  $\pm[L \times R]$  on which the classic classification is based. Both are direct products in the group-theoretic sense, but  $O(3) \times O(1)$  is a direct sum, a “Cartesian” product in a straightforward geometric sense, consisting of pairs of independent transformations in orthogonal subspaces, whereas the product  $\pm[L \times R]$ , which is specific to  $SO(4)$ , refers to the representation  $[l, r]$  by pairs of quaternions, which have by themselves a significance as operations  $[l]$  and  $[r]$  in  $SO(3)$ .

We will now derive the axial groups systematically. Let  $G_3^{+x_4} \leq O(3)$  be the subgroup of  $G_3$  of those elements that don’t negate the 4-th coordinate. That is,

$$G_3^{+x_4} := \{g \in O(3) \mid (g, +x_4) \in G\}.$$

The subgroup  $G_3^{+x_4}$  is either equal to  $G_3$ , or it is an index-2 subgroup of  $G_3$ .

If  $G_3^{+x_4} = G_3$ , there are two cases, which are both easy: we can form the “pyramidal” group  $G_3 \times \{+x_4\}$ , which does not move the 4-th dimension at all, or the full “prismatic” group  $G_3 \times \{+x_4, -x_4\}$ . This gives two axial groups for each three-dimensional polyhedral group  $G_3 \leq SO(3)$ , and they are listed in Table 13, together with their “CS names” following Conway and Smith [8], and their “Coxeter names”, which are explained in Table 15. The pyramidal groups are just the common 3-dimensional polyhedral groups, interpreted as operating in 4 dimensions.

The prismatic groups are never chiral. The pyramidal group  $G_3 \times \{+x_4\}$  is chiral iff  $G_3$  is: These are the groups  $+I$ ,  $+O$ , and  $+T$ .

We are left with the case that  $G_3^{+x_4}$  is an index-2 subgroup  $H$  of  $G_3$ . In this case, the group  $G$  is uniquely determined by  $H$  and  $G_3$ : It consists of the elements  $(g, +x_4)$  for  $g \in H$  and  $(g, -x_4)$  for  $g \in G_3 - H$ . We denote this group as “ $H$  in  $G_3$ ”. As an abstract group, it is isomorphic to  $G_3$ . There are seven index-2 containments among the three-dimensional polyhedral groups. (See [8, Figures 3.9 and 3.10] for an overview about all index-2 containments in  $O(3)$ .) They lead to seven “hybrid axial groups”, which are listed in Table 14.

There are several methods by which such an index-2 containment can be constructed, and we indicate in the table which methods are applicable:

---

$4 - \sqrt{8} \approx 1.17$ . The four short edges have length  $\sqrt{8(10 - \sqrt{98})} \approx 0.9$ , and the edge length of the 48-cell is  $6 - \sqrt{32} \approx 0.34$ .

$G_3$			pyramidal groups $G_3 \times \{+x_4\}$			prismatic groups $G_3 \times \{+x_4, -x_4\}$		
name	orbitope	I.T.	CS name	Cox.	order	CS name	Cox. name	order
$\pm I$	<b>*532</b>	53m	$+\frac{1}{60}[I \times I] \cdot 2_3$	[3, 5]	120	$\pm\frac{1}{60}[I \times I] \cdot 2$	2.[3, 5]	240
$+I$	<b>532</b>	532	$+\frac{1}{60}[I \times I]$	[3, 5] <sup>+</sup>	60	$+\frac{1}{60}[I \times I] \cdot 2_1$	[3, 5] <sup>°</sup>	120
$\pm O$	<b>*432</b>	m3m	$+\frac{1}{24}[O \times O] \cdot 2_3$	[3, 4]	48	$\pm\frac{1}{24}[O \times O] \cdot 2$	2.[3, 4]	96
$+O$	<b>432</b>	432	$+\frac{1}{24}[O \times O]$	[3, 4] <sup>+</sup>	24	$+\frac{1}{24}[O \times O] \cdot 2_1$	[3, 4] <sup>°</sup>	48
$TO$	<b>*332</b>	$\bar{4}3m$	$+\frac{1}{12}[T \times \bar{T}] \cdot 2_1$	[3, 3]	24	$+\frac{1}{24}[O \times \bar{O}] \cdot 2_1$	[2, 3, 3]	48
$\pm T$	<b>3*2</b>	m3	$+\frac{1}{12}[T \times T] \cdot 2_3$	[ <sup>+</sup> 3, 4]	24	$\pm\frac{1}{12}[T \times T] \cdot 2$	2.[ <sup>+</sup> 3, 4]	48
$+T$	<b>332</b>	23	$+\frac{1}{12}[T \times T]$	[3, 3] <sup>+</sup>	12	$+\frac{1}{12}[T \times T] \cdot 2_1$	[ <sup>+</sup> 3, 4] <sup>°</sup>	24

Table 13: Pyramidal and prismatic axial groups (except doubly axial groups)

hybrid axial groups				
$G_3^{+x_4}$ in $G_3$	CS name	Coxeter name	order	methods
$+I$ in $\pm I$	$\pm\frac{1}{60}[I \times I]$	2.[3, 5] <sup>+</sup>	120	center, chirality
$\pm T$ in $\pm O$	$+\frac{1}{24}[O \times \bar{O}] \cdot 2_3$	[2, 3, 3] <sup>°</sup>	48	edge orientation
$+O$ in $\pm O$	$\pm\frac{1}{24}[O \times O]$	2.[3, 4] <sup>+</sup>	48	center, chirality
$TO$ in $\pm O$	$\pm\frac{1}{12}[T \times \bar{T}] \cdot 2$	2.[3, 3]	48	center, alternation
$+T$ in $\pm T$	$\pm\frac{1}{12}[T \times T]$	2.[3, 3] <sup>+</sup>	24	center, chirality
$+T$ in $+O$	$+\frac{1}{12}[T \times \bar{T}] \cdot 2_3$	[3, 3] <sup>°</sup>	24	alternation
$+T$ in $TO$	$+\frac{1}{24}[O \times \bar{O}]$	[2, 3, 3] <sup>+</sup>	24	chirality

Table 14: Hybrid axial groups (except doubly axial groups)

- D2315 1. Chirality:  $G_3^{+x_4}$  is the chiral part of an achiral group  $G_3$ . In this case, the resulting group will be chiral, because the orientation-reversing elements of  $G_3$  are composed with the reflection of the axis. In other words,  $G$  is the chiral part  $(G_3 \times \{x_4, -x_4\})^+$  of the prismatic group  $G_3 \times \{x_4, -x_4\}$ .
- D2316
- D2317
- D2318
- D2319 2. Center:  $G_3^{+x_4}$  does not contain the central reflection. In this case, an index-2 extension  $G_3$  of  $G_3^{+x_4}$  can always be obtained by adjoining the central reflection (in  $\mathbb{R}^3$ ). The resulting group “ $G_3^{+x_4}$  in  $G_3$ ” is equivalently thought of as simply adjoining the central reflection (in  $\mathbb{R}^4$ ) to  $G_3^{+x_4}$ . These groups can be recognized as having their Coxeter names prefixed with “2.”.  $G$  is achiral iff  $G_3^{+x_4}$  is achiral, and in this case, the construction is simultaneously a case of the chirality method.
- D2320
- D2321
- D2322
- D2323
- D2324
- D2325 3. Alternation: This applies to the octahedral groups, which are symmetries of the cube. The vertices of the cube can be two-colored. The subgroup consists of those transformations that preserve the coloring.
- D2326
- D2327
- D2328 4. Edge orientation: There is only one case where this applies, namely the pyritohedral group  $\pm T$  as a subgroup of the full octahedral group  $\pm O$ . The edges of the octahedron can be *coherently* oriented in such a way that the boundary of every face is a directed cycle. The subgroup consists of those transformations that preserve this orientation (cf. the use of the edge orientation for the 24-cell and its polar, Section 8.6).
- D2329
- D2330
- D2331
- D2332

D2333 Often, the same result can be obtained by two methods. For example,  $TO$  in  $\pm O$  results both from alternation and from center.

D2334 The group “ $G_3^{+x_4}$  in  $G_3$ ” is chiral if and only if  $G_3^{+x_4}$  is chiral and  $G_3$  is achiral, because the elements of  $G_3 \setminus G_3^{+x_4}$  are flipped by the  $x_4$ -reflection. These are the case of the form “ $+G$  in  $\pm G$ ” in the table, plus the group “ $+T$  in  $TO$ ”.

D2335 The situation is very much analogous to the construction of the achiral groups in  $O(3)$  from the chiral groups in  $SO(3)$  and their index-2 subgroups in [8, §3.8], except that Conway and Smith prefer to extend by the algebraically simpler central inversion  $-\text{id}$  instead of the geometrically more natural reflection of the axial coordinate.

D2336 The maximal axial groups are  $\pm\frac{1}{60}[I \times I] \cdot 2 = 2.[3, 5]$  and  $\pm\frac{1}{24}[O \times O] \cdot 2 = 2.[3, 4]$ . Hence, the axial groups can be characterized as the symmetries of a 4-dimensional prism over an icosahedron

D2343

The 21 axial groups					
pyramidal groups $G_3 \times \{+x_4\}$					
$G_3$	CS name	Du Val # and name	Cox.	BBNZW	order
$\pm I$	$+\frac{1}{60}[I \times I] \cdot 2_3$	49' ( $I/C_1; I/C_1$ )*	[3, 5]	n.cryst.	120
$+I$	$+\frac{1}{60}[I \times I]$	31' ( $I/C_1; I/C_1$ )	[3, 5] <sup>+</sup>	n.cryst.	60
$\pm O$	$+\frac{1}{24}[O \times O] \cdot 2_3$	44' ( $O/C_1; O/C_1$ )*'	[3, 4]	25/10	48
$+O$	$+\frac{1}{24}[O \times O]$	26' ( $O/C_1; O/C_1$ )'	[3, 4] <sup>+</sup>	25/03	24
$TO$	$+\frac{1}{12}[T \times \bar{T}] \cdot 2_1$	40' ( $T/C_1; T/C_1$ )*	[3, 3]	24/04	24
$\pm T$	$+\frac{1}{12}[T \times T] \cdot 2_3$	39' ( $T/C_1; T/C_1$ )* <sub>c</sub>	[ <sup>+</sup> 3, 4]	25/02	24
$+T$	$+\frac{1}{12}[T \times T]$	21' ( $T/C_1; T/C_1$ )	[3, 3] <sup>+</sup>	24/01	12
prismatic groups $G_3 \times \{+x_4, -x_4\}$					
$G_3$	CS name	Du Val # and name	Cox.	BBNZW	order
$\pm I$	$\pm\frac{1}{60}[I \times I] \cdot 2$	49. ( $I/C_2; I/C_2$ )*	2.[3, 5]	n.cryst.	240
$+I$	$+\frac{1}{60}[I \times I] \cdot 2_1$	49' ( $I/C_1; I/C_1$ )* <sub>-</sub>	[3, 5] <sup>o</sup>	n.cryst.	120
$\pm O$	$\pm\frac{1}{24}[O \times O] \cdot 2$	44. ( $O/C_2; O/C_2$ )*	2.[3, 4]	25/11	96
$+O$	$+\frac{1}{24}[O \times O] \cdot 2_1$	44' ( $O/C_1; O/C_1$ )*' <sub>-</sub>	[3, 4] <sup>o</sup>	25/07	48
$TO$	$+\frac{1}{24}[O \times \bar{O}] \cdot 2_1$	44'' ( $O/C_1; O/C_1$ )*'' <sub>-</sub>	[2, 3, 3]	25/08	48
$\pm T$	$\pm\frac{1}{12}[T \times T] \cdot 2$	39. ( $T/C_2; T/C_2$ )* <sub>c</sub>	2.[ <sup>+</sup> 3, 4]	25/05	48
$+T$	$+\frac{1}{12}[T \times T] \cdot 2_1$	39' ( $T/C_1; T/C_1$ )* <sub>c-</sub>	[ <sup>+</sup> 3, 4] <sup>o</sup>	25/01	24
hybrid axial groups $G_3^{+x_4}$ in $G_3$					
$G_3^{+x_4}$ in $G_3$	CS name	Du Val # and name	Cox.	BBNZW	order
$+I$ in $\pm I$	$\pm\frac{1}{60}[I \times I]$	31. ( $I/C_2; I/C_2$ )	2.[3, 5] <sup>+</sup>	n.cryst.	120
$\pm T$ in $\pm O$	$+\frac{1}{24}[O \times \bar{O}] \cdot 2_3$	44'' ( $O/C_1; O/C_1$ )*''	[2, 3, 3] <sup>o</sup>	25/09	48
$+O$ in $\pm O$	$\pm\frac{1}{24}[O \times O]$	26. ( $O/C_2; O/C_2$ )	2.[3, 4] <sup>+</sup>	25/06	48
$TO$ in $\pm O$	$\pm\frac{1}{12}[T \times \bar{T}] \cdot 2$	40. ( $T/C_2; T/C_2$ )*	2.[3, 3]	24/05	48
$+T$ in $\pm T$	$\pm\frac{1}{12}[T \times T]$	21. ( $T/C_2; T/C_2$ )	2.[3, 3] <sup>+</sup>	24/02	24
$+T$ in $+O$	$+\frac{1}{12}[T \times \bar{T}] \cdot 2_3$	40' ( $T/C_1; T/C_1$ )* <sub>-</sub>	[3, 3] <sup>o</sup>	24/03	24
$+T$ in $TO$	$+\frac{1}{24}[O \times \bar{O}]$	26'' ( $O/C_1; O/C_1$ )''	[2, 3, 3] <sup>+</sup>	25/04	24

Table 15: Summary of the 21 axial groups (except doubly axial groups). We have included references to the list of crystallographic 4-dimensional groups by Brown, Bülow, Neubüser, Wondratschek, Zassenhaus (BBNWZ) [4], and the names of Du Val [15], together with his numbering which extends the numbering of Goursat.

We use two further adaptations of Coxeter's notation, following [8]:  $G^\circ$  is obtained by replacing the orientation-reversing elements  $g$  of  $G$  by  $-g$ . An initial "2." indicates doubling the group by adjoining negatives. The 2 in [2, 3, 3] indicates the presence of an extra "perpendicular" mirror  $R_1$  that commutes with the other reflections.

In Du Val's notation, achiral groups can be recognized by the \* superscript. Haploid groups (those whose CS name begins with a +) were not considered by Goursat, and Du Val denotes them by adding primes to the numbers of the corresponding diploid groups, such as 44' and 44''. Variations are indicated by various subscript and superscript decorations of the group names. In some cases, a unique notation is only achieved by considering the number and the name together. Thus, we are deviating from Du Val's notation by attaching the primes also to the names. For example, Du Val distinguishes two groups 26' and 26'' with the same name ( $O/C_1; O/C_1$ ). Accordingly, although this is overlooked in Du Val [15, p. 61], one must also make a distinction between the corresponding achiral groups 44' and 44''. Each of these two achiral extensions comes in two variations: ( $O/C_1; O/C_1$ )\* and ( $O/C_1; O/C_1$ )\*<sub>-</sub>. This omission in Du Val's list was already noted by Dunbar [16, p. 141, last paragraph].

or over an octahedron, and the subgroups of these. (This includes, however, the doubly axial groups, which we have classified under the toroidal groups.)

**Numerology.** Among the  $3 \times 7 = 21$  axial groups, there are 7 chiral ones and 14 achiral ones. Among the polyhedral groups, there are 14 chiral ones. In addition, there are 14 types of three-dimensional point groups, which split into 7 polyhedral groups and 7 infinite axial families (which correspond to the 7 frieze groups). We have no explanation for the frequent appearance of the magic number 7 and its multiples.

## 10 Computer calculations

We used the help of computers for investigating the groups and checking the results, as well as for the preparation of the figures and tables. We used SageMath [34] and its interface to the GAP [19] software for group-theoretic calculations. The computer code is available in <https://github.com/LaisRast/point-groups>.

### 10.1 Representation of transformations and groups

We represent the orthogonal transformations  $[l, r]$  and  $*[l, r]$  by the quaternion pair  $(l, r)$  and a bit for indicating orientation reversal. In a group, each transformation is represented twice, by the equivalent pairs  $(l, r)$  and  $(-l, -r)$ .

We used two different representations for quaternions: For the elements of  $2I$ ,  $2O$ , and  $2T$ , the quaternions  $x_1 + x_2i + x_3j + x_4$  are represented in the natural way with precise algebraic coefficients, using SageMath's support for algebraic extension fields. For the elements of  $2D_{2n}$ , we used a tailored representation: These elements are of the form  $e_n^s$  or  $e_n^s j$ , and we represent and manipulate them using the fraction  $s/n$ , and a bit that indicates whether the factor  $j$  is present. (An exact algebraic representation would have required extension fields of arbitrarily high degree.)

The left group and the right group don't have to use the same representation: For elements of tubical groups, like  $[l, r] \in \pm[I \times C_n]$ , each of  $l$  and  $r$  uses its own appropriate representation.

### 10.2 Fingerprinting

For preparing a catalog of groups, it is useful to have some easily computable invariants. We used the number of elements of each geometric type as a *fingerprint*. This technique was initiated by Hurley [23] in his classification of the 4-dimensional crystallographic groups.

We first discuss the classification of the individual 4-dimensional orthogonal transformations, as introduced in Section 3.1. Every orientation-preserving orthogonal transformation can be written as a block diagonal matrix  $R_{\alpha_1, \alpha_2}$  of two rotation matrices (1). We must be aware of other angle parameters  $R_{\alpha'_1, \alpha'_2}$  that describe geometrically the same operation, in other words, that are conjugate by an orientation-preserving transformation (see Section 7.3.3). If we swap the two invariant coordinate planes  $(x_1, x_2) \leftrightarrow (x_3, x_4)$ , this is an orientation-preserving transformation, and it turns  $R_{\alpha_1, \alpha_2}$  into  $R_{\alpha_2, \alpha_1}$ . A simultaneous reflection in both coordinate planes  $(x_1 \leftrightarrow x_2$  and  $x_3 \leftrightarrow x_4)$  is also orientation-preserving, and it turns  $R_{\alpha_1, \alpha_2}$  into  $R_{-\alpha_1, -\alpha_2}$ .

Thus,  $R_{\alpha_1, \alpha_2} \doteq R_{\alpha_2, \alpha_1} \doteq R_{-\alpha_1, -\alpha_2} \doteq R_{-\alpha_2, -\alpha_1}$ . On the other hand,  $R_{\alpha_1, \alpha_2}$  and  $R_{\alpha_1, -\alpha_2}$  are distinct unless one of the angles is 0 or  $\pm\pi$ . They are mirrors of each other.

The orientation-reversing transformations  $\bar{R}_\alpha$  of (2) are characterized by a single angle  $\alpha$ . Since the simultaneous negation of  $x_1$  and  $x_4$  turns  $\bar{R}_\alpha$  into  $\bar{R}_{-\alpha}$ , the parameter  $\alpha$  can be normalized to the range  $0 \leq \alpha \leq \pi/2$ .

Since the angles are rational multiples of  $\pi$ , it is possible to encode the data about the operation into a short code. By collecting the codes of the elements in a group into a string, we obtained a “fingerprint” of the group, which we used as a key for our catalog.<sup>21</sup> Experimentally,

<sup>21</sup>Here are some details: We actually use the quaternion pair  $[l, r]$  for computing the code for a rotation: If  $[l, 1]$  and  $[1, r]$  are rotations by  $a\pi$  and  $b\pi$ , respectively, we use the pair of rational numbers  $(a, b)$  with  $0 \leq a, b \leq 1$ . The pair  $[-l, -r]$ , which represents the same rotation, gives the pair  $(1-a, 1-b)$ , and hence we normalize by requiring that  $a < b$  or  $a = b \leq 1/2$ .

For example, the group  $\square_{2,4}^{\text{pg}}$  has the fingerprint 0|0:2 0|1:2 1|1/4:4 1|3/4:4 1|1/2:4 \*1/2:16. We tried to make the code concise while keeping it readable. The term /4 in 1|3/4:4 is a common denominator for both components, and hence 1|3/4 stands for the pair  $(a, b) = (\frac{1}{4}, \frac{3}{4})$ , denoting a rotation of the form  $[\exp \frac{\pi}{4}, \exp \frac{3\pi}{4}] \doteq R_{-\pi/2, \pi}$ . The number :4 after the colon denotes the multiplicity. Since our group representation contains both

in all cases that we encountered, this method was sufficient to distinguish groups up to conjugacy. (As reported below, we considered, from the infinite families of groups, at least all groups of order up to 100.)

The classification of the elements by Hurley [23] is almost equivalent, except that it disregards the orientation: He classified a transformation by the triplet of coefficients  $(c_3, c_2, c_0)$  of its characteristic equation  $\lambda^4 - c_3\lambda^3 + c_2\lambda^2 - c_1\lambda + c_0 = 0$ : the trace  $c_3$ , the second invariant  $c_2$ , and the determinant  $c_0$ . Since all eigenvalues have absolute value 1, the linear coefficient  $c_1$  is determined by the others through the formula  $c_1 = -c_0c_3$ . The Hurley triplet determines the eigenvalues and thus the geometric conjugacy type and the rotation angles  $\alpha_1, \alpha_2$ , but only up to orientation.  $R_{\alpha_1, \alpha_2}$  and  $R_{\alpha_1, -\alpha_2}$  have the same spectrum and the same Hurley symbol.

**The Hurley symbol.** Hurley was interested in the crystallographic groups, and the operations in these groups must have integer coefficients in their characteristic polynomial. This restricts the operations to a finite set. Hurley denoted them by 24 letters (the Hurley symbols).

They were also used in the monumental classification of the four-dimensional crystallographic space groups by Brown, Bülow, Neubüser, Wondratschek, Zassenhaus [4]. Brown et al. refined the classification by splitting the groups into conjugacy classes *under the group operations*, resulting in the *Hurley pattern*. It may happen that several operations are geometrically the same but not conjugate to each other by a transformation of the group that is under consideration.<sup>22</sup>

Brown et al. [4, p. 9] report that their classification, which is more refined than ours but in another respect coarser, since it does not distinguish enantiomorphic groups, was also found to be sufficient to characterize the crystallographic point groups uniquely (up to mirror congruence).

We could use the data in the Tables of [4] to match them with our classification. The results are tabulated in Tables 17–18 in Appendix D.

### 10.3 Computer checks

As mentioned, the classic approach to the classification following Goursat’s method yields the chiral groups, and with the exception of the toroidal groups, they are obtained quite painlessly. However, the achiral groups must be found and classified as index-2 extensions of the chiral groups.

This task has been carried out by Du Val [15] and Conway and Smith [8], but they only gave the results. Du Val [15, p. 61] explicitly lists the orientation-reversing elements of each achiral group. Conway and Smith [8, Tables 4.1–4.3] provide generating elements for each group.

A detailed derivation is not presented in the literature. The considerations about the extension from chiral groups to achiral ones are only briefly sketched by Conway and Smith [8, p. 51–52], see Figures 54–55. Since we found this situation unsatisfactory, we ran a brute-force computer check. We generated all subgroups of the groups  $\pm[I \times I]$ ,  $\pm[O \times O]$  and  $\pm[T \times T]$  and their achiral extensions. No missing groups were discovered. More details are given below.

For the achiral extension of the subgroups of  $\pm[C_n \times C_n]$ , and  $\pm[D_{2n} \times D_{2n}]$ , we have supplanted the classic classification by our own classification as toroidal groups. Nevertheless, we ran some computer checks also for these groups, see Section 10.5.

### 10.4 Checking the achiral polyhedral and axial groups

For each group  $\pm[I \times I]$ ,  $\pm[O \times O]$  and  $\pm[T \times T]$  in turn, we generated all subgroups. We kept only those subgroups for which the left and right subgroup is the full group  $2I$ ,  $2O$ , or  $2T$  respectively. (For an achiral group, we must extend a group whose left group is equal to its right group.)

pairs  $[l, r]$  and  $[-l, -r]$  for each rotation, the multiplicity is always overcounted by a factor of 2. The group actually contains only two operations  $R_{-\pi/2, \pi}$ . (The reader may wish to identify them as particular torus translations of this group, see Figure 23.) The symbol 0|0 denotes the identity. The orientation-reversing transformations are written with a star. The sign  $*a$  with a fraction  $a$  denotes  $\bar{R}_{(1-a)\pi}$ . In our example,  $*1/2:16$  denotes eight operations of the form  $\bar{R}_{\pi/2}$ . The sum of the written multiplicities is 32, in accordance with the fact that the group has order  $32/2 = 16$ .

<sup>22</sup>For example, the group 21/03 in [4] of order 12 has the Hurley pattern 1\*1I, 1\*1E, 2\*3E, 1\*2S', 1\*2B; in our classification, it corresponds to two enantiomorphic groups,  $\boxtimes_{1,3}^{c2mm}$  and  $\boxtimes_{3,1}^{c2mm}$ . The fingerprints of these groups are 0|0:2 0|2/3:4 1|1/2:14 3|5/6:4 and 0|0:2 1|3/6:4 1|3/3:4 1|1/2:14. Both groups contain 7 half-turns (code 1|1/2, Hurley symbol E). The second group, for example, is actually also a torus flip group:  $\boxtimes_{3,1}^{c2mm} \doteq \boxtimes_{3,2}$ . In this representation, it has 6 flip operations, which are half-turns. In addition, it contains the torus translation  $R_{\pi,0}$ , which is another half-turn. This half-turn is not conjugate to the other half-turns by operations of the group. It forms a conjugacy class of its own, as indicated by the code 1\*1E in the Hurley pattern. The 6 flip operations split into two conjugacy classes of size 3, as indicated by the code 2\*3E.

For each obtained subgroup, we identified the possible extending elements, using the considerations of Section 3.5. Each achiral group was classified by its fingerprint (the conjugacy types of its elements), and for each class, we managed to find geometric conjugations to show that all groups with the same fingerprint are geometrically the same.

We mention some details for the largest group  $[I \times I]$ . The group  $\pm[I \times I]$  was represented by its double-cover  $2I \times 2I$ , and converted to a permutation group, in order to let GAP generate the subgroups. There are 19,987 subgroups in total, and they were found in about 5 minutes. 14,896 subgroups of them contain the pair  $(-1, -1)$ , which is necessary to have a double cover of a rotation group in  $\pm[I \times I]$ , and only 241 of these groups have the left and right subgroups equal to  $2I$ . These represented the group  $\pm[I \times I]$  itself, and 60 different copies of each group  $\pm \frac{1}{60}[I \times I]$ ,  $\pm \frac{1}{60}[I \times \bar{I}]$ ,  $+\frac{1}{60}[I \times I]$ ,  $+\frac{1}{60}[I \times \bar{I}]$ .

For each of the 241 groups, we tried to extend it by an element  $*[1, c]$  in all possible ways, following Proposition 3.2. Actually, it is easy to see that elements  $c$  and  $c' = cx$  that are related by an element  $x$  in the kernel lead to the same extension, and thus they need not be tried separately.

This leads to 361 distinct groups. Again there are 60 representatives of each of the six achiral groups with fraction  $\frac{1}{60}$ , plus one for the group  $\pm[I \times I] \cdot 2$  itself.

Since we searched for conjugacies in a systematic but somewhat ad-hoc manner, it took about half a week for the computer to show that all 60 groups in each class are geometrically the same. With hindsight, the multiplicity 60 is not surprising, since there are 60 conjugacies that map the elements of  $2I$  to themselves.

## 10.5 Checking the toroidal groups

The toroidal groups form an infinite family, and hence we can only generate them up to some limit. We set the goal of checking all chiral toroidal groups up to order 200 and all achiral groups up to order 400. For this purpose, we generated all groups  $\pm[D_n \times D_n] \cdot 2$  (for even  $n$ ) and  $\pm[C_n \times C_n] \cdot 2$  in the range  $100 < n \leq 200$ , together with their subgroups.

For generating the subgroups, we took a different approach than for the polyhedral groups: We constructed a permutation group representation of the *achiral* group and computed all its subgroups. We took all subgroups, regardless of whether the left and right group is the full group  $C_n$  or  $D_n$ . For each chiral group up to order 200 and each achiral group up to order 400 that was generated, we checked that it is conjugate to one on the known groups according to our classification. We also checked whether all known toroidal groups within these size bounds are found. This turned out to be the case with a few exceptions. The exceptions were the chiral groups  $\square_{m,n}^{\text{cm}}$ ,  $\square_{n,m}^{\text{cm}}$ ,  $\square_{m,n}^{\text{cm}}$ , and  $\square_{n,m}^{\text{cm}}$ , for 14 pairs  $(m, n) = (3, 17), (3, 19), (3, 23), \dots, (7, 13), (9, 11)$  of relatively prime odd numbers  $m$  and  $n$ , of orders  $2mn$  between 100 and 200. The reason that these groups were missed is that they are of the form  $+\frac{1}{2}[D_{2m} \times C_{2n}] \leq +\frac{1}{2}[D_{2m} \times D_{4n}]$ , and the smallest group  $\pm[D_{n'} \times D_{n'}] \cdot 2$  that contains them has  $n' = 4 \cdot \text{lcm}(m, n)$ , which exceeds 200.

This computation requires a workstation with large memory. The group with the largest number of subgroups was  $\pm[D_{192} \times D_{192}] \cdot 2$ . It has 1,361,642 subgroups. For 1,249,563 of these groups, the order was within the limits. The whole computation took about 10 days on a computer with 256 gigabytes of main memory.

## 11 Higher dimensions

In the classification of Theorem 1.1, there are categories that we expect in any dimension: the polyhedral groups, which are related to the regular polytopes, the toroidal groups, and the axial groups, which come from direct sums of lower-dimensional groups. On the other hand, the tubical groups are more surprising. They rely on the covering  $\text{SO}(3) \times \text{SO}(3) \xrightarrow{2:1} \text{SO}(4)$ , which provides a different product structure in terms of lower-dimensional groups than the direct sum.

The scarcity of regular polytopes in high dimensions might be an indication that these groups are not very exciting. On the other hand, the root systems  $E_6$ ,  $E_7$ , and  $E_8$  in 6, 7, and 8 dimensions promise some richer structure in certain dimensions.

In five dimensions, the orientation-preserving case has been settled by Mecchia and Zimmermann [30], see [37, Corollary 2]:

**Theorem 11.1.** *The finite subgroups of the orthogonal group  $\text{SO}(5)$  are*

- (i) *subgroups of  $\text{O}(4) \times \text{O}(1)$  or  $\text{O}(3) \times \text{O}(2)$  (the reducible case);*

- (ii) *subgroups of the symmetry group  $(\mathbb{Z}_2)^5 \rtimes S_5$  of the hypercube;*  
 (iii) *or isomorphic to  $A_5$ ,  $S_5$ ,  $A_6$  or  $S_6$ . (This includes symmetries of the simplex and its polar.)*

The irreducible representations of the groups in (iii) can be looked up in the character tables of the books on Representation Theory. It would be interesting to know what the 5-dimensional representations are in geometric terms (besides the symmetries of the simplex).

This theorem gives only the chiral groups, but in odd dimensions like 5, it is in principle straightforward to derive the achiral groups from the chiral ones: All one needs to know are the chiral groups and their index-2 subgroups. See [8, §3.8] for the three-dimensional case. Briefly, one can say that nothing unexpected happens for the point groups in 5 dimensions.

**Six dimensions.** The richest part of the 4-dimensional groups were the toroidal groups, which have an invariant Clifford torus. The sphere  $S^5$  contains an analogous three-dimensional torus:

$$x_1^2 + x_2^2 = x_3^2 + x_4^2 = x_5^2 + x_6^2 = 1/3$$

A group that leaves this torus invariant behaves similarly to a three-dimensional space group, involving translations, reflections, and rotations in terms of torus coordinates  $\varphi_1, \varphi_2, \varphi_3$ . Thus, the three-dimensional space groups will make their appearance in the classification of 6-dimensional point groups.

The situation in 4 dimensions was similar: We have studied the toroidal groups in analogy to the wallpaper groups (the two-dimensional space groups). In contrast to the situation in the plane, a 6-fold rotation in 3-space is not inconsistent with the requirement that the lattice of translations contains a cubical lattice. Thus, we may expect that all of the 230 three-dimensional space groups show up in the 6-dimensional point groups. (In one dimension lower, we have another instance of this phenomenon: The frieze groups appear as the 3-dimensional axial point groups.)

Thus, a classification of the point groups in 6 dimensions will be much more laborious than in 5 dimensions. It has already been observed by Carl Hermann in 1952 [22, p. 33], in connection with the crystallographic groups, that “going up from an odd dimension to the next higher even one leads by far to more surprises than the opposite case”.

## References

- [1] Simon L. Altmann. Hamilton, Rodrigues, and the quaternion scandal. *Mathematics Magazine*, 62(5):291–308, 1989. doi:10.1080/0025570X.1989.11977459.
- [2] Thomas F. Banchoff. Torus decompositions of regular polytopes in 4-space. In Marjorie Senechal, editor, *Shaping Space*, pages 257–266. Springer, 2013. doi:10.1007/978-0-387-92714-5\_20.
- [3] Marcel Berger. *Geometry II*. Springer Science & Business Media, 2009.
- [4] Harold Brown, Rolf Bülow, Joachim Neubüser, Hans Wondratschek, and Hans Zassenhaus. *Crystallographic Groups of Four-Dimensional Space*. Wiley, New York, 1978.
- [5] Christopher Cashen. Quasi-isometries between tubular groups. *Groups, Geometry, and Dynamics*, 4(3):473–516, 2010. doi:10.4171/GGD.
- [6] John H. Conway, Heidi Burgiel, and Chaim Goodman-Strauss. *The Symmetries of Things*. A K Peters, 2008.
- [7] John H. Conway, Ronald H. Hardin, and Neil J. A. Sloane. Packing lines, planes, etc.: packings in Grassmannian spaces. *Experimental Mathematics*, 5(2):139–159, 1996. doi:em/1047565645.
- [8] John H. Conway and Derek A. Smith. *On Quaternions and Octonions*. CRC Press, 2003.
- [9] H. S. M. Coxeter. Symmetrical definitions for the binary polyhedral groups. In *Finite Groups*, volume 1 of *Proc. Sympos. Pure Math.*, pages 64–87. Amer. Math. Soc., 1959.
- [10] H. S. M. Coxeter. *Regular Polytopes*. Dover, 3rd edition, 1973.

- d2532 [11] H. S. M. Coxeter. Regular and semi-regular polytopes. II. *Math. Z.*, 188:559–591, 1985.  
d2533 doi:10.1007/BF01161657.
- d2534 [12] H. S. M. Coxeter. *Regular Complex Polytopes*. Cambridge Univ. Press, 2nd edition, 1991.
- d2535 [13] James Cruickshank and Seamus Kelly. Rearrangement inequalities and the alterna-  
d2536 hedron. *Discrete & Computational Geometry*, 35(2):241–254, 2006. doi:10.1007/  
d2537 s00454-005-1199-6.
- d2538 [14] Paul de Medeiros and José Figueroa-O’Farrill. Half-BPS M2-brane orbifolds. *Advances in*  
d2539 *Theoretical and Mathematical Physics*, 16(5):1349–1408, 2012. doi:10.4310/ATMP.2012.  
d2540 v16.n5.a1.
- d2541 [15] Patrick Du Val. *Homographies, Quaternions and Rotations*. Clarendon Press, 1964.
- d2542 [16] William D. Dunbar. Nonfibering spherical 3-orbifolds. *Transactions of the American Math-*  
d2543 *ematical Society*, 341(1):121–142, 1994. doi:10.2307/2154616.
- d2544 [17] Erik Friese and Frieder Ladisch. Affine symmetries of orbit polytopes. *Advances in Mathe-*  
d2545 *matics*, 288:386–425, 2016.
- d2546 [18] Erik Friese and Frieder Ladisch. Classification of affine symmetry groups of orbit polytopes.  
d2547 *Journal of Algebraic Combinatorics*, 48(3):481–509, 2018. URL: <https://rdcu.be/cDHw3>,  
d2548 doi:10.1007/s10801-017-0804-0.
- d2549 [19] The GAP Group. *GAP – Groups, Algorithms, and Programming, Version 4.11.1*, 2021.  
d2550 URL: <https://www.gap-system.org>.
- d2551 [20] Edouard Goursat. Sur les substitutions orthogonales et les divisions régulières de l’espace.  
d2552 *Annales scientifiques de l’É.N.S. 3<sup>e</sup> série*, 6:9–102, 1889. doi:10.24033/asens.317.
- d2553 [21] Norman F. M. Henry, editor. *International tables for X-ray crystallography, Vol. 1, Sym-*  
d2554 *metry Groups*. Kynoch Press, Birmingham, 2nd edition, 1952.
- d2555 [22] C. Hermann. Translationsgruppen in  $n$  Dimensionen. In H. O’Daniel, editor, *Zur Struktur*  
d2556 *und Materie der Festkörper*, pages 24–33. Springer-Verlag, Berlin, Göttingen, Heidelberg,  
d2557 1952. doi:10.1007/978-3-662-29427-7\_2.
- d2558 [23] A. C. Hurley. Finite rotation groups and crystal classes in four dimensions. *Mathematical*  
d2559 *Proceedings of the Cambridge Philosophical Society*, 47(4):650–661, 1951. doi:10.1017/  
d2560 S0305004100027109.
- d2561 [24] A. C. Hurley. Finite rotation groups and crystal classes in four dimensions: II. revised tables  
d2562 and projection of groups of antisymmetry in three dimensions. In Per Olov Löwdin, editor,  
d2563 *Quantum Theory of Atoms, Molecules, and the Solid State: A Tribute to John C. Slater*,  
d2564 pages 571–586. Academic Press, 1966.
- d2565 [25] Heuna Kim and Günter Rote. Congruence testing of point sets in 4 dimensions, March 2016.  
d2566 arXiv:1603.07269.
- d2567 [26] Heuna Kim and Günter Rote. Congruence testing of point sets in 4-space. In Sándor  
d2568 Fekete and Anna Lubiw, editors, *32st International Symposium on Computational Geometry*  
d2569 *(SoCG 2016)*, volume 51 of *Leibniz International Proceedings in Informatics (LIPIcs)*, pages  
d2570 48:1–48:16. Schloss Dagstuhl–Leibniz-Zentrum für Informatik, 2016. doi:10.4230/LIPIcs.  
d2571 SOCG.2016.48.
- d2572 [27] Christian Lange and Marina A. Mikhailova. Classification of finite groups generated by  
d2573 reflections and rotations. *Transformation Groups*, 21:1155–1201, 2016. doi:10.1007/  
d2574 s00031-016-9385-6.
- d2575 [28] David W. Lyons. An elementary introduction to the Hopf fibration. *Mathematics Magazine*,  
d2576 76(2):87–98, 2003. doi:10.2307/3219300.
- d2577 [29] M. A. Maerchik. Finite groups generated by pseudoreflections in four-dimensional Euclidean  
d2578 space. *Trudy Kirgiz Gos. Univ. Ser. Mat. Nauk*, 11:66–72, 1976. (in Russian).



- d2579 [30] Mattia Mecchia and Bruno Zimmermann. On finite groups acting on homology 4-spheres  
d2580 and finite subgroups of  $SO(5)$ . *Topology and its Applications*, 158(6):741–747, 2011. doi:  
d2581 10.1016/j.topol.2011.01.017.
- d2582 [31] J. L. Nicolas and G. Robin. Majorations explicites pour le nombre de diviseurs de  $n$ .  
d2583 *Canadian Mathematical Bulletin*, 26(4):485–492, 1983. doi:10.4153/CMB-1983-078-5.
- d2584 [32] G. de B. Robinson. On the orthogonal groups in four dimensions. *Mathematical*  
d2585 *Proceedings of the Cambridge Philosophical Society*, 27(1):37–48, 1931. doi:10.1017/  
d2586 S0305004100009312.
- d2587 [33] Henry Segerman and Saul Schleimer. Puzzling the 120-cell. *Notices of the AMS*, 62(11):1309–  
d2588 1316, 2015. doi:10.1090/noti1297.
- d2589 [34] The Sage Developers. *SageMath, the Sage Mathematics Software System (Version 9.5)*,  
d2590 2022. URL: <https://www.sagemath.org>.
- d2591 [35] W. Threlfall and H. Seifert. Topologische Untersuchung der Diskontinuitätsbereiche  
d2592 endlicher Bewegungsgruppen des dreidimensionalen sphärischen Raumes. *Math. Annalen*,  
d2593 104:1–70, 1931. doi:10.1007/BF01457920.
- d2594 [36] W. Threlfall and H. Seifert. Topologische Untersuchung der Diskontinuitätsbereiche  
d2595 endlicher Bewegungsgruppen des dreidimensionalen sphärischen Raumes (Schluß). *Math.*  
d2596 *Annalen*, 107:543–586, 1933. doi:10.1007/BF01448910.
- d2597 [37] Bruno P. Zimmermann. On finite groups acting on spheres and finite subgroups of orthogonal  
d2598 groups. *Sib. Elektron. Mat. Izv.*, 9:1–12, 2012. URL: [http://mi.mathnet.ru/eng/semr/  
d2599 v9/p1](http://mi.mathnet.ru/eng/semr/v9/p1), arXiv:1108.2602.

## A Generators for the polyhedral and axial groups

Table 16 gives a complete summary of the polyhedral (Table 10) and axial groups (Table 15), following the numbering by Goursat [20], as extended to the haploid groups by Du Val [15], together with a set of generators for each group. The axial groups can be recognized as having only two numbers different from 2 in their Coxeter name. Our adaptations of Du Val’s names was explained in Tables 10 (p. 66) and 15 (p. 75). The top part contains the chiral groups (#20–#32) and the bottom part the achiral ones (#39–#51).<sup>23</sup>

Where appropriate, we include a reference to the numbering of crystallographic point groups according to Brown, Bülow, Neubüser, Wondratschek, Zassenhaus (BBNWZ) [4], see also Appendix D.

In addition to the quaternions defined in (6) in Section 3.7, the following elements are used for generating the groups:

$$\bar{\omega} = \frac{1}{2}(-1 - i - j - k) \quad (\text{order } 3)$$

$$i_I^\dagger = \frac{1}{2}(i + \frac{-\sqrt{5}-1}{2}j + \frac{-\sqrt{5}+1}{2}k) \quad (\text{order } 4) \quad (26)$$

$$i_I' = \frac{1}{2}(-\frac{\sqrt{5}-1}{2}i - \frac{\sqrt{5}+1}{2}j + k) \quad (\text{order } 4) \quad (27)$$

$\bar{\omega}$  is simply the conjugate quaternion of  $\omega$ . We tried to reduce the number of generators by trial and error, confirming by computer whether the generated groups did not change.

For a few groups, the groups given by Conway and Smith are not identical to the groups of Du Val, and our table lists both possibilities.

Conway and Smith [8, Tables 4.2–4.3] specified the five groups of type  $[I \times \bar{I}]$  (#32, #32' and #51–#51'') by the generating set “ $[\omega, \omega], [i_I, \pm i_I']$ ”, possibly extended by  $*$  or  $-*$  for the achiral

<sup>23</sup>A similar table, containing some four-dimensional reflection groups and their subgroups, appears in Coxeter [11, p. 571], with correspondences between Coxeter’s own notation and Du Val’s names. The very first entry in that table,  $[3, 3, 2]^+$ , mistakenly refers to Du Val’s group #21 ( $T/C_2; T/C_2$ ) =  $\pm \frac{1}{12}[T \times T]$ , while it is actually #26'' ( $O/C_1; O/C_1$ )'' =  $+\frac{1}{24}[O \times \bar{O}]$ . The fifth entry,  $[3, 3, 2]$ , refers to Du Val’s group ( $O/C_1; O/C_1$ )\*, while it should actually be ( $O/C_1; O/C_1$ )\*, or more precisely #44'' ( $O/C_1; O/C_1$ )\*'' =  $+\frac{1}{24}[O \times \bar{O}] \cdot 2_1$ . The confusing ambiguity of Du Val’s names for the groups 44' and 44'' mentioned in the caption of Table 15 was apparently not realized by Coxeter.

Du Val # & name	CS name	generators	Cox. name	order	BBNWZ
20. $(T/T; T/T)$	$\pm[T \times T]$	$[i, \omega], [\omega, i]$	$[+3, 4, 3^+]$	288	33/13
21. $(T/C_2; T/C_2)$	$\pm \frac{1}{12}[T \times T]$	$[\omega, -\omega], [i, i]$	$2.[3, 3]^+$	24	24/02
21'. $(T/C_1; T/C_1)$	$+\frac{1}{12}[T \times T]$	$[\omega, \omega], [i, i]$	$[3, 3]^+$	12	24/01
22. $(T/V; T/V)$	$\pm \frac{1}{3}[T \times T]$	$[i, 1], [1, i], [\omega, \omega]$	$[+3, 3, 4^+]$	96	32/16
23. $(O/O; T/T)$	$\pm[O \times T]$	$[i_O, \omega], [\omega, i]$	$[[+3, 4, 3^+]]_L$	576	not cryst.
23. $(T/T; O/O)$	$\pm[T \times O]$	$[i, \omega], [\omega, i_O]$	$[[+3, 4, 3^+]]_R$	576	not cryst.
24. $(I/I; T/T)$	$\pm[I \times T]$	$[i_I, \omega], [\omega, i]$	$[3, 3, 5]^+_{\frac{1}{5}L}$	1440	not cryst.
24. $(T/T; I/I)$	$\pm[T \times I]$	$[i, \omega], [\omega, i_I]$	$[3, 3, 5]^+_{\frac{1}{5}R}$	1440	not cryst.
25. $(O/O; O/O)$	$\pm[O \times O]$	$[i_O, \omega], [\omega, i_O]$	$[[3, 4, 3]]^+$	1152	not cryst.
26. $(O/C_2; O/C_2)$	$\pm \frac{1}{24}[O \times O]$	$[\omega, -\omega], [i_O, i_O]$	$2.[3, 4]^+$	48	25/06
26'. $(O/C_1; O/C_1)'$	$+\frac{1}{24}[O \times O]$	$[\omega, \omega], [i_O, i_O]$	$[3, 4]^+$	24	25/03
26''. $(O/C_1; O/C_1)''$	$+\frac{1}{24}[O \times \bar{O}]$	$[\omega, \omega], [i_O, -i_O]$	$[2, 3, 3]^+$	24	25/04
27. $(O/V; O/V)$	$\pm \frac{1}{6}[O \times O]$	$[i, j], [\omega, \omega], [i_O, i_O]$	$[3, 3, 4]^+$	192	32/20
28. $(O/T; O/T)$	$\pm \frac{1}{2}[O \times O]$	$[\omega, 1], [1, \omega], [i_O, i_O]$	$[3, 4, 3]^+$	576	33/15
29. $(I/I; O/O)$	$\pm[I \times O]$	$[i_I, \omega], [\omega, i_O]$	$[[3, 3, 5]^+_{\frac{1}{5}L}]$	2880	not cryst.
29. $(O/O; I/I)$	$\pm[O \times I]$	$[i_O, \omega], [\omega, i_I]$	$[[3, 3, 5]^+_{\frac{1}{5}R}]$	2880	not cryst.
30. $(I/I; I/I)$	$\pm[I \times I]$	$[i_I, \omega], [\omega, i_I]$	$[3, 3, 5]^+$	7200	not cryst.
31. $(I/C_2; I/C_2)$	$\pm \frac{1}{60}[I \times I]$	$[\omega, \omega], [i_I, -i_I]$	$2.[3, 5]^+$	120	not cryst.
31'. $(I/C_1; I/C_1)$	$+\frac{1}{60}[I \times I]$	$[\omega, \omega], [i_I, i_I]$	$[3, 5]^+$	60	not cryst.
32. $(I^\dagger/C_2; I/C_2)^\dagger$		$[\omega, \omega], [i_I, -i_I^\dagger]$	$\left. \begin{array}{l} \\ \end{array} \right\} [[3, 3, 3]]^+$	120	31/06
	$\pm \frac{1}{60}[I \times \bar{I}]$	$[\omega, \omega], [i_I, -i_I']$			
32'. $(I^\dagger/C_1; I/C_1)^\dagger$		$[\omega, \omega], [i_I, i_I^\dagger]$	$\left. \begin{array}{l} \\ \end{array} \right\} [3, 3, 3]^+$	60	31/03
	$+\frac{1}{60}[I \times \bar{I}]$	$[\omega, \omega], [i_I, i_I']$			
39. $(T/C_2; T/C_2)_c^*$	$\pm \frac{1}{12}[T \times T] \cdot 2$	$[\omega, -\omega], *[i, -i]$	$2.[+3, 4]$	48	25/05
39'. $(T/C_1; T/C_1)_c^*$	$+\frac{1}{12}[T \times T] \cdot 2_3$	$[\omega, \omega], *[i, i]$	$[+3, 4]$	24	25/02
39'. $(T/C_1; T/C_1)_{c-}^*$	$+\frac{1}{12}[T \times T] \cdot 2_1$	$[\omega, \omega], *[i, -i]$	$[+3, 4]^\circ$	24	25/01
40. $(T/C_2; T/C_2)^*$		$[\omega, -\omega], *[i_O, -i_O]$	$\left. \begin{array}{l} \\ \end{array} \right\} 2.[3, 3]$	48	24/05
	$\pm \frac{1}{12}[T \times \bar{T}] \cdot 2$	$[\omega, -\bar{\omega}], *[i, -i]$			
40'. $(T/C_1; T/C_1)^*$		$[\omega, \omega], *[i_O, i_O]$	$\left. \begin{array}{l} \\ \end{array} \right\} [3, 3]$	24	24/04
	$+\frac{1}{12}[T \times \bar{T}] \cdot 2_1$	$[\omega, \bar{\omega}], *[i, i]$			
40'. $(T/C_1; T/C_1)_-^*$		$[\omega, \omega], *[i_O, -i_O]$	$\left. \begin{array}{l} \\ \end{array} \right\} [3, 3]^\circ$	24	24/03
	$+\frac{1}{12}[T \times \bar{T}] \cdot 2_3$	$[\omega, \bar{\omega}], *[i, -i]$			
41. $(T/V; T/V)^*$	$\pm \frac{1}{3}[T \times T] \cdot 2$	$*[i, 1], [\omega, \omega]$	$[+3, 3, 4]$	192	32/18
42. $(T/V; T/V)_-^*$	$\pm \frac{1}{3}[T \times \bar{T}] \cdot 2$	$*[i, 1], [\omega, \bar{\omega}]$	$[3, 3, 4]^+$	192	32/19
43. $(T/T; T/T)^*$	$\pm[T \times T] \cdot 2$	$[i, \omega], *[\omega, i]$	$[3, 4, 3]^+$	576	33/14
44. $(O/C_2; O/C_2)^*$	$\pm \frac{1}{24}[O \times O] \cdot 2$	$[\omega, -\omega], [i_O, i_O], -*$	$2.[3, 4]$	96	25/11
44'. $(O/C_1; O/C_1)^{*\prime}$	$+\frac{1}{24}[O \times O] \cdot 2_3$	$[\omega, \omega], [i_O, i_O], *$	$[3, 4]$	48	25/10
44'. $(O/C_1; O/C_1)^{*\prime}_-$	$+\frac{1}{24}[O \times O] \cdot 2_1$	$[\omega, \omega], [i_O, i_O], -*$	$[3, 4]^\circ$	48	25/07
44''. $(O/C_1; O/C_1)^{*\prime\prime}$	$+\frac{1}{24}[O \times \bar{O}] \cdot 2_3$	$[\omega, \omega], [i_O, -i_O], *$	$[2, 3, 3]^\circ$	48	25/09
44''. $(O/C_1; O/C_1)^{*\prime\prime}_-$	$+\frac{1}{24}[O \times \bar{O}] \cdot 2_1$	$[\omega, \omega], [i_O, -i_O], -*$	$[2, 3, 3]$	48	25/08
45. $(O/T; O/T)^*$	$\pm \frac{1}{2}[O \times O] \cdot 2$	$*[\omega, 1], [i_O, i_O]$	$[3, 4, 3]$	1152	33/16
46. $(O/T; O/T)_-^*$	$\pm \frac{1}{2}[O \times O] \cdot \bar{2}$	$[\omega, 1], *[1, i_O]$	$[[3, 4, 3]]^+$	1152	not cryst.
47. $(O/V; O/V)^*$	$\pm \frac{1}{6}[O \times O] \cdot 2$	$*[i\omega, \omega], [i_O, i_O]$	$[3, 3, 4]$	384	32/21
48. $(O/O; O/O)^*$	$\pm[O \times O] \cdot 2$	$*[1, \omega], [\omega, i_O]$	$[[3, 4, 3]]$	2304	not cryst.
49. $(I/C_2; I/C_2)^*$	$\pm \frac{1}{60}[I \times I] \cdot 2$	$[\omega, -\omega], *[i_I, -i_I]$	$2.[3, 5]$	240	not cryst.
49'. $(I/C_1; I/C_1)^*$	$+\frac{1}{60}[I \times I] \cdot 2_3$	$[\omega, \omega], *[i_I, i_I]$	$[3, 5]$	120	not cryst.
49'. $(I/C_1; I/C_1)_-^*$	$+\frac{1}{60}[I \times I] \cdot 2_1$	$[\omega, \omega], *[i_I, -i_I]$	$[3, 5]^\circ$	120	not cryst.
50. $(I/I; I/I)^*$	$\pm[I \times I] \cdot 2$	$[i_I, \omega], [\omega, i_I], *$	$[3, 3, 5]$	14400	not cryst.
51. $(I^\dagger/C_2; I/C_2)^{\dagger*}$		$[\omega, -\omega], *[i_I i_O i, i_I^\dagger i_O i]$	$\left. \begin{array}{l} \\ \end{array} \right\} [[3, 3, 3]]$	240	31/07
	$\pm \frac{1}{60}[I \times \bar{I}] \cdot 2$	$[\omega, -\omega], *[i_I, i_I']$			
51'. $(I^\dagger/C_1; I/C_1)^{\dagger*}$		$[\omega, \omega], *[i_I i_O i, i_I^\dagger i_O i]$	$\left. \begin{array}{l} \\ \end{array} \right\} [3, 3, 3]$	120	31/05
	$+\frac{1}{60}[I \times \bar{I}] \cdot 2_1$	$[\omega, \omega], [i_I, i_I'], -*$			
51'. $(I^\dagger/C_1; I/C_1)_-^{\dagger*}$		$[\omega, \omega], *[i_I i_O i, -i_I^\dagger i_O i]$	$\left. \begin{array}{l} \\ \end{array} \right\} [[3, 3, 3]]^+$	120	31/04
	$+\frac{1}{60}[I \times \bar{I}] \cdot 2_3$	$[\omega, \omega], *[i_I, i_I']$			

Table 16: Polyhedral and axial groups with generators

groups, but they did not define what  $i'_I$  is.<sup>24</sup> We tried all 120 elements of  $2I$ , and it turned out that (27) is the only value that works in this way. We don't see how we could have predicted precisely this element, and we have no explanation for it.

Du Val [15], on the other hand, specifies generators for these five groups in terms of the quaternion  $i_I^\dagger$  defined in (26), which is obtained by flipping the sign of  $\sqrt{5}$  in the expression for  $i_I = \frac{1}{2}(i + \frac{\sqrt{5}-1}{2}j + \frac{\sqrt{5}+1}{2}k)$ . This alternative choice generates a group  $2I^\dagger$  that is different from  $2I$ . With this setup, it is not possible to use the simple extending elements  $*$  and  $-*$  for the three achiral extensions #51–#51'': For example, the square of the element  $*[i_I^\dagger, i_I]$  is  $[i_I i_I^\dagger, i_I^\dagger i_I]$  with  $i_I i_I^\dagger = \frac{1}{4} + \frac{\sqrt{5}}{4}(i + j - k)$ , and this element is in neither of the groups  $2I$  or  $2I^\dagger$ . Du Val [15, p. 55–56] gives a thorough and transparent exposition of these groups and explains why they represent the symmetries of the 4-simplex.

For the axial groups of type  $\frac{1}{12}[T \times \bar{T}]$  (#40 and #40'), the natural generators from an algebraic viewpoint involve the quaternion  $\bar{\omega}$ , and these were chosen by Conway and Smith. However, the axis that is kept invariant by the groups is then spanned by the quaternion  $j - k$ . With  $*[i_O, \pm i_O]$  as the orientation-reversing generator, the invariant axis becomes the real axis, and only in this representation, the groups are subgroups of the larger axial group  $\pm\frac{1}{24}[O \times O]$  (#44).

## B Orbit polytopes for tubical groups with special starting points

We show polar orbit polytopes for the tubical groups of cyclic type with all choices of special starting points.

Each subsection considers a left tubical group  $G$  together with a representative  $f$ -fold rotation center  $p$  of  $G^h$ , corresponding to an entry in Table 3. The particular data are given in the caption. In addition, we indicate the subgroup  $H$  of  $G$  of elements that preserve  $K_p$ . An *alternate group* refers to an index-2 dihedral-type supergroup of  $G$  that, for an appropriate starting point on  $K_p$ , produces the same orbit as  $G$ .

Two of these groups were already illustrated in the main text (Figures 12 and 13), and we follow the same conventions as in these figures: On the top left, we show the  $G^h$ -orbit polytope of  $p$ , and on the top right the spherical Voronoi diagram of that orbit. Then we show the cells of the polar  $G$ -orbit polytopes of a starting point on  $K_p$ , for different values of  $n$ , in increasing order of the size of the orbit. For each cell, we indicate the values of  $n$ , and in addition, the counterclockwise angle (as seen from the top) by which the group rotates the cell as it proceeds to the next cell above. A blue vertical line indicates the cell axis, the direction towards the next cell along  $K_p$ . For small values of  $n$ , this axis sometimes exits through a vertex or an edge of the cell, but for large enough  $n$  it goes through the top face where the next cell is attached.

When the same orbit arises for several values of  $n$ , then the specified rotation angle is the unique valid angle only for the smallest value  $n_0$  that is given. For a larger value  $n = n_0 f$ , this can be combined with arbitrary multiples of an  $f$ -fold rotation. For example, in Figure 36, we have the same cell for  $n = 5$  and  $n = 15$ . The specified rotation angle  $(\frac{1}{3} + \frac{1}{30}) \cdot 2\pi$  is the unique valid angle between consecutive cells in the group  $\pm[I \times C_5]$ , but in the larger group  $\pm[I \times C_{15}]$ , it can be combined with all multiples of  $\frac{2}{3}\pi$ . That is, all three rotation angles  $\frac{1}{15}\pi$ ,  $(\frac{2}{3} + \frac{1}{15})\pi$ , and  $(\frac{4}{3} + \frac{1}{15})\pi$  are valid. In some cases, such as  $n = 18$ , the angle is never unique, and this is indicated by a free parameter  $k$  in the angle specification, which can take any integer value.

By observing the rotation angles for the successive cells in the figures, one can recognize the pattern that they follow.

<sup>24</sup>Five years later, the tables were almost literally reproduced in another book [6, Chapter 26], still without a definition of  $i'_I$ .

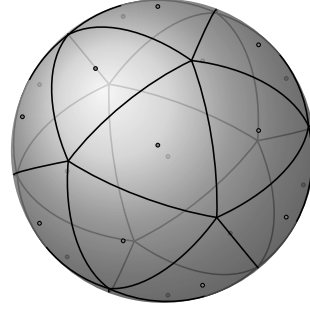
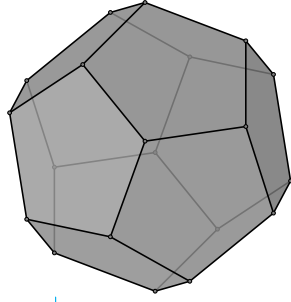
D2663

**B.1**  $\pm[I \times C_n]$ 

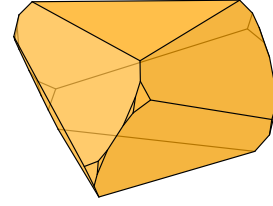
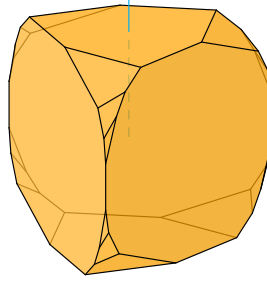
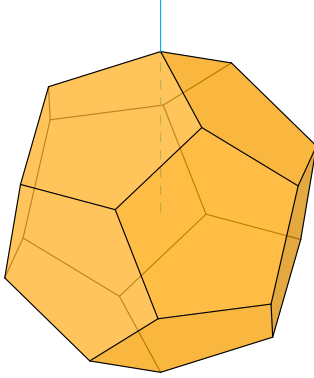
D2664

**B.1.1**  $\pm[I \times C_n]$ , **3-fold rotation center**

D2665



D2666



$$n = 1, 3$$

$$\left(\frac{2}{3} + \frac{1}{6}\right) \cdot 2\pi$$

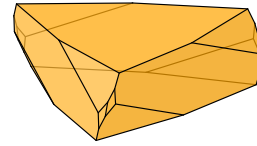
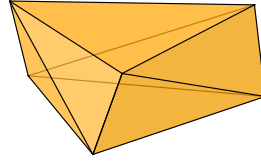
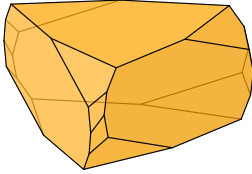
$$n = 2, 6$$

$$\left(\frac{1}{3} + \frac{1}{12}\right) \cdot 2\pi$$

$$n = 9$$

$$\left(\frac{k}{3} + \frac{1}{18}\right) \cdot 2\pi$$

D2667



$$n = 4, 12$$

$$\left(\frac{2}{3} + \frac{1}{24}\right) \cdot 2\pi$$

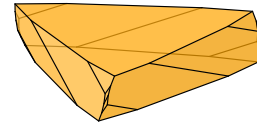
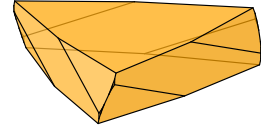
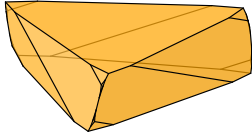
$$n = 5, 15$$

$$\left(\frac{1}{3} + \frac{1}{30}\right) \cdot 2\pi$$

$$n = 18$$

$$\left(\frac{k}{3} + \frac{1}{36}\right) \cdot 2\pi$$

D2668



$$n = 7, 21$$

$$\left(\frac{2}{3} + \frac{1}{42}\right) \cdot 2\pi$$

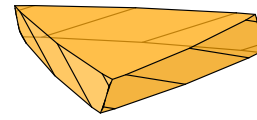
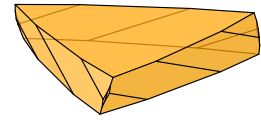
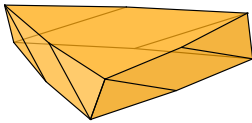
$$n = 8, 24$$

$$\left(\frac{1}{3} + \frac{1}{48}\right) \cdot 2\pi$$

$$n = 27$$

$$\left(\frac{k}{3} + \frac{1}{54}\right) \cdot 2\pi$$

D2669



$$n = 10, 30$$

$$\left(\frac{2}{3} + \frac{1}{60}\right) \cdot 2\pi$$

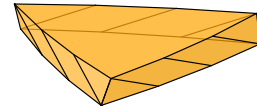
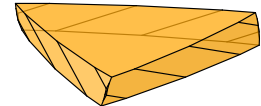
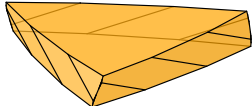
$$n = 11, 33$$

$$\left(\frac{1}{3} + \frac{1}{66}\right) \cdot 2\pi$$

$$n = 36$$

$$\left(\frac{k}{3} + \frac{1}{72}\right) \cdot 2\pi$$

D2670



$$n = 13, 39$$

$$\left(\frac{2}{3} + \frac{1}{78}\right) \cdot 2\pi$$

$$n = 14, 42$$

$$\left(\frac{1}{3} + \frac{1}{84}\right) \cdot 2\pi$$

$$n = 45$$

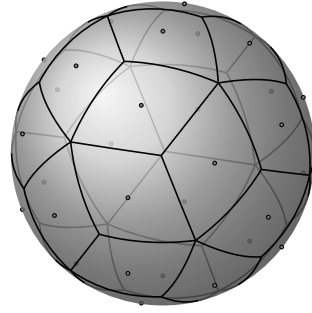
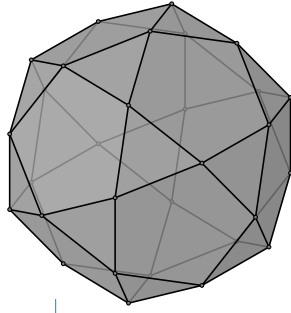
$$\left(\frac{k}{3} + \frac{1}{90}\right) \cdot 2\pi$$

Figure 36:  $G = \pm[I \times C_n]$ ,  $G^h = +I$ , 3-fold rotation center  $p = \frac{1}{\sqrt{3}}(-1, -1, -1)$ .  $H = \langle [-\omega, 1], [1, e_n] \rangle$ . 20 tubes, each with  $\text{lcm}(2n, 6)$  cells. Alternate group:  $\pm[I \times D_{2n}]$ . When  $n = 1$  or  $n = 3$ , the cells of a tube are disconnected from each other.

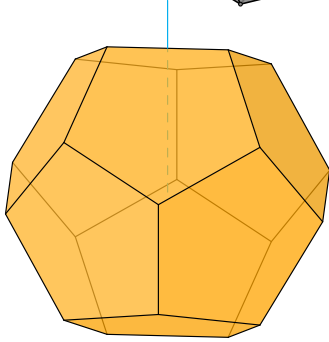
D2671

**B.1.2  $\pm[I \times C_n]$ , 2-fold rotation center**

D2672

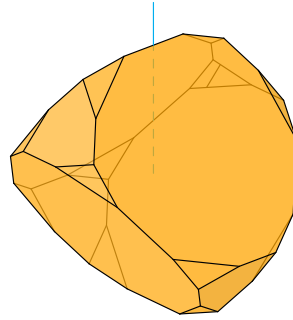


D2673



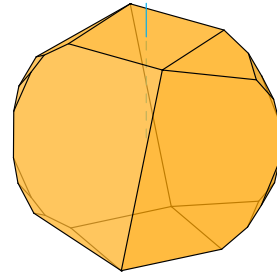
$$n = 1, 2$$

$$\left(\frac{1}{2} + \frac{1}{4}\right) \cdot 2\pi$$



$$n = 4$$

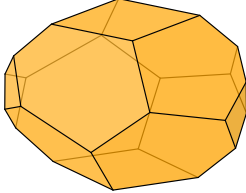
$$\left(\frac{k}{2} + \frac{1}{8}\right) \cdot 2\pi$$



$$n = 3, 6$$

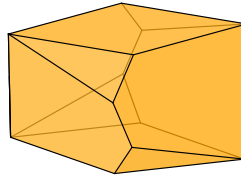
$$\left(\frac{1}{2} + \frac{1}{12}\right) \cdot 2\pi$$

D2674



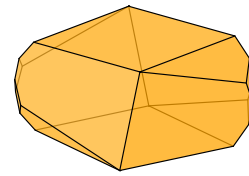
$$n = 8$$

$$\left(\frac{k}{2} + \frac{1}{16}\right) \cdot 2\pi$$



$$n = 5, 10$$

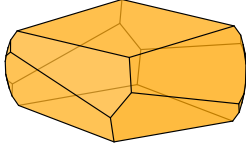
$$\left(\frac{1}{2} + \frac{1}{20}\right) \cdot 2\pi$$



$$n = 12$$

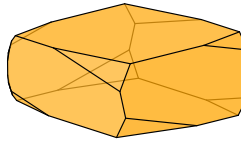
$$\left(\frac{k}{2} + \frac{1}{24}\right) \cdot 2\pi$$

D2675



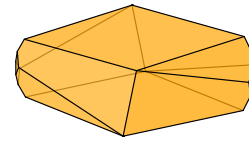
$$n = 7, 14$$

$$\left(\frac{1}{2} + \frac{1}{28}\right) \cdot 2\pi$$



$$n = 16$$

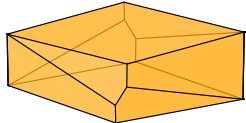
$$\left(\frac{k}{2} + \frac{1}{32}\right) \cdot 2\pi$$



$$n = 9, 18$$

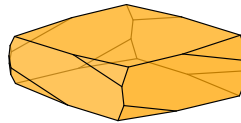
$$\left(\frac{1}{2} + \frac{1}{36}\right) \cdot 2\pi$$

D2676



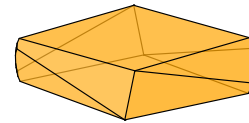
$$n = 20$$

$$\left(\frac{k}{2} + \frac{1}{40}\right) \cdot 2\pi$$



$$n = 11, 22$$

$$\left(\frac{1}{2} + \frac{1}{44}\right) \cdot 2\pi$$



$$n = 24$$

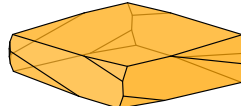
$$\left(\frac{k}{2} + \frac{1}{48}\right) \cdot 2\pi$$

D2677



$$n = 13, 26$$

$$\left(\frac{1}{2} + \frac{1}{52}\right) \cdot 2\pi$$



$$n = 28$$

$$\left(\frac{k}{2} + \frac{1}{56}\right) \cdot 2\pi$$



$$n = 15, 30$$

$$\left(\frac{1}{2} + \frac{1}{60}\right) \cdot 2\pi$$

Figure 37:  $G = \pm[I \times C_n]$ ,  $G^h = +I$ , 2-fold rotation center  $p = \frac{1}{2}(1, \frac{1}{\varphi}, \varphi)$ , where  $\varphi = \frac{1+\sqrt{5}}{2}$ . The  $G^h$ -orbit polytope is an icosidodecahedron. The corresponding Voronoi diagram on the 2-sphere has the structure of a rhombic triacontahedron.  $H = \langle [i_I, 1], [1, e_n] \rangle$ . 30 tubes, each with  $\text{lcm}(2n, 4)$  cells. Alternate group:  $\pm[I \times D_{2n}]$ . When  $n = 1, 2$ , or 4, the cells of a tube are disconnected from each other.

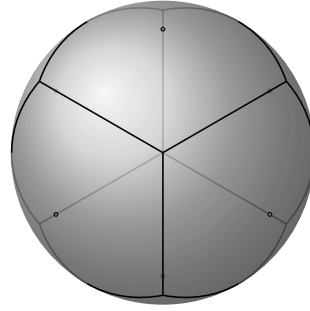
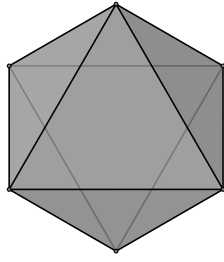
D2678

**B.2**  $\pm[O \times C_n]$ 

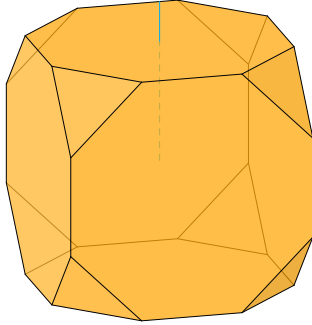
D2679

**B.2.1**  $\pm[O \times C_n]$ , 4-fold rotation center

D2680

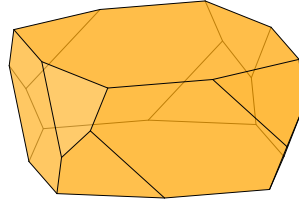


D2681



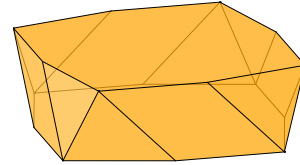
$$n = 1, 2, 4$$

$$\left(\frac{3}{4} + \frac{1}{8}\right) \cdot 2\pi$$



$$n = 8$$

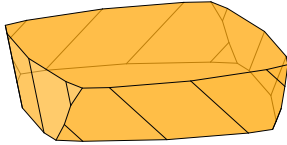
$$\left(\frac{k}{4} + \frac{1}{16}\right) \cdot 2\pi$$



$$n = 3, 6, 12$$

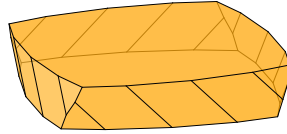
$$\left(\frac{1}{4} + \frac{1}{24}\right) \cdot 2\pi$$

D2682



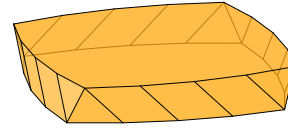
$$n = 16$$

$$\left(\frac{k}{4} + \frac{1}{32}\right) \cdot 2\pi$$



$$n = 5, 10, 20$$

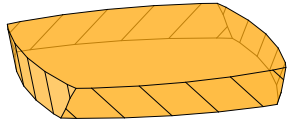
$$\left(\frac{3}{4} + \frac{1}{40}\right) \cdot 2\pi$$



$$n = 24$$

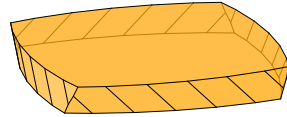
$$\left(\frac{k}{4} + \frac{1}{48}\right) \cdot 2\pi$$

D2683



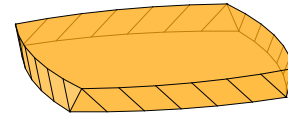
$$n = 7, 14, 28$$

$$\left(\frac{1}{4} + \frac{1}{56}\right) \cdot 2\pi$$



$$n = 32$$

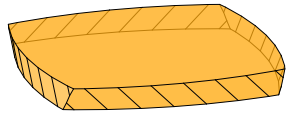
$$\left(\frac{k}{4} + \frac{1}{64}\right) \cdot 2\pi$$



$$n = 9, 18, 36$$

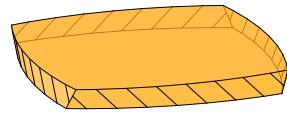
$$\left(\frac{3}{4} + \frac{1}{72}\right) \cdot 2\pi$$

D2684



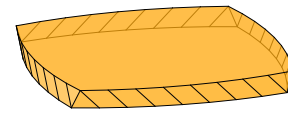
$$n = 40$$

$$\left(\frac{k}{4} + \frac{1}{80}\right) \cdot 2\pi$$



$$n = 11, 22, 44$$

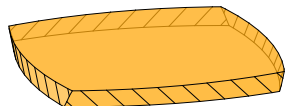
$$\left(\frac{1}{4} + \frac{1}{88}\right) \cdot 2\pi$$



$$n = 48$$

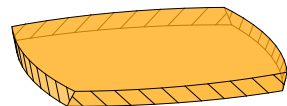
$$\left(\frac{k}{4} + \frac{1}{96}\right) \cdot 2\pi$$

D2685



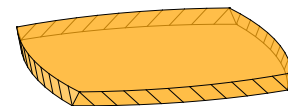
$$n = 13, 26, 52$$

$$\left(\frac{3}{4} + \frac{1}{104}\right) \cdot 2\pi$$



$$n = 56$$

$$\left(\frac{k}{4} + \frac{1}{112}\right) \cdot 2\pi$$



$$n = 15, 30, 60$$

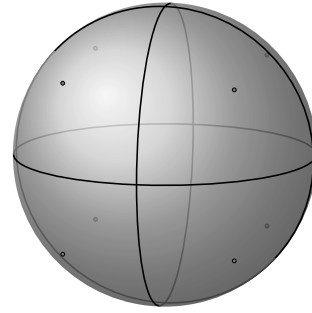
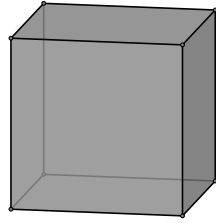
$$\left(\frac{1}{4} + \frac{1}{120}\right) \cdot 2\pi$$

Figure 38:  $G = \pm[O \times C_n]$ ,  $G^h = +O$ , 4-fold rotation center  $p = (0, 1, 0)$ .  $H = \langle [-\omega i_O, 1], [1, e_n] \rangle$ . 6 tubes, each with  $\text{lcm}(2n, 8)$  cells. Alternate group:  $\pm[O \times D_{2n}]$ .

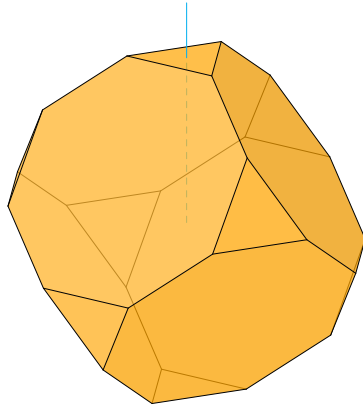
D2686

**B.2.2  $\pm[O \times C_n]$ , 3-fold rotation center**

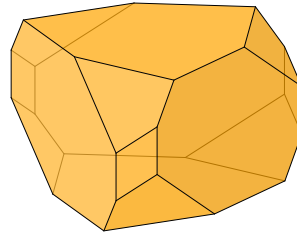
D2687



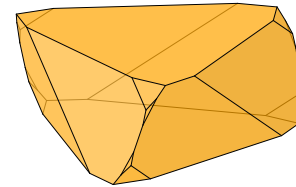
D2688



$$n = 1, 3 \\ \left(\frac{2}{3} + \frac{1}{6}\right) \cdot 2\pi$$

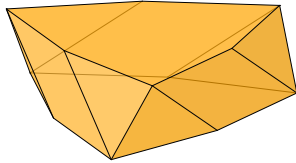


$$n = 2, 6 \\ \left(\frac{1}{3} + \frac{1}{12}\right) \cdot 2\pi$$

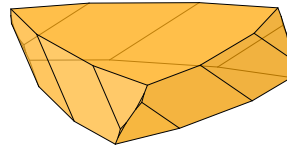


$$n = 9 \\ \left(\frac{k}{3} + \frac{1}{18}\right) \cdot 2\pi$$

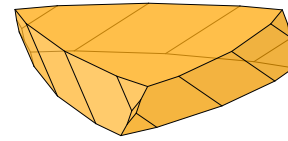
D2689



$$n = 4, 12 \\ \left(\frac{2}{3} + \frac{1}{24}\right) \cdot 2\pi$$

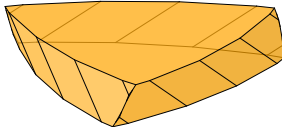


$$n = 5, 15 \\ \left(\frac{1}{3} + \frac{1}{30}\right) \cdot 2\pi$$

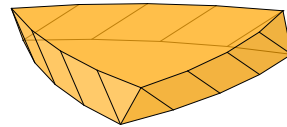


$$n = 18 \\ \left(\frac{k}{3} + \frac{1}{36}\right) \cdot 2\pi$$

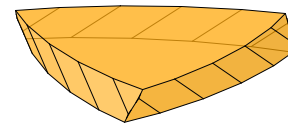
D2690



$$n = 7, 21 \\ \left(\frac{2}{3} + \frac{1}{42}\right) \cdot 2\pi$$

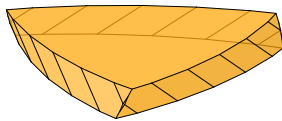


$$n = 8, 24 \\ \left(\frac{1}{3} + \frac{1}{48}\right) \cdot 2\pi$$

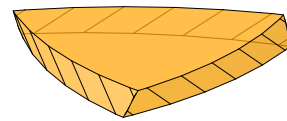


$$n = 27 \\ \left(\frac{k}{3} + \frac{1}{54}\right) \cdot 2\pi$$

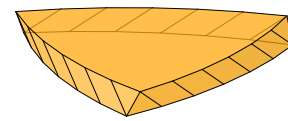
D2691



$$n = 10, 30 \\ \left(\frac{2}{3} + \frac{1}{60}\right) \cdot 2\pi$$

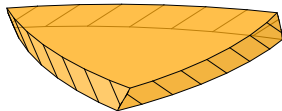


$$n = 11, 33 \\ \left(\frac{1}{3} + \frac{1}{66}\right) \cdot 2\pi$$

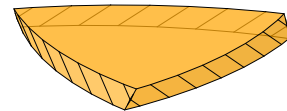


$$n = 36 \\ \left(\frac{k}{3} + \frac{1}{72}\right) \cdot 2\pi$$

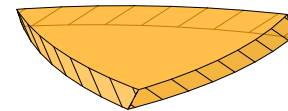
D2692



$$n = 13, 39 \\ \left(\frac{2}{3} + \frac{1}{78}\right) \cdot 2\pi$$



$$n = 14, 42 \\ \left(\frac{1}{3} + \frac{1}{84}\right) \cdot 2\pi$$



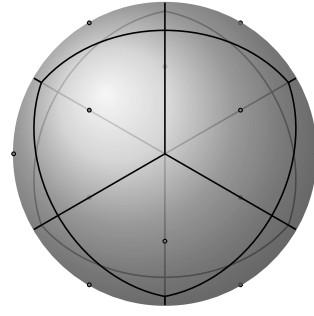
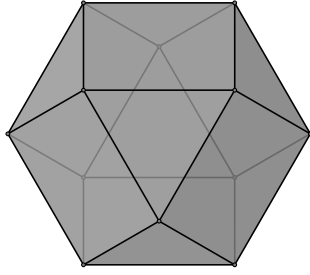
$$n = 45 \\ \left(\frac{k}{3} + \frac{1}{90}\right) \cdot 2\pi$$

Figure 39:  $G = \pm[O \times C_n]$ ,  $G^h = +O$ , 3-fold rotation center  $p = \frac{1}{\sqrt{3}}(-1, -1, -1)$ .  $H = \langle [-\omega, 1], [1, e_n] \rangle$ . 8 tubes, each with  $\text{lcm}(2n, 4)$  cells. Alternate group:  $\pm[O \times D_{2n}]$ .

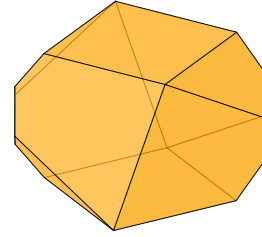
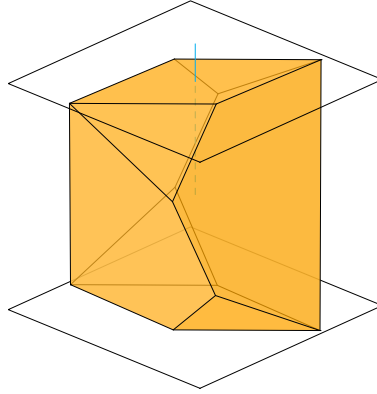
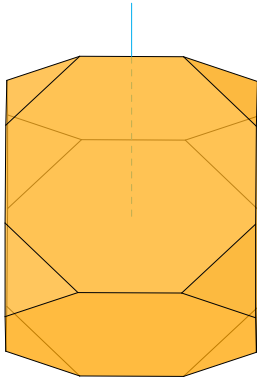
D2693

**B.2.3  $\pm[O \times C_n]$ , 2-fold rotation center**

D2694



D2695



$$n = 1, 2$$

$$\left(\frac{1}{2} + \frac{1}{4}\right) \cdot 2\pi$$

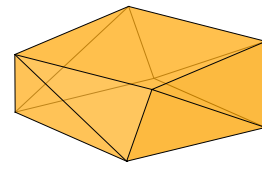
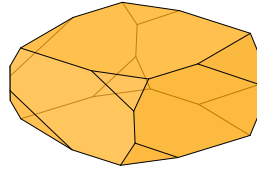
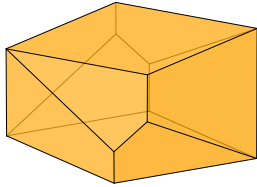
$$n = 4$$

$$\left(\frac{k}{2} + \frac{1}{8}\right) \cdot 2\pi$$

$$n = 3, 6$$

$$\left(\frac{1}{2} + \frac{1}{12}\right) \cdot 2\pi$$

D2696



$$n = 8$$

$$\left(\frac{k}{2} + \frac{1}{16}\right) \cdot 2\pi$$

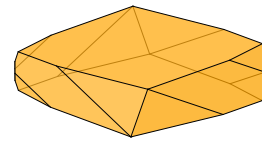
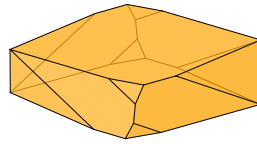
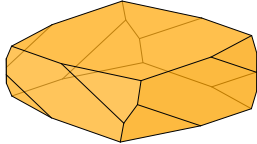
$$n = 5, 10$$

$$\left(\frac{1}{2} + \frac{1}{20}\right) \cdot 2\pi$$

$$n = 12$$

$$\left(\frac{k}{2} + \frac{1}{24}\right) \cdot 2\pi$$

D2697



$$n = 7, 14$$

$$\left(\frac{1}{2} + \frac{1}{28}\right) \cdot 2\pi$$

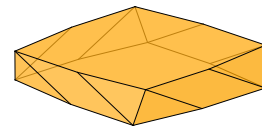
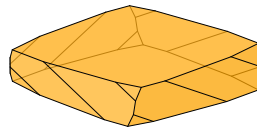
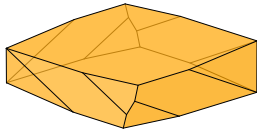
$$n = 16$$

$$\left(\frac{k}{2} + \frac{1}{32}\right) \cdot 2\pi$$

$$n = 9, 18$$

$$\left(\frac{1}{2} + \frac{1}{36}\right) \cdot 2\pi$$

D2698



$$n = 20$$

$$\left(\frac{k}{2} + \frac{1}{40}\right) \cdot 2\pi$$

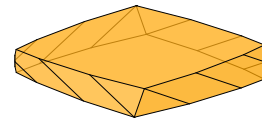
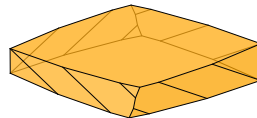
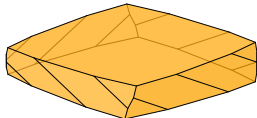
$$n = 11, 22$$

$$\left(\frac{1}{2} + \frac{1}{44}\right) \cdot 2\pi$$

$$n = 24$$

$$\left(\frac{k}{2} + \frac{1}{48}\right) \cdot 2\pi$$

D2699



$$n = 13, 26$$

$$\left(\frac{1}{2} + \frac{1}{52}\right) \cdot 2\pi$$

$$n = 28$$

$$\left(\frac{k}{2} + \frac{1}{56}\right) \cdot 2\pi$$

$$n = 15, 30$$

$$\left(\frac{1}{2} + \frac{1}{60}\right) \cdot 2\pi$$

Figure 40:  $G = \pm[O \times C_n]$ ,  $G^h = +O$ , 2-fold rotation center  $p = \frac{1}{\sqrt{2}}(0, 1, 1)$ .  $H = \langle [i_O, 1], [1, e_n] \rangle$ . 12 tubes, each with  $\text{lcm}(2n, 4)$  cells. Alternate group:  $\pm[O \times D_{2n}]$ . When  $n = 1$  or  $n = 2$ , the cells of a tube are disconnected from each other. For  $n = 4$ , we have drawn squares in the planes around the top and bottom face, to indicate that these faces are horizontal and parallel.



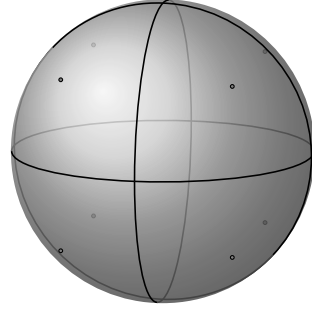
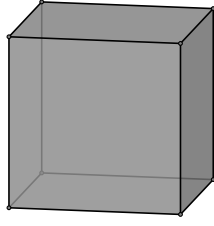
D2700

**B.3**  $\pm \frac{1}{2}[O \times C_{2n}]$ 

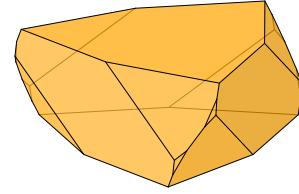
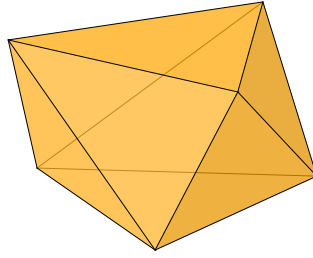
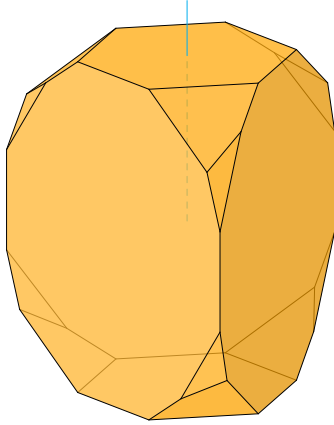
D2701

**B.3.1**  $\pm \frac{1}{2}[O \times C_{2n}]$ , 3-fold rotation center

D2702



D2703



$$n = 1, 3$$

$$\left(\frac{2}{3} + \frac{1}{6}\right) \cdot 2\pi$$

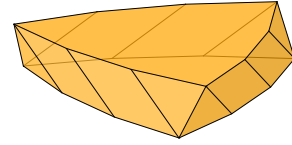
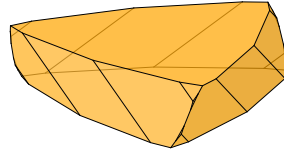
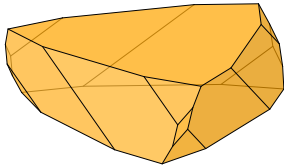
$$n = 2, 6$$

$$\left(\frac{1}{3} + \frac{1}{12}\right) \cdot 2\pi$$

$$n = 9$$

$$\left(\frac{k}{3} + \frac{1}{18}\right) \cdot 2\pi$$

D2704



$$n = 4, 12$$

$$\left(\frac{2}{3} + \frac{1}{24}\right) \cdot 2\pi$$

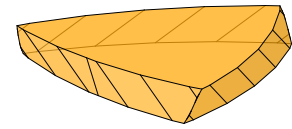
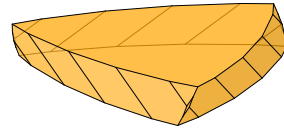
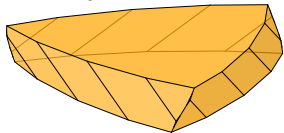
$$n = 5, 15$$

$$\left(\frac{1}{3} + \frac{1}{30}\right) \cdot 2\pi$$

$$n = 18$$

$$\left(\frac{k}{3} + \frac{1}{36}\right) \cdot 2\pi$$

D2705



$$n = 7, 21$$

$$\left(\frac{2}{3} + \frac{1}{42}\right) \cdot 2\pi$$

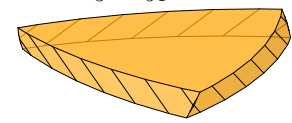
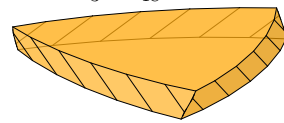
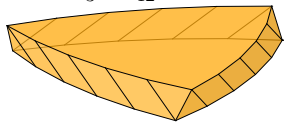
$$n = 8, 24$$

$$\left(\frac{1}{3} + \frac{1}{48}\right) \cdot 2\pi$$

$$n = 27$$

$$\left(\frac{k}{3} + \frac{1}{54}\right) \cdot 2\pi$$

D2706



$$n = 10, 30$$

$$\left(\frac{2}{3} + \frac{1}{60}\right) \cdot 2\pi$$

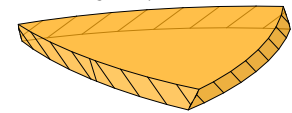
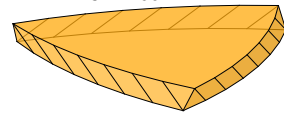
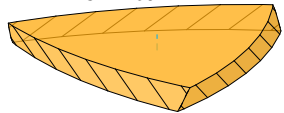
$$n = 11, 33$$

$$\left(\frac{1}{3} + \frac{1}{66}\right) \cdot 2\pi$$

$$n = 36$$

$$\left(\frac{k}{3} + \frac{1}{72}\right) \cdot 2\pi$$

D2707



$$n = 13, 39$$

$$\left(\frac{2}{3} + \frac{1}{78}\right) \cdot 2\pi$$

$$n = 14, 42$$

$$\left(\frac{1}{3} + \frac{1}{84}\right) \cdot 2\pi$$

$$n = 45$$

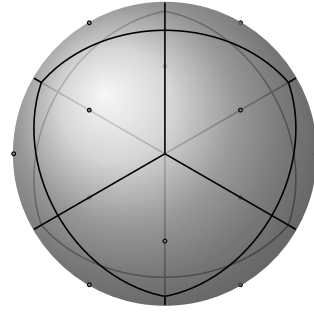
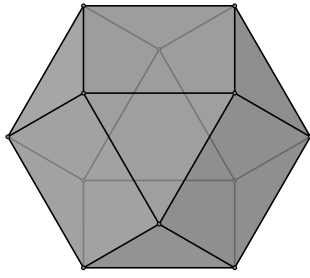
$$\left(\frac{k}{3} + \frac{1}{90}\right) \cdot 2\pi$$

Figure 41:  $G = \pm \frac{1}{2}[O \times C_{2n}]$ ,  $G^h = +O$ , 3-fold rotation center  $p = \frac{1}{\sqrt{3}}(-1, -1, -1)$ .  $H = \langle [-\omega, 1], [1, e_n] \rangle$ . 8 tubes, each with  $\text{lcm}(2n, 6)$  cells. Alternate group:  $\pm \frac{1}{2}[O \times \overline{D}_{4n}]$ .

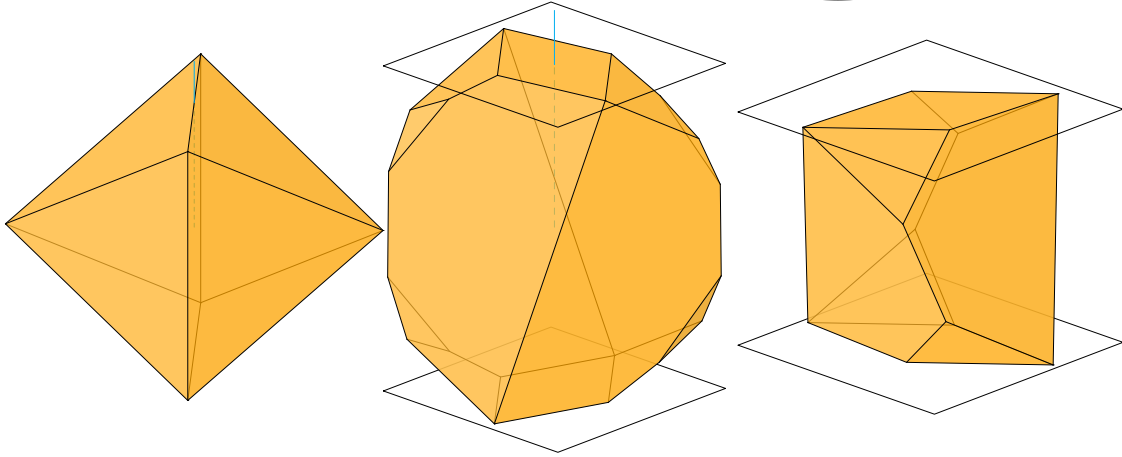
D2708

**B.3.2**  $\pm \frac{1}{2}[O \times C_{2n}]$ , 2-fold rotation center

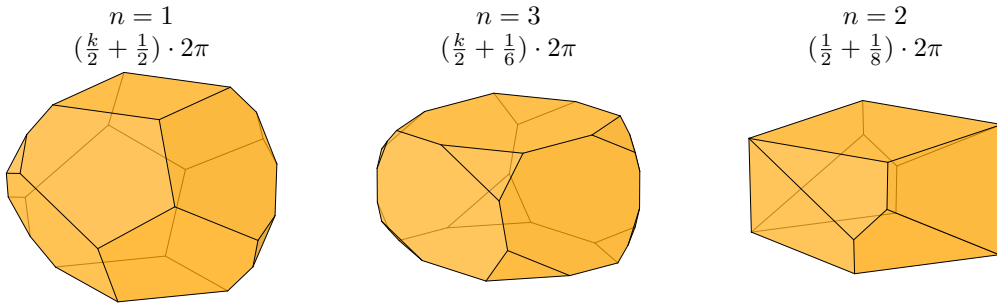
D2709



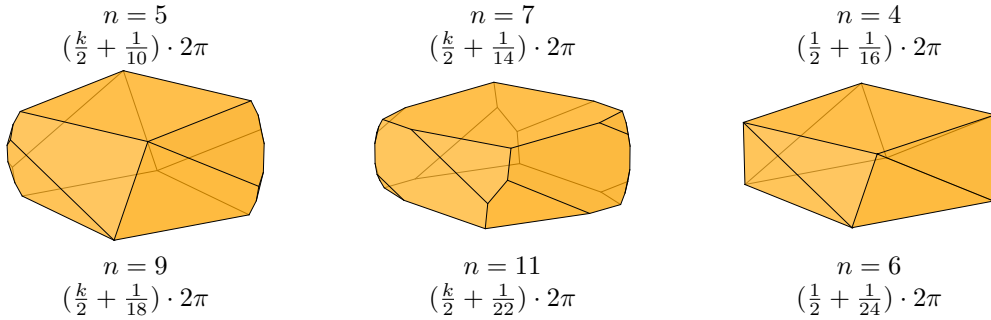
D2710



D2711



D2712



D2713

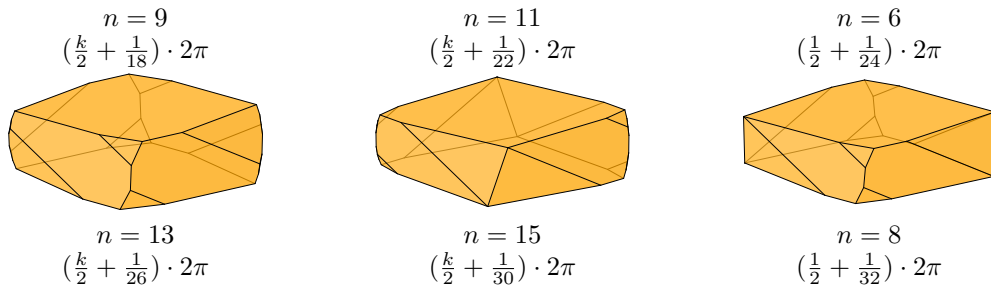


Figure 42:  $G = \pm \frac{1}{2}[O \times C_{2n}]$ ,  $G^h = +O$ , 2-fold rotation center  $p = \frac{1}{\sqrt{2}}(0, 1, 1)$ . The  $G^h$ -orbit polytope is a cuboctahedron. The corresponding Voronoi diagram on the 2-sphere has the structure of a rhombic dodecahedron.  $H = \langle [i_O, e_{2n}], [1, e_n] \rangle$ . 12 tubes, each with  $\frac{4n}{\gcd(n-1, 2)}$  cells. Alternate group:  $\pm \frac{1}{2}[O \times \overline{D}_{4n}]$ . When  $n = 1$ , the cells of a tube are disconnected from each other. For  $n = 2$  and  $n = 3$ , we have drawn squares in the planes around the top and bottom face, to indicate that these faces are horizontal and parallel.

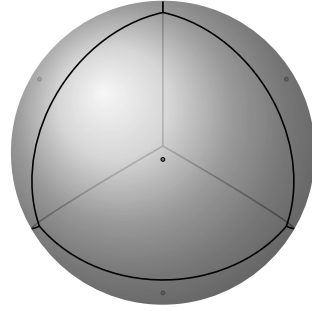
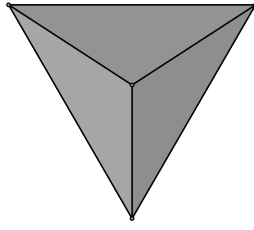
D2714

**B.4**  $\pm[T \times C_n]$ 

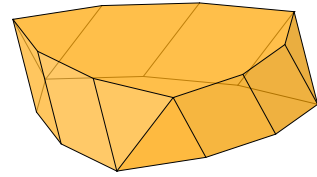
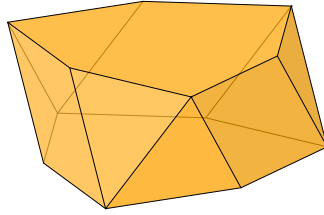
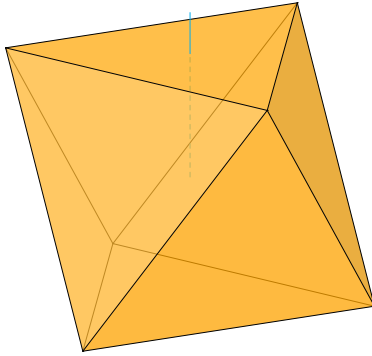
D2715

**B.4.1**  $\pm[T \times C_n]$ , 3-fold rotation center

D2716



D2717



$$n = 1, 3$$

$$\left(\frac{2}{3} + \frac{1}{6}\right) \cdot 2\pi$$

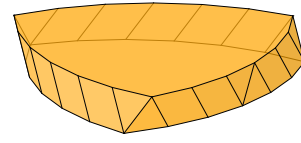
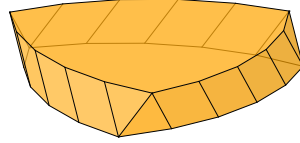
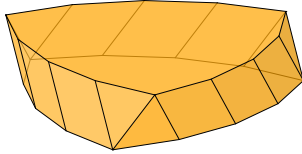
$$n = 2, 6$$

$$\left(\frac{1}{3} + \frac{1}{12}\right) \cdot 2\pi$$

$$n = 9$$

$$\left(\frac{k}{3} + \frac{1}{18}\right) \cdot 2\pi$$

D2718



$$n = 4, 12$$

$$\left(\frac{2}{3} + \frac{1}{24}\right) \cdot 2\pi$$

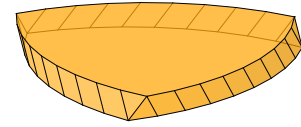
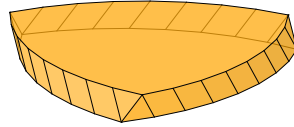
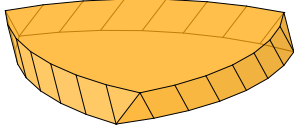
$$n = 5, 15$$

$$\left(\frac{1}{3} + \frac{1}{30}\right) \cdot 2\pi$$

$$n = 18$$

$$\left(\frac{k}{3} + \frac{1}{36}\right) \cdot 2\pi$$

D2719



$$n = 7, 21$$

$$\left(\frac{2}{3} + \frac{1}{42}\right) \cdot 2\pi$$

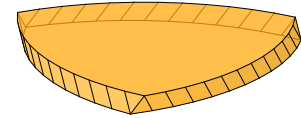
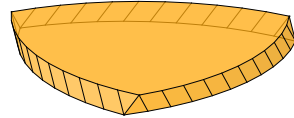
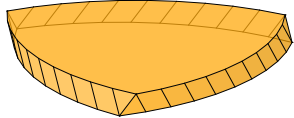
$$n = 8, 24$$

$$\left(\frac{1}{3} + \frac{1}{48}\right) \cdot 2\pi$$

$$n = 27$$

$$\left(\frac{k}{3} + \frac{1}{54}\right) \cdot 2\pi$$

D2720



$$n = 10, 30$$

$$\left(\frac{2}{3} + \frac{1}{60}\right) \cdot 2\pi$$

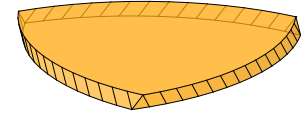
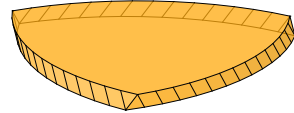
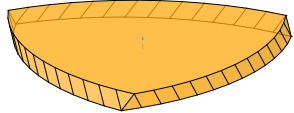
$$n = 11, 33$$

$$\left(\frac{1}{3} + \frac{1}{66}\right) \cdot 2\pi$$

$$n = 36$$

$$\left(\frac{k}{3} + \frac{1}{72}\right) \cdot 2\pi$$

D2721



$$n = 13, 39$$

$$\left(\frac{2}{3} + \frac{1}{78}\right) \cdot 2\pi$$

$$n = 14, 42$$

$$\left(\frac{1}{3} + \frac{1}{84}\right) \cdot 2\pi$$

$$n = 45$$

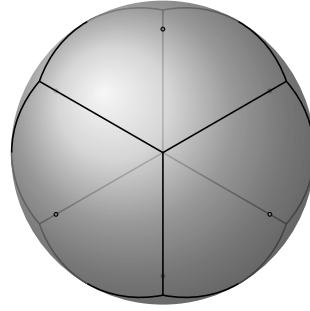
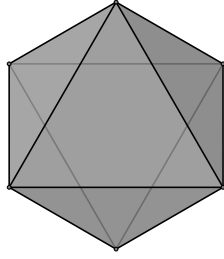
$$\left(\frac{k}{3} + \frac{1}{90}\right) \cdot 2\pi$$

Figure 43:  $G = \pm[T \times C_n]$ ,  $G^h = +T$ , 3-fold (type I) rotation center  $p = \frac{1}{\sqrt{3}}(-1, -1, -1)$ .  $H = \langle [-\omega, 1], [1, e_n] \rangle$ . 4 tubes, each with  $\text{lcm}(2n, 6)$  cells. Alternate group:  $\pm \frac{1}{2}[O \times D_{2n}]$ .

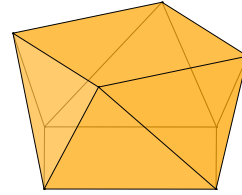
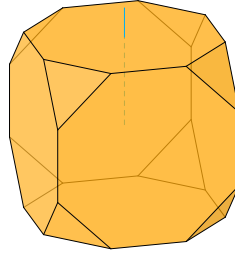
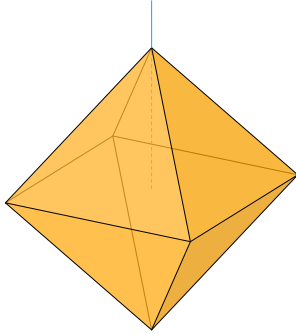
D2722

**B.4.2  $\pm[T \times C_n]$ , 2-fold rotation center**

D2723



D2724



$$n = 1, 2$$

$$\left(\frac{1}{2} + \frac{1}{4}\right) \cdot 2\pi$$

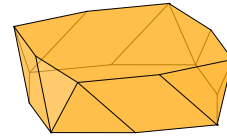
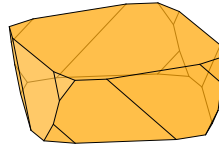
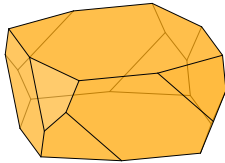
$$n = 4$$

$$\left(\frac{k}{2} + \frac{1}{8}\right) \cdot 2\pi$$

$$n = 3, 6$$

$$\left(\frac{1}{2} + \frac{1}{12}\right) \cdot 2\pi$$

D2725



$$n = 8$$

$$\left(\frac{k}{2} + \frac{1}{16}\right) \cdot 2\pi$$

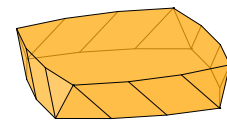
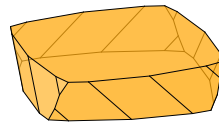
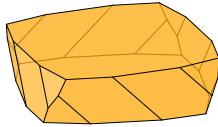
$$n = 5, 10$$

$$\left(\frac{1}{2} + \frac{1}{20}\right) \cdot 2\pi$$

$$n = 12$$

$$\left(\frac{k}{2} + \frac{1}{24}\right) \cdot 2\pi$$

D2726



$$n = 7, 14$$

$$\left(\frac{1}{2} + \frac{1}{28}\right) \cdot 2\pi$$

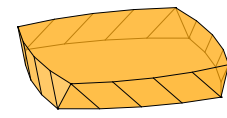
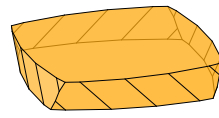
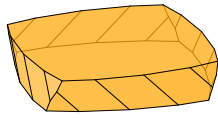
$$n = 16$$

$$\left(\frac{k}{2} + \frac{1}{32}\right) \cdot 2\pi$$

$$n = 9, 18$$

$$\left(\frac{1}{2} + \frac{1}{36}\right) \cdot 2\pi$$

D2727



$$n = 20$$

$$\left(\frac{k}{2} + \frac{1}{40}\right) \cdot 2\pi$$

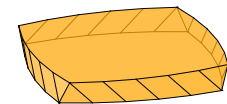
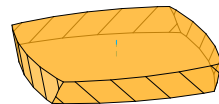
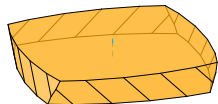
$$n = 11, 22$$

$$\left(\frac{1}{2} + \frac{1}{44}\right) \cdot 2\pi$$

$$n = 24$$

$$\left(\frac{k}{2} + \frac{1}{48}\right) \cdot 2\pi$$

D2728



$$n = 13, 26$$

$$\left(\frac{1}{2} + \frac{1}{52}\right) \cdot 2\pi$$

$$n = 28$$

$$\left(\frac{k}{2} + \frac{1}{56}\right) \cdot 2\pi$$

$$n = 15, 30$$

$$\left(\frac{1}{2} + \frac{1}{60}\right) \cdot 2\pi$$

Figure 44:  $G = \pm[T \times C_n]$ ,  $G^h = +T$ , 2-fold rotation center  $p = (1, 0, 0)$ .  $H = \langle [i, 1], [1, e_n] \rangle$ . 6 tubes, each with  $\text{lcm}(2n, 4)$  cells. Alternate groups:  $\pm[T \times D_{2n}]$  and  $\pm\frac{1}{2}[O \times D_{2n}]$  (also their common supergroup  $\pm[O \times D_{2n}]$ ) if  $n \equiv 0 \pmod{4}$ , else  $\pm[T \times D_{2n}]$  (and its supergroup  $\pm\frac{1}{2}[O \times \overline{D}_{4n}]$ ). When  $n = 1$  or  $n = 2$ , consecutive cells of a tube touch only via vertices.

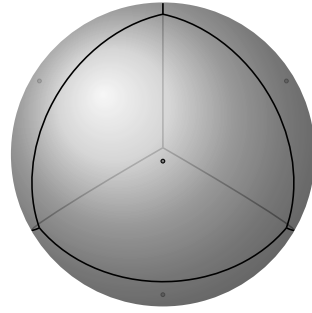
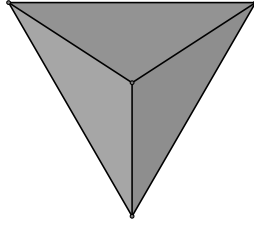
D2729

**B.5**  $\pm \frac{1}{3}[T \times C_{3n}]$ 

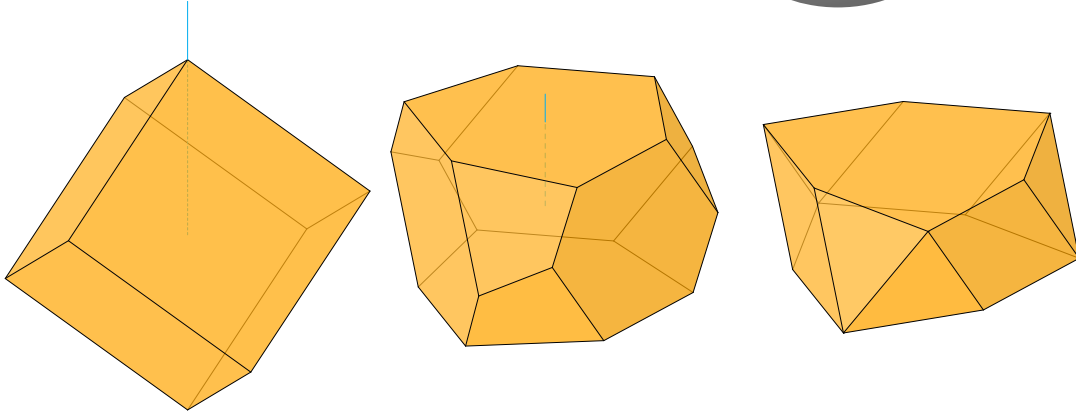
D2730

**B.5.1**  $\pm \frac{1}{3}[T \times C_{3n}]$ , **3-fold (type I) rotation center**

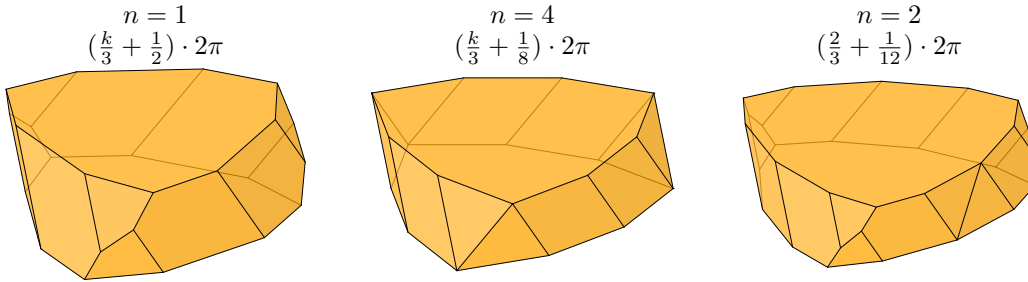
D2731



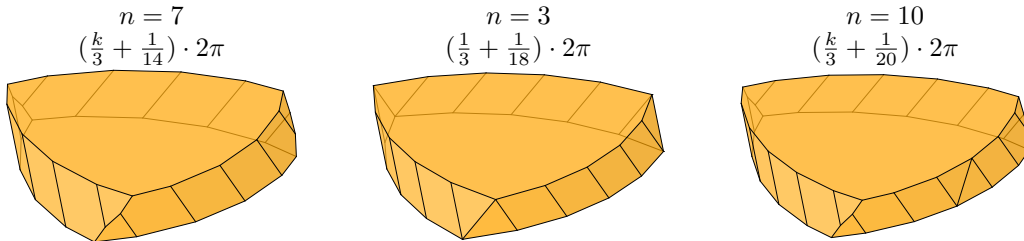
D2732



D2733



D2734



D2735

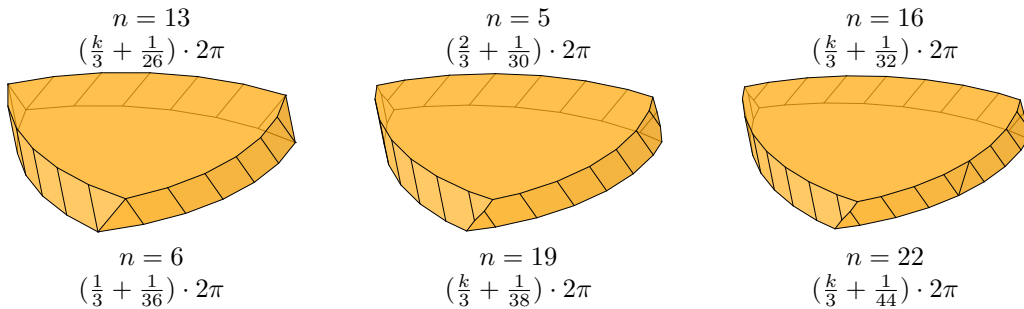
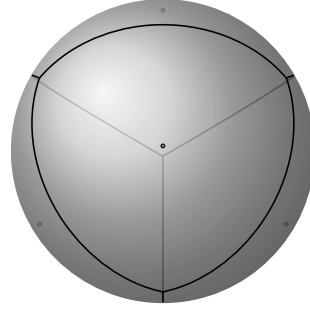
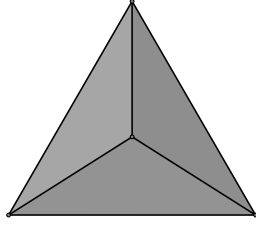


Figure 45:  $G = \pm \frac{1}{3}[T \times C_{3n}]$ ,  $G^h = +T$ , 3-fold (type I) rotation center  $p = \frac{1}{\sqrt{3}}(-1, -1, -1)$ .  $H = \langle [-\omega, e_{3n}], [1, e_n] \rangle$ . 4 tubes, each with  $\frac{6n}{\gcd(n-1, 3)}$  cells. Alternate groups:  $\pm \frac{1}{6}[O \times D_{6n}]$  (and its supergroup  $\pm \frac{1}{2}[O \times D_{6n}]$  if  $n \not\equiv 1 \pmod{3}$ ). When  $n = 1$ , the cells of a tube are disconnected from each other.

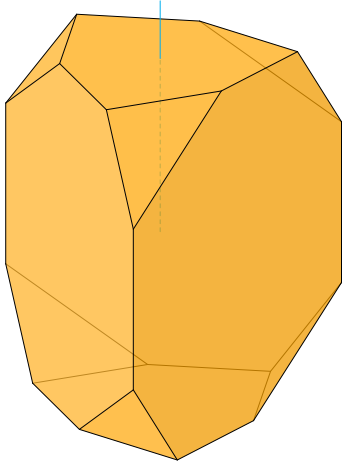
D2736

**B.5.2**  $\pm \frac{1}{3}[T \times C_{3n}]$ , 3-fold (type II) rotation center

D2737

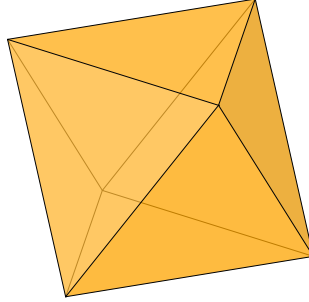


D2738



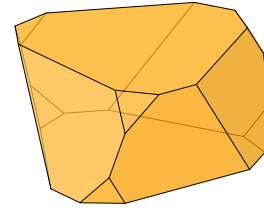
$$n = 2$$

$$\left(\frac{k}{3} + \frac{1}{4}\right) \cdot 2\pi$$



$$n = 1$$

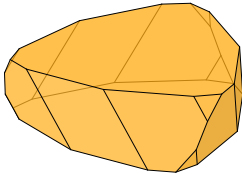
$$\left(\frac{1}{3} + \frac{1}{6}\right) \cdot 2\pi$$



$$n = 5$$

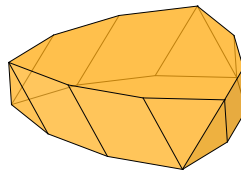
$$\left(\frac{k}{3} + \frac{1}{10}\right) \cdot 2\pi$$

D2739



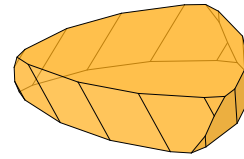
$$n = 8$$

$$\left(\frac{k}{3} + \frac{1}{16}\right) \cdot 2\pi$$



$$n = 3$$

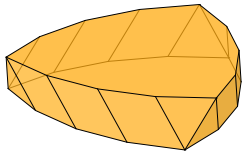
$$\left(\frac{2}{3} + \frac{1}{18}\right) \cdot 2\pi$$



$$n = 11$$

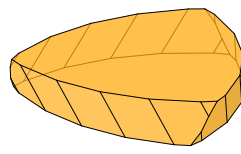
$$\left(\frac{k}{3} + \frac{1}{22}\right) \cdot 2\pi$$

D2740



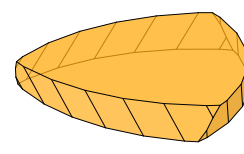
$$n = 4$$

$$\left(\frac{1}{3} + \frac{1}{24}\right) \cdot 2\pi$$



$$n = 14$$

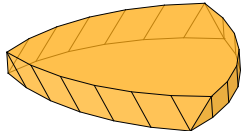
$$\left(\frac{k}{3} + \frac{1}{28}\right) \cdot 2\pi$$



$$n = 17$$

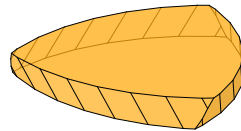
$$\left(\frac{k}{3} + \frac{1}{34}\right) \cdot 2\pi$$

D2741



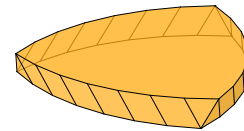
$$n = 6$$

$$\left(\frac{2}{3} + \frac{1}{36}\right) \cdot 2\pi$$



$$n = 20$$

$$\left(\frac{k}{3} + \frac{1}{40}\right) \cdot 2\pi$$



$$n = 7$$

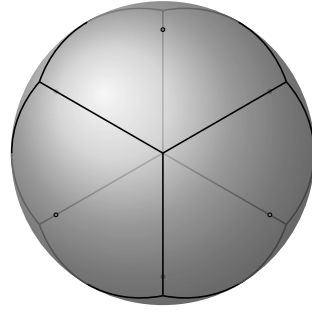
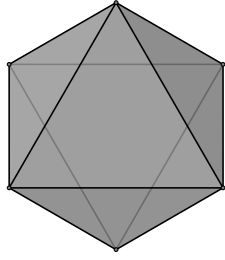
$$\left(\frac{1}{3} + \frac{1}{42}\right) \cdot 2\pi$$

Figure 46:  $G = \pm \frac{1}{3}[T \times C_{3n}]$ ,  $G^h = +T$ , 3-fold (type II) rotation center  $p = \frac{1}{\sqrt{3}}(1, 1, 1)$ .  $H = \langle [-\omega^2, e_{3n}^2], [1, e_n] \rangle$ . 4 tubes, each with  $\frac{6n}{\gcd(n-2, 3)}$  cells. Alternate groups:  $\pm \frac{1}{6}[O \times D_{6n}]$  (and its supergroup  $\pm \frac{1}{2}[O \times D_{6n}]$  if  $n \not\equiv 2 \pmod{3}$ ).

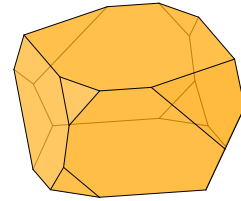
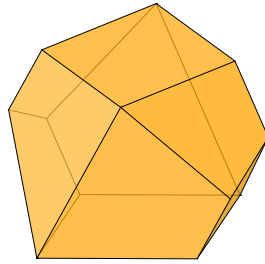
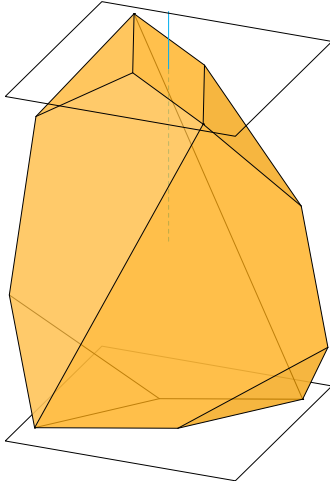
D2742

**B.5.3**  $\pm \frac{1}{3}[T \times C_{3n}]$ , 2-fold rotation center

D2743



D2744



$$n = 1, 2$$

$$\left(\frac{1}{2} + \frac{1}{4}\right) \cdot 2\pi$$

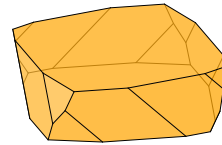
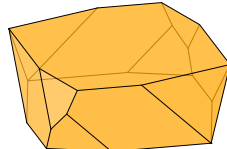
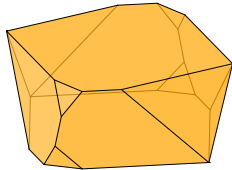
$$n = 4$$

$$\left(\frac{k}{2} + \frac{1}{8}\right) \cdot 2\pi$$

$$n = 3, 6$$

$$\left(\frac{1}{2} + \frac{1}{12}\right) \cdot 2\pi$$

D2745



$$n = 8$$

$$\left(\frac{k}{2} + \frac{1}{16}\right) \cdot 2\pi$$

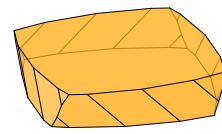
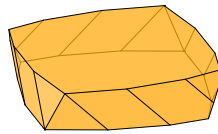
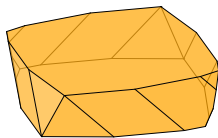
$$n = 5, 10$$

$$\left(\frac{1}{2} + \frac{1}{20}\right) \cdot 2\pi$$

$$n = 12$$

$$\left(\frac{k}{2} + \frac{1}{24}\right) \cdot 2\pi$$

D2746



$$n = 7, 14$$

$$\left(\frac{1}{2} + \frac{1}{28}\right) \cdot 2\pi$$

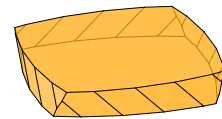
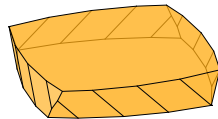
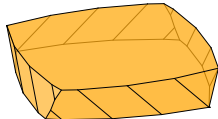
$$n = 16$$

$$\left(\frac{k}{2} + \frac{1}{32}\right) \cdot 2\pi$$

$$n = 9, 18$$

$$\left(\frac{1}{2} + \frac{1}{36}\right) \cdot 2\pi$$

D2747



$$n = 20$$

$$\left(\frac{k}{2} + \frac{1}{40}\right) \cdot 2\pi$$

$$n = 11, 22$$

$$\left(\frac{1}{2} + \frac{1}{44}\right) \cdot 2\pi$$

$$n = 24$$

$$\left(\frac{k}{2} + \frac{1}{48}\right) \cdot 2\pi$$

Figure 47:  $G = \pm \frac{1}{3}[T \times C_{3n}]$ ,  $G^h = +T$ , 2-fold rotation center  $p = (1, 0, 0)$ .  $H = \langle [i, 1], [1, e_n] \rangle$ . 6 tubes, each with  $\text{lcm}(2n, 4)$  cells. Alternate group:  $\pm \frac{1}{6}[O \times D_{6n}]$ . For  $n = 1$  and  $n = 2$ , we have drawn squares in the planes around the top and bottom face, to indicate that these faces are horizontal and parallel.

## C The number of groups of given order

We will see that the number of groups of order  $N$  is always at least  $N/2$ , and less than  $O(N^2)$ . If  $N$  is an odd prime, there are exactly  $(N+3)/2$  groups, namely the torus translation groups  $\square_{1,N}^{(s)}$  for  $0 \leq s \leq (N-1)/2$  and  $\square_{N,1}^{((1-N)/2)}$ .

The richest class of groups are the toroidal groups, and among them, the most numerous groups are the torus translation groups, of type  $\square$ : For each divisor  $m$  of  $N$ , there are  $\sim n/2$  groups  $\square_{m,n}^{(s)}$ , where  $n = N/m$ . Thus, the number of groups is about  $1/2$  times the sum  $\sigma(N)$  of divisors of  $N$ , which is bounded by  $N^{1+\frac{1+O(1/\log \log n)}{\log 2 \ln N}} \leq N^2$  [31]. The upper bound of  $O(N^2)$  is very weak; the actual bound is slightly superlinear.

The number of groups of type  $\square$  is of similar magnitude, provided that  $N$  is even. For all the other types, there is at most one group for every divisor of  $N$ , except for the swaptorn groups, whose number is related to the number of integer points on the circle  $a^2 + b^2 = N/4$ , and this number is at most  $N$ .

From all the remaining classes of groups (tubical, polyhedral, or axial), there can be only a constant number of groups of a given order.

**The number of groups of order 100.** As an exercise, let us compute the number of point groups of order  $N = 100$ .

We proceed through the toroidal classes of groups in Table 6 one by one. For the pure translation groups of type  $\square$ , we can write  $100 = mn = 1 \cdot 100 = 2 \cdot 50 = 4 \cdot 25 = 5 \cdot 20 = 10 \cdot 10 = 20 \cdot 5 = 25 \cdot 4 = 50 \cdot 2 = 100 \cdot 1$  with accordingly  $50+26+13+10+6+3+2+2+1 = 113$  choices of  $s$ , see the remark after (20) in Section 7.5. For the flip groups of type  $\square$  of order  $100 = 2mn$ , we have to factor 50 instead of 100. The possibilities are  $50 = 1 \cdot 50 = 2 \cdot 25 = 5 \cdot 10 = 10 \cdot 5 = 25 \cdot 2 = 50 \cdot 1$  with  $25 + 13 + 5 + 3 + 1 + 1 = 48$  choices of  $s$ .

For the swap groups  $\square_{m,n}^{\mathbf{pm}}$  of order  $4mn$ , we have to split  $25 = mn$  into two factors  $m, n$  larger than 1. There is one possibility:  $25 = 5 \times 5$ . For the groups  $\square_{m,n}^{\mathbf{pg}}$ , only the first factor  $m$  must be larger than 1. This gives 2 choices. For  $\square_{m,n}^{\mathbf{cm}}$  of order  $2mn$ ,  $mn = 50$  must be split into two factors of the same parity. This is impossible since  $mn \equiv 2 \pmod{4}$ . Thus, in total we have 3 swap groups of type  $\square$ . Clearly, there is the same number of 3 swap groups of type  $\square$ .

Finally, for the full torus swap groups, almost all types have order  $8mn$ , which cannot equal 100. We only need to consider the groups of type  $\square_{m,n}^{\mathbf{c2mm}}$ , of order  $4mn$ . We have to split  $100/4 = 25$  into two factors  $\geq 3$  of the same parity. There is one possibility:  $25 = 5 \times 5$ .

In total, we get  $113 + 48 + 3 + 3 + 1 = 168$  chiral toroidal groups of order 100.

Let us turn to the achiral groups: For the reflection groups  $\square$ , we have to consider all factorizations  $100 = 2mn$  (types  $\mathbf{pm}$  and  $\mathbf{pg}$ ) or  $100 = 4mn$  (type  $\mathbf{cm}$ ). This gives  $2 \times \sigma_0(50) + \sigma_0(25) = 2 \times 6 + 3 = 15$  groups, where  $\sigma_0$  denotes the number of divisors of a number.

For the full reflection groups  $\square$ , we have to consider all factorizations  $100 = 4mn$  or  $100 = 8mn$ , respectively, where in one case ( $\mathbf{p2mg}$ ), we distinguish the order of the factors. We get  $2 + 3 + 2 + 0 = 7$  possibilities. For general  $N$ , there are  $2[\sigma_0(\frac{N}{4})/2] + \sigma_0(\frac{N}{4}) + [\sigma_0(\frac{N}{8})/2]$  full reflection groups of order  $N$ , where  $\sigma_0(x) = 0$  if  $x$  is not an integer.

For  $\square$ , we must have  $100 = 4(a^2 + b^2)$  with  $a \geq b \geq 0$ . There are two possibilities:  $(a, b) = (5, 0)$  or  $(4, 3)$ .

For the full torus groups  $\square$ , the order would have to be a multiple of 8; so there are no such groups of order 100.

In total, we get  $15 + 7 + 2 = 24$  achiral toroidal groups of order 100, and 192 toroidal groups altogether.

$N = 100$  does not occur as the order of any of the other types of groups. So 192 is the total number of 4-dimensional point groups of order 100.

**Enantiomorphic pairs.** As an advanced exercise, we can ask, how many of the 168 chiral groups of order 100 are their own mirror image?

For the groups of type  $\square$ , we are looking for a lattice of translations of size 100 that has an orientation-reversing symmetry. If it is symmetric with respect to a horizontal axis, then, according to Lemma 7.7, the possibilities are an  $m \times n$  rectangular grid of  $mn$  points or a rhombic grid of  $2mn$  points. In this case, it is also symmetric with respect to a vertical axis.

Thus, we have to split  $100 = mn$  and  $50 = mn$  into two factors  $m$  and  $n$ . The order of the factors plays no role, because the reflection  $\square$  swaps the factors. We have 5 possibilities for  $100 = 1 \cdot 100 = 2 \cdot 50 = 4 \cdot 25 = 5 \cdot 20 = 10 \cdot 10$  and 3 possibilities for  $50 = 1 \cdot 50 = 2 \cdot 25 = 5 \cdot 10$ ,



which gives  $5 + 3 = 8$  possibilities in total. (Alternatively, adding a vertical and horizontal mirror to such a translational subgroup will produce a group of type  $\boxplus \mathbf{p2mm}$  or  $\boxplus \mathbf{c2mm}$ . So we can equivalently count the groups of these types of order  $4N = 400$ .)

There is also the possibility that the lattice is symmetric with respect to a swapturn operation  $\boxtimes$ . The number of these groups equals the number of groups of type  $\boxtimes$  of order  $4N = 400$ . It can be computed as the number of integer points  $(a, b)$  on the circle  $100 = a^2 + b^2$  with  $a \geq b \geq 0$ . There are two possibilities:  $(10, 0)$  and  $(8, 6)$ .

We have overcounted the lattices that are symmetric with respect to both  $\boxplus$  and  $\boxtimes$ , in other words, the upright or slanted square lattices. There is one lattice of this type: the  $10 \times 10$  upright lattice.

In total,  $8 + 2 - 1 = 9$  groups among the 113 groups of type  $\boxtimes$  are equal to their own mirror.

For the groups of type  $\boxtimes$ , we can repeat the same game, except that we are looking for a translation lattice of half the size, 50. For the lattices with  $\boxplus$  symmetry, we have 3 possibilities for  $50 = 1 \cdot 50 = 2 \cdot 25 = 5 \cdot 10$ , and 2 possibilities for  $25 = 1 \cdot 25 = 5 \cdot 5$ , giving  $3 + 2 = 5$  possibilities in total. There are two possibilities for  $50 = a^2 + b^2$  with  $a \geq b \geq 0$ :  $(7, 1)$  and  $(5, 5)$ . We have to subtract 1 for the slanted  $5 \times 5$  grid, for a total of  $5 + 2 - 1 = 6$  groups among the 48 flip groups.

The mirrors of the groups of type  $\boxtimes$  are the groups of type  $\boxtimes$ , and hence none of them is its own mirror. The groups of type  $\boxtimes$  are easy to handle: The two parameters  $m$  and  $n$  must be equal. We have one such group,  $\boxtimes_{5,5} \mathbf{c2mm}$ . In total,  $9 + 6 + 1 = 16$  chiral groups are their own mirror images. The remaining  $168 - 16 = 152$  chiral groups consist of enantiomorphic pairs.

**The number of groups of order 7200.** To look at a more interesting example, let us count the groups of order 7200. The count of toroidal groups follows the same calculation as above, and it amounts to 19,319 chiral and 216 achiral groups. In addition, we have 22 tubical groups:  $\pm[I \times C_{60}], \pm[I \times D_{60}], \pm[O \times C_{150}], \pm[O \times D_{150}], \pm[T \times C_{300}], \pm[T \times D_{300}], \pm\frac{1}{2}[O \times D_{300}], \pm\frac{1}{2}[O \times \overline{D}_{300}], \pm\frac{1}{2}[O \times C_{300}], \pm\frac{1}{6}[O \times D_{900}], \pm\frac{1}{3}[T \times C_{900}]$ , and their mirrors. Finally, there is one polyhedral group  $\pm[I \times I]$ . In total, we have  $19,319 + 22 + 1 = 19,342$  chiral groups and 216 achiral ones.

**The number of groups of order at most  $M$ .** While the number of groups of a given order  $N$  fluctuates between a linear lower bound and a slightly superlinear upper bound, the “average number” can be estimated quite precisely: We have seen that the number of groups of order  $N$  is of order  $\Theta(\sigma(N))$ , where  $\sigma(N)$  is the sum of divisors of  $N$ . If we look at all groups of order at most  $M$ , we can sum over all potential divisors  $d$  and get

$$\sum_{N=1}^M \sigma(N) = \sum_{d=1}^M d \lfloor M/d \rfloor = \Theta(M^2).$$

Thus, the number of four-dimensional groups of order at most  $M$  is  $\Theta(M^2)$ . The majority of these groups is chiral, but the achiral ones alone are already of the order  $\Theta(M^2)$ : There is essentially one swapturn group for each integer point  $(a, b)$  in the disk  $a^2 + b^2 \leq M/4$ , with roughly a factor 8 of overcounting of symmetric points, and this gives  $\Theta(M^2)$  chiral groups.

## D The crystallographic point groups

Brown, Bülow, Neubüser, Wondratschek, Zassenhaus classified the four-dimensional crystallographic space groups in 1978 [4]. They grouped them by the underlying point groups (geometric crystal classes, or  $\mathbb{Q}$ -classes), and assigned numbers to these groups. The crystallographic point groups are characterized as having some lattice that they leave invariant.

There are 227 crystallographic point groups, sorted into 33 crystal systems according to the holohedry, i.e., the symmetry group of the underlying lattice. Tables 17–18 give a reference from the 227 groups in the list of [4, Table 1C, pp. 79–260] to our notation (for the toroidal groups) or Conway and Smith’s notation (for the remaining groups). When appropriate, we list two enantiomorphic groups.

The first classification of the four-dimensional crystallographic point groups was obtained by Hurley in 1951 [23], see Section 10.2. A few mistakes were later corrected [24].

order			order			order		
01/01	$\square_{1,1}$	1	13/01	$\square_{4,1}^{pm}$	8	20/01	$\square_{1,12}^{(3)}$	12
01/02	$\square_{2,1}$	2	13/02	$\square_{2,1}^{cm}$	8	20/02	$\square_{1,12}^{(2)}$	12
02/01	$\square_{1,1}^{pg}$	2	13/03	$\square_{1,4}^{(1)}$	8	20/03	$\square_{2,3}^{pg}$	12
02/02	$\square_{1,1}^{pm}$	2	13/04	$\square_{1,4}^{(0)}$	8	20/04	$\square_{4,3}^{pm}$	24
02/03	$\square_{1,1}^{cm}$	4	13/05	$\square_{4,2}^{pm}$	16	20/05	$\square_{2,12}^{(4)}$	24
03/01	$\square_{1,1}^{cm}$	2	13/06	$\square_{4,1}^{p2mg}$	16	20/06	$\square_{3,4}^{pm}$	24
03/02	$\square_{2,2}^{pm}$	4	13/07	$\square_{2,1}^{c2mm}$	16	20/07	$\square_{1,12}^{(3)}$	24
04/01	$\square_{1,1}^{p2gg}$	4	13/08	$\square_{4,1}^{p2mm}$	16	20/08	$\square_{3,4}^{pg}$	24
04/02	$\square_{1,1}^{p2mg}$	4	13/09	$\square_{2,4}^{(0)}$	16	20/09	$\square_{2,3}^{cm}$	24
04/03	$\square_{1,1}^{p2mm}$	4	13/10	$\square_{4,2}^{p2mm}$	32	20/10	$\square_{3,2}^{cm}$	24
04/04	$\square_{1,1}^{c2mm}$	8	14/01	$\square_{3,1}^{pm}$	6	20/11	$\square_{1,12}^{(2)}$	24
05/01	$\square_{1,1}^{c2mm}$	4	14/02	$\square_{3,1}^{pg}$	6	20/12	$\square_{3,2}^{p2gg}$	24
05/02	$\square_{2,2}^{p2mm}$	8	14/03	$\square_{1,3}^{(0)}$	6	20/13	$\square_{3,2}^{p2mg}$	24
06/01	$\square_{2,1}^{p2mg}$	8	14/04	$\square_{3,1}^{cm}$	12	20/14	$\square_{2,6}^{pg}$	24
06/02	$\square_{2,1}^{p2mm}$	8	14/05	$\square_{2,3}^{(0)}$	12	20/15	$\square_{4,6}^{pm}$	48
06/03	$\square_{2,2}^{p2mm}$	16	14/06	$\square_{3,1}^{p2mg}$	12	20/16	$\square_{4,3}^{p2mm}$	48
07/01	$\square_{1,4}^{(1)}$	4	14/07	$\square_{3,1}^{p2mm}$	12	20/17	$\square_{4,3}^{p2mg}$	48
07/02	$\square_{1,4}^{(0)}$	4	14/08	$\square_{3,1}^{p2gg}$	12	20/18	$\square_{6,4}^{pm}$	48
07/03	$\square_{2,4}^{(0)}$	8	14/09	$\square_{1,3}^{p2mg}$	12	20/19	$\square_{2,12}^{(4)}$	48
07/04	$\square_{1,2}^{cm}$	8	14/10	$\square_{3,1}^{c2mm}$	24	20/20	$\square_{3,2}^{c2mm}$	48
07/05	$\square_{1,4}^{pm}$	8	15/01	$\square_{6,1}^{pm}$	12	20/21	$\square_{6,2}^{p2mg}$	48
07/06	$\square_{1,4}^{pg}$	8	15/02	$\square_{3,2}^{pg}$	12	20/22	$\square_{6,4}^{p2mm}$	96
07/07	$\square_{2,4}^{pm}$	16	15/03	$\square_{3,2}^{pm}$	12	21/01	$\square_{1,3}^{cm} \mid \square_{3,1}^{cm}$	6
08/01	$\square_{1,3}^{(0)}$	3	15/04	$\square_{1,6}^{(0)}$	12	21/02	$\square_{2,6}^{pm} \mid \square_{6,2}^{pm}$	12
08/02	$\square_{2,3}^{(0)}$	6	15/05	$\square_{1,6}^{(2)}$	12	21/03	$\square_{1,3}^{c2mm} \mid \square_{3,1}^{c2mm}$	12
08/03	$\square_{1,3}^{pg}$	6	15/06	$\square_{6,1}^{p2mg}$	24	21/04	$\square_{2,6}^{p2mm} \mid \square_{6,2}^{p2mm}$	24
08/04	$\square_{1,3}^{pm}$	6	15/07	$\square_{2,3}^{p2mg}$	24	22/01	$\square_{3,3}^{(0)}$	9
08/05	$\square_{1,3}^{cm}$	12	15/08	$\square_{6,2}^{pm}$	24	22/02	$\square_{6,3}^{(-3)}$	18
09/01	$\square_{1,6}^{(0)}$	6	15/09	$\square_{6,1}^{p2mm}$	24	22/03	$\square_{3,3}^{pg}$	18
09/02	$\square_{1,6}^{(2)}$	6	15/10	$\square_{3,2}^{p2mm}$	24	22/04	$\square_{3,3}^{pm}$	18
09/03	$\square_{2,6}^{(0)}$	12	15/11	$\square_{2,6}^{(0)}$	24	22/05	$\square_{3,3}^{(0)}$	18
09/04	$\square_{1,6}^{pg}$	12	15/12	$\square_{6,2}^{p2mm}$	48	22/06	$\square_{3,3}^{cm}$	36
09/05	$\square_{1,6}^{pm}$	12	16/01	$\square_{2,2}^{p2gm} \mid \square_{2,2}^{p2mg}$	8	22/07	$\square_{6,3}^{(-3)}$	36
09/06	$\square_{2,3}^{pm}$	12	17/01	$\square_{1,3}^{cm} \mid \square_{3,1}^{cm}$	6	22/08	$\square_{3,3}^{p2gg}$	36
09/07	$\square_{2,6}^{pm}$	24	17/02	$\square_{2,6}^{pm} \mid \square_{6,2}^{pm}$	12	22/09	$\square_{3,3}^{p2mg}$	36
10/01	$\square_{2,2}^{pg} \mid \square_{2,2}^{pg}$	4	18/01	$\square_{2,2}^{p2gg}$	8	22/10	$\square_{3,3}^{p2mm}$	36
11/01	$\square_{1,3}^{(1)} \mid \square_{3,1}$	3	18/02	$\square_1^{p4gmS}$	16	22/11	$\square_{3,3}^{c2mm}$	72
11/02	$\square_{2,3}^{(-1)} \mid \square_{6,1}$	6	18/03	$\square_{2,0}$	16	23/01	$\square_{3,6}^{(0)}$	18
12/01	$\square_{1,0}$	4	18/04	$\square_{2,2}^{c2mm}$	16	23/02	$\square_{6,6}^{(0)}$	36
12/02	$\square_{1,1}$	8	18/05	$\square_2^{p4mmU}$	32	23/03	$\square_{3,6}^{pm}$	36
12/03	$\square_1^{p4gmU}$	8	19/01	$\square_{2,4}^{pg}$	16	23/04	$\square_{3,6}^{pg}$	36
12/04	$\square_1^{p4mmU}$	8	19/02	$\square_{4,4}^{(0)}$	16	23/05	$\square_{3,6}^{(0)}$	36
12/05	$\square_1^{p4mmS}$	16	19/03	$\square_{4,4}^{pm}$	32	23/06	$\square_{6,3}^{pm}$	36
			19/04	$\square_{4,2}^{p2mg}$	32	23/07	$\square_{6,6}^{pm}$	72
			19/05	$\square_{4,4}^{(0)}$	32	23/08	$\square_{6,6}^{(0)}$	72
			19/06	$\square_{4,4}^{p2mm}$	64	23/09	$\square_{6,3}^{p2mm}$	72
						23/10	$\square_{6,3}^{p2mg}$	72
						23/11	$\square_{6,6}^{p2mm}$	144

Table 17: The 227 crystallographic point groups in four dimensions, part 1

order			order		
24/01	$+\frac{1}{12}[T \times T]$	12	31/01	$\boxtimes_{2,1}$	20
24/02	$\pm\frac{1}{12}[T \times T]$	24	31/02	$\boxtimes_{3,1}$	40
24/03	$+\frac{1}{12}[T \times \bar{T}] \cdot 2_3$	24	31/03	$+\frac{1}{60}[I \times \bar{I}]$	60
24/04	$+\frac{1}{12}[T \times \bar{T}] \cdot 2_1$	24	31/04	$+\frac{1}{60}[I \times \bar{I}] \cdot 2_3$	120
24/05	$\pm\frac{1}{12}[T \times \bar{T}] \cdot 2$	48	31/05	$+\frac{1}{60}[I \times \bar{I}] \cdot 2_1$	120
25/01	$+\frac{1}{12}[T \times T] \cdot 2_1$	24	31/06	$\pm\frac{1}{60}[I \times \bar{I}]$	120
25/02	$+\frac{1}{12}[T \times T] \cdot 2_3$	24	31/07	$\pm\frac{1}{60}[I \times \bar{I}] \cdot 2$	240
25/03	$+\frac{1}{24}[O \times O]$	24	32/01	$\boxtimes_{2,4}^{\text{pg}} \mid \boxtimes_{4,2}^{\text{pg}}$	8
25/04	$+\frac{1}{24}[O \times \bar{O}]$	24	32/02	$\boxtimes_{2,4}^{\text{cm}} \mid \boxtimes_{4,2}^{\text{cm}}$	16
25/05	$\pm\frac{1}{12}[T \times T] \cdot 2$	48	32/03	$\boxtimes_{2,4}^{\text{p2gg}} \mid \boxtimes_{4,2}^{\text{p2gg}}$	16
25/06	$\pm\frac{1}{24}[O \times O]$	48	32/04	$\boxtimes_{4,2}^{\text{p2mg}} \mid \boxtimes_{2,4}^{\text{p2gm}}$	16
25/07	$+\frac{1}{24}[O \times O] \cdot 2_1$	48	32/05	$\pm\frac{1}{3}[T \times C_3] \mid \pm\frac{1}{3}[C_3 \times T]$	24
25/08	$+\frac{1}{24}[O \times \bar{O}] \cdot 2_1$	48	32/06	$\boxtimes_{2,4}^{\text{c2mm}} \mid \boxtimes_{4,2}^{\text{c2mm}}$	32
25/09	$+\frac{1}{24}[O \times \bar{O}] \cdot 2_3$	48	32/07	$\boxtimes_{4,4}^{\text{p2gg}}$	32
25/10	$+\frac{1}{24}[O \times O] \cdot 2_3$	48	32/08	$\boxtimes_{4,4}^{\text{cm}} \mid \boxtimes_{4,4}^{\text{cm}}$	32
25/11	$\pm\frac{1}{24}[O \times O] \cdot 2$	96	32/09	$\boxtimes_2^{\text{p4gmU}}$	32
26/01	$\boxtimes_{2,4}^{\text{pg}} \mid \boxtimes_{4,2}^{\text{pg}}$	8	32/10	$\boxtimes_{4,4}^{\text{p2mm}}$	32
26/02	$\boxtimes_{2,4}^{\text{p2mg}} \mid \boxtimes_{4,2}^{\text{p2gm}}$	16	32/11	$\pm\frac{1}{6}[O \times D_6] \mid \pm\frac{1}{6}[D_6 \times O]$	48
27/01	$\boxtimes_{1,5}^{(1)}$	5	32/12	$\boxtimes_{4,4}^{\text{c2mm}}$	64
27/02	$\boxtimes_{2,5}^{(1)}$	10	32/13	$\boxtimes_2^{\text{p4gmS}}$	64
27/03	$\boxtimes_{1,5}^{(1)}$	10	32/14	$\boxtimes_2^{\text{p4mmS}}$	64
27/04	$\boxtimes_{2,5}^{(1)}$	20	32/15	$\boxtimes_{4,0}$	64
28/01	$\boxtimes_{2,6}^{\text{pg}} \mid \boxtimes_{6,2}^{\text{pg}}$	12	32/16	$\pm\frac{1}{3}[T \times T]$	96
28/02	$\boxtimes_{2,6}^{\text{p2mg}} \mid \boxtimes_{6,2}^{\text{p2gm}}$	24	32/17	$\boxtimes_4^{\text{p4mmU}}$	128
29/01	$\boxtimes_{3,3}^{\text{cm}} \mid \boxtimes_{3,3}^{\text{cm}}$	18	32/18	$\pm\frac{1}{3}[T \times T] \cdot 2$	192
29/02	$\boxtimes_{6,6}^{\text{pm}} \mid \boxtimes_{6,6}^{\text{pm}}$	36	32/19	$\pm\frac{1}{3}[T \times \bar{T}] \cdot 2$	192
29/03	$\boxtimes_{3,3}^{\text{c2mm}}$	36	32/20	$\pm\frac{1}{6}[O \times O]$	192
29/04	$\boxtimes_{3,0}$	36	32/21	$\pm\frac{1}{6}[O \times O] \cdot 2$	384
29/05	$\boxtimes_{6,6}^{\text{p2mm}}$	72	33/01	$\boxtimes_{4,6}^{\text{pg}} \mid \boxtimes_{6,4}^{\text{pg}}$	24
29/06	$\boxtimes_{3,3}$	72	33/02	$\boxtimes_{4,6}^{\text{pg}} \mid \boxtimes_{6,4}^{\text{pg}}$	24
29/07	$\boxtimes_3^{\text{p4gmU}}$	72	33/03	$\pm[C_1 \times T] \mid \pm[T \times C_1]$	24
29/08	$\boxtimes_3^{\text{p4mmU}}$	72	33/04	$\boxtimes_{4,6}^{\text{p2gg}} \mid \boxtimes_{6,4}^{\text{p2gg}}$	48
29/09	$\boxtimes_3^{\text{p4mmS}}$	144	33/05	$\pm[C_2 \times T] \mid \pm[T \times C_2]$	48
30/01	$\boxtimes_{2,6}^{\text{pg}} \mid \boxtimes_{6,2}^{\text{pg}}$	12	33/06	$\pm\frac{1}{2}[O \times C_2] \mid \pm\frac{1}{2}[C_2 \times O]$	48
30/02	$\boxtimes_{2,6}^{\text{p2gg}} \mid \boxtimes_{6,2}^{\text{p2gg}}$	24	33/07	$\pm[C_3 \times T] \mid \pm[T \times C_3]$	72
30/03	$\boxtimes_{2,6}^{\text{cm}} \mid \boxtimes_{6,2}^{\text{cm}}$	24	33/08	$\pm[D_4 \times T] \mid \pm[T \times D_4]$	96
30/04	$\boxtimes_{2,6}^{\text{p2gm}} \mid \boxtimes_{6,2}^{\text{p2mg}}$	24	33/09	$\pm\frac{1}{2}[O \times D_4] \mid \pm\frac{1}{2}[D_4 \times O]$	96
30/05	$\boxtimes_{6,6}^{\text{pg}} \mid \boxtimes_{6,6}^{\text{pg}}$	36	33/10	$\pm\frac{1}{2}[O \times C_4] \mid \pm\frac{1}{2}[C_4 \times O]$	96
30/06	$\boxtimes_{2,6}^{\text{c2mm}} \mid \boxtimes_{6,2}^{\text{c2mm}}$	48	33/11	$\pm\frac{1}{2}[O \times D_6] \mid \pm\frac{1}{2}[D_6 \times O]$	144
30/07	$\boxtimes_{6,6}^{\text{cm}} \mid \boxtimes_{6,6}^{\text{cm}}$	72	33/12	$\pm\frac{1}{2}[O \times \bar{D}_8] \mid \pm\frac{1}{2}[\bar{D}_8 \times O]$	192
30/08	$\boxtimes_{6,6}^{\text{p2mg}} \mid \boxtimes_{6,6}^{\text{p2gm}}$	72	33/13	$\pm[T \times T]$	288
30/09	$\boxtimes_{6,6}^{\text{p2gg}}$	72	33/14	$\pm[T \times T] \cdot 2$	576
30/10	$\boxtimes_{6,6}^{\text{c2mm}}$	144	33/15	$\pm\frac{1}{2}[O \times O]$	576
30/11	$\boxtimes_{6,0}$	144	33/16	$\pm\frac{1}{2}[O \times O] \cdot 2$	1152
30/12	$\boxtimes_3^{\text{p4gmS}}$	144	—	$\boxtimes_{4,6}^{\text{p2gm}} \mid \boxtimes_{6,4}^{\text{p2mg}}$	48
30/13	$\boxtimes_6^{\text{p4mmU}}$	288	—	$\boxtimes_{4,6}^{\text{p2mg}} \mid \boxtimes_{6,4}^{\text{p2gm}}$	48
			—	$\pm[D_6 \times T] \mid \pm[T \times D_6]$	144

Table 18: The 227 crystallographic point groups, part 2, and three pseudo-crystal groups

All these groups are subgroups of only four maximal groups:

- $31/07 = \pm \frac{1}{60}[I \times \bar{I}] \cdot 2 = [[3, 3, 3]]$  (the simplex and its polar, order 240)
- $33/16 = \pm \frac{1}{2}[O \times O] \cdot 2 = [3, 4, 3]$  (the 24-cell, order 1152). Taking the permutations of  $(\pm 1, \pm 1, 0, 0)$  as the vertices of a 24-cell, this set generates a lattice, and this lattice is invariant under the group. The symmetries of the hypercube/cross-polytope,  $32/21 = \pm \frac{1}{6}[O \times O] \cdot 2 = [3, 3, 4]$ , are contained in this group as a subgroup.
- $30/13 = \boxtimes_6^{\mathbf{p4mmU}} = \pm \frac{1}{2}[\bar{D}_{12} \times \bar{D}_{12}] \cdot 2$ , order 288. The invariant lattice is the Cartesian product of two hexagonal plane lattices.
- $20/22 = \boxplus_{6,4}^{\mathbf{p2mm}} = \pm \frac{1}{24}[D_{24} \times D_{24}^{(5)}] \cdot 2^{(0,0)}$ , order 96. The invariant lattice is the Cartesian product of a hexagonal lattice and a square lattice.

The last three items in Table 18 are the “pseudo crystal groups” of Hurley [24]: Each such group consists of transformations that can individually occur in crystallographic groups, but as a whole, it is not a crystallographic group. All its proper subgroups are crystallographic groups.

## E Geometric interpretation of oriented great circles

Section 4.1.2 introduced the notation  $\vec{K}_p^q$  to denote oriented great circles on  $S^3$ . Here we give a geometric interpretation of the orientation. In fact, we will give two equivalent geometric interpretations. However, at the boundary cases  $p = q$  and  $q = -p$ , one or the other of the interpretations loses its meaning, and only by combining both interpretations we get a consistent definition that covers all cases.

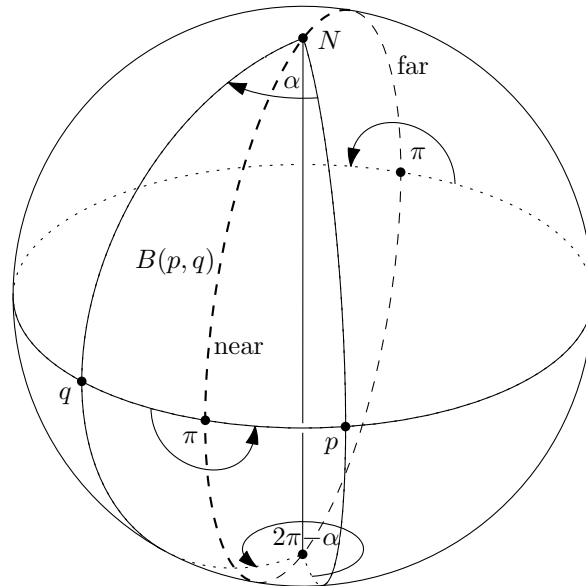
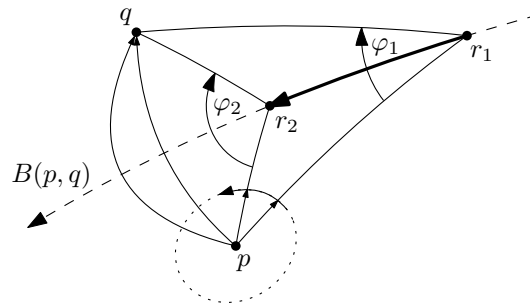


Figure 48: The centers of the rotations mapping  $p$  to  $q$  lie on the bisecting circle  $B(p, q)$ .

We start from the definition (7) of  $K_p^q$  as the set of rotations  $[x]$  that map  $p$  to  $q$  in  $S^2$ . The centers  $r$  of these rotations lie on the bisecting circle  $B(p, q)$  between  $p$  and  $q$ . In Figure 48, we have drawn  $p$  and  $q$  on the equator, with  $p$  east of  $q$ . If we observe the clockwise rotation angle  $\varphi$  as  $r$  moves along  $B(p, q)$ , we see that  $\varphi$  has two extrema: If the angular distance between  $p$  and  $q$  is  $\alpha$ , the minimum clockwise angle  $\varphi = \alpha$  is achieved when  $r$  is at the North Pole. The maximum  $2\pi - \alpha$  is achieved at the South Pole. The poles bisect  $B(p, q)$  into two semicircles, the *near semicircle* and the *far semicircle*, according to the distance from  $p$  and  $q$ .

To define an orientation, we let  $r$  move continuously on  $B(p, q)$ , see Figure 49 for an illustration on a small patch of  $S^2$ . We make the movement in such a way that

- the rotation center  $r$  moves in counterclockwise direction around  $p$ ;
- simultaneously, the clockwise rotation angle  $\varphi$  increases when  $r$  is on the near semicircle and decreases when  $r$  is on the far semicircle.

Figure 49: Orienting the great circle  $K_p^q$ 

In Figure 49, as  $r$  moves from  $r_1$  to  $r_2$  along the thick arrow, the angle  $\varphi$  increases from  $\varphi_1$  to  $\varphi_2$ . These rules define an orientation of  $B(p, q)$ .

When we want to transfer this orientation to  $K_p^q$ , we must be aware of the 2 : 1 relation between quaternions  $x = \cos \frac{\varphi}{2} + r \cdot \sin \frac{\varphi}{2}$  and rotations  $[x]$  of  $S^2$ . The angle  $\varphi$  is defined only up to multiples of  $2\pi$ , and hence a rotation corresponds to two opposite quaternions  $x$  and  $-x$ . Thus, there are two ways of defining a continuous dependence from  $r$  via  $\varphi$  to  $x$ . Both possibilities lead to the same orientation of  $K_p^q$ , but we can select one of them by restricting  $\varphi$  to the interval  $0 \leq \varphi < 2\pi$ . Once this mapping is chosen, two opposite points  $r$  and  $-r$  on  $B(p, q)$ , which define the same rotation  $[r]$  of  $S^2$ , correspond to opposite quaternions  $x$  and  $-x$  on  $K_p^q$ . (The easiest way to check this is for the midpoint of  $p$  and  $q$  in Figure 48 and the opposite point. Both have the same rotation angle  $\varphi = \pi$ . Generally, the transition from  $\varphi$  to  $2\pi - \varphi$  changes the sign of  $\cos \frac{\varphi}{2}$  and leaves  $\sin \frac{\varphi}{2}$  unchanged.) Thus, as  $r$  traverses  $B(p, q)$ ,  $x$  traverses  $K_p^q$  once, and this traversal defines the orientation  $\vec{K}_p^q$ .

The rules break down in the degenerate situations when  $q = \pm p$ . Luckily, in each situation, there is one rule that works.

- When  $p = q$ , the only rotations centers are  $r = p$  and  $r = -p$ . In this case, we can maintain rule (ii): We consider increasing rotation angles around  $r = p$  (or decreasing rotation angles around  $r = -p$ , which corresponds to the far semicircle).
- When  $p = -q$ , the rotation angle  $\varphi = 180^\circ$  is constant, but we can stick to rule (i): The rotation centers  $r$  lie on the circle  $B(p, -p)$  that has  $p$  and  $-p$  as poles, and we let them move counterclockwise around  $p$ .

Considering the definition (7) of  $K_p^q$ , it is actually surprising that  $K_p^q$  makes a smooth transition when  $q$  approaches  $p$ : The locus  $B(p, q)$  of rotation centers changes discontinuously from a circle to a set of opposite points.

When  $p$  and  $q$  are exchanged with  $-p$  and  $-q$ , the circle  $K_p^q$  of rotations remains the same, but everything changes its direction: A counterclockwise movement of  $r$  around  $p$  becomes a clockwise movement when seen from  $-p$ , and  $r$  is on the near semicircle of  $p$  and  $q$  if it is on the far semicircle of  $-p$  and  $-q$ . Thus,  $\vec{K}_{-p}^{-q}$  has the opposite orientation.

## F Subgroup relations between tubical groups

Figure 50 shows the subgroup structure between different tubical groups. Some types are included multiple times with different parameters to indicate common supergroups. However, all the types appear at least once with the parameter “ $n$ ”. (Those are the ones in red.)

## G Conway and Smith’s classification of the toroidal groups

We describe the parameterization of the lattice translations for the Conway–Smith classification of the groups of types  $\pm[C \times C]$  and  $+[C \times C]$  in geometric terms and relate them to our torus translations groups (type  $\square$ ). This might be interesting for readers who want to study the classic classification for the toroidal groups and understand the connections.

As before, we describe the groups in terms of the lattice of torus translations in the  $(\alpha_1, \alpha_2)$  coordinate system, see Figure 51. We put the origin at the top right corner  $(2\pi, 2\pi)$  because the

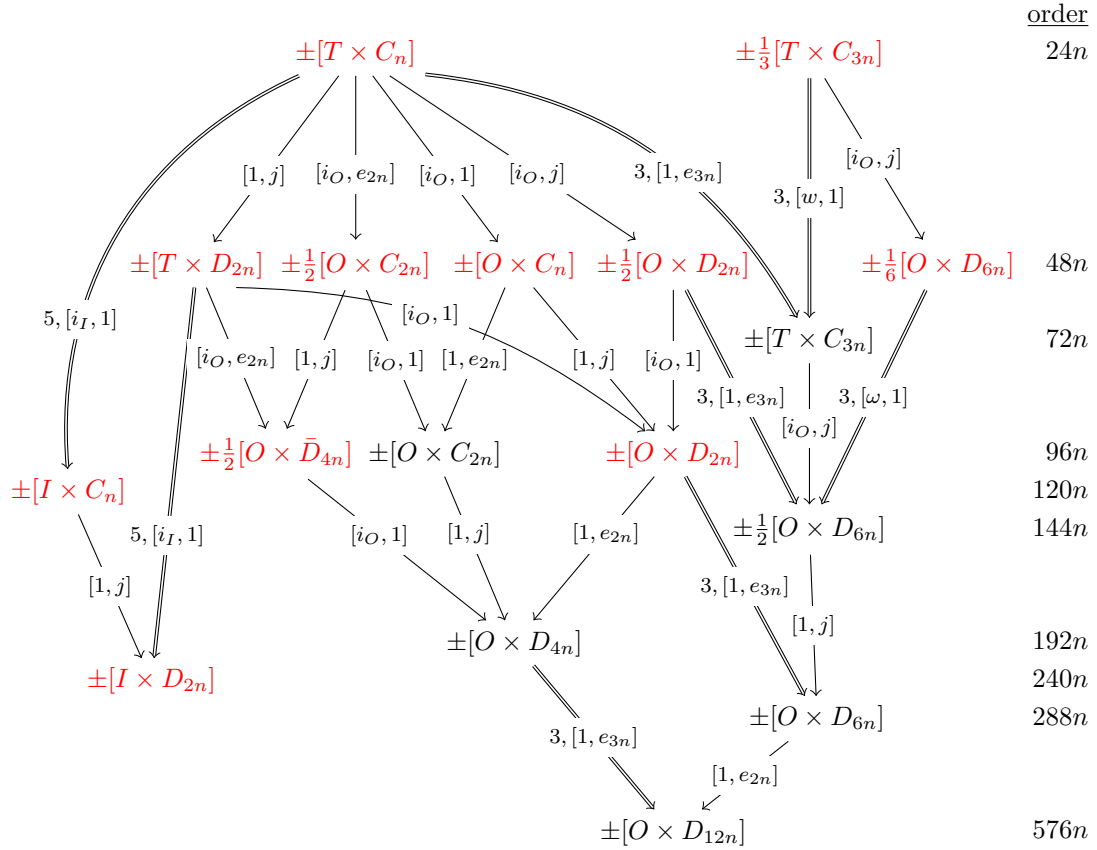


Figure 50: Small-index containments between left tubical groups. Each arrow is marked with an extending element. Single arrows indicate index-2 containments. Double arrows denote index-3 or index-5 containments, as specified with the extending element. The red groups have the “natural” parameter  $n$  (as in Table 2). Groups at the same horizontal level have the same order, which is given in the rightmost column.

left rotations  $[e_m, 1]$  is a shift by  $\pi/m$  along the negative  $\alpha_1 = \alpha_2$  axis. This is the axis for the left rotations, and we call it the  $L$ -axis. The right rotations move on the  $\alpha_2 = -\alpha_1$  axis in the southeast direction, and we call this the  $R$ -axis.

We first describe the diploid groups  $\pm \frac{1}{f}[C_m^{(s)} \times C_n]$ , and we related them to our groups  $\square_{m',n}^{(s')}$ . The left and right groups are determined by the grid formed by drawing  $\pm 45^\circ$  lines through all points. If  $2m$  grid lines cross the  $L$ -axis between  $(0,0)$  and  $(2\pi, 2\pi)$ , then the left group is  $C_m$ . Similarly, if there are  $2n$  grid intervals on the  $R$ -axis between  $(2\pi, 2\pi)$  and  $(4\pi, 0)$ , (or equivalently, on the  $-45^\circ$  diagonal of the square), the right group is  $C_n$ . The translation vectors on these diagonals form the left kernel  $C_{m/f}$  and the right kernel  $C_{n/f}$ . The factor  $f$  is determined by the number of grid steps along the diagonal from one point to the next. In the picture, these are  $f = 5$  steps. The parameter  $m'$  for our parameterization is hence  $2m/f$ . The kernels span a slanted rectangular grid; one rectangular box of this grid is shaded in the picture. In terms of grid lines, the diagonal is an  $f \times f$  square, and it contains exactly one point per grid line of either direction, for a total of  $f$  points (counting the four corners only once). In geometric terms, Conway and Smith parameterize the lattice by looking at the first grid line below the  $L$ -axis, as in our parameterization. They measure  $s$  as the number of grid steps to the first lattice point, starting from the  $R$ -axis in southwest direction. The number  $s$  must be relatively prime to  $f$ , because otherwise, additional points on the  $R$ -axis would be generated.

By contrast, the parameter  $s'$  in our setup (Figure 20) is effectively measured in the same units along the same diagonal line, but starting from the intersection with the  $\alpha_1$ -axis, in the northeast direction. Our parameterization is simpler because we don't specify in advance the number of points on the  $R$ -axis. This allows us to freely choose  $s'$  within some range.

The group  $\pm \frac{1}{f}[C_m^{(s)} \times C_n]$  is therefore generated by the translation vectors  $[e_m^f, 1]$  along the  $L$ -axis,  $[1, e_n^f]$  along the  $R$ -axis, and the additional vector  $[e_m^s, e_n]$ . (The second generator  $[1, e_n^f]$

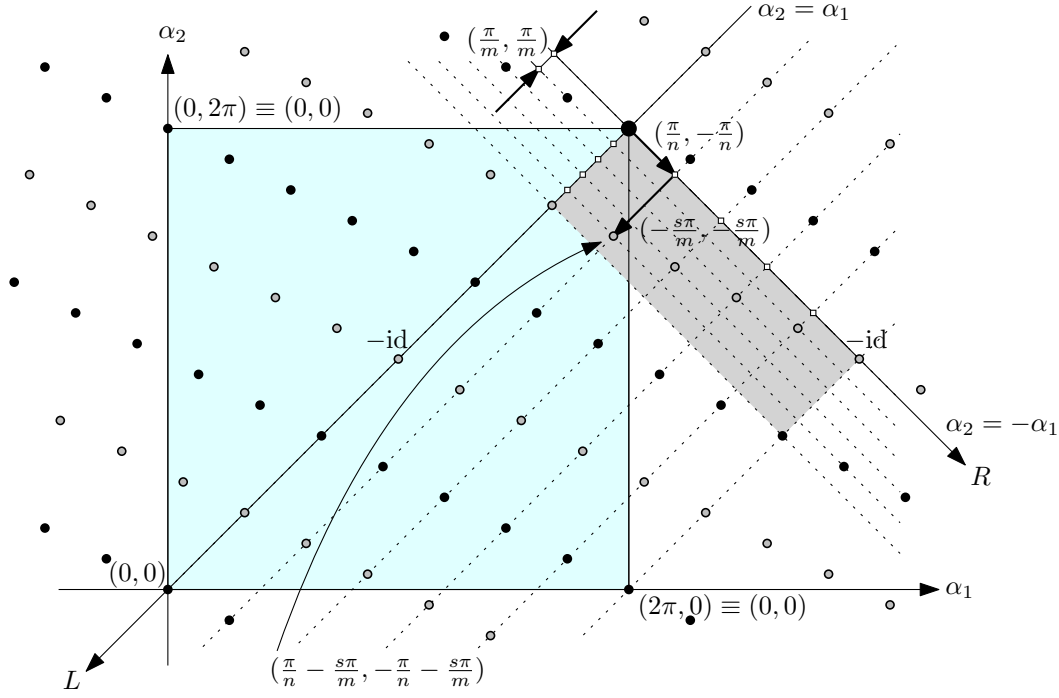


Figure 51: Parameterization of the translation groups in Conway and Smith. The black and gray points together form the diploid group  $\pm \frac{1}{5}[C_{15}^{(4)} \times C_5] = \square_{6,5}^{(-2)}$  of order 30. The black points alone form the haploid group  $+\frac{1}{5}[C_{15}^{(9)} \times C_5] = \square_{3,5}^{(-1)}$  of order 15.

is actually redundant because  $[e_m^s, e_n]^f [e_m^f, 1]^{-s} = [1, e_n^f]$ .

For our group  $\square_{m',n}^{(s')}$ , the parameter  $n$  is the same, and  $m' = 2m/f$ . The parameter  $s'$  can be computed as follows. Choose generators for  $\pm \frac{1}{f}[C_m^{(s)} \times C_n]$  as in Figure 20. These generators are then  $t_1 = (\frac{f\pi}{m}, \frac{f\pi}{m})$  and  $t_2 = (\frac{\pi}{n} - \frac{s\pi}{m} + \frac{f\pi}{m}, -\frac{\pi}{n} - \frac{s\pi}{m} + \frac{f\pi}{m})$ . Comparing them with the generators in Proposition 7.5, we get  $s' = \frac{-m+(f-s)n}{f}$ .

As mentioned in footnote 14 on p. 51, we have swapped the roles of the left and right groups with respect to Conway and Smith's convention, to get a closer correspondence. In the original convention of Conway and Smith, the group  $\pm \frac{1}{f}[C_m \times C_n^{(s)}]$  is considered, whose third generator is  $[e_m, e_n^s]$ . This group is the mirror of the group  $\pm \frac{1}{f}[C_n^{(s)} \times C_m]$ .

A haploid group  $+\frac{1}{f}[C_m^{(s)} \times C_n]$  exists if both  $m/f$  and  $n/f$  are odd. We modify the first generator to  $[e_m^{2f}, 1]$ . This omits every other point on the  $L$ -axis (and on every line parallel to it) and thus avoids the point  $(\pi, \pi) = -\text{id}$ . In addition to being relatively prime to  $f$ ,  $s$  must be odd, because otherwise, since  $[e_m^s, e_n]^n [e_m^{2f}, 1]^{-n/f \cdot s/2} = [1, e_n^n] = [1, -1]$ , we would nevertheless generate the point  $(\pi, \pi) = -\text{id}$ .

Reflection in the  $L$ -axis gives the same group. Hence  $\pm \frac{1}{5}[C_{15}^{(4)} \times C_5] \doteq \pm \frac{1}{5}[C_{15}^{(1)} \times C_5] = \square_{6,5}^{(1)}$ , and  $+\frac{1}{5}[C_{15}^{(9)} \times C_5] \doteq +\frac{1}{5}[C_{15}^{(1)} \times C_5] = \square_{3,5}^{(2)}$ . This reflection changes the parameter  $s$  to  $f-s$  for the diploid groups and to  $2f-s$  for the haploid groups. To eliminate these duplications, the parameter  $s$  should be constrained to the interval  $0 \leq s \leq f/2$  for the diploid groups and  $0 \leq s \leq f$  for the haploid groups. As mentioned in footnote 15 on p. 53, these constraints are not stated in Conway and Smith. This concerns the last four entries of [8, Table 4.2], see Figure 53.

With the help of the geometric picture of Figure 51 for the parameterization of Conway and Smith, one can give a geometric interpretation to the conditions  $s = fg \pm 1$  of [8, pp. 52–53] for the last 4 lines of Table 4.3: The condition  $s = fg - 1$  expresses the fact that a square lattice is generated, as is necessary for the torus swaptorn groups  $\square$  (type  $[D \times D] \cdot \bar{2}$ ). The condition  $s = fg + 1$  characterizes a rectangular lattice, as required for the groups of type  $\square$  and  $\square$ . (Accordingly, for the two types of groups  $\pm [C \times C] \cdot 2^{(\gamma)}$  and  $+[C \times C] \cdot 2^{(\gamma)}$  in the upper half of [8, pp. 53], the condition  $s = fg - 1$  must be corrected to  $s = fg + 1$ , see Figure 56.)

## G.1 Index-4 subgroups of $D_{4m}$

There is one ambiguity that is notorious for causing oversights and omissions. It arises when the group  $C_m$  is used as an index-4 subgroup of  $D_{4m}$ .

$D_{4m}$  is the chiral symmetry group of a regular  $2m$ -gon  $P_{2m}$  in space. In Figure 52 we show such a  $2m$ -gon with an alternating 2-coloring of its vertices.  $C_m$  is the normal subgroup of rotations around the principal axis, perpendicular to the polygon, by multiples of  $2\pi/m$  (those that respect the coloring).  $C_m$  has three cosets in  $D_{4m}$ : The “cyclic coset”  $C'_m$  of rotations by odd multiples of  $\pi/m$  (those that swap the coloring), and two “half-turn cosets”  $C_m^0$  and  $C_m^1$ . One of these contains the half-turns through the vertices of  $P_{2m}$  (the dashed axes, keeping the colors), and the other the half-turns through the edge midpoints of  $P_{2m}$  (the dotted axes, swapping colors). However, when we rotate  $P_{2m}$  by  $\pi/(2m)$ , the involved groups and subgroups don’t change, and hence we see that  $C_m^0$  and  $C_m^1$  are geometrically the same, whereas  $C'_m$  is clearly distinguishable (unless  $m = 1$ ).

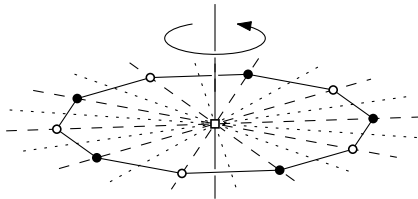


Figure 52: The operations of  $D_{20}$  on a regular 10-gon  $P_{10}$

The case of the index-4 subgroups  $C_m$  and  $C_n$  of  $D_{4m}$  and  $D_{4n}$  is denoted in Conway and Smith [8] by the notation  $\frac{1}{4}[D_{4m} \times D_{4n}]$ , possibly with some decoration to distinguish different cases.

The actual group is determined by an isomorphism between the cosets of  $D_{4m}/C_m$  and  $D_{4n}/C_n$ . For this there are two possibilities.

- (a) The cyclic coset  $C'_m$  is matched with the cyclic coset  $C'_n$ .
- (b) The cyclic coset  $C'_m$  and the cyclic coset  $C'_n$  are not matched to each other.

**Goursat’s omission.** In the earliest enumeration by Goursat from 1889, the less natural possibility (b) has been overlooked. This was noted by Threlfall and Seifert in 1931, [35, footnote 9 on p. 14]<sup>25</sup> and by Hurley in 1951 [23, bottom of p. 652],<sup>26</sup> who consequently extended the classification by adding an additional class XIII’ of groups to Goursat’s list. Du Val [15] followed Goursat and omitted case (b) again.

**A missed duplication in Conway and Smith.** Conway and Smith [8] denote case (b) by adding a bar to the second factor as follows:

$$\pm \frac{1}{4}[D_{4m} \times \bar{D}_{4n}] \text{ or } + \frac{1}{4}[D_{4m} \times \bar{D}_{4n}]$$

When  $n = 1$ , the distinction between case (a) and (b) disappears.  $D_4$  is the Vierergruppe, whose nontrivial operations are half-turns around three perpendicular axes, and these elements are geometrically indistinguishable.

Conway and Smith express this succinctly in the concluding sentence of their classification (see Figure 56): “In the last eight lines, it is always permissible to replace  $D_2$  by  $C_2$  and  $\bar{D}_4$  by  $D_4$ .” However, this formulation in connection with the choice of notation might lead an

<sup>25</sup>Referring to Goursat’s work: “Gruppen dieser Substitutionen – mit unseren Paargruppen 1-isomorph – sind mit einer Ausnahme (§ 4 S. 18 Fußnote und § 4 S. 22) vollständig angegeben.” (Groups of these substitutions – which are 1-isomorphic to our pair groups – are completely specified with one exception, see § 4 p. 18 footnote 13 and § 4 p. 22.) In fact, in footnote 13 on p. 18, they use two such groups as an example of groups with equal normal subgroups  $L_0$  and  $R_0$  that are different already as abstract groups. It is curious that Threlfall and Seifert, in the same paper, when they came to the actual classification, overlooked this class of groups again. They noted the gap themselves and filled it in part II [36, pp. 585–586, Appendix II, Note 5].

<sup>26</sup>“In the course of this calculation we find that Goursat has omitted one family of groups. This omission appears to have passed unnoticed by subsequent writers.”



unwary reader into a trap:<sup>27</sup> The choice (b) of an alternative mapping between the index-4 cosets in  $\frac{1}{4}[D_{4m} \times D_{4n}]$  is not a property associated to  $D_{4n}$  and its chosen normal subgroup, and it would more appropriate to add the bar to the  $\times$  operator or the whole expression. The distinction disappears when at least *one* of  $D_{4m}$  and  $D_{4n}$  is  $D_4$ , and hence, the bar can also be removed in a case like  $[D_4 \times \bar{D}_{4n}]$  when the first factor is  $D_4$ . This duplication example has been treated in detail in Section 7.11.2.

Conway and Smith use the bar notation  $\bar{D}_{4n}$  also for something different, namely in the index-2 case, for example in  $\pm \frac{1}{2}[O \times \bar{D}_{4n}]$ , see Table 2. It indicates that, as the kernel  $R_0$  (or  $L_0$ ) of  $D_{4n}$ , the normal subgroup  $\bar{D}_{2n}$  is used, as opposed to  $C_{2n}$ . Also in this case, the distinction disappears for  $n = 1$ , but this time, it is a property of the group  $D_{4n}$  and its normal subgroup, and hence the notation of attaching the bar to  $D_{4n}$  causes no confusion.

**Another duplication in Conway and Smith.** Our computer check unveiled another duplication in Conway and Smith's classification. It concerns the groups  $\boxplus_{m,n}^{p2mg}$  for  $m = n$ :

$$\begin{aligned}\boxplus_{n,n}^{p2mg} &\doteq \pm \frac{1}{4}[D_{2n} \times D_{2n}^{(1)}] \cdot 2^{(1,0)} \doteq \pm \frac{1}{4}[D_{2n} \times D_{2n}^{(1)}] \cdot 2^{(1,1)} && \text{for even } n \\ \boxplus_{n,n}^{p2mg} &\doteq + \frac{1}{2}[D_{2n} \times D_{2n}^{(1)}] \cdot 2^{(0,0)} \doteq + \frac{1}{2}[D_{2n} \times D_{2n}^{(1)}] \cdot 2^{(0,2)} && \text{for odd } n\end{aligned}$$

Neither of these duplications is warranted according to the equalities listed in [8, pp. 52–53]. For example, for  $\pm \frac{1}{4}[D_{2n} \times D_{2n}^{(s)}] \cdot 2^{(\alpha,\beta)}$  in the first line, we need a transition from  $(\alpha, \beta) = (1, 0)$  to  $(\alpha, \beta) = (1, 1)$ . In this example,  $f = 2$  and  $g = 0$ . The only rule according to [8, bottom of p. 52] that allows this change is the transition from  $\langle s, \alpha, \beta \rangle$  to  $\langle s + f, \alpha, \beta - \alpha \rangle$  (see Figure 55), but it comes with a simultaneous change of  $s$  from  $s = 1$  to  $s + f = 3$ . The parameter  $s$  is regarded modulo  $2f = 4$ .

We did not investigate the reason for this duplication. Since  $f = 2$  in both cases, it may have to do with “... the easy cases when  $f \leq 2$ , which we exclude” [8, p. 52, line 2], see Figure 55.

The book of Conway and Smith [8] is otherwise a very nice book on topics related to quaternions and octonions, but it suffers from a concentration of mistakes near the end of Chapter 4, in particular, concerning the achiral groups. As an “erratum” to [8, §4], we attach in Figures 53–56 the Tables 4.1–4.2 and the last three pages of Chapter 4 of [8] with our additional explanations and corrections, as far as we could ascertain them, but we certainly did not fix all problems.

<sup>27</sup>Besides, the rule should also apply to entries that are not in the last eight lines of the tables. Accordingly, the constraint  $n \geq 2$ , which is stated for five of the eleven tubical groups in Table 2, should also be applied to the corresponding groups in [8, Table 4.1]. For the group  $+\frac{1}{2}[D_{2m} \times C_{2n}]$  in the penultimate line of Table 4.1, the obvious condition that  $m$  and  $n$  should be odd was forgotten. This omission has already been noted by Medeiros and Figueroa-O'Farrill [14, p. 1405].

Group	Generators	
$\pm[I \times O]$	$[i_I, 1], [\omega, 1], [1, i_O], [1, \omega];$	
$\pm[I \times T]$	$[i_I, 1], [\omega, 1], [1, i], [1, \omega];$	
$\pm[I \times D_{2n}]$	$[i_I, 1], [\omega, 1], [1, e_n], [1, j];$	$(n \geq 2)$
$\pm[I \times C_n]$	$[i_I, 1], [\omega, 1], [1, e_n];$	
$\pm[O \times T]$	$[i_O, 1], [\omega, 1], [1, i], [1, \omega];$	
$\pm[O \times D_{2n}]$	$[i_O, 1], [\omega, 1], [1, e_n], [1, j];$	$(n \geq 2)$
$\pm\frac{1}{2}[O \times D_{2n}]$	$[i, 1], [\omega, 1], [1, e_n], [i_O, j];$	$(n \geq 2)$
$\pm\frac{1}{2}[O \times \overline{D}_{4n}]$	$[i, 1], [\omega, 1], [1, e_n], [1, j]; [i_O, e_{2n}]$	$(n \geq 2)$
$\pm\frac{1}{6}[O \times D_{6n}]$	$[i, 1], [j, 1], [1, e_n], [i_O, j], [\omega, e_{3n}]$	
$\pm[O \times C_n]$	$[i_O, 1], [\omega, 1], [1, e_n];$	
$\pm\frac{1}{2}[O \times C_{2n}]$	$[i, 1], [\omega, 1], [1, e_n], [i_O, e_{2n}]$	
$\pm[T \times D_{2n}]$	$[i, 1], [\omega, 1], [1, e_n], [1, j];$	$(n \geq 2)$
$\pm[T \times C_n]$	$[i, 1], [\omega, 1], [1, e_n];$	
$\pm\frac{1}{3}[T \times C_{3n}]$	$[i, 1], [1, e_n], [\omega, e_{3n}]$	
$\pm\frac{1}{2}[D_{2m} \times \overline{D}_{4n}]$	$[e_m, 1], [1, e_n], [1, j], [j, e_{2n}]$	$(m \geq 2, n \geq 2)$
$\pm[D_{2m} \times C_n]$	$[e_m, 1], [j, 1], [1, e_n];$	$(m \geq 2)$
$\pm\frac{1}{2}[D_{2m} \times C_{2n}]$	$[e_m, 1], [1, e_n], [j, e_{2n}]$	$(m \geq 2, n \geq 2)$
$\pm\frac{1}{2}[D_{2m} \times C_{2n}]$	$- , - ; +$	$m \text{ and } n \text{ odd } (m \geq 2, n \geq 2)$
$\pm\frac{1}{2}[\overline{D}_{4m} \times C_{2n}]$	$[e_m, 1], [j, 1], [1, e_n], [e_{2m}, e_{2n}]$	$(m \geq 2)$

**Table 4.1.** Chiral groups, I. These are most of the “metachiral” groups—see section 4.6—some others appear in the last few lines of Table 4.2.

Group	Generators	Coxeter Name
$\pm[I \times I]$	$[i_I, 1], [\omega, 1], [1, i_I], [1, \omega];$	$[3, 3, 5]^+$
$\pm\frac{1}{60}[I \times I]$	$[\omega, \omega], [i_I, i_I]$	$2.[3, 5]^+$
$+\frac{1}{60}[I \times I]$	$; + , +$	$[3, 5]^+$
$\pm\frac{1}{60}[I \times \overline{I}]$	$[\omega, \omega], [i_I, i'_I]$	$2.[3, 3, 3]^+$
$+\frac{1}{60}[I \times \overline{I}]$	$; + , +$	$[3, 3, 3]^+$
$\pm[O \times O]$	$[i_O, 1], [\omega, 1], [1, i_O], [1, \omega];$	$[3, 4, 3]^+ : 2$
$\pm\frac{1}{2}[O \times O]$	$[i, 1], [\omega, 1], [1, i], [1, \omega]; [i_O, i_O]$	$[3, 4, 3]^+$
$\pm\frac{1}{6}[O \times O]$	$[i, 1], [j, 1], [1, i], [1, j]; [\omega, \omega], [i_O, i_O]$	$[3, 3, 4]^+$
$\pm\frac{1}{24}[O \times O]$	$[\omega, \omega], [i_O, i_O]$	$2.[3, 4]^+$
$+\frac{1}{24}[O \times O]$	$; + , +$	$[3, 4]^+$
$+\frac{1}{24}[O \times \overline{O}]$	$; + , -$	$[2, 3, 3]^+$
$\pm[T \times T]$	$[i, 1], [\omega, 1], [1, i], [1, \omega];$	$[^+3, 4, 3^+]$
$\pm\frac{1}{3}[T \times T]$	$[i, 1], [j, 1], [1, i], [1, j]; [\omega, \omega]$	$[^+3, 3, 4^+]$
$\cong \pm\frac{1}{3}[T \times \overline{T}]$	$[i, 1], [j, 1], [1, i], [1, j]; [\omega, \overline{\omega}]$	“
$\pm\frac{1}{12}[T \times T]$	$[\omega, \omega], [i, i]$	$2.[3, 3]^+$
$\cong \pm\frac{1}{12}[T \times \overline{T}]$	$[\omega, \overline{\omega}], [i, -i]$	“
$+\frac{1}{12}[T \times T]$	$; + , +$	$[3, 3]^+$
$\cong +\frac{1}{12}[T \times \overline{T}]$	$; + , +$	“
$\pm[D_{2m} \times D_{2n}]$	$[e_m, 1], [j, 1], [1, e_n], [1, j];$	$\left. \begin{array}{l} \text{Conditions} \\ m, n \text{ odd} \\ (s, f) = 1 \\ m, n \text{ odd}, (s, 2f) = 1 \\ (s, f) = 1 \\ m, n \text{ odd}, (s, 2f) = 1 \end{array} \right\} (m \geq 2, n \geq 2)$
$\pm\frac{1}{2}[\overline{D}_{4m} \times \overline{D}_{4n}]$	$[e_m, 1], [j, 1], [1, e_n], [1, j]; [e_{2m}, e_{2n}]$	
$\pm\frac{1}{4}[D_{4m} \times \overline{D}_{4n}]$	$[e_m, 1], [1, e_n], [e_{2m}, j], [j, e_{2n}]$	
$+\frac{1}{4}[D_{4m} \times \overline{D}_{4n}]$	$- , - ; + , +$	
$\pm\frac{1}{2f}[D_{2mf} \times D_{2nf}^{(s)}]$	$[e_m, 1], [1, e_n], [e_{mf}, e_{nf}^s], [j, j]$	$(s, f) = 1$
$+\frac{1}{2f}[D_{2mf} \times D_{2nf}^{(s)}]$	$- , - ; + , +$	$m, n \text{ odd}, (s, 2f) = 1$
$\pm\frac{1}{f}[C_{mf} \times C_{nf}^{(s)}]$	$[e_m, 1], [1, e_n], [e_{mf}, e_{nf}^s]$	$(s, f) = 1$
$+\frac{1}{f}[C_{mf} \times C_{nf}^{(s)}]$	$- , - ; +$	$m, n \text{ odd}, (s, 2f) = 1$

**Table 4.2.** Chiral groups, II. These groups are mostly “orthochiral,” with a few “parachiral” groups in the last few lines. The generators should be taken with both signs except in the haploid cases, for which we just indicate the proper choice of sign. The “Coxeter names” are explained in Section 4.4.

Figure 53: Corrections and remarks for [8, Tables 4.1 and 4.2, p. 44 and 46].

### The Completeness of Table 4.3

Here we obtain  $G$  from the “half-group”  $H$  corresponding to some isomorphism  $L/L_0 \cong R/R_0$  by adjoining an extending element  $*[a, b]$ , which must normalize  $H$ . We shall show that (at some cost) the extending element may be reduced to the form  $*[1, c]$ , and also that (at no cost)  $c$  can be multiplied by any element of  $R_0$ , or altered by any inner automorphism of  $R$ , while finally  $c$  must be in the part of  $R$  that is fixed (mod  $R_0$ ) by the isomorphism (since  $(*[1, c])^2 = [c, c]$  must be in  $H$ ).

For, conjugation by  $[1, a]$  replaces  $*[a, b]$  by

$$(*[a, b])^{[1, a]} = [1, \bar{a}] * [a, b][1, a] = *[\bar{a}a, ba] = *[1, c], \text{ say,}$$

at the cost of replacing  $[l, r]$  by  $[l, \bar{a}ra]$ , which changes the isomorphism to a geometrically equivalent one. If  $r_0 \in R_0$ ,  $*[1, cr_0]$  defines the same group as does  $*[l_1, cr_1]$  for any  $[l_1, r_1] \in H$ , and this reduces to  $*[1, cr_1 l_1]$  on conjugation by  $[1, l_1]$ , which replaces the  $r$  in  $[l, r]$  by  $\bar{l}_1 r l_1$ , its image under an arbitrary inner automorphism of  $R$ .

These considerations almost always suffice to restrict the extending element to

$$*[1, \pm 1] = * \text{ or } -*,$$

notated respectively by  $\cdot 2_3$  or  $\cdot 2_1$  (the subscript being the dimension of the negated space). The exceptions are the “ $D \times D$ ” and “ $C \times C$ ” cases, for which Table 4.3 lists every  $c$ , and just two more cases, denoted

$$\pm \frac{1}{2}[O \times O] \cdot \bar{2} \quad \text{and} \quad \pm \frac{1}{4}[\bar{D}_{4n} \times \bar{D}_{4n}] \cdot \bar{2}$$

in which we can take  $c = i_O$  and  $e_{2n}$ , respectively.

As we remarked, the reduction to the form  $*[1, c]$  comes at the cost of replacing the isomorphism by a geometrically equivalent one, and in the “ $T \times T$ ” case, this sometimes replaces the identity isomorphism by the one we indicate by  $\bar{T}$ , namely

$$\omega \rightarrow \bar{\omega} \quad \text{and} \quad i \rightarrow \bar{i} = -i.$$

### The Last Eight Lines of Table 4.3

For  $\pm[D \times D] \cdot 2$ , we start from the fact that the extending element  $*[a, b]$  may be reduced (mod  $H$ ) and must normalize  $H$ , and therefore also  $E$ , the



subgroup of elements of the form  $[e^\gamma, e^\delta]$ , in  $H$ , since  $E$  is a characteristic subgroup of  $H$  (except in the easy cases when  $f \leq 2$ , which we exclude). MISSING  
 This puts  $a$  and  $b$  in  $e^{\mathbb{R}}(1 \text{ or } j)$ , and so (since  $[j, j] \in H$ ) we can take  $*[a, b] = *[e^\lambda, e^\mu]$  (leading to  $\pm[D \times D] \cdot 2^{(\alpha, \beta)}$ ) or  $*[a, b] = *[e^\lambda, e^\mu j]$  (leading to  $\pm[D \times D] \cdot 2$ —see footnote 4.) In the first case, we must have

$$[j, j]^{*[e^\lambda, e^\mu]} = [j, j]^{[e^\lambda, e^\mu]} = [je^{2\lambda}, je^{2\mu}] \in H,$$

which forces  $\lambda = \frac{\alpha}{2}$  and  $\mu = \frac{\alpha s + \beta f}{2}$ , where  $\alpha, \beta \in \mathbb{Z}$ . The fact that the square of this is in  $H$  imposes the condition  $\alpha g + \beta f \equiv 0 \pmod{2}$ .

$G$  is unaltered when we increase  $\alpha$  or  $\beta$  by 2 since  $[e, e^s], [1, e^f] \in H$ . For a similar reason,  $s$  is initially only defined  $\pmod{f}$ , but the equation

$$*[e^{\frac{\alpha}{2}}, e^{\frac{\alpha s + \beta f}{2}}] = *[e^{\frac{\alpha}{2}}, e^{\frac{\alpha(s+f) + (\beta-\alpha)f}{2}}]$$
DEFINED HERE

shows that

$$\langle s, \alpha, \beta \rangle \approx \langle s + f, \alpha, \beta - \alpha \rangle,$$

so from now on it is better to regard  $s$  as defined  $\pmod{2f}$ . Since  $[e^s, e^f] = [e, e^s]^{*[a, b]}$  and  $[e, e^{s^2}]$  are both in  $H$ , we must have  $s^2 = fg + 1$  for some integer  $g \in \mathbb{Z}$ . e

To discuss equalities, we must consider all possibilities for an element that transforms this group  $\langle s, \alpha, \beta \rangle$  to a similar one  $\langle s', \alpha', \beta' \rangle$ . The transforming element can also be reduced  $\pmod{H}$  and after taking account of  $*$  and  $[1, j]$  (which takes  $\langle s, \alpha, \beta \rangle$  to itself or  $\langle -s, \alpha, -\beta \rangle$ ), can be supposed to normalize  $H$  and therefore have the form  $[e^{\frac{a}{2}}, e^{\frac{as + bf}{2}}]$ , with  $a, b \in \mathbb{Z}$ . We find that transforming by this adds some multiple (which can be odd) of  $(f, g)$  to  $(\alpha, \beta)$ , so the only further relation is  $\langle s, \alpha, \beta \rangle \approx \langle s, \alpha + f, \beta + g \rangle$ .

To summarize, we have for this group

Variables	Conditions	Equalities
$\alpha \pmod{2}$	$s^2 = fg + 1$	$\langle s, \alpha, \beta \rangle$
$\beta \pmod{2}$	$\alpha g + \beta f \equiv 0 \pmod{2}$	$\approx \langle -s, \alpha, -\beta \rangle$
$s \pmod{2f}$		$\approx \langle s + f, \alpha, \beta - \alpha \rangle$
		$\approx \langle s, \alpha + f, \beta + g \rangle,$

<sup>4</sup> In the second case we can choose new generators to simplify the group; namely, conjugation by  $[1, e^\lambda]$  fixes  $E$  and replaces  $*[e^\lambda, e^\mu j]$  by  $*[1, e^{\mu-\lambda} j] = *[1, J]$ , and then  $J$  can replace  $j$ , since  $(*[1, J])^2 = [J, J]$  must be in  $H$ .

Figure 55: Corrections and remarks for [8, p. 52].

## Appendix: Completeness of the Tables

53

while for  $\pm[D \times D^{(s)}] \cdot \bar{2}$  we have

Variables	Conditions	Equalities
$s \pmod{f}$	$s^2 = fg - 1$	$\langle s \rangle \approx \langle -s \rangle$ .

Equalities in the other cases are summarized as:

Group	Variables	Conditions	Equalities
$[D \times D^{(s)}] \cdot 2^{(\alpha, \beta)}$	$\alpha \pmod{2}$ $\beta \pmod{4}$ $s \pmod{4f}$	$s^2 = fg + 1$ $\alpha g \equiv 0 \pmod{4}$ $n \text{ odd, } g \text{ even}$	$\langle s, \alpha, \beta \rangle$ $\approx \langle -s, \alpha, -\beta \rangle$ $\approx \langle s + 2f, \alpha, \beta - 2\alpha \rangle$ $\approx \langle s, \alpha, \beta + 2h \rangle$
$[D \times D] \cdot \bar{2}$	$s \pmod{2f}$	$s^2 = fg - 1, g = 2h \text{ even}$	$\langle s \rangle \approx \langle -s \rangle$
$\pm[C \times C] \cdot 2^{(\gamma)}$	$s \pmod{f}$ $\gamma \pmod{2}$ $*[1, e^{\frac{\gamma(f, s+1)}{2}}]$	$s^2 = fg - 1$ $(g, s-1)\gamma \equiv 0 \pmod{2}$ $(f, s+1)\gamma \equiv 0 \pmod{2}$ $g \text{ even}$	$\langle s, \gamma \rangle$ $\approx \langle s, -\gamma \rangle$
$[C \times C] \cdot 2^{(\gamma)}$	$s \pmod{2f}$ $\gamma \pmod{2d}$ $*[1, e^{\frac{\gamma(f, s+1)}{2}}]$ $d = \frac{(2f, s+1)}{(f, s+1)}$	$s^2 = fg - 1$ $(g, s-1)\gamma \equiv 0 \pmod{4}$ $(f, s+1)\gamma \equiv 0 \pmod{2}$ $n \text{ odd, } g = 2h \text{ even}$	$\langle s, \gamma \rangle$ $\approx \langle s, -\gamma \rangle$

Table 4.4 summarizes the different achiral groups among the last four lines of Table 4.3. In the last eight lines, it is always permissible to replace  $D_2$  by  $C_2$  and  $\bar{D}_4$  by  $D_4$ .

• ALSO IN THE OTHER TABLES

• ALSO  $\frac{1}{4}[D_4 \times \bar{D}_{4m}]$  BY  $\frac{1}{4}[D_4 \times D_{4m}]$

$f, g \text{ even}$	:	$\cdot 2^{(0,0)}, \cdot 2^{(0,1)}, \cdot 2^{(1,0)}, \cdot 2^{(1,1)}$ and $\cdot \bar{2}$
else	:	$\cdot 2$ and $\cdot \bar{2}$
$f, h \text{ even}$	:	$\cdot 2^{(0,0)}, \cdot 2^{(0,2)}, \cdot 2^{(1,0)}, \cdot 2^{(1,2)}$ and $\cdot \bar{2}$
else	:	$\cdot 2$ and $\cdot \bar{2}$ <span style="color: green;">(<math>\cdot 2</math>) STANDS FOR <math>\cdot 2^{(0,0)} (= \cdot 2_3)</math></span>
$g/2 \text{ even}$	:	$\cdot 2^{(0)}, \cdot 2^{(1)}$ and $\cdot \bar{2}$
else	:	$\cdot 2$ and $\cdot \bar{2}$
$h \text{ even}$	:	$\cdot 2^{(0)}, \cdot 2^{(d)}$ and $\cdot \bar{2}$ <span style="color: green;">(<math>\cdot 2</math>) STANDS FOR <math>\cdot 2^{(0)}</math> (OR <math>\cdot 2_3</math>)</span>
else	:	$\cdot 2$ and $\cdot \bar{2}$

Table 4.4. Different achiral groups.

Figure 56: Corrections and remarks for [8, p. 53].